A new perspective to strongly-interacting lattice fermions in the framework of density functional theory

From ground-state correlations to spin-charge separation at finite temperatures

Dissertation zur Erlangung des akademischen Grades

Doktor der Naturwissenschaften (Dr. rer. nat.)

Vorgelegt im Fachbereich Mathematik und Naturwissenschaften der Universität Kassel

Vorgelegt von

Tobias Müller

Betreut durch

Prof. Dr. Gustavo M. Pastor

Verteidigt am 2. Dezember 2020

Abstract

A density functional theory for lattice models of strongly-interacting fermions is formulated, which applies both to the ground state and to the thermodynamic equilibrium in the canonical and grand-canonical ensembles. The single-particle density matrix (SPDM) γ plays the role of the central variable in the sense that all physical observables can be expressed as functionals of it. The actual SPDM γ which corresponds to the ground state or to the thermodynamic equilibrium is obtained by minimizing the appropriate thermodynamic potential: the energy $E[\gamma] = K[\gamma] + W[\gamma]$, if one is interested in ground-state properties, and the Helmholtz free-energy $F[\gamma] = E[\gamma] - TS[\gamma]$ or grand potential $\Omega[\gamma] = F[\gamma] - \mu N[\gamma]$ in the case of the thermodynamic equilibrium at finite temperatures. Here $K[\gamma]$, $W[\gamma]$, $S[\gamma]$, and $N[\gamma]$ are the SPDM functionals giving, respectively, the kinetic and interaction energies, the entropy, and the number of particles in the system. While the exact forms of $K[\gamma]$ and $N[\gamma]$ are known, explicit expressions for the interaction energy $W[\gamma]$ and the entropy $S[\gamma]$ are not available at present. Therefore, the very first and crucial challenge in the framework of the present lattice density functional theory (LDFT), as in any density functional approach, is to develop accurate and physically sound approximations to these highly non-trivial functionals. Clearly, the functional dependence of $W[\gamma]$ and $S[\gamma]$ will crucially depend on the nature and strength of the interactions between the Fermions. In this work we focus on local interactions as described by the Hubbard model, which is considered to be the paradigm of correlated itinerant electrons in narrow bands.

A simple, transparent approximation to the interaction-energy functional $W[\gamma]$ is proposed, which is based on an analogy between the effects of electronic correlations and finite-temperature excitations leading to occupation-number redistributions in momentum space. In this framework, the ground-state properties of the single-band Hubbard model are investigated as functions of the Coulomb-repulsion strength U/t. Remarkably accurate results are obtained for the most relevant ground-state properties, such as the ground-state energy E_0, the SPDM γ, the average number of double occupations D, and the spin-resolved momentum distribution $\eta_\sigma(k)$ in the complete range of interaction strengths, from weak correlations ($U/t \ll 1$) to the strongly-correlated limit ($U/t \gg 1$). A wide variety of physical situations is successfully explored, including finite and infinite lattices in 1–3 and infinite dimensions, bipartite and frustrated antiferromagnetic (AFM) structures, spin-polarized systems, attractive

interactions leading to electronic pairing, and different band-fillings.

Following the reasoning behind Mermin's theorem, we extend the scope of LDFT to the thermodynamic equilibrium at finite temperatures. A simple scaling-approximation to the correlation part $G_c[\boldsymbol{\gamma}] = G[\boldsymbol{\gamma}] - G_s[\boldsymbol{\gamma}]$ of the free-energy functional $F[\boldsymbol{\gamma}] = K[\boldsymbol{\gamma}] + G[\boldsymbol{\gamma}]$ is proposed, where $G_s[\boldsymbol{\gamma}] = W_{\mathrm{HF}}[\boldsymbol{\gamma}] - TS_s[\boldsymbol{\gamma}]$ incorporates the interaction-energy and entropy functionals of independent fermions. The scaling approximation is subsequently applied to the half-filled Hubbard model in 1–3 dimensions. The comparison with the exact solution in 1D and quantum Monte Carlo simulations or numerical linked-cluster expansion in higher dimensions demonstrates the predictive power of our method. Most notably, the separation of spin and charge degrees of freedom, a subtle effect of strong electronic correlations, is accurately described. This effect is most clearly reflected by the temperature dependence of the specific heat C_V in the strongly-correlated limit, which displays two distinct peaks corresponding to the low-lying spin- and the high-energy charge-excitations. In particular, the temperature $T_N \propto t^2/U$ at which the low-temperature peak occurs in C_V, marking the Néel transition from the AFM ground-state to the paramagnetic phase, is accurately reproduced. The same applies to the temperature $T_C \propto U$, corresponding to the high-temperature peak, marking the onset of charge excitations across the Hubbard gap. The scaling approximation is also applied away from half band-filling in order to determine how the changes in the electron density affect the most relevant equilibrium properties, such as the kinetic energy K, the double occupations D, and the specific heat C_V. Furthermore, the scaling approximation is extended to spin-polarized systems, which allows us to study the effect of an external magnetic field on various finite-temperature properties of the 1D Hubbard model. The comparison with exact results confirms the very good accuracy of our LDFT approach.

The theory formulated in this thesis opens a new perspective to the many-body problem of interacting fermions on a lattice. Practical applications, enabled by the new approximations to the central functionals $W[\boldsymbol{\gamma}]$ and $G_c[\boldsymbol{\gamma}]$ introduced in this work, demonstrate the flexibility and the predictive power of the theory. This applies both to the ground state, where our functionals are able to take advantage of the full universality of LDFT, as well as to the equilibrium at finite temperatures, where subtle effects such as the spin-charge separation are, to our knowledge, reproduced for the first time in the framework of a density-functional description.

Zusammenfassung

Eine Dichtefunktionaltheorie für Gittermodelle stark wechselwirkender Fermionen wird formuliert, welche sowohl für den Grundzustand als auch für das thermodynamische Gleichgewicht im kanonischen und großkanonischen Ensemble anwendbar ist. Die Einteilchen-Dichtematrix (SPDM) γ spielt hierbei die Rolle der zentralen Variable in dem Sinne, dass alle physikalischen Observablen als Funktionale von ihr dargestellt werden können. Die SPDM γ, welche zum Grundzustand oder zum Gleichgewichtszustand gehört, erhält man durch die Minimierung des entsprechenden thermodynamischen Potentials: Die Energie $E[\gamma] = K[\gamma] + W[\gamma]$, wenn man an den Grundzustandseigenschaften interessiert ist und die Helmholtz'sche freie Energie $F[\gamma] = E[\gamma] - TS[\gamma]$ bzw. das großkanonische Potential $\Omega[\gamma] = F[\gamma] - \mu N[\gamma]$, im Falle des thermodynamischen Gleichgewichts bei endlichen Temperaturen. Hierbei sind $K[\gamma]$, $W[\gamma]$, $S[\gamma]$ und $N[\gamma]$ die SPDM Funktionale der Kinetischen- und Wechselwirkungsenergie, der Entropie sowie der Teilchenzahl. Während die genaue Form von $K[\gamma]$ und $N[\gamma]$ bekannt ist, existieren bislang keine expliziten Ausdrücke für $W[\gamma]$ und $S[\gamma]$. Daher besteht die erste wichtige Herausforderung in der vorliegenden Gitterdichtefunktionaltheorie (LDFT), genau wie in jedem anderen Dichtefunktional Ansatz, darin, genaue und physikalisch sinnvolle Näherungen für diese hochgradig nichttrivialen Funktionale zu entwickeln. Natürlich wird die funktionale Abhängigkeit von $W[\gamma]$ und $S[\gamma]$ stark von der Art und Stärke der Wechselwirkung zwischen den Fermionen beeinflusst. In dieser Arbeit konzentrieren wir uns auf lokale Wechselwirkungen die durch das Hubbard-Modell beschrieben werden, welches das Paradebeispiel zur Beschreibung korrelierter Elektronen in schmalen Energiebändern darstellt.

Wir schlagen eine einfache Näherung für das Wechselwirkungsfunktional $W[\gamma]$ vor, welche auf einer Analogie zwischen den Effekten elektronischer Korrelationen und thermischen Anregungen basiert, die zu Umverteilungen der Besetzungszahlen im Impulsraum führen. In diesem Rahmen untersuchen wir die Grundzustandseigenschaften des Einband Hubbard-Modells als Funktionen der Coulomb Abstoßung U/t. Wir erhalten bemerkenswert genaue Resultate für die wichtigsten Grundzustandseigenschaften, wie z. B. die Grundzustandsenergie E_0, die SPDM γ, die mittlere Anzahl der Doppelbesetzungen D und die Spin-aufgelöste Impulsverteilung $\eta_\sigma(\boldsymbol{k})$ im gesamten Bereich, beginnend bei schwachen Wechselwirkungen ($U/t \ll 1$) bis hin zum stark korrelierten Grenzfall ($U/t \gg 1$). Eine Vielzahl physikalischer Situationen wird

erfolgreich untersucht, darunter endliche und unendliche Gitter in 1–3 und unendlichen Dimensionen, bipartite und antiferromagnetisch (AFM) frustrierte Strukturen, Spin-polarisierte Systeme, attraktive Wechselwirkungen, welche zur elektronischen Paarbildung führen, sowie unterschiedliche Bandfüllungen.

Der Argumentation des Mermin-Theorems folgend erweitern wir den Anwendugsbereich der LDFT auf das thermodynamische Gleichgewicht bei endlichen Temperaturen. Wir schlagen eine einfache Skalierungsnäherung für den Korrelationsanteil $G_c[\gamma] = G[\gamma] - G_s[\gamma]$ des Funktionals der freien Energie $F[\gamma] = K[\gamma] + G[\gamma]$ vor, wobei $G_s[\gamma] = W_{\mathrm{HF}}[\gamma] - TS_s[\gamma]$ die Funktionale der Wechselwirkungsenergie und der Entropie unabhängiger Fermionen beinhaltet. Die Skalierungsnäherung wird anschließend auf das halbgefüllte Hubbard-Modell in 1–3 Dimensionen angewandt. Der Vergleich mit der exakten Lösung in 1D und Quanten Monte Carlo Simulationen sowie numerischen linked-Cluster Entwicklungen in höheren Dimensionen demonstriert die Genauigkeit und Vorhersagekraft unserer Methode. Vor allem die Trennung der Freiheitsgrade von Spin- und Ladungsfluktuationen, welche ein subtiler Effekt von starken elektronischen Korrelationen ist, wird hierbei sehr genau wiedergegeben. Dies zeigt sich am deutlichsten in der Temperaturabhängigkeit der spezifischen Wärme C_V im stark korrelierten Grenzfall, welche zwei getrennte Maxima aufweist, die zu den tiefliegenden Spinanregungen und den hochenergetischen Ladungsanregungen gehören. Insbesondere wird die Temperatur $T_N \propto t^2/U$, bei welcher der Tieftemperaturpeak in C_V entsteht und welche den Néel-Übergang vom AFM Grundzustand zur paramagnetischen Phase markiert, genau reproduziert. Dasselbe gilt auch für die Temperatur $T_C \propto U$, bei welcher der Hochtemperaturpeak entsteht und welche den Beginn der Ladungsanregungen über die Hubbard-Lücke markiert. Wir wenden die Skalierungsnäherung auch auf das weniger als halb gefüllte Hubbard-Modell an und untersuchen wie Änderungen der Elektronendichte die wichtigsten Gleichgewichtseigenschaften beeinflussen, wie z. B. die kinetische Energie K, die Doppelbesetzungen D und die spezifische Wärme C_V. Außerdem erweitern wir die Skalierungsnäherung auf Spin-polarisierte Systeme, was uns die Möglichkeit gibt die Auswirkungen externer Magnetfelder auf unterschiedliche Gleichgewichtseigenschaften des 1D Hubbard-Modells zu studieren. Der Vergleich mit entsprechenden exakten Resultaten bestätigt die Genauigkeit unseres LDFT Ansatzes.

Die in dieser Arbeit formulierte Theorie betrachtet das Vielteilchenproblem wechselwirkender Fermionen auf einem Gitter aus einem neuen Blickwinkel. Praktische Anwendungen, welche durch die neuen Näherungen für die zentralen Funktionale $W[\gamma]$ und $G_c[\gamma]$ ermöglicht werden, zeigen die Flexibilität und die Vorhersagekraft der Theorie. Dies gilt sowohl für den Grundzustand, wo unsere Funktionale die volle Universalität der LDFT ausnutzen, als auch für das thermodynamische Gleichgewicht, wo subtile Effekte wie die Spin-Ladungs Separation, nach unserem Wissen, zum ersten Mal im Rahmen einer Dichtefunktionaltheorie reproduziert werden.

The most beautiful experience we can have is the mysterious.
It is the fundamental emotion that stands at the cradle
of true art and true science.

— Albert Einstein

Acknowledgements

It is my greatest pleasures to express my sincere gratitude to all those who supported and motivated me during the course of this work.

I would first like to thank my supervisor Prof. Dr. G. M. Pastor, whose guidance and advice made this work possible. His door was always open whenever I ran into troubles and his inspiring words where always a great source of motivation to me.

Moreover, I would like to express my deepest gratitude to my wonderful girlfriend Claudia Itzel Jauregui Caballero for her tireless support and motivation during this challenging but very fruitful time.

I would also like to thank my colleagues and friends Gunnar Stegmann, Matthieu Saubanère, and Waldemar Töws for many interesting and inspiring discussions which were of great help during the course of this work.

Finally, I like to thank my parents Klaus and Dorothea Müller as well as my sisters Damaris Weil and Judith Müller for all their love, support, and encouragement.

Contents

List of Figures

Acronyms

AFM Antiferromagnetic

BCS Bardeen, Cooper, and Schrieffer

BZ First Brillouin Zone

DF Density Functional

DFT Density Functional Theory

DMFT Dynamical Mean-Field Theory

DOS Density of States

eq-SPDM Equilibrium Single-Particle Density Matrix

FM Ferromagnetic

FT-DFT Finite-Temperature Density Functional Theory

FT-LDFT Finite-Temperature Lattice Density Functional Theory

GGA Generalized Gradient Approximation

gs-SPDM Ground-State Single-Particle Density Matrix

HF Hartree-Fock

HK Hohenberg-Kohn

IFE Independent-Fermion Entropy

KS Kohn-Sham

LDA Local Density Approximation

LDFT Lattice Density Functional Theory

LL Levy-Lieb

LSDA Local Spin-Density Approximation

NLCE Numerical Linked-Cluster Expansion

NN Nearest Neighbor

PM Paramagnetic

QMC Quantum Monte Carlo

SPDM Single-Particle Density Matrix

TF Thomas-Fermi

XC Exchange-Correlation

Introduction

The formulation of quantum mechanics and the accompanying progress in our understanding of the physical properties of matter and the solid state in particular is undoubtedly one of the major breakthroughs in the physics of the last century. It has led to an understanding of the chemical composition, structure, and particular properties of solids according to which we categorize them as metals, insulators, semiconductors, superconductors, and magnetic materials. The technical applications which arose from the understanding of matter at the quantum level have revolutionized our lives in a way which is unparalleled since the industrialization of the 19th century. The development and progressive miniaturization of essential building blocks, such as transistors, magnetic and solid-state storage devices, dynamic and magnetic random access memories, solid-state lasers, and sensors, has led to a wide variety of modern electronic devices, such as computers and mobile phones.

Among the most important advances in condensed-matter physics and the quantum many-body problem in general is the development of Hohenberg-Kohn-Sham's density functional theory (DFT), in which the ground-state properties of a many-particle system subject to an arbitrary external potential $v(\boldsymbol{r})$ can be regarded as functionals of the many-particle density $n(\boldsymbol{r})$ [2, 3]. The underlying one-to-one correspondence between the ground state $|\Psi_0\rangle$ and the corresponding density $n_0(\boldsymbol{r})$ allows us, in principle, to avoid the calculation of the far more complicated ground-state wave function. Thus, in the framework of DFT, the density $n(\boldsymbol{r})$ takes the role of the fundamental variable of the many-body problem.

The first attempt to formulate the quantum many-body problem solely in terms of the particle density $n(\boldsymbol{r})$ dates back to 1927, where Thomas and Fermi (TF) proposed the first, from today's perspective very rudimentary, approach to compute atomic energies on the basis of the electronic density [4, 5]. The TF theory approximates the local contribution to the kinetic-energy functional $K[n(\boldsymbol{r})]$ of the interacting many-electron system by the kinetic energy of noninteracting electrons with the homogeneous density $n = n(\boldsymbol{r})$, and the interaction energy $W[n(\boldsymbol{r})]$ is approximated by the classical Hartree-energy $W_{\mathrm{H}}[n(\boldsymbol{r})]$. However, shortly after its formulation it turned out that the TF theory is unable to account for any kind of molecular bonding, which

---

Some passages of this chapter have been published in Ref. [1], ©2018 American Physical Society.

is mostly due to the oversimplified approximation to the kinetic-energy functional, and thus has been rapidly abandoned.

After the failure of the TF theory, the density functional (DF) approach was not used very intensively, until in 1964 Hohenberg and Kohn (HK) [2] demonstrated that in principle all ground-state observables of a many-particle system can be exactly obtained from the ground-state electron density $n_0(\mathbf{r})$ alone. The HK theorem ensures the existence of a universal functional

$$F_{\text{HK}}[n(\mathbf{r})] = K[n(\mathbf{r})] + W[n(\mathbf{r})]\,, \tag{1.1}$$

representing the optimal sum of the kinetic energy $T[n(\mathbf{r})]$ and the interaction energy $W[n(\mathbf{r})]$ of a many-particle system having the density $n(\mathbf{r})$. The variational principle of the corresponding energy functional

$$E[n(\mathbf{r})] = \int v(\mathbf{r})\, n(\mathbf{r})\, \mathrm{d}\mathbf{r} + F_{\text{HK}}[n(\mathbf{r})] \tag{1.2}$$

gives access to the ground-state density $n_0(\mathbf{r})$ and thus to all ground-state properties in principle. Just a few month after the formulation of the seminal HK theorem, an extension to the important case of the thermodynamic equilibrium at a finite temperature was formulated by Mermin [6], who proved that in principle all equilibrium averages of an interacting many-particle system can be obtained from the equilibrium particle density $n_{\text{eq}}(\mathbf{r})$ alone.

Most practical applications of DFT are performed within the Kohn-Sham (KS) scheme, which reduces the interacting many-particle problem to a set of selfconsistent single-particle equations [3]. Although formally exact, practical applications of DFT must resort to some kind of approximation to the universal functional $F_{\text{HK}}[n(\mathbf{r})]$. The first such approximation, known as the local density approximation (LDA), was introduced by Kohn and Sham [3], who expressed the local contribution to the nontrivial exchange and correlation (XC) part $E_{\text{xc}}[n(\mathbf{r})]$ of the universal functional (1.1) in terms of the XC energy of a homogeneous electron gas with density $n = n(\mathbf{r})$. Noticeable improvements over the LDA have been proposed later on, such as the local spin-density approximation (LSDA) [7], which accounts for spin-polarized systems, the generalized gradient approximations (GGAs), which take into account the density gradient [8–14], and the hybrid functionals [15–19], which combine the exchange energy computed with the KS orbitals and some appropriate approximation to the XC energy. More recently, related methods based on the single-particle density matrix (SPDM) $\gamma(\mathbf{r}, \mathbf{r}')$ have also been developed [20–32].

Hohenberg-Kohn-Sham's DFT, in combination with the LDA and its extensions, has demonstrated its predictive power in countless applications throughout the most large variety of fields. For example, ionization energies of atoms, dissociation energies

of molecules, bond-lengths, and molecular geometries are predicted with astonishing accuracy. There are, however, several situations where the conventional XC functionals perform poorly. One prominent example is the semiconductor band-gap, for example in silicon, which is largely underestimated by conventional DFT [33]. Another example are van der Waals interactions, which are caused by dynamical density fluctuations, and are therefore beyond the scope of LDA based XC functionals [34]. Particularly relevant in the context of the present thesis is the fact that conventional DFT systematically fails to account for the effects caused by strong electron correlations. This applies, for example, to the physics of spin-fluctuations, the Kondo-screening, heavy-fermion materials [35], high-temperature superconductivity [36, 37], and Mott-insulators [38–40]. Finding an accurate description of the effects caused by strong electronic correlations remains therefore a serious challenge in the framework of DFT.

Strongly-correlated electron systems are usually best described in the framework of lattice-model Hamiltonians, in which the electronic dynamics is simplified by focusing on the most relevant contributions which dominate the low-energy or low-temperature physics. Motivated at the origin by the description of molecular bonding [41, 42], magnetic impurities in metals [43], and itinerant electrons in narrow bands [44–46], the theory of many-body models has grown to a high level of sophistication, not only from a methodological perspective, but also concerning the physical effects that are taken into account in the modelization. In this way, subtle phenomena, such as valence and spin fluctuations, the separation of charge and spin degrees of freedom, superconductivity, correlation-induced localization, etc., have been revealed [37, 47, 48]. Despite these achievements, and although the electron dynamics is largely simplified with respect to the full first-principles problem, deriving the properties of these many-body lattice models remains a very difficult task. Exact analytical results are rare [38, 39, 49–56] and accurate numerical solutions are either inaccessible or very demanding [36, 57–68]. Consequently, developing theoretical methods capable of describing the physics of many-body lattice models is a subject of considerable interest.

Taking into account the universality of DFT and its remarkable success in handling the first-principles problem in the continuum, it is reasonable to expect that a suitable extension of the fundamental concepts of DFT combined with appropriate approximations to the corresponding functionals could provide an alternative, potentially most effective approach towards the physics of strongly-correlated electrons on a lattice. Indeed, in the past decades a number of very successful methods have been developed by applying the concepts of DFT to lattice models [1, 69–87]. Early studies have addressed the band-gap problem in semiconductors [69–71] and the role of the off-diagonal elements of the density matrix in the description of strong electron correlations [72]. Density-matrix energy functionals based on the exact Bethe-ansatz solution have been proposed and applied to the Hubbard and Anderson models in or-

der to describe itinerant electrons in narrow energy bands and the transport trough an Anderson junction as well as the related Kondo effect [75, 88, 89]. Also time-dependent approaches for lattice models of strongly-correlated electrons have been developed in the framework of DFT [76]. Most relevant in the context of the present work is the lattice density functional theory (LDFT), which considers the SPDM γ as the central variable of the many-body problem [77, 78].

Several important lattice models of strongly interacting electrons have been addressed within the framework of LDFT. This includes the single-impurity Anderson model [81–83] as well as the Hubbard model with homogeneous and inhomogeneous local potentials, dimerized chains, attractive pairing interactions, and inhomogeneous local repulsions [77–80, 83–87]. The basic idea behind the functionals proposed in previous approaches is to adopt a real-space perspective and to take advantage of scaling properties of the interaction energy W as a function of the bond order $\gamma_{12\sigma}$, which measures the degree of charge fluctuations between nearest neighbors (NNs). The actual dependence of W on $\gamma_{12\sigma}$ can then be inferred from the exact solution of a reference system, such as the two-site problem (dimer), or other exactly solvable systems. In its simplest form, this scaling approach gives access only to the diagonal and NN elements of the ground-state single-particle density matrix (gs-SPDM). Therefore, more complex observables whose functional dependence $O[\gamma]$ involves long-range SPDM elements, as well as physical situations requiring interatomic hoppings beyond NNs, remain out of scope, although an extension has been recently proposed which overcomes the latter limitation [87]. Nevertheless, the domain of applicability of the functionals proposed so far in the framework of LDFT, and the physical properties that can be derived from them, are somewhat limited. Moreover, in order to take full advantage of the universality of LDFT, it is necessary to account for the dependence of W on the complete density matrix γ. In fact, only in this case the interaction-energy functional $W[\gamma]$ is independent of the topology, dimensionality, and structure of the system. A more flexible formulation would also allow us to account for the distance dependence of $\gamma_{ij\sigma}$ and thus for the long-range electron mobility, which is most interesting in the context of strong electron correlations, even if the actual hybridizations are short-ranged, as it is usually the case in narrow-band systems. In this way, it should be possible to investigate how electron localization develops in real space as the Coulomb-repulsion strength increases, which is also relevant for transport properties.

It is therefore one of the central goals of this work (Chapter 4) to develop an interaction-energy functional $W[\gamma]$ for the Hubbard-model, which takes into account its dependence on the full SPDM γ, and thus leverages the universality of LDFT. To this aim, we will adopt a delocalized $\boldsymbol{k}$-space perspective and exploit a newly discovered connection between the interaction energy W in the ground state of the model and the entropy of the corresponding Bloch-state occupation-number distri-

bution $\eta_{k\sigma}$. We apply our functional to finite and infinite lattices in 1–3 dimensions as well as to the limit of infinite dimensions. The universal character of our functional is demonstrated by considering a large variety of interesting physical situations, including spin-polarized systems, correlated fermions subject to an attractive interaction, and we will study systems with different electron densities exhibiting Luttinger-liquid behavior.

Another fundamental limitation of current LDFT is the lack of a rigorous formulation which applies to the thermodynamic equilibrium at a finite temperature. A finite-temperature formulation exists in the framework of conventional DFT, which is based on Mermin's fundamental theorem [6], however, despite some efforts to derive sound approximations to the corresponding functionals, no practical implementation of the finite-temperature method is available so far [88, 90, 91]. This precludes the current DF approaches to account for a myriad of important physical phenomena, which can not be described within a ground-state formalism. For example, phase transitions in magnetic or superconducting materials, the Kondo-effect, and metal-insulator transitions are the consequence of specific qualitative features in the many-body spectral density of the electronic system. These effects therefore manifest themselves at specific temperatures, such as the Curie or Néel ordering temperatures in ferromagnets and antiferromagnets, or the Kondo temperature for magnetic impurities in metals.

A further important contribution of the present work is therefore the rigorous formulation of finite-temperature lattice density functional theory (FT-LDFT) in Section 3.2. Practical applications of FT-LDFT are provided in Chapter 5, where we focus on the Hubbard model and propose a simple scaling approximation to the correlation part $G_c[\gamma] = G[\gamma] - G_s[\gamma]$ of the central free-energy functional $F[\gamma] = K[\gamma] + G[\gamma]$. Here, $K[\gamma]$ represents the kinetic energy of the lattice electrons and $G_s[\gamma] = W_{\mathrm{HF}}[\gamma] - TS_s[\gamma]$ incorporates the interaction energy and entropy of independent fermions. The flexibility and predictive power of FT-LDFT in combination with our new scaling approximation is demonstrated in numerous applications to the Hubbard model with different band fillings in 1–3 dimensions. This applies in particular to the regime of strong Coulomb-interactions $U \gg t$, where the scaling approximation accurately reproduces the subtle effects of the separation between the spin- and charge-degrees of freedom.

The remainder of this thesis is organized as follows. In Chapter 2 we will give a short introduction to the Hubbard model, which is among the most emblematic models for strongly correlated electrons on a lattice, and which is therefore the main model of interest in the applications of our methods. Chapter 3 provides a rigorous formulation of LDFT for the ground state as well as for the thermodynamic equilibrium at finite temperatures. We will formulate the fundamentals of FT-LDFT in two different flavours, accounting for canonical and grand-canonical ensembles. In Chapter 4 we discover a remarkable one-to-one correspondence between the interaction energy W

in the ground state of the Hubbard model and the entropy S of the corresponding Bloch-state occupation-number distribution $\eta_{k\sigma}$. This newly discovered connection between W and S leads us to a very intuitive approximation to the interaction-energy functional $W[\gamma]$, which takes into account its dependence on the full SPDM γ and reproduces the exact interaction energy in the important limits of idempotent and scalar SPDMs, which are characteristic for weak and strong electronic correlations. The accuracy and universal nature of our method is demonstrated in applications to a large variety of physical situations. In Chapter 5 we focus on the thermal equilibrium at finite temperatures and develop a very intuitive scaling approximation for the correlation contribution $G_c[\gamma]$ to the free energy of the Hubbard model. The predictive power of our scaling approximation is demonstrated in applications to the half-filled Hubbard model on bipartite lattices in 1–3 dimensions. We also go beyond half band-filling and employ the scaling approximation in order to investigate the influence of the electron density on the most important equilibrium observables, such as the specific heat C_V and the average number of double occupations D. Furthermore, we extend our method to spin-polarized systems, which allows us to study the effects of external magnetic fields. The final Chapter 6 summarizes our results and provides an outlook on future challenges in the framework of LDFT.

The Hubbard model

<div style="text-align: right; font-size: 2em; color: #8B1538;">**2**</div>

The accurate description of electronic interactions is one of the major challenges in modern condensed matter physics. Strong electronic interactions arise, for example, in transition or rare-earth metals having partially filled d or f shells. Since these orbitals are rather localized around the ions, the mutual Coulomb repulsion of the corresponding electrons is, in contrast to the delocalized s or p shells, not treated with sufficient accuracy by mean-field approximations. The partially filled d and f shells are, however, also hybridized in the bulk, and in this way contribute to the chemical bonding. Consequently, neither a delocalized free-electron picture nor a fully-localized picture is suitable to describe the physical properties of transition-metal systems. In order to understand the physics of these systems it is important to have a theory which takes into account the interplay between electronic interactions and hybridizations. In this context Hubbard, Gutzwiller, and Kanamori [44–46] independently proposed a model Hamiltonian, usually referred to as Hubbard model, which intends to capture the most relevant contributions to the competition between electronic delocalization driven by hybridization and localization due to the mutual Coulomb repulsion between the electrons. In its most simple form, the Hubbard model describes a single orbital per lattice site and the hybridization is realized by the hopping of electrons between the orbitals located at nearest neighbor (NN) sites. Furthermore, the Coulomb interaction between the electrons is simplified to an effective onsite repulsion, i.e., only the interaction between electrons within the same orbital is taken into account.

Despite its apparent simplicity, no general solution of the Hubbard model is available to date. An exact solution exist only in two special cases, namely for the two extremes of lattice coordination numbers two and infinity. The solution for the first case, i.e., the one-dimensional Hubbard model, was derived by Lieb and Wu [49], and it is based on Bethe's solution for the spin-1/2 Heisenberg chain [92]. The latter case is handled by mapping the Hubbard model to a single-impurity Anderson model supplemented by a self-consistency condition. This provides a mean-field like picture, which becomes exact if the spatial dimension tends to infinity [38, 39]. After having introduced the Hubbard model in Section 2.1 and discussed the profound approximations involved in its derivation from the first-principles many-body Hamiltonian, we review the exact Lieb-Wu solution for the ground state of the infinite Hubbard chain

in Section 2.2. In the subsequent Section 2.3 we discuss some important limiting cases of the Hubbard model, most notably the case of strong Coulomb repulsions, where the low-lying excitations of the half-filled Hubbard model are described by an effective spin-1/2 Heisenberg model. Furthermore, we review the mean-field approximation for the Hubbard model in Section 2.4 and present the corresponding ground-state phase diagram.

2.1 Approximating the full many-body Hamiltonian

In order to derive the Hubbard model from the full many-body Hamiltonian of interacting electrons in a solid, we start by assuming that the ions form a static lattice, such that their interaction with the electrons can be described by a static potential $v(\boldsymbol{r})$. This assumption is justified, since the electron mass is several orders of magnitude smaller than the mass of the ions in typical solids, and consequently, the electronic system is able to adapt almost instantly to changes of the ionic structure. Within this approximation the dynamics of interacting electrons in a solid is governed by the electronic Hamiltonian

$$\hat{H} = \sum_{\sigma} \int \hat{\psi}_{\sigma}^{\dagger}(\boldsymbol{r}) \left[-\frac{\hbar^2}{2m} \nabla^2 + v(\boldsymbol{r}) \right] \hat{\psi}_{\sigma}(\boldsymbol{r}) \, \mathrm{d}\boldsymbol{r}$$

$$+ \frac{1}{2} \sum_{\sigma\sigma'} \int \hat{\psi}_{\sigma}^{\dagger}(\boldsymbol{r}) \, \hat{\psi}_{\sigma'}^{\dagger}(\boldsymbol{r}') \, \frac{e^2}{|\boldsymbol{r} - \boldsymbol{r}'|} \, \hat{\psi}_{\sigma'}(\boldsymbol{r}') \, \hat{\psi}_{\sigma}(\boldsymbol{r}) \, \mathrm{d}\boldsymbol{r} \, \mathrm{d}\boldsymbol{r}', \quad (2.1)$$

where $\hat{\psi}_{\sigma}^{\dagger}(\boldsymbol{r})$ $[\hat{\psi}_{\sigma}(\boldsymbol{r})]$ is the usual fermionic field operator creating (annihilating) an electron with spin polarization σ at the position $\boldsymbol{r}$. The first term in Eq. (2.1) represents the kinetic energy of the electrons and their interaction with the static ion potential $v(\boldsymbol{r})$, and the second term describes their mutual Coulomb interaction.

We aim to describe the dynamics of electrons in narrow energy bands, such as the d or f electrons in solids, and therefore it is appropriate to work in a basis of Wannier states $\phi_{\alpha}(\boldsymbol{r} - \boldsymbol{R}_i)$ which are localized around the lattice sites $i = 1, \dots, N_a$. Here α is the band index, and if we introduce the corresponding creation operator $\hat{c}_{i\alpha\sigma}^{\dagger}$ which creates an electron with spin polarization σ in the Wannier orbital $\phi_{\alpha}(\boldsymbol{r} - \boldsymbol{R}_i)$, we can express the fermionic field operator as

$$\hat{\psi}_{\sigma}^{\dagger}(\boldsymbol{r}) = \sum_{i\alpha} \phi_{\alpha}^{*}(\boldsymbol{r} - \boldsymbol{R}_i) \, \hat{c}_{i\alpha\sigma}^{\dagger} \,. \quad (2.2)$$

Consequently, within the basis of the single-particle Wannier orbitals we can write

the Hamiltonian (2.1) as

$$\hat{H} = \sum_{ij\alpha\beta\sigma} t_{ij}^{\alpha\beta} \, \hat{c}_{i\alpha\sigma}^{\dagger} \hat{c}_{j\beta\sigma} + \frac{1}{2} \sum_{\sigma\sigma'} \sum_{\substack{ijkl \\ \alpha\beta\gamma\delta}} W_{ijkl}^{\alpha\beta\gamma\delta} \hat{c}_{i\alpha\sigma}^{\dagger} \, \hat{c}_{j\beta\sigma'}^{\dagger} \hat{c}_{l\delta\sigma'} \hat{c}_{k\gamma\sigma} \,, \tag{2.3}$$

where the hopping integrals are given by

$$t_{ij}^{\alpha\beta} = \int \phi_{\alpha}^{*}(r - R_i) \left[-\frac{\hbar^2}{2m} \nabla^2 + v(r) \right] \phi_{\beta}(r - R_j) \, dr \,, \tag{2.4}$$

and similarly, the interaction-energy integrals are given by

$$W_{ijkl}^{\alpha\beta\gamma\delta} = \int \phi_{\alpha}^{*}(r - R_i) \, \phi_{\beta}^{*}(r' - R_j) \, \frac{e^2}{|r - r'|} \, \phi_{\delta}(r' - R_l) \, \phi_{\gamma}(r - R_k) \, dr \, dr' \,. \tag{2.5}$$

The Hubbard model is obtained from the general many-body Hamiltonian (2.3) by several profound approximations. First, since we are interested in the dynamics of electrons in open d or f shells, it is justified to approximate their interaction with the electrons in the closed s and p shells by some static mean-field potential which, added to the ionic potential $v(r)$, results in an effective potential describing the interaction of the conduction band electrons and the screened ions. If one furthermore assumes that the Fermi surface lies within a single conduction band and all other bands are far away from the Fermi level, it is justified to focus on the conduction band exclusively, which means that one can discard the band indices denoted by Greek letters in the general Hamiltonian (2.3). A further profound approximation in the Hubbard model is to neglect any kind of interatomic Coulomb interaction between the electrons, i. e., to neglect all interaction parameters except for the dominating term W_{iiii}, which accounts for the Coulomb repulsion between two electrons occupying the same Wannier orbital localized at a given lattice site. According to Eq. (2.5) the intra-atomic Coulomb integral W_{iiii} is independent of the specific lattice site under consideration, such that one can set $W_{iiii} = U$ for all i. In this way, the second term in the Hamiltonian (2.3), which accounts for the Coulomb interaction between the electrons, is reduced to the simple form

$$\frac{U}{2} \sum_{\sigma\sigma'} \sum_{i} \hat{c}_{i\sigma}^{\dagger} \hat{c}_{i\sigma'}^{\dagger} \hat{c}_{i\sigma'} \hat{c}_{i\sigma} = U \sum_{i} \hat{n}_{i\uparrow} \hat{n}_{i\downarrow} \,, \tag{2.6}$$

where $\hat{n}_{i\sigma} = \hat{c}_{i\sigma}^{\dagger} \hat{c}_{i\sigma}$ is the usual number operator for electrons with spin polarization σ in the Wannier orbital located at R_i. Consequently, one obtains the Hubbard-model Hamiltonian as

$$\hat{H} = \hat{K} + \hat{W} = \sum_{ij\sigma} t_{ij} \, \hat{c}_{i\sigma}^{\dagger} \hat{c}_{j\sigma} + U \sum_{i} \hat{n}_{i\uparrow} \hat{n}_{i\downarrow} \,. \tag{2.7}$$

9

A further simplification usually made in the context of the Hubbard model on periodic lattice structures is to assume that the hopping integrals (2.4) are isotropic, i. e., that they solely depend on the distance between the lattice sites, such that $t_{ij} = t(|\boldsymbol{R}_i - \boldsymbol{R}_j|)$, and based on the assumption that the Wannier functions $\phi_\alpha(\boldsymbol{r} - \boldsymbol{R}_i)$ are strongly localized around the corresponding lattice sites, one often neglects all hopping-matrix elements beyond the NN terms $t_{ij} = -t$. In this way, the Hubbard-model Hamiltonian (2.7) is further simplified to

$$\hat{H} = \hat{K} + \hat{W} = -t \sum_{\langle i,j\rangle\sigma} \hat{c}^\dagger_{i\sigma}\hat{c}_{j\sigma} + U \sum_i \hat{n}_{i\uparrow}\hat{n}_{i\downarrow}\,, \qquad (2.8)$$

where $\langle i,j\rangle$ indicates the summation over NN lattice sites.[1] We have ignored the on-site terms $t_{ii} = \varepsilon$ since, due to the assumed homogeneity, they solely contribute a constant $N\varepsilon$ to the energy if the number of electrons N is kept fixed, and otherwise they can be absorbed in the chemical potential when working in a grand-canonical ensemble.

The physical processes described by the single-band Hubbard model (2.8) are quite intuitive. The first term $\hat{K}$ describes the hopping of electrons between the orbitals located at NN sites, which leads to a delocalized electronic state and, due to the interaction with the screened ions, to an effective bonding among the lattice. The second term $\hat{W}$ describes the local Coulomb repulsion U between electrons located at the same lattice site. Equation (2.8) describes a single band, such that there is only one orbital per lattice site, and consequently, due to Pauli's exclusion principle, two electrons occupying the Wannier orbital at a given lattice site must have opposite spin polarization. The two processes described by the Hubbard model are in strong competition with one another, since the kinetic energy $\hat{K}$ favors a delocalized electronic state in order to achieve a strong bonding among the lattice, while the local Coulomb interaction $\hat{W}$ favors a localized state in order to minimize the number of doubly occupied Wannier orbitals.

In order to take a closer look at the two contributions, $\hat{K}$ and $\hat{W}$, which make up the Hubbard-model Hamiltonian, we consider two cases in which the Hubbard model can be solved easily. The first one concerns the atomic limit $t = 0$, in which the Hubbard model Hamiltonian reduces to the interaction-energy term

$$\hat{H} = \hat{W} = U\,\hat{D}\,, \qquad (2.9)$$

where the operator $\hat{D} = \sum_i \hat{n}_{i\uparrow}\hat{n}_{i\downarrow}$ counts the number of doubly occupied Wannier orbitals. The corresponding eigenstates are given by

$$|\Psi\rangle = \left(\prod_{i\in\mathcal{I}_\uparrow} \hat{c}^\dagger_{i\uparrow}\right)\left(\prod_{i\in\mathcal{I}_\downarrow} \hat{c}^\dagger_{i\downarrow}\right)|\text{vac}\rangle\,, \qquad (2.10)$$

---

[1] Notice, that some authors use the notation $\langle i,j\rangle$ in order to indicate the summation over NN *pairs*, while in our convention there are two terms in the sum for each pair of NNs.

where $\mathcal{I}_\sigma$ is an arbitrary subset of $\{1, \ldots, N_a\}$ which represents the local orbitals that are occupied by spin-σ electrons, such that the corresponding cardinality $|\mathcal{I}_\sigma|$ equals the number N_σ of spin-σ electrons. The energy eigenvalue of this state is given by

$$E = \sum_{\mathcal{I}_\uparrow \cap \mathcal{I}_\downarrow} U = U\,D\,, \tag{2.11}$$

where $D = |\mathcal{I}_\uparrow \cap \mathcal{I}_\downarrow|$ is the number of doubly occupied local orbitals. The ground state is obtained by choosing subsets $\mathcal{I}_\sigma$ having minimal intersection. Clearly, for $N = N_\uparrow + N_\downarrow \leq N_a$, i.e., if the band is not more than half-filled, one can always find subsets having $\mathcal{I}_\uparrow \cap \mathcal{I}_\downarrow = \varnothing$, resulting in a vanishing ground-state energy $E_0 = 0$. In the case of a more than half-filled band ($N > N_a$) there must be at least $N - N_a$ sites which are occupied by two electrons, such that the ground-state energy is given by $E_0 = U(N - N_a)$.

The second case in which the Hubbard model (2.8) allows for a straight forward solution concerns noninteracting systems, i.e., a vanishing local Coulomb repulsion $U = 0$. The Hubbard-model Hamiltonian then reduces to the tight-binding term

$$\hat{H} = \hat{K} = -t \sum_{\langle i,j \rangle \sigma} \hat{c}_{i\sigma}^\dagger \hat{c}_{j\sigma}\,. \tag{2.12}$$

Like every periodic tight-binding Hamiltonian it can be diagonalized by introducing the corresponding Bloch states

$$\hat{c}_{k\sigma}^\dagger = \frac{1}{\sqrt{N_a}} \sum_{i=1}^{N_a} e^{i\boldsymbol{k} \cdot \boldsymbol{R}_i} \, \hat{c}_{i\sigma}^\dagger\,, \tag{2.13}$$

which correspond to the wave vectors $\boldsymbol{k}$ in the first Brillouin zone (BZ). It is straight forward to verify that, in terms of the Bloch-states (2.13), the tight-binding Hamiltonian (2.12) assumes the form

$$\hat{H} = \hat{K} = \sum_{\boldsymbol{k} \in \text{BZ}} \sum_{\sigma = \uparrow, \downarrow} \varepsilon_{\boldsymbol{k}} \, \hat{n}_{\boldsymbol{k}\sigma} \tag{2.14}$$

with the single-particle energies

$$\varepsilon_{\boldsymbol{k}} = -t \sum_{\Delta \in \text{NN}} \cos(\boldsymbol{k} \cdot \Delta)\,, \tag{2.15}$$

where the sum is taken over the unique vectors $\Delta \in \text{NN}$ connecting a given lattice site to its NNs. For example, in the case of a one-dimensional lattice with lattice constant $a = 1$ one has $\varepsilon_k = -2t \cos(k)$, and the corresponding N_a discrete wave

numbers k are distributed equally spaced within the BZ $[-\pi, \pi)$. The eigenstates of the Hamiltonian (2.14) are given by

$$|\Psi_K\rangle = \left(\prod_{k \in \mathcal{K}_\uparrow} \hat{c}^\dagger_{k\uparrow} \right) \left(\prod_{k \in \mathcal{K}_\downarrow} \hat{c}^\dagger_{k\downarrow} \right) |\text{vac}\rangle , \tag{2.16}$$

where $\mathcal{K}_\sigma$ is an arbitrary subset of the k-vectors in the BZ, representing the Bloch states that are occupied by spin-σ electrons. The corresponding energy eigenvalue is then given by

$$E_K = \sum_\sigma \sum_{k \in \mathcal{K}_\sigma} \varepsilon_k . \tag{2.17}$$

The ground state of (2.14) is consequently obtained by choosing $\mathcal{K}_\sigma$ as the set of wave-vectors which correspond to the N_σ lowest-lying Bloch-state energies (2.15). This kind of "filling the band from the bottom" is illustrated in Fig. 2.1 for the case of a one-dimensional ring having $N_a = 10$ sites and $N = 10$ electrons. As another specific example, let us consider the infinite one-dimensional Hubbard chain. Since the corresponding wave numbers k are dense within the BZ $[-\pi, \pi)$, one can replace sums within the BZ by integrals according to the rule

$$\sum_{k \in \text{BZ}} \longrightarrow \frac{N_a}{2\pi} \int_{-\pi}^{\pi} \mathrm{d}k . \tag{2.18}$$

Furthermore, since the dispersion relation of the infinite chain $\varepsilon(k) = -2t \cos(k)$ increases monotonously with $|k|$ for $k \in$ BZ, all Bloch states having $|k| < k_{F\sigma}$ are occupied in the ground state, while states with $|k| > k_{F\sigma}$ are unoccupied. Here, the Fermi wave-number $k_{F\sigma}$ for electrons with spin polarization σ is determined from the corresponding electron density $n_\sigma = N_\sigma/N_a$ as

$$N_\sigma = \frac{N_a}{2\pi} \int_{-k_{F\sigma}}^{k_{F\sigma}} \mathrm{d}k \quad \Rightarrow \quad k_{F\sigma} = \pi n_\sigma . \tag{2.19}$$

The ground-state energy of the infinite noninteracting Hubbard chain is thus obtained as

$$E_0 = \frac{N_a}{2\pi} \sum_\sigma \int_{-k_{F\sigma}}^{k_{F\sigma}} \varepsilon(k) \, \mathrm{d}k = -\frac{2t N_a}{\pi} \sum_\sigma \sin(\pi n_\sigma) . \tag{2.20}$$

Despite the apparent simplicity of the Hubbard model (2.8), it incorporates a plethora of interesting physical phenomena observed in interacting many-electron systems. It has been used in order to study the band magnetism in transition metals [93], to investigate the Mott metal-insulator transition [40, 94], and it is believed to incorporate the fundamental processes responsible for high-T_c superconductivity [95, 96]. Clearly, a model which incorporates such a diversity of subtle many-body
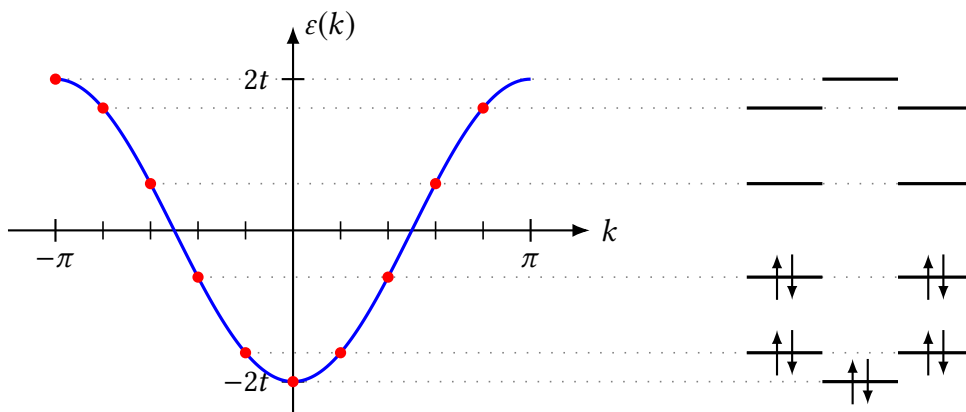
Figure 2.1: Schematic illustration of the noninteracting ground state of a 10-site Hubbard ring having $N = 10$ electrons with $N_\uparrow = N_\downarrow = 5$. The dispersion relation $\varepsilon(k) = -2t \cos(k)$ of the one-dimensional Hubbard chain is shown by the blue curve on the left and the single-particle energy levels ε_k of the 10-site ring are marked by red dots. The diagram on the right illustrates the "filling" of the energy levels from the bottom by electrons with opposite spin polarization, which leads to the noninteracting ground state.

effects can not be expected to allow for an easy general solution. In fact, despite the profound simplifications involved in the derivation of the Hubbard model (2.8), and the simple solution of its two individual constituents $\hat{K}$ and $\hat{W}$ discussed above, there are only few exact results available at present. An exact solution exists for the ground state of the infinite one-dimensional chain, which will be reviewed in the subsequent section, as well as in the limit of infinite spatial dimensions [38, 39]. Furthermore, there are a number of rigorous results for the ground state and excited states in some limiting cases [55].

2.2 Lieb-Wu equations for the ground state

One of the few situations in which the Hubbard model (2.8) allows for an exact analytical solution is the case of the infinite one-dimensional chain. The ground-state problem of the infinite one-dimensional Hubbard chain has been solved by Lieb and Wu [49]. Later developments by Jüttner *et al.* [56] have extended the exact analytical solution of the one-dimensional Hubbard chain to the equilibrium at finite temperatures. In this section we briefly review the solution of Lieb and Wu for the ground state, which is based on the *Bete-ansatz* [92] and reduces the Schrödinger equation for the one-dimensional Hubbard model to a set of algebraic equations. In the thermodynamic limit $N_a \to \infty$, with the electron density N/N_a and the density $N_\downarrow/N_a$ of the down spins kept fixed, the solution of Lieb and Wu is expressed in terms of

two density functions $\rho(k)$ and $\sigma(\lambda)$, which are obtained from the coupled integral equations

$$\rho(k) = \frac{1}{2\pi} + \cos(k) \int_{-B}^{B} K[\sin(k) - \lambda]\,\sigma(\lambda)\,\mathrm{d}\lambda\,, \tag{2.21}$$

$$\sigma(\lambda) = \int_{-Q}^{Q} K[\sin(k) - \lambda]\,\rho(k)\,\mathrm{d}k - \int_{-B}^{B} K^2[\lambda - \lambda']\,\sigma(\lambda')\,\mathrm{d}\lambda'\,. \tag{2.22}$$

The functions $K[x]$ and $K^2[x]$ entering the integral equations are defined as

$$K[x] = \frac{1}{2\pi}\left[\frac{8u}{u^2 + 16x^2}\right] \quad \text{and} \quad K^2[x] = \frac{1}{2\pi}\left[\frac{4u}{u^2 + 4x^2}\right]\,, \tag{2.23}$$

where $u = U/t$ is the ratio between the Coulomb repulsion strength U and the hopping integral t. The parameters $0 \leq Q \leq \pi$ and $0 \leq B \leq \infty$, which appear in Eqs. (2.21) and (2.22), are determined by the conditions

$$\int_{-Q}^{Q} \rho(k)\,\mathrm{d}k = \frac{N}{N_a} \quad \text{and} \quad \int_{-B}^{B} \sigma(\lambda)\,\mathrm{d}\lambda = \frac{N_\downarrow}{N_a}\,. \tag{2.24}$$

Finally, the ground-state energy of the infinite one-dimensional Hubbard chain is obtained from the density function $\rho(k)$ as

$$E_0 = -2t N_a \int_{-Q}^{Q} \rho(k)\,\cos(k)\,\mathrm{d}k\,. \tag{2.25}$$

In the case of a half-filled band with vanishing magnetization, i. e., $N = N_a$ and $N_\uparrow = N_\downarrow = N/2$, one can show that Eq. (2.24) is satisfied for $Q = \pi$ and $B = \infty$ [97]. In this case, Eqs. (2.21) and (2.22) can be solved in a closed form, and one obtains the ground-state energy of the half-filled one-dimensional Hubbard chain as

$$E_0 = -4t N_a \int_0^{\infty} \frac{J_0(\omega)\,J_1(\omega)}{\omega\left(1 + e^{\omega u/2}\right)}\,\mathrm{d}\omega\,, \tag{2.26}$$

where $J_0(\omega)$ and $J_1(\omega)$ are Bessel functions of order zero and one. Another important quantity that can be obtained from the Lieb-Wu solution is the average number of double occupations $D = \sum_i \langle \hat{n}_{i\uparrow} \hat{n}_{i\downarrow} \rangle$ which, regarding the Hamiltonian (2.8) of the Hubbard model, is obtained as the derivative of the ground-state energy E_0 with respect to the Coulomb integral U. From the ground-state energy (2.26) of the half-filled unpolarized Hubbard chain one obtains the corresponding average number of double occupations as

$$D = \frac{\partial E_0}{\partial U} = N_a \int_0^{\infty} \frac{J_0(\omega)\,J_1(\omega)}{1 + \cosh(\omega u/2)}\,. \tag{2.27}$$

The unpolarized case $N_\uparrow = N_\downarrow = N/2$ with arbitrary electron density $n = N/N_a \leq 1$ has been investigated by Shiba [51]. Vanishing magnetization corresponds to $B = \infty$, and Shiba has demonstrated that in this case Eqs. (2.21) and (2.22) can be reduced to the single integral equation

$$\rho(k) = \frac{1}{2\pi} + \frac{\cos(k)}{u} \int_{-Q}^{Q} R\left(\frac{4\left(\sin k - \sin k'\right)}{u}\right) \rho(k')\,dk',\tag{2.28}$$

where

$$R(x) = \frac{4}{\pi} \sum_{n=1}^{\infty} (-1)^{n+1} \frac{2n}{x^2 + (2n)^2} = \frac{1}{\pi} \int_{-\infty}^{\infty} \frac{\mathrm{sech}(\pi t/2)}{1 + (x + t)^2}\,dt.\tag{2.29}$$

The parameter Q which enters Eq. (2.28) is determined by the first condition of Eq. (2.24), and after $\rho(x)$ is obtained from the solution of Eq. (2.28), the ground-state energy follows from Eq. (2.25). Again, the average number of double occupations is obtained from the derivative of the ground-state energy with respect to the Coulomb repulsion strength U

$$D = \frac{\partial E_0}{\partial U} = -2N_a \frac{\partial}{\partial u}\left(\int_{-Q}^{Q} \rho(k)\,\cos(k)\,dk\right).\tag{2.30}$$

Here one has to take into account that not only $\rho(k)$ but also Q depends on $u = U/t$. In fact, from the conservation of particles $\partial N/\partial u = 0$ and the first condition of Eq. (2.24) one obtains

$$\frac{\partial Q}{\partial u} = -\frac{1}{2\rho(Q)} \int_{-Q}^{Q} \frac{\partial \rho(k)}{\partial u}\,dk,\tag{2.31}$$

where we have used $\rho(Q) = \rho(-Q)$.[2] Combining Eqs. (2.30) and (2.31) one obtains

$$D = 2N_a \int_{-Q}^{Q} (\cos Q - \cos k) \frac{\partial \rho(k)}{\partial u}\,dk.\tag{2.32}$$

For the derivative of the density function $\rho(k)$ one obtains from Eqs. (2.28) and (2.31) the following integral equation

$$\frac{\partial \rho(k)}{\partial u} = \frac{\cos(k)}{u^2} \int_{-Q}^{Q} \Phi\left(\frac{4\left(\sin k - \sin k'\right)}{u}\right) \rho(k')\,dk' + \frac{\cos(k)}{u} \int_{-Q}^{Q} dk' \frac{\partial \rho(k')}{\partial u} \times$$

$$\times \left[R\left(\frac{4\left(\sin k - \sin k'\right)}{u}\right) - \frac{1}{2} R\left(\frac{4\left(\sin k - \sin Q\right)}{u}\right) - \frac{1}{2} R\left(\frac{4\left(\sin k + \sin Q\right)}{u}\right)\right],\tag{2.33}$$

---

[2]The fact, that $\rho(k)$ is an even function follows from the uniqueness of the solution of Eq. (2.28), which has been demonstrated by Lieb and Wu [97], together with the fact that if $\rho(k)$ is a solution of Eq. (2.28) then $\rho(-k)$ is a solution too.

where the function $R(x)$ is defined in Eq. (2.29) and

$$\Phi(x) = -R(x) - x\,\frac{\partial R(x)}{\partial x} = \frac{8}{\pi}\sum_{n=1}^{\infty}(-1)^{n+1}\,n\,\frac{x^2 - (2n)^2}{\left[x^2 + (2n)^2\right]^2}\,. \tag{2.34}$$

In the strongly correlated limit $u = U/t \to \infty$, Shiba's integral equations (2.28) and (2.33) yield $\rho(k) = 1/(2\pi)$ and $\partial\rho(k)/\partial u = 0$. Therefore, one obtains $D = 0$ from Eq. (2.32), i. e., the expected result that there are no double occupations in the ground state of the strongly-correlated Hubbard model with $n = N/N_a \leq 1$. Furthermore, the first condition in Eq. (2.24) must be fulfilled, i. e.,

$$\int_{-Q}^{Q}\rho(k)\,\mathrm{d}k = \frac{2Q}{2\pi} = \frac{N}{N_a} \quad\Rightarrow\quad Q = \pi n\,, \tag{2.35}$$

and consequently, from Eq. (2.25) one obtains the ground-state energy of the strongly correlated infinite Hubbard chain as

$$E_0 = -\frac{tN_a}{\pi}\int_{-\pi n}^{\pi n}\cos(k)\,\mathrm{d}k = -\frac{2tN_a}{\pi}\sin(\pi n)\,. \tag{2.36}$$

This energy is due to the correlated electronic hopping between vacant lattice sites, which does not lead to double occupations. Clearly, in a half-filled band ($n = 1$) there are no vacancies, since a state with vanishing double occupations must be attained, and consequently the ground-state energy of the strongly correlated Hubbard chain vanishes at half band-filling.

In Appendix D we present a method for solving Shiba's integral equations (2.28) and (2.33), which utilizes the trapezoidal rule in order to approximate the integrals and, in turn, leads to a set of coupled linear algebraic equations. Results for the ground-state energy E_0 and the average number of double occupations D as a function of the electron density N/N_a are presented in Fig. 2.2 for some representative values of the Coulomb-repulsion strength U/t. From Fig. 2.2 (a) one concludes that correlation effects are rather negligible for low electron densities ($N/N_a \lesssim 0.3$), since the electrons can effectively avoid each other without much impact on their kinetic energy. Correlations in the electronic ground state become more noticeable as the electron density increases, and reach the maximum in the case of a half-filled band $N/N_a = 1$. The ground-state energy is thus most affected by changes in the Coulomb-repulsion strength U/t if the band is half filled, where it varies from $E_0 = -4tN_a/\pi$ in the non-interacting case $U/t = 0$ to $E_0 = 0$ in the strongly interacting limit $U/t \to \infty$. In the strongly interacting limit the electrons can reduce their kinetic energy only by hopping processes which involve vacant lattice sites and consequently, the ground-state energy is minimal if the number of vacant sites equals the number of electrons, i. e.,
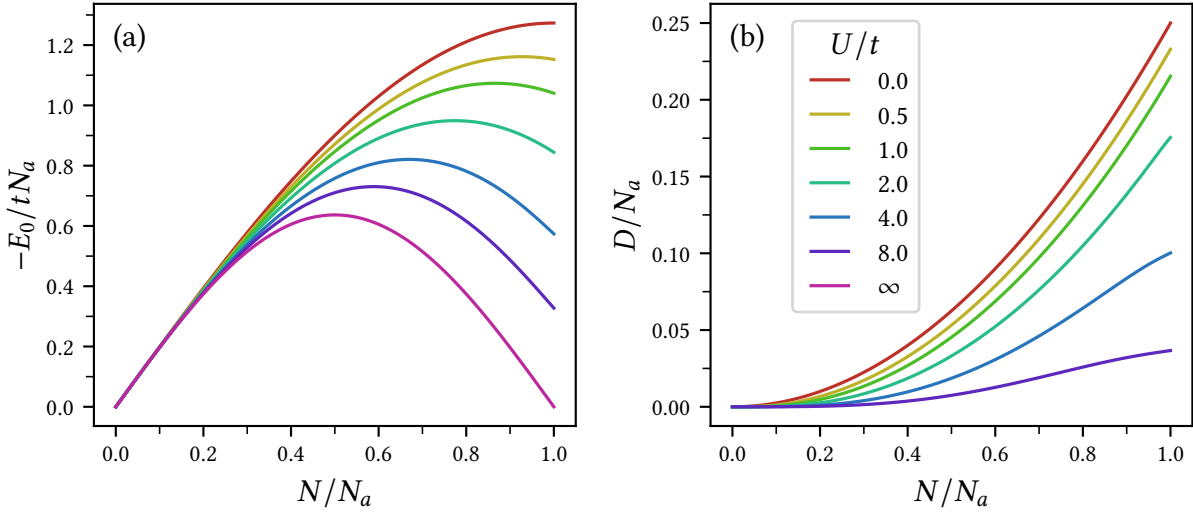
Figure 2.2: Ground-state properties of the infinite one-dimensional Hubbard chain as functions of the electron density N/N_a, obtained by solving Shiba's integral equations (2.28) and (2.33). In (a) the ground-state energy E_0 is shown for a number of representative values of the Coulomb-repulsion strength U/t, and the corresponding average number of double occupations D is displayed in subfigure (b).

for $N/N_a = 1/2$. This is in sharp contrast to the noninteracting case $U/t = 0$, where the electrons fill the band from the bottom such that the minimal value of the ground-state energy is attained at half band-filling $N/N_a = 1$. The position of the minimum in the ground-state energy E_0 shifts continuously with increasing U/t, starting from the noninteracting limit where the minimum is attained at $N/N_a = 1$, to the strongly-interacting limit where the minimum in E_0 occurs at $N/N_a = 1/2$. Furthermore, the electrons tend to reduce the average number of double occupations D at the expense of a kinetic-energy gain as U/t increases, and consequently one observes in Fig. 2.2 (b) a gradual suppression of D with increasing values of U/t, starting from $D = N^2/(4N_a)$ in the noninteracting case to $D = 0$ in the strongly correlated limit.

2.3 Symmetries and related models

The Hubbard model has many symmetries, some of them are general while others, such as the particle-hole symmetry, depend on the topology described by the hopping integrals t_{ij}. In the following we will focus on the symmetries that are most relevant for the remainder of this thesis. These are the particle-number conservation, the invariance with respect to rotations in spin space, as well as the particle-hole symmetry. An excellent overview of all symmetries of the Hubbard model can be found in the

book of Essler *et al.* [98]. Furthermore, we will consider the strongly interacting limit of the Hubbard model and demonstrate that the low-lying excitations in this limit are described by the *t-J* model, which reduces to the well known antiferromagnetic (AFM) Heisenberg model in the case of a half-filled band.

2.3.1 Selected symmetries of the Hubbard model

The fact, that the Hamiltonian of the Hubbard model (2.7) commutes with the number operator $\hat{N}_\sigma = \sum_i \hat{c}^\dagger_{i\sigma} \hat{c}_{i\sigma}$ for electrons with spin polarization σ is obvious, since each term in $\hat{H}$ contains as many creation operators $\hat{c}^\dagger_{i\sigma}$ as annihilation operators $\hat{c}_{j\sigma}$. Consequently, the number N_σ of electrons with spin polarization σ is a conserved quantity in the Hubbard model. It follows that the total number of electrons $N = N_\uparrow + N_\downarrow$ and the z-component of the spin $S_z = (N_\uparrow - N_\downarrow)/2$ are conserved quantities as well. In order to demonstrate that $\hat{H}$ also commutes with the spin components $\hat{S}_x$ and $\hat{S}_y$, one considers the ladder operators

$$\hat{S}_+ = \hat{S}_x + \mathrm{i}\,\hat{S}_y = \sum_i \hat{c}^\dagger_{i\uparrow} \hat{c}_{i\downarrow} \quad \text{and} \quad \hat{S}_- = \hat{S}_x - \mathrm{i}\,\hat{S}_y = \sum_i \hat{c}^\dagger_{i\downarrow} \hat{c}_{i\uparrow} \,. \tag{2.37}$$

Using the fundamental fermionic anticommutator relations $\{\hat{c}_\alpha, \hat{c}_\beta\} = 0$ and $\{\hat{c}_\alpha, \hat{c}^\dagger_\beta\} = \delta_{\alpha\beta}$, it is straight forward to verify that both terms of the Hubbard-model Hamiltonian (2.7), i. e., the kinetic energy $\hat{K}$ and the local Coulomb repulsion $\hat{W}$, individually commute with the operators $\hat{S}_\pm$. Consequently, both terms commute with all three components of the spin $\hat{S}_x = (\hat{S}_+ + \hat{S}_-)/2$, $\hat{S}_y = -\mathrm{i}(\hat{S}_+ - \hat{S}_-)/2$, and $\hat{S}_z$, which means that they are invariant with respect to arbitrary rotations in spin-space.

In order to introduce the particle-hole symmetry, let us consider the Hubbard model on a bipartite lattice, i. e., a lattice $\mathcal{T}$ that can be divided into two sublattices $\mathcal{T}_A$ and $\mathcal{T}_B$ with $\mathcal{T} = \mathcal{T}_A \cup \mathcal{T}_B$ such that there is no hopping within the two sublattices, i. e., $t_{ij} = 0$ if $i, j \in \mathcal{T}_A$ or $i, j \in \mathcal{T}_B$. In this case, the unitary transformation which maps $\hat{c}^\dagger_{i\sigma} \to \pm\hat{c}_{i\sigma}$, where the positive sign applies if $i \in \mathcal{T}_A$ and the negative if $i \in \mathcal{T}_B$, transforms the Hamiltonian of the Hubbard model (2.7) into

$$\hat{H}_\mathrm{h} = -\sum_{ij\sigma} t_{ij}\,\hat{c}_{i\sigma}\hat{c}^\dagger_{j\sigma} + U \sum_i \hat{c}_{i\uparrow}\hat{c}^\dagger_{i\uparrow}\hat{c}_{i\downarrow}\hat{c}^\dagger_{i\downarrow} = \sum_{ij\sigma} t^*_{ij}\,\hat{c}^\dagger_{i\sigma}\hat{c}_{j\sigma} + U \sum_i \hat{n}_{i\uparrow}\hat{n}_{i\downarrow} + U\,(N_a - \hat{N})\,. \tag{2.38}$$

Therefore, if the hopping matrix t is real, i. e., $t_{ij} \in \mathbb{R}$ for all i, j, the Hamiltonian $\hat{H}_\mathrm{h}$ differs from (2.7) only by the term $U\,(N_a - \hat{N})$, which is an irrelevant constant if one works in a basis with a fixed number of particles. Since the transformation under consideration maps electrons into holes and vice versa, it follows that one can infer the N-electron spectrum and eigenstates of the Hubbard model on a bipartite lattice from the corresponding problem with $2N_a - N$ electrons. This means, for a bipartite

lattice it is sufficient to analyze the case $N \leq N_a$, since the solution of the more than half-filled band $N > N_a$ can be derived from it.

Let us now restrict the electron-hole transformation to the down spins, i. e., let us consider the transformation which maps $\hat{c}_{i\downarrow}^{\dagger} \rightarrow \pm\hat{c}_{i\downarrow}$, where, again, the positive sign applies if $i \in \mathcal{T}_A$ and the negative if $i \in \mathcal{T}_B$. This transformation maps the Hubbard-model Hamiltonian (2.7) into

$$
\begin{aligned}
\hat{H}_{\mathrm{a}} &= \sum_{ij} t_{ij} \left(\hat{c}_{i\uparrow}^{\dagger}\hat{c}_{j\uparrow} - \hat{c}_{i\downarrow}\hat{c}_{j\downarrow}^{\dagger} \right) + U \sum_{i} \hat{c}_{i\uparrow}^{\dagger}\hat{c}_{i\uparrow}\hat{c}_{i\downarrow}\hat{c}_{i\downarrow}^{\dagger} = \\
&= \sum_{ij} t_{ij}\, \hat{c}_{i\uparrow}^{\dagger}\hat{c}_{j\uparrow} + \sum_{ij} t_{ij}^{*}\, \hat{c}_{i\downarrow}^{\dagger}\hat{c}_{j\downarrow} - U \sum_{i} \hat{n}_{i\uparrow}\hat{n}_{i\downarrow} + U\hat{N}_{\uparrow}\,.
\end{aligned}
\tag{2.39}
$$

If the hopping matrix t is real, the transformed Hamiltonian (2.39) differs from the Hubbard-model Hamiltonian (2.7) by the sign of the Coulomb integral U and the term $U\hat{N}_{\uparrow}$, which only contributes an irrelevant constant if one works in a basis with a fixed number of up spins. This means, the electron-hole transformation of the down spins effectively maps the Hubbard model with repulsive Coulomb interaction onto a corresponding model with attractive interaction. Therefore, on a bipartite lattice one can obtain the solution of the attractive Hubbard model with coupling constant $U < 0$ and $N_{\downarrow}$ down spins from the corresponding solution of the repulsive Hubbard model with $U > 0$ and $N_a - N_{\downarrow}$ down spins.

2.3.2 Related models of strongly interacting electrons

In Section 2.1 we have already analyzed the noninteracting limit $U = 0$, where the Hubbard model reduces to a simple tight-binding Hamiltonian. Furthermore, we have reviewed the atomic limit $t_{ij} = 0$ for all i, j, where all states with minimal number of double occupations are ground states, such that the corresponding ground-state energy is highly degenerate. Let us now consider the limit of strong Coulomb interactions, where the hopping integrals are non-vanishing but several orders of magnitude smaller than the Coulomb-repulsion strength, i. e., $U \gg |t_{ij}|$ for all i, j. In this case, the large ground-state degeneracy encountered in the atomic limit is lifted by the kinetic-energy term $\hat{K}$, which can be treated like a small perturbation to the interaction energy $\hat{W}$. The ground state is then obtained by diagonalizing $\hat{K}$ in the lower Hubbard subband $\mathcal{D}_0$, which is the subspace formed by all states having minimal double occupations, i. e., $D = 0$ if $N \leq N_a$ and $D = N - N_a$ else. In the following we will derive an effective Hamiltonian which describes the low-lying excitations of the strongly correlated Hubbard model, i. e., the excitations within the low-energy subspace $\mathcal{D}_0$. To this aim, let us split the kinetic-energy term $\hat{K}$ defined in Eq. (2.7) into

the following projected hopping operators

$$\hat{K}_0 = \sum_{ij\sigma} t_{ij} \left[\left(1 - \hat{n}_{i,-\sigma}\right) \hat{c}^\dagger_{i\sigma}\hat{c}_{j\sigma} \left(1 - \hat{n}_{j,-\sigma}\right) + \hat{n}_{i,-\sigma}\, \hat{c}^\dagger_{i\sigma}\hat{c}_{j\sigma}\, \hat{n}_{j,-\sigma} \right], \tag{2.40}$$

$$\hat{K}_+ = \sum_{ij\sigma} t_{ij}\, \hat{n}_{i,-\sigma}\, \hat{c}^\dagger_{i\sigma}\hat{c}_{j\sigma} \left(1 - \hat{n}_{j,-\sigma}\right), \tag{2.41}$$

$$\hat{K}_- = \sum_{ij\sigma} t_{ij} \left(1 - \hat{n}_{i,-\sigma}\right) \hat{c}^\dagger_{i\sigma}\hat{c}_{j\sigma}\, \hat{n}_{j,-\sigma}\,. \tag{2.42}$$

It is easy to verify that $\hat{K} = \hat{K}_0 + \hat{K}_+ + \hat{K}_-$. The first term $\hat{K}_0$ neither creates nor annihilates double occupations, but represents the hopping of double occupations and vacancies across the lattice. Consequently, the term $\hat{K}_0$ does not lead out of the lower subband $\mathcal{D}_0$. In contrast to $\hat{K}_0$, the operators $\hat{K}_\pm$ lead to transitions between the low-energy and the high-energy subspaces by creating or annihilating double occupations. However, higher order hopping processes, such as $\hat{K}_-\hat{K}_+$, generate and subsequently eliminate double occupations, and thus do not lead out of $\mathcal{D}_0$. These intermediate double occupations are called *virtual* and they are generated by hopping processes of second or higher order in the operators $\hat{K}_\pm$. In order to find an effective Hamiltonian which describes the action of the Hubbard model (2.7) in the subspace $\mathcal{D}_0$, we follow the work of Schrieffer and Wolff [99] and seek for a unitary transformation

$$\hat{H}_{\text{eff}} = e^{i\hat{S}}\, \hat{H}\, e^{-i\hat{S}} = \hat{H} + i\,[\hat{S},\hat{H}] - \frac{1}{2}\,[\hat{S},[\hat{S},\hat{H}]] + \cdots \tag{2.43}$$

which eliminates all terms in $\hat{H}$ that give rise to transitions between the lower and upper Hubbard subbands. It turns out that this goal cannot be achieved in a finite number of steps, since, for example, all terms that are of odd order in the operators $\hat{K}_\pm$ lead to transitions between the Hubbard subbands. Therefore, we will restrict ourselves to the elimination of the leading term $\hat{K}_1 = \hat{K}_+ + \hat{K}_-$ in the Hamiltonian $\hat{H}$ which, regarding Eq. (2.43), can be achieved by choosing the generator $\hat{S}$ such that

$$i\,[\hat{W},\hat{S}] = \hat{K}_1\,. \tag{2.44}$$

Since the operator $\hat{K}_+$ ($\hat{K}_-$) increases (decreases) the number of doubly occupied sites by one, it holds

$$[\hat{W},\hat{K}_\pm] = U \left(\hat{D}\hat{K}_\pm - \hat{K}_\pm\hat{D}\right) = \pm U\,\hat{K}_\pm\,, \tag{2.45}$$

and consequently one has

$$[\hat{W},\hat{K}_+ - \hat{K}_-] = U\,\hat{K}_1\,, \tag{2.46}$$

such that by comparison with Eq. (2.44) one finds

$$\hat{S} = -\frac{i}{U}\left(\hat{K}_+ - \hat{K}_-\right). \tag{2.47}$$

This means that $\hat{S}$ is of the order $t/U \ll 1$ where $t = \max_{ij} |t_{ij}|$. Using $i\,[\hat{S}, \hat{K}_1] = 2\,[\hat{K}_+, \hat{K}_-]/U$, one obtains by substituting Eq. (2.47) into Eq. (2.43)

$$\hat{H}_{\text{eff}} = \hat{K}_0 + \hat{W} + i\,[\hat{S}, \hat{K}_0] + \frac{1}{U}\,[\hat{K}_+, \hat{K}_-] + O\!\left(t^3/U^2\right). \tag{2.48}$$

Let us now focus on the case $n = N/N_a \leq 1$, where the lower Hubbard subband $\mathcal{D}_0$ is formed by the states without doubly occupied sites. Consequently, there is no contribution from $\hat{W}$ in the effective Hamiltonian (2.48) in this case. Furthermore, the term in $\hat{K}_0$ which accounts for the hopping of double occupations does not contribute, such that within $\mathcal{D}_0$ one has

$$\hat{K}_0 = \sum_{ij\sigma} t_{ij}\left(1 - \hat{n}_{i,-\sigma}\right) \hat{c}_{i\sigma}^\dagger \hat{c}_{j\sigma}\left(1 - \hat{n}_{j,-\sigma}\right). \tag{2.49}$$

Let us now consider the commutator $[\hat{K}_+, \hat{K}_-]$. If $\hat{K}_+^{(ij)}$ and $\hat{K}_-^{(kl)}$ denote the terms in Eqs. (2.41) and (2.42) which account for the site pairs (ij) and (kl), it is clear that $[\hat{K}_+^{(ij)}, \hat{K}_-^{(kl)}] = 0$ if both pairs are disjoint. Therefore, only terms involving two or three sites contribute to $[\hat{K}_+, \hat{K}_-]$. The same is true for the commutator $[\hat{S}, \hat{K}_0]$. It is easy to see that only three-site terms contribute to $[\hat{S}, \hat{K}_0]$ and, furthermore, one can show (see for example [100, Chapter 5]) that the two-site terms of the operator $[\hat{K}_+, \hat{K}_-]/U$ can be expressed as

$$\hat{H}_{\text{spin}} = \sum_{ij} J_{ij}\left(\hat{\sigma}_i \cdot \hat{\sigma}_j - \frac{\hat{n}_i\,\hat{n}_j}{4}\right) \quad \text{with} \quad J_{ij} = \frac{2t_{ij}^2}{U}, \tag{2.50}$$

where $\hat{\sigma}_i = \hat{S}_i/\hbar$ with the local spin operator $\hat{S}_i$, and $\hat{n}_i = \hat{n}_{i\uparrow} + \hat{n}_{i\downarrow}$ is the local electron-number operator. Consequently, if we neglect all three-site contributions, the effective Hamiltonian (2.48) reduces to the so-called t-J model

$$\hat{H}_{tJ} = \sum_{ij\sigma} t_{ij}\left(1 - \hat{n}_{i,-\sigma}\right) \hat{c}_{i\sigma}^\dagger \hat{c}_{j\sigma}\left(1 - \hat{n}_{j,-\sigma}\right) + \sum_{ij} J_{ij}\left(\hat{\sigma}_i \cdot \hat{\sigma}_j - \frac{\hat{n}_i\,\hat{n}_j}{4}\right). \tag{2.51}$$

It is often argued that the omission of the three-site contributions is well justified close to half band-filling, however, a complete treatment of the effective Hamiltonian (2.48), including three-site terms up to order t^2/U, is desirable in many situations and can be found, for example, in the excellent book of Fazekas [100]. The first term in the t-J model (2.51) represents the correlated motion of the electrons through the lattice, which avoids the creation of double occupations altogether. The second term describes an AFM interaction between the spins ($J_{ij} = 2t_{ij}^2/U > 0$), which is reduced by a density-density interaction. At exactly half band-filling ($n = 1$) the electrons can not

move without creating doubly occupied sites, such that in this case the t-J model (2.51) reduces to the well-known AFM Heisenberg model

$$\hat{H}_{\mathrm{H}} = \sum_{ij} J_{ij}\, \hat{\boldsymbol{\sigma}}_i \cdot \hat{\boldsymbol{\sigma}}_j \,. \tag{2.52}$$

Here we have omitted the density-density interaction term $\hat{n}_i\,\hat{n}_j$ which appears in Eq. (2.50), since at half band-filling it only contributes an irrelevant constant due to the fact that the electrons can not move such that $\langle \hat{n}_i\,\hat{n}_j \rangle = \langle \hat{n}_i \rangle \langle \hat{n}_j \rangle = 1$ for all i, j.

2.4 Mean-field approximation

The mean-field approximation reduces the Hamiltonian of an interacting many-electron system to an effective single-particle Hamiltonian by neglecting electronic correlations. Clearly, the negligence of electronic correlations rules out the accurate description of many interesting effects observed in many-electron systems, but nevertheless, the mean-field approximation is often useful in order to gain a rough insight into the basic physical properties of a given many-body system. In order to introduce the mean-field approximation for the Hubbard model (2.8), let us notice that

$$\hat{n}_{i\uparrow}\hat{n}_{i\downarrow} = \Delta\hat{n}_{i\uparrow}\,\Delta\hat{n}_{i\downarrow} + \hat{n}_{i\uparrow}\langle\hat{n}_{i\downarrow}\rangle + \hat{n}_{i\downarrow}\langle\hat{n}_{i\uparrow}\rangle - \langle\hat{n}_{i\uparrow}\rangle\langle\hat{n}_{i\downarrow}\rangle\,, \tag{2.53}$$

where we have introduced the density fluctuation $\Delta\hat{n}_{i\sigma} = \hat{n}_{i\sigma} - \langle\hat{n}_{i\sigma}\rangle$. The mean-field approximation is obtained by neglecting the product $\Delta\hat{n}_{i\uparrow}\Delta\hat{n}_{i\downarrow}$ of the density fluctuations, such that the Hubbard-model Hamiltonian (2.8) becomes equivalent to

$$\hat{H}_{\mathrm{MF}} = -t \sum_{\langle i,j\rangle\sigma} \hat{c}_{i\sigma}^{\dagger}\hat{c}_{j\sigma} + \frac{U}{2} \sum_{i\sigma} \hat{n}_{i\sigma}\langle\hat{n}_{i,-\sigma}\rangle\,. \tag{2.54}$$

If one assumes that the charge distribution is homogeneous, i. e., $\langle\hat{n}_{i\sigma}\rangle = n_\sigma\;\forall i$, it is straight forward to express the Hamiltonian (2.54) in terms of the Bloch states (2.13)

$$\hat{H}_{\mathrm{MF}} = \sum_{\boldsymbol{k}\sigma} \left(\varepsilon_{\boldsymbol{k}} + \frac{U n_{-\sigma}}{2} \right) \hat{n}_{\boldsymbol{k}\sigma}\,, \tag{2.55}$$

where $\varepsilon_{\boldsymbol{k}}$ are the single-particle energies (2.15). This mean-field Hamiltonian is also referred to as *Stoner model*, and it describes noninteracting fermions in a band-structure which is shifted for the up and down spins by $\Delta\varepsilon = U\,|n_\uparrow - n_\downarrow|/2 > 0$ if the underlying state is ferromagnetic (FM), i. e., if $n_\uparrow \neq n_\downarrow$. In the following we would like to investigate if this splitting of the spin-dependent subbands is energetically favorable, and in this way determine the stability of the FM phase versus the paramagnetic (PM) phase.

To this aim, let us first notice that the ground-state energy of the Hamiltonian (2.55) is given by

$$\frac{E_{\text{MF}}}{N_a} = \sum_\sigma \int_{-\infty}^{\mu_\sigma} \varepsilon \, \rho(\varepsilon) \, d\varepsilon + U \, n_\uparrow n_\downarrow \,, \tag{2.56}$$

where we have introduced the tight-binding density of states (DOS)

$$\rho(\varepsilon) = \frac{1}{N_a} \sum_{k \in \text{BZ}} \delta(\varepsilon - \varepsilon_k) \,, \tag{2.57}$$

and the chemical potential μ_σ for electrons with spin polarization σ is determined by the condition

$$\int_{-\infty}^{\mu_\sigma} \rho(\varepsilon) \, d\varepsilon = n_\sigma \,. \tag{2.58}$$

Clearly, in the PM phase one has $n_\uparrow = n_\downarrow = n/2$ and consequently $\mu_\uparrow = \mu_\downarrow = \mu$, such that the corresponding ground-state energy is given by

$$\frac{E_{\text{PM}}}{N_a} = 2 \int_{-\infty}^{\mu} \varepsilon \, \rho(\varepsilon) \, d\varepsilon + \frac{U n^2}{4} \,. \tag{2.59}$$

Let us now consider a slightly ferromagnetic configuration, i. e., $n_\sigma = n/2 + \sigma \, \delta n$ with $|\delta n| \ll n$. If one assumes that the DOS is approximately constant in a small region around the Fermi energy $\varepsilon_F = \mu$, one can approximate Eq. (2.58) as

$$n_\sigma = \frac{n}{2} + \sigma \, \delta n = \int_{-\infty}^{\mu} \rho(\varepsilon) \, d\varepsilon + \int_{\mu}^{\mu_\sigma} \rho(\varepsilon) \, d\varepsilon \approx \frac{n}{2} + \rho(\mu) \, \delta\mu_\sigma \tag{2.60}$$

$$\Rightarrow \quad \delta\mu_\sigma = \mu_\sigma - \mu = \sigma \, \frac{\delta n}{\rho(\mu)} \,. \tag{2.61}$$

Similarly, one obtains

$$\int_{-\infty}^{\mu_\sigma} \varepsilon \, \rho(\varepsilon) \, d\varepsilon \approx \int_{-\infty}^{\mu} \varepsilon \, \rho(\varepsilon) \, d\varepsilon + \rho(\mu) \left(\mu \, \delta\mu_\sigma + \frac{\delta\mu_\sigma^2}{2} \right), \tag{2.62}$$

such that with Eq. (2.61) and $n_\uparrow n_\downarrow = n^2/4 - \delta n^2$ the energy (2.56) of the FM configuration is given by

$$\frac{E_{\text{FM}}}{N_a} = \frac{E_{\text{PM}}}{N_a} + \delta n^2 \left(\frac{1}{\rho(\mu)} - U \right) . \tag{2.63}$$

This means that the FM configuration is more stable if

$$U \rho(\mu) > 1 \,. \tag{2.64}$$

This is the well-known *Stoner criterion*, which states that ferromagnetism should be favorable for strong Coulomb interactions as well as for large values of the DOS at the Fermi level. The corresponding equality $U\rho(\mu) = 1$ marks the boundary where, according to the present mean-field approximation, a transition between the PM and the FM phase is expected. As an example we have indicated the Stoner transition for the one-dimensional chain and the two-dimensional square lattice in Fig. 2.3.

In Section 2.3.2 we have seen, that the low-lying excitations in the half-filled Hubbard model are described by the AFM Heisenberg model if strong Coulomb interactions are considered. Consequently, we expect that AFM configurations play an important role especially in the region around $n = 1$. In order to adapt our present mean-field approximation for the Hubbard model such that AFM configurations can be taken into account, we divide the given lattice into unit cells containing two sites. Thus, in the following we denote by $\boldsymbol{R}_i$ the lattice vector which belongs to a given (two-site) unit cell, and the individual sites within this unit cell are indicated by the index $\alpha = 1, 2$. Using this notation the Hubbard-model Hamiltonian (2.8) is written as

$$\hat{H} = \hat{K} + \hat{W} = \sum_{ij\alpha\alpha'\sigma} t_{ij}^{\alpha\alpha'} \hat{c}_{i\alpha\sigma}^{\dagger} \hat{c}_{j\alpha'\sigma} + U \sum_{i\alpha} \hat{n}_{i\alpha\uparrow} \hat{n}_{i\alpha\downarrow} , \tag{2.65}$$

where the operator $\hat{c}_{i\alpha\sigma}^{\dagger}$ ($\hat{c}_{i\alpha\sigma}$) creates (annihilates) an electron with spin polarization σ in the Wannier orbital localized at the site α in the unit cell $\boldsymbol{R}_i$. For the hopping integrals we have $t_{ij}^{\alpha\alpha'} = -t$ if the site α in the unit cell $\boldsymbol{R}_i$ and the site α' in the unit cell $\boldsymbol{R}_j$ are NNs, and $t_{ij}^{\alpha\alpha'} = 0$ otherwise. In analogy to Eq. (2.13) we introduce the Fourier transform of the localized Wannier states

$$\hat{c}_{\boldsymbol{k}\alpha\sigma}^{\dagger} = \frac{1}{\sqrt{N_c}} \sum_{i=1}^{N_c} e^{i\boldsymbol{k}\cdot\boldsymbol{R}_i} \hat{c}_{i\alpha\sigma}^{\dagger} , \tag{2.66}$$

where $N_c = N_a/2$ denotes the number of two-site unit cells and the vectors $\boldsymbol{k}$ belong to the BZ of the given lattice structure. It is straight forward to verify that the kinetic-energy operator $\hat{K}$, expressed in terms of the creation operators (2.66), assumes the form

$$\hat{K} = \sum_{\boldsymbol{k}\alpha\alpha'\sigma} \varepsilon_{\boldsymbol{k}}^{\alpha\alpha'} \hat{c}_{\boldsymbol{k}\alpha\sigma}^{\dagger} \hat{c}_{\boldsymbol{k}\alpha'\sigma} \quad \text{with} \quad \varepsilon_{\boldsymbol{k}}^{\alpha\alpha'} = \sum_{i=1}^{N_c} t^{\alpha\alpha'}(\boldsymbol{R}_i) e^{-i\boldsymbol{k}\cdot\boldsymbol{R}_i} . \tag{2.67}$$

Here we made use of the translational symmetry of the underlying lattice, such that the hopping integrals $t_{ij}^{\alpha\alpha'} = t^{\alpha\alpha'}(\boldsymbol{R}_l)$ depend only on the lattice vector $\boldsymbol{R}_l = \boldsymbol{R}_i - \boldsymbol{R}_j$ connecting the unit cells at $\boldsymbol{R}_i$ and $\boldsymbol{R}_j$. Let us now apply the mean-field approximation

$$\hat{n}_{i\alpha\uparrow} \hat{n}_{i\alpha\downarrow} \approx \hat{n}_{i\alpha\uparrow} \langle \hat{n}_{i\alpha\downarrow} \rangle + \hat{n}_{i\alpha\downarrow} \langle \hat{n}_{i\alpha\uparrow} \rangle - \langle \hat{n}_{i\alpha\uparrow} \rangle \langle \hat{n}_{i\alpha\downarrow} \rangle \tag{2.68}$$

to the Hubbard-model Hamiltonian (2.65). If we use the result (2.67) and assume that the charge distribution is the same within each of the two-site unit cells, i. e.,

$\langle \hat{n}_{i\alpha\sigma} \rangle = n_{\alpha\sigma}$ $\forall i$, we readily obtain the mean-field approximation for the Hubbard-model Hamiltonian (2.65) as

$$\hat{H}_{\mathrm{MF}} = \sum_{\boldsymbol{k}\alpha\alpha'\sigma} h_{\boldsymbol{k}\sigma}^{\alpha\alpha'} \, \hat{c}_{\boldsymbol{k}\alpha\sigma}^{\dagger} \hat{c}_{\boldsymbol{k}\alpha'\sigma} \quad \text{with} \quad h_{\boldsymbol{k}\sigma}^{\alpha\alpha'} = \varepsilon_{\boldsymbol{k}}^{\alpha\alpha'} + \delta_{\alpha\alpha'} \frac{U n_{\alpha,-\sigma}}{2} \, . \tag{2.69}$$

The mean-field Hamiltonian $\hat{H}_{\mathrm{MF}}$ is already diagonal in $\boldsymbol{k}\sigma$, and in order to diagonalize it with respect to α, α' one seeks for the solutions of the eigenvalue equation

$$H_{\sigma}(\boldsymbol{k}) \, \boldsymbol{v}_{s\sigma}(\boldsymbol{k}) = \varepsilon_{s\sigma}(\boldsymbol{k}) \, \boldsymbol{v}_{s\sigma}(\boldsymbol{k}) \, , \tag{2.70}$$

where $H_{\sigma}(\boldsymbol{k})$ is the 2×2 matrix formed by $h_{\boldsymbol{k}\sigma}^{\alpha\alpha'}$ with $\alpha, \alpha' \in \{1, 2\}$. Introducing the states

$$\hat{b}_{\boldsymbol{k}s\sigma}^{\dagger} = \sum_{\alpha} v_{s\alpha\sigma}(\boldsymbol{k}) \, \hat{c}_{\boldsymbol{k}\alpha\sigma}^{\dagger} \, , \tag{2.71}$$

we readily obtain

$$\hat{H}_{\mathrm{MF}} = \sum_{\boldsymbol{k}s\sigma} \varepsilon_{s\sigma}(\boldsymbol{k}) \, \hat{n}_{\boldsymbol{k}s\sigma} \quad \text{with} \quad \hat{n}_{\boldsymbol{k}s\sigma} = \hat{b}_{\boldsymbol{k}s\sigma}^{\dagger} \hat{b}_{\boldsymbol{k}s\sigma} \, . \tag{2.72}$$

The single-particle eigenvalues $\varepsilon_{s\sigma}(\boldsymbol{k})$ of the mean-field Hamiltonian $\hat{H}_{\mathrm{MF}}$ form the two energy bands $s = 1, 2$ that are expected for a lattice having two orbitals per unit cell, however, due to the mean-field interaction both bands split into subbands for up- and down spins. Just like in the case of the Stoner model, this spin-dependent splitting of the energy bands is controlled by the Coulomb-repulsion strength U and the charge distribution, which is characterized by the spin-dependent electron density $n_{\alpha\sigma}$ at the sites $\alpha = 1, 2$.

In the following we would like to investigate the equilibrium properties of the mean-field Hamiltonian (2.72). To this aim we work in a grand-canonical ensemble at a given temperature T. Since $\hat{H}_{\mathrm{MF}}$ describes an effective noninteracting system, we have in equilibrium

$$\langle \hat{n}_{\boldsymbol{k}s\sigma} \rangle = \mathrm{Tr}\{\hat{\rho} \, \hat{n}_{\boldsymbol{k}s\sigma}\} = f\big(\varepsilon_{s\sigma}(\boldsymbol{k})\big) \, , \tag{2.73}$$

where $\hat{\rho}$ is the grand-canonical density matrix and

$$f(\varepsilon) = \frac{1}{1 + e^{\beta(\varepsilon-\mu)}} \quad \text{with} \quad \beta = \frac{1}{k_{\mathrm{B}}T} \tag{2.74}$$

the well-known Fermi-Dirac distribution. The chemical potential μ is determined by the electron density $n = N/N_a$, i.e., from the condition

$$n = \frac{1}{N_a} \sum_{\boldsymbol{k}s\sigma} f\big(\varepsilon_{s\sigma}(\boldsymbol{k})\big) \, . \tag{2.75}$$

Furthermore, it is straight forward to verify that the number of spin-σ electrons at the site α within each of the unit cells is given by

$$n_{\alpha\sigma} = \frac{1}{N_c} \sum_{k\in BZ} \langle \hat{c}_{k\alpha\sigma}^\dagger \hat{c}_{k\alpha\sigma} \rangle = \frac{1}{N_c} \sum_{ks} |v_{s\alpha\sigma}(k)|^2 f\big(\varepsilon_{s\sigma}(k)\big) . \tag{2.76}$$

Notice, however, that the vectors $v_{s\sigma}(k)$ depend on $n_{\alpha\sigma}$ themselves [see Eqs. (2.69) and (2.70)], such that these equations must be solved in a selfconsistent manner:

1. Start from some initial guess $n_{\alpha\sigma}^{(0)}$ for the number of spin-σ electrons at the site α within each unit cell. In particular choose

   a) $n_{\alpha\sigma}^{(0)} = n/2$ for all α, σ in order to start from a PM configuration,

   b) $n_{\alpha\uparrow}^{(0)} = n/2 + \delta n$ and $n_{\alpha\downarrow}^{(0)} = n/2 - \delta n$ for $\alpha = 1, 2$ with $|\delta n| > 0$ in order to start from a FM configuration,

   c) $n_{1\uparrow}^{(0)} = n_{2\downarrow}^{(0)} = n/2 + \delta n$ and $n_{1\downarrow} = n_{2\uparrow} = n/2 - \delta n$ with $|\delta n| > 0$ in order to start from an AFM configuration.

2. Solve the eigenvalue equation (2.70) in order to obtain the band structure $\varepsilon_{s\sigma}(k)$ and the eigenvectors $v_{s\sigma}(k)$.

3. Determine the chemical potential μ by means of Eq. (2.75) and, subsequently, obtain new values for $n_{\alpha\sigma}$ from Eq. (2.76).

4. Exit if convergence is achieved, i. e., $n_{\alpha\sigma} = n_{\alpha\sigma}^{(0)} \; \forall \alpha\sigma$. Otherwise, return to step 2 after having updated $n_{\alpha\sigma}^{(0)}$ with $n_{\alpha\sigma}$.

In order to determine the phase which corresponds to the equilibrium, one solves the selfconsistent procedure for all three phases and computes the corresponding free energy $F = E - TS$, with the energy

$$E = \sum_{ks\sigma} \varepsilon_{s\sigma}(k) f\big(\varepsilon_{s\sigma}(k)\big) \tag{2.77}$$

and the entropy

$$S = -k_B \sum_{ks\sigma} \left\{ f\big(\varepsilon_{s\sigma}(k)\big) \log\big[f\big(\varepsilon_{s\sigma}(k)\big)\big] + \big[1 - f\big(\varepsilon_{s\sigma}(k)\big)\big] \log\big[1 - f\big(\varepsilon_{s\sigma}(k)\big)\big] \right\} . \tag{2.78}$$

The phase which corresponds to the equilibrium is then identified as the one having the lowest free energy F. Notice, however, that solutions within the FM and AFM phases are not guaranteed, i. e., the selfconsistent iteration, starting from an
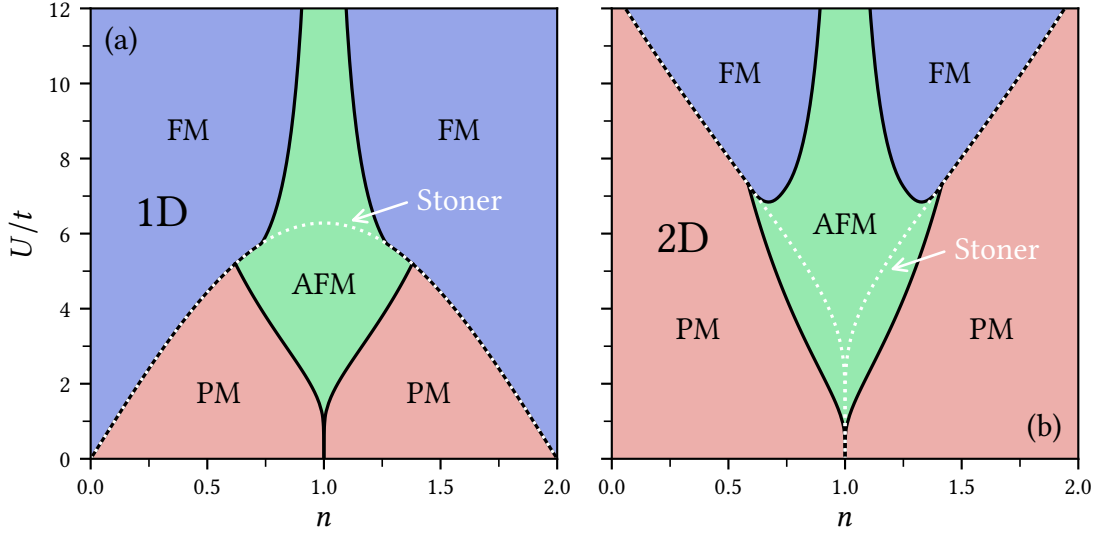
Figure 2.3: Ground-state phase diagram of the Hubbard model, obtained from the mean-field approximation. Subfigure (a) shows the phase diagram for the 1D chain as function of the band-filling n and the Coulomb-repulsion strength U/t. Subfigure (b) shows similar results for the 2D square lattice. In both subfigures the PM–FM transition predicted by the Stoner criterion (2.64) is indicated by a white dashed line.

(anti)ferromagnetic configuration having $|\delta n| > 0$ might lead to a PM solution with $\delta n = 0$.

Using the thus described selfconsistent procedure for the solution of the mean-field equations, we have determined the ground-state phase diagram of the Hubbard model on the infinite chain as well as on the two-dimensional square lattice. In our results presented in Fig. 2.3 one notices an apparent symmetry around half-band filling ($n = 1$), which is a simple consequence of the particle-hole symmetry in the bipartite Hubbard model, as already discussed in Section 2.3.1. Furthermore, one observes the general trend that paramagnetism dominates in the weakly interacting regime, while ferromagnetism or antiferromagnetism dominates for strong Coulomb interactions. This can be readily understood by noting that the subbands $\varepsilon_{s\sigma}(\boldsymbol{k})$ do not split if a noninteracting system ($U = 0$) is concerned, such that the most stable configuration must be PM in this case. In the other extreme where the Coulomb repulsion is strong, the subband-splitting is very pronounced, and the most stable configuration is achieved if the low-lying subbands are filled fist, which results in a FM or AFM configuration. Comparing Figs. 2.3 (a) and (b) one concludes that the mean-field approximation predicts a greatly enhanced stability of the FM phase in 1D for small and large values of the band-filling n. This can be easily understood by the Stoner

criterion (2.64), since the DOS in 1D is significantly larger at the band edges than its equivalent in 2D. In contrast to the FM phase, we find a stability region of the AFM configuration which is qualitatively very similar for the 1D and 2D lattices. As expected, an AFM configuration is most stable in the region around half band-filling, where the antiparallel alignment of the spins is crucial in order to reduce the kinetic energy by hopping processes.

Density functional theory on a lattice 3

The quantum many-body problem has always been one of the most important and challenging problems in condensed-matter physics. One of the major breakthroughs in this area is the development of Hohenberg-Kohn-Sham's density functional theory (DFT), in which the many-particle wave function $|\Psi\rangle$ is replaced by the many-particle density $n(\boldsymbol{r})$ as the central variable [2, 3]. For readers not familiar with conventional DFT in the continuum we present a concise overview in Appendix A, which accounts for the ground-state formalism as well as to the equilibrium at finite temperatures. Although DFT is an exact theory for many-body systems, practical applications must resort to approximations for the unknown exchange-correlation functional $E_{\mathrm{xc}}[n(\boldsymbol{r})]$. While the available approximations have been very successful in a wide range of applications, there are many situations where the current DFT approaches lead to qualitatively wrong results. This applies in particular to strong electron-correlation phenomena, including the physics of heavy-fermion materials [35], high-temperature superconductivity [36, 37], and Mott-insulators [38–40]. Strongly-correlated electron systems are usually best described in the framework of lattice Hamiltonians, in which the electronic dynamics is simplified by focusing on the most relevant contributions which dominate the low-energy or low-temperature physics. Taking into account the remarkable success of DFT to handle the first-principles problem in the continuum, it is reasonable to expect that a suitable extension of the fundamental concepts of DFT to many-body lattice models could provide an alternative, potentially most effective new perspective to the physics of strongly-correlated electrons on a lattice. It is therefore the purpose of this chapter to develop a DFT formalism which applies to strongly-interacting electron systems described by lattice and minimal-basis Hamiltonians.

The main differences between lattice models and the first-principles treatment of interacting-electron systems are that lattice-model Hamiltonians are described in terms of a discrete and drastically reduced set of single-particle basis states $\phi_{i\sigma}(\boldsymbol{r})$, and that the Coulomb-interactions as well as the hybridizations are simplified. Nevertheless, the formulation of lattice density functional theory (LDFT) is in many aspects similar to the conventional DFT in the continuum, however, some significant differences between both formulations exist. Most notably, the particle density $n(\boldsymbol{r})$, which

is the fundamental variable in the formulation of conventional DFT, is replaced by the single-particle density matrix (SPDM) $\boldsymbol{\gamma}$ in the framework of LDFT.

The remainder of this chapter is organized as follows. In Section 3.1 we present a formulation of LDFT which applies to the ground state of lattice-model Hamiltonians. After having established in Section 3.1.1 a unique connection between the hopping matrix $\boldsymbol{t}$, which characterizes the system under study, and the ground-state single-particle density matrix (gs-SPDM) $\boldsymbol{\gamma}$, we will employ a constrained-search method in Section 3.1.2 which leads to an interaction-energy functional from which the gs-SPDM and, in turn, all ground-state observables can be obtained in principle. In the following Section 3.1.3 we will demonstrate that the gs-SPDM of a given interacting system can be obtained from the solution of effective single-particle equations. In contrast to the Kohn and Sham (KS) scheme discussed in Appendix A.1.3, we will consider an auxiliary noninteracting system at a fictitious finite temperature $T_a > 0$ and chose its parameters such that the corresponding equilibrium single-particle density matrix (eq-SPDM) $\boldsymbol{\gamma}$ equals the one in the ground state of the given interacting system. Section 3.2 is devoted to the development of a DFT for lattice models in equilibrium at a finite temperature. We will formulate the theoretical foundations in two different flavours: Section 3.2.1 accounts for a grand-canonical ensemble formalism, where the system is open with respect to exchange of energy and particles with the environment, while Section 3.2.2 applies to a canonical ensemble, where the system only exchanges energy with the environment. Within both formulations of finite-temperature lattice density functional theory (FT-LDFT) we will establish a unique connection between the hopping matrix $\boldsymbol{t}$ and the eq-SPDM $\boldsymbol{\gamma}$, and we will derive a functional from which the eq-SPDM and thus the equilibrium values of arbitrary observables can be obtained in principle. Furthermore, we will demonstrate that a given interacting system can be mapped to an auxiliary noninteracting system which yields the same eq-SPDM. In this way, the solution of the finite-temperature problem for a given lattice model of interacting Fermions can be obtained from the selfconsistent solution of effective single-particle equations.

3.1 Ground-state formalism

In order to formulate the basic principles of ground-state LDFT, we consider N interacting particles described by the general Hamiltonian

$$\hat{H} = \hat{K} + \hat{W} = \sum_{ij\sigma} t_{ij\sigma}\, \hat{c}_{i\sigma}^{\dagger} \hat{c}_{j\sigma} + \frac{1}{2} \sum_{\substack{ijkl \\ \sigma\sigma'}} W_{ijkl}^{\sigma\sigma'}\, \hat{c}_{i\sigma}^{\dagger} \hat{c}_{j\sigma'}^{\dagger} \hat{c}_{l\sigma'} \hat{c}_{k\sigma}\,, \tag{3.1}$$

where $\hat{c}_{i\sigma}^{\dagger}$ ($\hat{c}_{i\sigma}$) creates (annihilates) a particle with spin polarization σ in the single-particle basis state $\phi_{i\sigma}(\boldsymbol{r})$. The parameters $t_{ij\sigma}$ are single-particle matrix elements,

where the diagonal terms $\varepsilon_{i\sigma} = t_{ii\sigma}$ refer to the (spin-dependent) energy levels, and the off-diagonal terms $t_{ij\sigma}$, $i \neq j$ are the hopping integrals. Furthermore, the parameters $W_{ijkl}^{\sigma\sigma'}$ specify the interaction between the particles. In order to make a connection between the Hamiltonians (A.1) and (3.1), we consider in Eq. (A.1) a spin-dependent external potential $v_\sigma(\mathbf{r})$ and a spin-dependent interaction $w_{\sigma\sigma'}(\mathbf{r}, \mathbf{r}')$ between the particles. If we expand the fermionic field

$$\hat{\psi}_\sigma^\dagger(\mathbf{r}) = \sum_i \phi_{i\sigma}^*(\mathbf{r}) \, \hat{c}_{i\sigma}^\dagger \tag{3.2}$$

in terms of the single-particle states $\phi_{i\sigma}(\mathbf{r})$, it is easy to verify that the single-particle matrix elements in Eq. (3.1) are given by

$$t_{ij\sigma} = \int \phi_{i\sigma}^*(\mathbf{r}) \left[-\frac{\hbar^2}{2m} \nabla^2 + v_\sigma(\mathbf{r}) \right] \phi_{j\sigma}(\mathbf{r}) \, \mathrm{d}\mathbf{r} \,, \tag{3.3}$$

and the interaction integrals are given by

$$W_{ijkl}^{\sigma\sigma'} = \int \phi_{i\sigma}^*(\mathbf{r}) \, \phi_{j\sigma'}^*(\mathbf{r}') \, w_{\sigma\sigma'}(\mathbf{r}, \mathbf{r}') \, \phi_{l\sigma'}(\mathbf{r}') \, \phi_{k\sigma}(\mathbf{r}) \, \mathrm{d}\mathbf{r} \, \mathrm{d}\mathbf{r}' \,. \tag{3.4}$$

Clearly, only the single-particle matrix elements $t_{ij\sigma}$ are associated with the external potential $v_\sigma(\mathbf{r})$ which, in the spirit of DFT, defines the system under study. The interaction integrals (3.4) are specified by the type of interaction $w_{\sigma\sigma'}(\mathbf{r}, \mathbf{r}')$ between the particles and the choice of the single-particle basis $\{\phi_{i\sigma}(\mathbf{r})\}$. Therefore, if we focus on a given type of particles and keep the single-particle basis fixed, we can regard the system described by the Hamiltonian (3.1) as uniquely characterized by the single-particle matrix elements $t_{ij\sigma}$. This is also clear from the lattice-model perspective, since the hopping integrals and energy levels are the single-particle parameters which define the lattice structure and the range of hybridizations.

Using Eq. (3.2) we can express the electron-density operator as

$$\hat{n}(\mathbf{r}) = \sum_\sigma \hat{\psi}_\sigma^\dagger(\mathbf{r}) \, \hat{\psi}_\sigma(\mathbf{r}) = \sum_{ij\sigma} \phi_{i\sigma}^*(\mathbf{r}) \, \phi_{j\sigma}(\mathbf{r}) \, \hat{c}_{i\sigma}^\dagger \hat{c}_{j\sigma} \,. \tag{3.5}$$

Consequently, the electron density in an arbitrary many-particle state $|\Psi\rangle$ is given by

$$n(\mathbf{r}) = \langle \Psi | \hat{n}(\mathbf{r}) | \Psi \rangle = \sum_{ij\sigma} \gamma_{ij\sigma} \, \phi_{i\sigma}^*(\mathbf{r}) \, \phi_{j\sigma}(\mathbf{r}) \,, \tag{3.6}$$

where we have introduced the single-particle density matrix (SPDM)

$$\gamma_{ij\sigma} = \langle \Psi | \hat{c}_{i\sigma}^\dagger \hat{c}_{j\sigma} | \Psi \rangle \tag{3.7}$$

which corresponds to the many-particle state $|\Psi\rangle$. Therefore, once a set $\{\phi_{i\sigma}(\boldsymbol{r})\}$ of single-particle basis states is adopted, the particle density $n(\boldsymbol{r})$ of any many-particle state $|\Psi\rangle$ is fully determined by the corresponding SPDM $\boldsymbol{\gamma} = \{\gamma_{ij\sigma}\}$. Conversely, the knowledge of the full SPDM $\boldsymbol{\gamma}$, including in particular its off-diagonal elements, is necessary in order to express an arbitrary electron density $n(\boldsymbol{r})$ in terms of the single-particle basis states $\{\phi_{i\sigma}(\boldsymbol{r})\}$. For this reason, the SPDM takes the role of the fundamental variable in LDFT in the same sense as the particle density $n(\boldsymbol{r})$ is the fundamental variable in conventional DFT.

3.1.1 Connection between the hopping matrix and the SPDM

In the following we consider the type of particle interaction specified by the parameters $W_{ijkl}^{\sigma\sigma'}$ as fixed, such that the matrix $\boldsymbol{t} = \{t_{ij\sigma}\}$ of the hopping integrals and energy levels characterizes the system described by the Hamiltonian (3.1). We have already identified the SPDM $\boldsymbol{\gamma}$ as the fundamental variable in LDFT, and we would now like to formulate a statement with the same fundamental character as the Hohenberg-Kohn (HK) Theorem A.1 in the formulation of conventional DFT in the continuum. Thus, we would like to establish a unique connection between the hopping matrix $\boldsymbol{t}$, which characterizes the system, and the SPDM associated to the ground state. Before we can do so, we need to ascertain under which conditions two hopping matrices $\boldsymbol{t}$ and $\boldsymbol{t}'$ lead to different ground states. In Lemma A.1 we have already shown that external potentials which differ by more than a constant must lead to different ground states. It is straight forward to adapt the proof of Lemma A.1 to the case of spin-dependent potentials and to demonstrate that two potentials $v_\sigma(\boldsymbol{r})$ and $v'_\sigma(\boldsymbol{r})$ must lead to different ground states if they differ by more than a possibly spin-dependent constant, i. e., if $v'_\sigma(\boldsymbol{r}) \neq v_\sigma(\boldsymbol{r}) + c_\sigma$ with $c_\sigma \in \mathbb{R}$.[1] From Eq. (3.3) it is clear, that a spin-dependent shift in the external potential $v'_\sigma(\boldsymbol{r}) = v_\sigma(\boldsymbol{r}) + c_\sigma$ does not change the hopping integrals $t_{ij\sigma}$, $i \neq j$, but leads to a spin-dependent shift $\varepsilon'_{i\sigma} = t'_{ii\sigma} = \varepsilon_{i\sigma} + c_\sigma$ of the energy levels. This immediately proves the following

Lemma 3.1. *Two hopping matrices $\boldsymbol{t} = \{t_{ij\sigma}\}$ and $\boldsymbol{t}' = \{t'_{ij\sigma}\}$ lead to different ground states of the Hamiltonian (3.1) if they differ by more than a spin-dependent shift in the energy levels, i. e., if $t'_{ij\sigma} \neq t_{ij\sigma} + \delta_{ij}c_\sigma$ with $c_\sigma \in \mathbb{R}$.*

We are now prepared to formulate a HK-like theorem and to establish a unique connection between the hopping matrix $\boldsymbol{t}$, which characterizes the system under study,

---

[1] Notice, however, that two potentials which differ by a spin-dependent constant not *necessarily* lead to the same ground state. For example, the coupling to an external magnetic-field via a Zeeman term corresponds to a spin-dependent shift in the external potential which leads to a polarized ground state if the field is sufficiently strong.

and the corresponding ground-state single-particle density matrix (gs-SPDM). We will focus on systems having nondegenerate ground states, however, the inclusion of degenerate ground-states poses no problem, as discussed further below.

Theorem 3.1 (Töws and Pastor [81])**.** *The hopping matrix t of the interacting many-particle system described by the Hamiltonian (3.1) is (apart from an irrelevant spin-dependent shift in the energy levels) a functional[2] of the gs-SPDM γ.*

Proof. The proof is carried out in close analogy to the proof of the HK Theorem A.1. Assume that the ground state $|\Psi_0\rangle$ of the Hamiltonian $\hat{H}$ with the hopping matrix t is nondegenerate and that there exists *another* hopping matrix t' which differs from t by more than a spin-dependent shift in the energy levels but, nevertheless, leads to the *same* gs-SPDM γ as the hopping matrix t. If $\hat{H}'$ and $|\Psi'_0\rangle$ denote the Hamiltonian and ground state associated with t', the corresponding ground-state energy is given by

$$E'_0 = \langle\Psi'_0|\hat{H}'|\Psi'_0\rangle = \sum_{ij\sigma} t'_{ij\sigma}\,\gamma_{ij\sigma} + \langle\Psi'_0|\hat{W}|\Psi'_0\rangle\,. \tag{3.8}$$

Since the hopping matrices t and t' differ by more than a spin-dependent shift in the energy levels, the corresponding ground states $|\Psi_0\rangle$ and $|\Psi'_0\rangle$ must be different according to Lemma 3.1. Therefore, from the minimal principle for the ground-state energy $E_0 = \langle\Psi_0|\hat{H}|\Psi_0\rangle$ of the Hamiltonian $\hat{H}$ it follows that

$$E_0 < \langle\Psi'_0|\hat{H}|\Psi'_0\rangle = \sum_{ij\sigma} t_{ij\sigma}\,\gamma_{ij\sigma} + \langle\Psi'_0|\hat{W}|\Psi'_0\rangle = E'_0 + \sum_{ij\sigma}\left(t_{ij\sigma} - t'_{ij\sigma}\right)\gamma_{ij\sigma}\,. \tag{3.9}$$

Notice that the strict inequality holds because we assumed that the ground state associated with t is nondegenerate. By interchanging primed and unprimed quantities one obtains

$$E'_0 \leq \langle\Psi_0|\hat{H}'|\Psi_0\rangle = E_0 + \sum_{ij\sigma}\left(t'_{ij\sigma} - t_{ij\sigma}\right)\gamma_{ij\sigma}\,, \tag{3.10}$$

where no strict inequality holds, since the ground state associated with t' could be degenerate. Adding Eqs. (3.9) and (3.10) the contradiction

$$E_0 + E'_0 < E'_0 + E_0 \tag{3.11}$$

is obtained. This proves that two hopping matrices t and t' which differ by more than a spin-dependent shift in the energy levels cannot lead to the same gs-SPDM γ. One concludes that t is (apart from a spin-dependent shift in the energy levels) a functional of γ. □

---

[2]Here and in the following we will sometimes use the term "functional" for quantities which are ordinary functions in the strict mathematical sense. We choose to do so in order to match the terminology in conventional DFT and to highlight the corresponding similarities.

Theorem 3.1 states that the hopping matrix *t* is, apart from a spin-dependent shift in the energy levels, a functional of the gs-SPDM. A spin-dependent energy shift is, however, of little physical relevance, since it could be absorbed in a spin-dependent chemical potential and, most importantly, since it does not change the set of eigenstates of the Hamiltonian. Therefore, we conclude that the physically relevant part of the Hamiltonian $\hat{H}$, and thus the full set of corresponding eigenstates as well as all physical properties derived from it, are functionals of the gs-SPDM γ. Notice, however, that the one-to-one correspondence between the gs-SPDM γ and the hopping matrix *t* established by Theorem 3.1 is no longer valid in the presence of ground-state degeneracies. Clearly, if the ground state is degenerate the gs-SPDM γ is no longer unique. Nevertheless, due to the variational principle and the simple fact that all ground states share the same energy, a one-to-one correspondence between the set $\{\gamma_\alpha\}$ formed by the SPDMs of all degenerate ground-states and the hopping matrix *t* can be established. Thus, the gs-SPDM of any one of the degenerate ground-states determines the hopping matrix *t* up to a spin-dependent energy-level shift. Furthermore, in practical applications we will resort to a Levy-Lieb (LL) like formulation of LDFT, which will be formulated in Section 3.1.2 and where degeneracies pose no problem by default. Returning to the case of a nondegenerate ground-state, where the unique gs-SPDM γ determines the hopping matrix *t* up to a spin-dependent energy-level shift and thus all the eigenstates of the Hamiltonian, we may immediately formulate the important

Corollary 3.1. *The ground state $|\Psi_0\rangle$ of the interacting many-particle system described by the Hamiltonian (3.1) is a functional of the gs-SPDM γ.*

Moreover, the converse statement is also true, i. e., the gs-SPDM $\gamma_{ij\sigma} = \langle\Psi_0|\hat{c}_{i\sigma}^\dagger\hat{c}_{j\sigma}|\Psi_0\rangle$ is a functional of the ground state $|\Psi_0\rangle$. This establishes a bijective map between the set Ψ_0 containing all nondegenerate ground states and the corresponding set Γ_0 of the gs-SPDMs. Furthermore, from Corollary 3.1 we obtain the important

Corollary 3.2. *The ground-state expectation value of any observable $\hat{O}$ is a functional of the gs-SPDM γ.*

Proof. From Corollary 3.1 we know that the ground state $|\Psi_0\rangle = |\Psi_0[\gamma]\rangle$ is a functional of the gs-SPDM γ. Therefore, the ground-state expectation value of any observable $\hat{O}$ can be obtained from the gs-SPDM as

$$O[\gamma] = \langle\Psi_0[\gamma]|\hat{O}|\Psi_0[\gamma]\rangle . \tag{3.12}$$

$\square$

In particular, the functional representing the sum of the kinetic and potential energy

$$K[\gamma] = \langle\Psi_0[\gamma]|\hat{K}|\Psi_0[\gamma]\rangle = \sum_{ij\sigma} t_{ij\sigma}\,\gamma_{ij\sigma} \tag{3.13}$$

is explicitly known in the framework of LDFT and a simple linear form in $\boldsymbol{\gamma}$. In the following we will, as it is common practice, refer to $\hat{K}$ as "kinetic energy", even though it contains the contribution from the external potential $v_\sigma(\boldsymbol{r})$ [see Eqs. (3.1) and (3.3)]. It is one of the major advantages of LDFT over the conventional formulation of DFT in the continuum that the functional dependence $K[\boldsymbol{\gamma}]$ of the kinetic energy is explicitly known. From Corollary 3.2 it follows furthermore that the interaction energy

$$W[\boldsymbol{\gamma}] = \langle \Psi_0[\boldsymbol{\gamma}] | \hat{W} | \Psi_0[\boldsymbol{\gamma}] \rangle \tag{3.14}$$

is a functional of the gs-SPDM $\boldsymbol{\gamma}$. The interaction-energy functional (3.14) has a universal character in the sense that it does not depend on the hopping integrals $t_{ij\sigma}$, which define the system under study, i. e., the dimensionality and structure of the underlying lattice as well as the range of the hybridizations. The interaction-energy functional (3.14) depends on the interaction integrals $W_{ijkl}^{\sigma\sigma'}$. Furthermore, it depends on the many-particle Hilbert space under consideration, since the ground state $|\Psi_0[\boldsymbol{\gamma}]\rangle$ is a state within this Hilbert space. Using Eqs. (3.13) and (3.14), the functional corresponding to the ground-state energy is obtained as

$$E[\boldsymbol{\gamma}] = \sum_{ij\sigma} t_{ij\sigma} \, \gamma_{ij\sigma} + W[\boldsymbol{\gamma}] \,. \tag{3.15}$$

Clearly, for the actual gs-SPDM $\boldsymbol{\gamma}_0$ the energy functional $E[\boldsymbol{\gamma}]$ assumes its minimum and equals the ground-state energy E_0 associated with the given hopping matrix $\boldsymbol{t}$. If the interaction energy functional $W[\boldsymbol{\gamma}]$ were known, the ground-state energy and SPDM corresponding to arbitrary hopping matrices $\boldsymbol{t}$ could be obtained by minimizing the energy functional $E[\boldsymbol{\gamma}]$. Therefore, the main challenge in practical applications of ground-state LDFT is to determine the functional $W[\boldsymbol{\gamma}]$. In the next section we will see that already the characterization of the domain of definition of $W[\boldsymbol{\gamma}]$ poses some difficulties. We will circumvent these difficulties by introducing a constrained-search method for the interaction-energy functional, which is similar to the LL procedure discussed in Appendix A.1.2.

3.1.2 Constrained-search functional for the interaction energy

In the previous section we have seen that the ground-state energy and SPDM can be obtained by minimizing the energy functional (3.15) with respect to all matrices $\boldsymbol{\gamma}$ that can be derived as the gs-SPDM of the N-particle problem described by the Hamiltonian (3.1) with *some* hopping matrix $\boldsymbol{t}$. We call this class of matrices *pure-state t-representable*, in close analogy to the corresponding terminology in conventional DFT. At first, the pure-state t-representability does not seem to pose a major restriction on $\boldsymbol{\gamma}$, since all SPDMs of physical interest for the ground-state problem must

fulfill this criterion. However, any practical implementation of the variational principle for the ground-state energy (3.15) must in principle ensure that the minimization is constrained to the set of pure-state *t*-representable SPDMs, since otherwise the interaction-energy functional (3.14) would be ill-defined and the result of the minimization would be uncontrolled or simply unphysical. This raises the problem of characterizing pure-state *t*-representable SPDMs, which has not been solved to date. Therefore, in order to render the variational principle for the ground-state energy useful in practice, the domain of definition of the functional (3.15) must be extended to a larger set of SPDMs. To this aim we follow the work of Valone [101, 102] and consider the set $\Gamma_e(N)$ of *ensemble N-representable* SPDMs. By definition, a SPDM is said to be ensemble *N*-representable if it can be associated with *some N*-particle mixed-state, i. e., if it can be expressed as

$$\gamma_{ij\sigma} = \text{Tr}_N\left\{\hat{\rho}\,\hat{c}_{i\sigma}^\dagger\hat{c}_{i\sigma}\right\},\qquad(3.16)$$

where

$$\hat{\rho} = \sum_n p_n\,|\Psi_n\rangle\langle\Psi_n|\quad\text{with}\quad p_n\geq 0\quad\text{and}\quad\text{Tr}_N\{\hat{\rho}\} = \sum_n p_n = 1\qquad(3.17)$$

is the density matrix characterizing the *N*-particle mixed state. Here, Tr_N means the trace in the *N*-particle Hilbert space and the sums go over the complete set of *N*-particle eigenstates $|\Psi_n\rangle$ of the density matrix $\hat{\rho}$. We will denote by $\mathcal{P}_N$ the set of all density matrices of the form (3.17), i. e., the set of all positive semidefinite operators with unit trace in *N*-particle Hilbert space. One can show (see for example Ref. [103]) that a matrix $\boldsymbol{\gamma}$ is ensemble *N*-representable if, and only if, it is hermitian, i. e., $\gamma_{ji\sigma} = \gamma_{ij\sigma}^*$, and its eigenvalues $\eta_{k\sigma}$ fulfill the requirements

$$0 \leq \eta_{k\sigma} \leq 1\quad\forall k\sigma\quad\text{and}\quad\sum_{k\sigma}\eta_{k\sigma} = N\,.\qquad(3.18)$$

In order to extend the domain of the interaction-energy functional (3.14) to the set $\Gamma_e(N)$ of ensemble *N*-representable SPDMs, we adopt the idea of LL (see Appendix A.1.2) and propose the constrained-search functional

$$W_e[\boldsymbol{\gamma}] = \min_{\hat{\rho}\to\boldsymbol{\gamma}}\text{Tr}_N\left\{\hat{\rho}\,\hat{W}\right\}.\qquad(3.19)$$

Here the notation $\hat{\rho}\to\boldsymbol{\gamma}$ indicates the minimization with respect to all density matrices $\hat{\rho}\in\mathcal{P}_N$ which yield the given SPDM $\boldsymbol{\gamma}$ via Eq. (3.16). In order to render the functional (3.19) useful in practice, we have to prove the following statement.

Theorem 3.2. *The constrained-search interaction-energy functional* (3.19) *is a reasonable extension of the interaction-energy functional* (3.14) *in the sense that*

(a) it holds

$$W_e[\boldsymbol{\gamma}] = W[\boldsymbol{\gamma}] \tag{3.20}$$

for all pure-state t-representable SPDMs $\boldsymbol{\gamma}$, and

(b) the minimum of the corresponding energy functional

$$E_e[\boldsymbol{\gamma}] = \sum_{ij\sigma} t_{ij\sigma}\, \gamma_{ij\sigma} + W_e[\boldsymbol{\gamma}] \tag{3.21}$$

equals the ground-state energy E_0 associated with the hopping matrix $\boldsymbol{t}$ and is assumed at, and only at, the unique gs-SPDM $\boldsymbol{\gamma}_0$ if the ground state is nondegenerate. In case of ground-state degeneracies, the energy functional (3.21) assumes its minimum E_0 only for linear combinations of the SPDMs generated by the degenerate ground-states.

Proof. It is clear that the Rayleigh-Ritz principle (A.20) remains valid if the minimization is extended to the set of N-particle mixed-states characterized by density matrices $\hat{\rho} \in \mathcal{P}_N$ of the form (3.17), since any normalized N-particle state $|\Psi\rangle$ is associated with the density matrix $\hat{\rho} = |\Psi\rangle\langle\Psi|$. Thus, it is easy to verify that the minimal value of the energy functional (3.21) equals the ground-state energy E_0 associated with the hopping matrix $\boldsymbol{t}$, by performing the minimization in the extended Rayleigh-Ritz principle in two consecutive steps:

$$E_0 = \min_{\hat{\rho} \in \mathcal{P}_N} \text{Tr}_N\left\{\hat{\rho}\left(\hat{K} + \hat{W}\right)\right\} = \min_{\boldsymbol{\gamma} \in \Gamma_e(N)} \left\{\sum_{ij\sigma} t_{ij\sigma}\, \gamma_{ij\sigma} + \min_{\hat{\rho} \to \boldsymbol{\gamma}} \text{Tr}_N\left\{\hat{\rho}\,\hat{W}\right\}\right\} =$$
$$\tag{3.22}$$
$$= \min_{\boldsymbol{\gamma} \in \Gamma_e(N)} \left\{\sum_{ij\sigma} t_{ij\sigma}\, \gamma_{ij\sigma} + W_e[\boldsymbol{\gamma}]\right\} = \min_{\boldsymbol{\gamma} \in \Gamma_e(N)} E_e[\boldsymbol{\gamma}].$$

If the ground state $|\Psi_0\rangle$ associated with the hopping matrix $\boldsymbol{t}$ is nondegenerate, the minimum in Eq. (3.22) is unique and must be assumed for the pure-state density $\hat{\rho}_0 = |\Psi_0\rangle\langle\Psi_0|$. This means, the only SPDM which yields a minimum of the energy functional (3.21) is the corresponding unique gs-SPDM $\gamma_{ij\sigma} = \langle\Psi_0|\hat{c}_{i\sigma}^\dagger \hat{c}_{j\sigma}|\Psi_0\rangle$. If the hopping matrix $\boldsymbol{t}$ leads to a degenerate ground-state, only density matrices $\hat{\rho} = \sum_n p_n |\Psi_0^{(n)}\rangle\langle\Psi_0^{(n)}|$ constructed from the degenerate ground states $|\Psi_0^{(n)}\rangle$ lead to minima in Eq. (3.22). In this case, SPDMs of the form $\gamma_{ij\sigma} = \sum_n p_n \langle\Psi_0^{(n)}|\hat{c}_{i\sigma}^\dagger \hat{c}_{j\sigma}|\Psi_0^{(n)}\rangle = \sum_n p_n \gamma_{ij\sigma}^{(n)}$, i.e., linear combinations of the SPDMs generated by the degenerate ground states, are the only ones which lead to minima of the energy functional (3.21). This concludes the proof of statement (b).

Let us now consider an arbitrary pure-state t-representable SPDM $\boldsymbol{\gamma}$, and let $\boldsymbol{t}$ be the hopping matrix associated with it according to Theorem 3.1. Then, the density

matrix which yields the minimum in Eq. (3.22) for this hopping matrix t must be the pure-state density $\hat{\rho}_0 = |\Psi_0[\gamma]\rangle\langle\Psi_0[\gamma]|$ constructed from the ground state $|\Psi_0[\gamma]\rangle$ associated with γ. Therefore, $W_e[\gamma] = \mathrm{Tr}_N\{\hat{\rho}_0\hat{W}\} = \langle\Psi_0[\gamma]|\hat{W}|\Psi_0[\gamma]\rangle$ must hold, which coincides with Eq. (3.14). This concludes the proof of statement (a). $\qquad\square$

The constrained-search formulation (3.19) extends the interaction-energy functional (3.14) to the domain $\Gamma_e(N)$ of ensemble N-representable SPDMs, which are easy to characterize by the condition (3.18). This opens the way to practical implementations of the variational principle for the energy functional (3.21), from which the ground-state energy and gs-SPDM, and in principle all ground-state observables can be obtained by virtue of Corollary 3.2. The next section addresses the problem of implementing the variational principle for the ground-state energy in practice. It will be shown that the interacting many-particle system can be mapped to a system of N noninteracting particles with an effective hopping matrix $t^s[\gamma]$ which is a functional of the SPDM γ itself. In this way, the ground-state problem for N interacting particles can be formally reduced to the selfconsistent solution of single-particle equations.

3.1.3 Mapping to an effective noninteracting system

Similar to the KS method presented in Appendix A.1.3, we would like to map a given system of N interacting particles to an auxiliary noninteracting system whose gs-SPDM equals the one of the interacting system. To this aim, let us consider a noninteracting system characterized by a hopping matrix t^s, such that the corresponding energy functional is given by

$$E_s[\gamma] = \sum_{ij\sigma} t^s_{ij\sigma}\, \gamma_{ij\sigma}\,. \tag{3.23}$$

In order to minimize $E_s[\gamma]$ within the set $\Gamma_e(N)$ of ensemble N-representable SPDMs, i.e., within the set of all hermitian matrices γ having the same dimensionality as the hopping matrix t^s and fulfill the requirements (3.18), we express the spin-resolved SPDM γ_σ in terms of its normalized eigenvectors $u_{k\sigma}$ and its eigenvalues or *occupation numbers* $\eta_{k\sigma}$

$$\gamma_{ij\sigma} = \sum_k u_{ik\sigma}\, \eta_{k\sigma}\, u^*_{jk\sigma}\,. \tag{3.24}$$

Here we have used the fact that γ_σ is hermitian, such that its eigenvectors $u_{k\sigma}$ can be chosen to be mutually orthogonal. Consequently, the matrix constructed from the normalized eigenvectors is unitary, i.e.,

$$\sum_k u^*_{ik\sigma}\, u_{jk\sigma} = \delta_{ij}\,. \tag{3.25}$$

For the SPDM $\boldsymbol{\gamma}$ which minimizes $E_s[\boldsymbol{\gamma}]$, i. e., for the gs-SPDM associated with the non-interacting system characterized by the hopping matrix $\boldsymbol{t}^s$, the corresponding Euler-Lagrange functional

$$\mathcal{L}_s = E_s[\boldsymbol{\gamma}] - \sum_{k\sigma} \lambda_{k\sigma} \left(\sum_i u^*_{ik\sigma} u_{ik\sigma} - 1 \right) - \mu \left(\sum_{k\sigma} \eta_{k\sigma} - N \right) \qquad (3.26)$$

must be stationary. Lagrange multipliers $\lambda_{k\sigma}$ and μ have been introduced in order to enforce the normalization of the eigenvectors $\boldsymbol{u}_{k\sigma}$ and to satisfy the second condition in Eq. (3.18) which accounts for the number of particles. At a stationary point of $\mathcal{L}_s$ its derivative with respect to $u^*_{jk\sigma}$ must vanish, and by using Eqs. (3.23) and (3.24) we thus obtain the following eigenvalue equation for the vectors $\boldsymbol{u}_{k\sigma}$

$$\eta_{k\sigma} \sum_i t^s_{ij\sigma} u_{ik\sigma} = \lambda_{k\sigma} u_{jk\sigma} \quad \forall jk\sigma \,. \qquad (3.27)$$

For $\eta_{k\sigma} = 0$ the SPDM (3.24) is independent of the eigenvector $\boldsymbol{u}_{k\sigma}$ and therefore it can be chosen as an arbitrary normalized vector. For $\eta_{k\sigma} > 0$ we can recast Eq. (3.27) in the form

$$\left(\boldsymbol{t}^s_\sigma \right)^\top \boldsymbol{u}_{k\sigma} = \varepsilon_{k\sigma} \boldsymbol{u}_{k\sigma} \quad \forall k\sigma \,, \qquad (3.28)$$

with the spin-resolved hopping matrix $\boldsymbol{t}^s_\sigma$ and $\varepsilon_{k\sigma} = \lambda_{k\sigma}/\eta_{k\sigma}$. Equation (3.28) demonstrates that the eigenvectors $\boldsymbol{u}_{k\sigma}$ of the gs-SPDM associated with the given noninteracting system are common eigenvectors of the corresponding transposed[3] spin-resolved hopping matrix $\left(\boldsymbol{t}^s_\sigma \right)^\top$. The fact that $\boldsymbol{t}^s_\sigma$ is hermitian ensures that the eigenvectors $\boldsymbol{u}_{k\sigma}$ of the gs-SPDM can be chosen to be mutually orthogonal.

Having identified the eigenvectors $\boldsymbol{u}_{k\sigma}$ of the gs-SPDM as the eigenvectors of the transposed hopping matrix $\left(\boldsymbol{t}^s_\sigma \right)^\top$, it remains to determine the corresponding occupation numbers $\eta_{k\sigma}$. To this aim, we combine Eqs. (3.23), (3.24), and (3.28), and obtain the single-particle energy functional in diagonal form

$$E_s[\boldsymbol{\gamma}] = \sum_{k\sigma} \varepsilon_{k\sigma} \eta_{k\sigma} \,. \qquad (3.29)$$

Thus, the occupation numbers $0 \leq \eta_{k\sigma} \leq 1$ which correspond to the ground state of the given noninteracting system are immediately identified as

$$\eta_{k\sigma} = 1 \quad \text{for} \quad \varepsilon_{k\sigma} < \mu$$
$$\eta_{k\sigma} = 0 \quad \text{for} \quad \varepsilon_{k\sigma} > \mu \qquad (3.30)$$
$$0 \leq \eta_{k\sigma} \leq 1 \quad \text{for} \quad \varepsilon_{k\sigma} = \mu \,,$$

---

[3]Notice, that the hopping matrix $\boldsymbol{t}^s_\sigma$ is hermitian, such that transposition is equivalent to complex conjugation and therefore this operation can be discarded in the usual case of a real hopping matrix.

where the chemical potential μ must be chosen such that the condition $\sum_{k\sigma} \eta_{k\sigma} = N$ is satisfied. If the Fermi level $\varepsilon_{k\sigma} = \mu$ is nondegenerate and the number $N_\sigma = \sum_k \eta_{k\sigma}$ of particles with spin polarization σ is integer, we have $\eta_{k\sigma} \in \{0, 1\}$ for all k and the corresponding SPDM is thus idempotent, i. e., $\boldsymbol{\gamma}_\sigma^2 = \boldsymbol{\gamma}_\sigma$. The ground state $|\Psi_0\rangle$ of the given noninteracting system is then a single Slater determinant of the form

$$|\Psi_0\rangle = \prod_{k\sigma} \left(\hat{b}_{k\sigma}^\dagger \right)^{\eta_{k\sigma}} |\text{vac}\rangle, \tag{3.31}$$

where

$$\hat{b}_{k\sigma}^\dagger = \sum_i u_{ik\sigma}^* \hat{c}_{i\sigma}^\dagger \tag{3.32}$$

are the creation operators associated to single-particle states which we will refer to as *natural orbitals*. Conversely it is clear, that the only kind of many-body state which can give rise to an idempotent SPDM is a single Slater determinant of the form (3.31). Notice, however, that the ground state of an interacting system can not be represented by a single Slater determinant, and that the corresponding gs-SPDM $\boldsymbol{\gamma}$ is consequently not idempotent. This means $\boldsymbol{\gamma}$ must always involve fractional occupation numbers $0 < \eta_{k\sigma} < 1$ if it is associated with the ground state of an interacting many-particle system. Therefore, if we try to map a given interacting system to an auxiliary noninteracting system which is supposed to yield the same gs-SPDM, we will face the difficulty that the Fermi level $\varepsilon_{k\sigma} = \mu_\sigma$ of the auxiliary noninteracting system must be degenerate in order to produce fractional ground-state occupation numbers. This means that the gs-SPDM of the auxiliary noninteracting system can not be unique, since variations of the occupation numbers $\eta_{k\sigma}$ at the degenerate Fermi level have no impact on the energy as long as the number of particles is kept fixed. In order to resolve these difficulties we will further below propose to map the given interacting system to an auxiliary noninteracting system in equilibrium at a fictitious finite temperature $T_a > 0$, since the occupation numbers in equilibrium at a finite temperature are always fractional.

Before doing so, let us return to the given interacting system and minimize the energy functional (3.21) with respect to all ensemble N-representable SPDMs $\boldsymbol{\gamma} \in \Gamma_e(N)$. To this aim, we seek for the stationary points of the corresponding Euler-Lagrange functional

$$\mathcal{L} = E_e[\boldsymbol{\gamma}] - \sum_{k\sigma} \lambda_{k\sigma} \left(\sum_i u_{ik\sigma}^* u_{ik\sigma} - 1 \right) - \mu \left(\sum_{k\sigma} \eta_{k\sigma} - N \right). \tag{3.33}$$

Again, we have introduced Lagrange multipliers $\lambda_{k\sigma}$ and μ in order to enforce the normalization of the eigenvectors $\boldsymbol{u}_{k\sigma}$ of the SPDM and to obtain the desired particle

number. At a stationary point, the derivative of $\mathcal{L}$ with respect to $u^*_{jk\sigma}$ vanishes, such that we obtain the following eigenvalue equation for the eigenvectors $\boldsymbol{u}_{k\sigma}$

$$\eta_{k\sigma} \sum_i \left(t_{ij\sigma} + \frac{\partial W_e[\boldsymbol{\gamma}]}{\partial \gamma_{ij\sigma}} \right) u_{ik\sigma} = \lambda_{k\sigma} \, u_{jk\sigma} \quad \forall jk\sigma \, . \tag{3.34}$$

This eigenvalue equation is formally identical to the corresponding equation (3.27) for the noninteracting system if we choose the hopping integrals of the auxiliary system as

$$t^s_{ij\sigma}[\boldsymbol{\gamma}] = t_{ij\sigma} + \frac{\partial W_e[\boldsymbol{\gamma}]}{\partial \gamma_{ij\sigma}} \, . \tag{3.35}$$

Therefore, the gs-SPDM $\boldsymbol{\gamma}$ of the interacting system is also a gs-SPDM of the auxiliary noninteracting system with the hopping integrals $t^s_{ij\sigma}[\boldsymbol{\gamma}]$. Equations (3.24), (3.28), (3.30), and (3.35) make up an iterative scheme, by which the gs-SPDM of a given interacting system can be determined from the solution of an effective single-particle problem. These equations must be solved in a selfconsistent manner, since the effective hopping integrals (3.35) depend on the SPDM $\boldsymbol{\gamma}$ itself. As already discussed above, a difficulty arises from the fact that fractional occupation numbers $0 < \eta_{k\sigma} < 1$, which are characteristic for interacting ground states, are obtained only if the auxiliary noninteracting system has a degenerate ground state. In this case, the fractional occupation numbers $\eta_{k\sigma}$ at the Fermi level are not unique and only constrained by the condition $N = \sum_{k\sigma} \eta_{k\sigma}$. This renders the practical implementation of the iterative scheme based on the ground state of the auxiliary noninteracting system impractical.

One possibility to resolve the issues arising from the requirement of fractional occupation numbers was proposed by Saubanére, Lepetit, and Pastor [87]. They suggested to consider an auxiliary noninteracting system at a fictitious finite temperature $T_a > 0$, such that the corresponding eq-SPDM equals the one in the ground state of the given interacting system. The advantage of an auxiliary noninteracting system at a finite temperature is that the occupation numbers in equilibrium are fractional. In order to introduce the method of Saubanére *et al.*, let us consider the eigenvectors $\boldsymbol{u}_{k\sigma}$ of the SPDM as fixed for the moment, such that the energy (3.21) can be regarded as a functional of the occupation numbers $\eta_{k\sigma}$ alone, i. e., $E = E_e[\boldsymbol{\eta}]$. In order to seek for an extremum of the energy functional $E_e[\boldsymbol{\eta}]$ under the constraint of a given particle number N, we consider the corresponding Euler-Lagrange functional

$$\mathcal{L} = E_e[\boldsymbol{\eta}] - \mu \left(\sum_{k\sigma} \eta_{k\sigma} - N \right) . \tag{3.36}$$

At a stationary point of $\mathcal{L}$ its variation with respect to all $\eta_{k\sigma}$ vanishes, such that

$$\frac{\partial E_e[\boldsymbol{\eta}]}{\partial \eta_{k\sigma}} = \mu \quad \forall k\sigma \, . \tag{3.37}$$

Let us now consider an auxiliary noninteracting system with spin-resolved hopping matrix t_σ^s which is chosen such that Eq. (3.28) is fulfilled for the given set of eigenvectors $\boldsymbol{u}_{k\sigma}$ and some set of corresponding eigenvalues $\varepsilon_{k\sigma}$. The energy of this noninteracting system is then given by

$$E_s = \sum_{k\sigma} \varepsilon_{k\sigma}\,\eta_{k\sigma}\,, \tag{3.38}$$

where $\eta_{k\sigma}$ are the occupation numbers of the natural orbitals associated with the creation operators (3.32). Working in a grand-canonical ensemble at a temperature $T_a > 0$ and chemical potential μ, the equilibrium occupation numbers of the noninteracting system follow a Fermi-Dirac distribution

$$\eta_{k\sigma} = \frac{1}{1 + e^{(\varepsilon_{k\sigma}-\mu)/k_{\mathrm{B}}T_a}}\,. \tag{3.39}$$

We require that the equilibrium occupation numbers of the auxiliary noninteracting system coincide with the eigenvalues of the gs-SPDM of the given interacting system, such that they lead to a stationary point of $\mathcal{L}$. This means, the equilibrium occupation numbers of the auxiliary noninteracting system must satisfy the conditions (3.37) and (3.39) together. The energy levels of the auxiliary noninteracting system are therefore obtained as

$$\varepsilon_{k\sigma}[\boldsymbol{\eta}] = \frac{\partial E_{\mathrm{e}}[\boldsymbol{\eta}]}{\partial \eta_{k\sigma}} + k_{\mathrm{B}}T_a\,\log\!\left(\frac{1-\eta_{k\sigma}}{\eta_{k\sigma}}\right). \tag{3.40}$$

Since these energy levels depend on the occupation numbers $\eta_{k\sigma}$ themselves, Eqs. (3.39) and (3.40) must be solved in a selfconsistent manner. The full iterative procedure for the minimization of the energy functional $E_{\mathrm{e}}[\boldsymbol{\gamma}]$ can be implemented as follows:

1. Start from an arbitrary ensemble N-representable SPDM $\boldsymbol{\gamma}$, compute its eigenvalues $\eta_{k\sigma}$ and the effective hopping integrals (3.35). Solve the eigenvalue equation (3.28) for the eigenvectors $\boldsymbol{u}_{k\sigma}$.

2. Optimize the occupation numbers $\eta_{k\sigma}$ by keeping the current $\boldsymbol{u}_{k\sigma}$ fixed. To this aim, select a fixed auxiliary temperature $T_a > 0$, compute the effective energy levels (3.40) and use them to update $\eta_{k\sigma}$ via Eq. (3.39). Iterate until convergence is achieved.

3. Compute the new SPDM $\gamma_{ij\sigma} = \sum_k u_{ik\sigma}\eta_{k\sigma}u_{jk\sigma}^*$ from the current eigenvectors $\boldsymbol{u}_{k\sigma}$ and the optimized occupation numbers $\eta_{k\sigma}$. Use Eq. (3.35) to determine new effective hopping integrals $t_{ij\sigma}^s$.

4. Solve the eigenvalue equation (3.28) with the updated hopping integrals $t_{ij\sigma}^s$ in order to obtain new eigenvectors $\boldsymbol{u}_{k\sigma}'$.

5. Exit if convergence is achieved, i. e., $u'_{ik\sigma} = u_{ik\sigma} \ \forall ik\sigma$. Otherwise, return to step 2 after having updated $\boldsymbol{u}_{k\sigma}$ with $\boldsymbol{u}'_{k\sigma}$.

The rate of convergence in the presented iterative procedure is affected by the choice of the initial SPDM $\boldsymbol{\gamma}$ and the auxiliary temperature $T_a > 0$. Practical implementations for model Hamiltonians, such as the Hubbard model, have shown that a good choice for the initial SPDM $\boldsymbol{\gamma}$ is obtained from the ground state of the corresponding noninteracting system which is obtained by setting $\hat{W} = 0$. If the noninteracting ground state is degenerate, one can freely choose the occupation numbers at the Fermi level such that the condition $\sum_{k\sigma} \eta_{k\sigma} = N$ is satisfied. Concerning the auxiliary temperature T_a, it is clear that extreme values should be avoided. Good values for the auxiliary temperature are found in the order of the hopping integrals $k_{\mathrm{B}} T_a \simeq |t_{ij\sigma}|$. Moreover, T_a may be tuned to some extend, depending on the specific lattice model and interaction strength under consideration, in order to further improve the rate of convergence.

3.2 Finite-temperature ensembles

Having formulated a density functional theory which applies to the ground state of lattice-model Hamiltonians, we would now like to extend the formalism to the equilibrium at finite temperatures. Having a density functional theory which applies to the physical properties of lattice models in thermodynamic equilibrium at a finite temperature is not only desirable from a theoretical point of view, but also crucial for applications to systems exhibiting strong electronic correlations. A natural way of describing electron correlation effects is to focus on the most relevant many-body dynamics of the valence electrons, and to derive a simplified lattice Hamiltonian. The ground-state properties of these lattice-model Hamiltonians can be treated in the framework of ground-state LDFT presented in the previous section. There are, however, a myriad phenomena which can not be described within a ground-state formalism. For example, phase transitions in magnetic or superconducting materials, the Kondo effect, and metal-insulator transitions. These effects manifest themselves at specific temperatures, such as the Curie or Néel ordering temperatures in ferromagnets and antiferromagnets, or the Kondo temperature for magnetic impurities in metals. Consequently, extending the scope of LDFT to the regime of finite temperatures in order to describe the equilibrium properties of strongly interacting electrons in the framework of lattice-model Hamiltonians is indispensable.

Let us begin by noting that the state of a system at a finite temperature $T > 0$ must be described by a mixed state which is characterized by a density matrix $\hat{\rho}$. Using the expansion of the fermionc fields (3.2) in terms of a given set $\{\phi_{i\sigma}(\boldsymbol{r})\}$ of single-particle

orbitals, we can express the electronic density in a mixed state as

$$n(\boldsymbol{r}) = \sum_\sigma \mathrm{Tr}\big\{\hat{\rho}\,\hat{\psi}_\sigma^\dagger(\boldsymbol{r})\,\hat{\psi}_\sigma(\boldsymbol{r})\big\} = \sum_{ij\sigma} \gamma_{ij\sigma}\,\phi_{i\sigma}^*(\boldsymbol{r})\,\phi_{j\sigma}(\boldsymbol{r})\,, \qquad (3.41)$$

where

$$\gamma_{ij\sigma} = \mathrm{Tr}\big\{\hat{\rho}\,\hat{c}_{i\sigma}^\dagger\hat{c}_{j\sigma}\big\} \qquad (3.42)$$

is the SPDM of the mixed state characterized by the density matrix $\hat{\rho}$. Clearly, once a set $\{\phi_{i\sigma}(\boldsymbol{r})\}$ of single-particle basis states is adopted, the particle density $n(\boldsymbol{r})$ in an arbitrary mixed state is fully determined by the corresponding SPDM $\boldsymbol{\gamma}$. Thus, we readily identify the SPDM (3.42) as the fundamental variable in the formulation of finite-temperature lattice density functional theory (FT-LDFT). We will formulate the fundamentals of FT-LDFT in two different flavours. In Section 3.2.1 we present a grand-canonical ensemble formulation of FT-LDFT, while the following Section 3.2.2 accounts for a canonical-ensemble.

3.2.1 Grand-canonical ensembles

In order to develop a grand-canonical formulation of FT-LDFT, we closely follow the formulation of finite-temperature density functional theory (FT-DFT) in Appendix A.2.1. First, we formulate a statement which establishes a unique connection between the hopping matrix $\boldsymbol{t}$, which characterizes the lattice model under study, and the corresponding equilibrium single-particle density matrix (eq-SPDM) $\boldsymbol{\gamma}$. This theorem has the same fundamental character as the Mermin Theorem A.3 in the formulation of FT-DFT. It enables us to propose a functional which incorporates a variational principle from which the eq-SPDM and, in turn, the equilibrium average value of all physical observables can be obtained in principle. Subsequently, we will demonstrate that the interacting many-particle system can be mapped to an auxiliary system of noninteracting particles with an effective hopping matrix $\boldsymbol{t}^s[\boldsymbol{\gamma}]$ which is a functional of the SPDM itself. In this way, the equilibrium properties of interacting electrons on a lattice can be formally obtained from the selfconsistent solution of single-particle equations.

Connection between the hopping matrix and the eq-SPDM

Let us consider a system described by a general Hamiltonian $\hat{H}$ of the form (3.1), where we regard the type of particle interaction specified by the parameters $W_{ijkl}^{\sigma\sigma'}$ as fixed, such that the hopping integrals $t_{ij\sigma}$ define the system under study. We will consider a system which is open with respect to exchange of energy and particles with the environment, where the latter is characterized by a fixed temperature T and chemical potential μ_σ for particles with spin polarization σ. Before we establish a unique

connection between the hopping matrix t and the corresponding eq-SPDM γ, let us first record Gibbs variational principle for the grand potential, which is the finite-temperature analog of the Rayleigh-Ritz variational principle (A.20) for the ground-state energy. To this aim we consider the functional

$$\Omega[\hat{\rho}] = \mathrm{Tr}\left\{\hat{\rho}\left(\hat{H} + \frac{1}{\beta}\log\hat{\rho} - \sum_\sigma \mu_\sigma \hat{N}_\sigma\right)\right\}, \tag{3.43}$$

where $\beta = (k_\mathrm{B} T)^{-1}$ with the Boltzmann constant k_B. Gibbs variational principle states that the grand potential is given by

$$\Omega_0 = \min_{\hat{\rho}\in\mathcal{P}} \Omega[\hat{\rho}], \tag{3.44}$$

where the minimization is performed within the set $\mathcal{P}$ of all positive semidefinite density matrices with unit trace representing physical mixed states with arbitrary particle number [see Eq. (A.37)]. It is easy to show that the functional (3.43) has a local minimum at the grand-canonical density matrix

$$\hat{\rho}_0 = \frac{e^{-\beta(\hat{H}-\sum_\sigma \mu_\sigma \hat{N}_\sigma)}}{\mathrm{Tr}\left\{e^{-\beta(\hat{H}-\sum_\sigma \mu_\sigma \hat{N}_\sigma)}\right\}}, \tag{3.45}$$

which characterizes the equilibrium state of the system described by the Hamiltonian $\hat{H}$. Furthermore, Mermin [6] has demonstrated that the minimum is unique and global within $\mathcal{P}$, i. e., that the strict inequality

$$\Omega[\hat{\rho}] > \Omega[\hat{\rho}_0] = \Omega_0, \quad \hat{\rho} \neq \hat{\rho}_0 \tag{3.46}$$

holds for any density matrix $\hat{\rho} \in \mathcal{P}$ different from $\hat{\rho}_0$. With these preliminaries we are now able to formulate the following statement, which plays the same fundamental role in the formulation of FT-LDFT as the Mermin Theorem A.3 in the formulation of FT-DFT.

Theorem 3.3. *For any fixed temperature $T > 0$ and chemical potential μ_σ for particles with spin polarization σ, the hopping matrix t of the interacting many-particle system described by the Hamiltonian (3.1) is a functional of the eq-SPDM γ.*

Proof. The proof is carried out in close analogy to the one shown for the Mermin Theorem A.3. Assume there would be *another* hopping matrix t' which differs from t but, nevertheless, at the given temperature T and chemical potential μ_σ leads to the *same* eq-SPDM γ as the hopping matrix t. If $\hat{H}'$ and $\hat{\rho}_0'$ denote the Hamiltonian and grand-canonical density matrix of the system with the hopping matrix t', the corresponding grand potential is given by given by

$$\Omega_0' = \sum_{ij\sigma} t_{ij\sigma}' \gamma_{ij\sigma} + \mathrm{Tr}\left\{\hat{\rho}_0'\left(\hat{W} + \frac{1}{\beta}\log\hat{\rho}_0' - \sum_\sigma \mu_\sigma \hat{N}_\sigma\right)\right\}. \tag{3.47}$$

Since the hopping matrices t and t' are by assumption different from each other, it follows from Eq. (3.45) that the associated grand-canonical density matrices $\hat{\rho}_0$ and $\hat{\rho}_0'$ must be different as well. Thus, from the minimal principle (3.46) it follows that

$$\Omega_0 < \Omega[\hat{\rho}_0'] = \mathrm{Tr}\left\{\hat{\rho}_0'\left(\hat{H} + \frac{1}{\beta}\log\hat{\rho}_0' - \sum_\sigma \mu_\sigma \hat{N}_\sigma\right)\right\} = \Omega_0' + \sum_{ij\sigma}\left(t_{ij\sigma} - t_{ij\sigma}'\right)\gamma_{ij\sigma} \,. \quad (3.48)$$

By interchanging primed and unprimed quantities one obtains

$$\Omega_0' < \Omega_0 + \sum_{ij\sigma}\left(t_{ij\sigma}' - t_{ij\sigma}\right)\gamma_{ij\sigma} \,. \quad (3.49)$$

Adding Eqs. (3.48) and (3.49) the contradiction

$$\Omega_0 + \Omega_0' < \Omega_0' + \Omega_0 \quad (3.50)$$

is obtained, which proves that two different hopping matrices t and t' cannot lead to the same eq-SPDM γ at a given temperature $T > 0$ and chemical potential μ_σ. One concludes that t is a functional of γ. □

Notice that Theorem 3.3 establishes a *unique* connection between hopping matrix t and the corresponding eq-SPDM γ, whereas the similar Theorem 3.1 for the ground state connects the gs-SPDM and the hopping matrix t only up to a spin-dependent shift in the energy levels. Clearly, this is due to the fact that we work in a grand-canonical ensemble with fixed chemical potential μ_σ for particles with spin polarization σ, such that there is no ambiguity with respect to a spin-dependent shift of the energy levels.

Since we consider the particle interaction specified by the parameters $W_{ijkl}^{\sigma\sigma'}$ as fixed, the hopping matrix t characterizes the system described by the Hamiltonian (3.1) uniquely. The hopping matrix is in turn uniquely determined by the eq-SPDM γ, such that the full Hamiltonian $\hat{H}$ and all physical properties derived from it must be functionals of the eq-SPDM as well. This applies in particular to the grand-canonical density matrix (3.45), which immediately proves the important

Corollary 3.3. *For any fixed temperature $T > 0$ and chemical potential μ_σ for electrons with spin polarization σ, the grand-canonical density matrix $\hat{\rho}_0$ of the interacting many-particle system described by the Hamiltonian (3.1) is a functional of the eq-SPDM γ.*

Obviously the converse statement is also true, namely that the eq-SPDM $\gamma_{ij\sigma} = \mathrm{Tr}\{\hat{\rho}_0\,\hat{c}_{i\sigma}^\dagger\hat{c}_{j\sigma}\}$ is a functional of the grand-canonical density matrix $\hat{\rho}_0$. This establishes a bijective map between the set of the grand-canonical density matrices and the corresponding set of the eq-SPDMs. A further important consequence of Theorem 3.3 is

Corollary 3.4. *For a fixed temperature $T > 0$ and chemical potential μ_σ for electrons with spin polarization σ, the equilibrium average-value of any observable $\hat{O}$ is a functional of the eq-SPDM $\boldsymbol{\gamma}$.*

Proof. From Corollary 3.3 we know that the grand-canonical density matrix $\hat{\rho}_0 = \hat{\rho}_0[\boldsymbol{\gamma}]$ is a functional of the eq-SPDM $\boldsymbol{\gamma}$. Therefore, the equilibrium average-value of any observable $\hat{O}$ can be obtained from the eq-SPDM as

$$O[\boldsymbol{\gamma}] = \text{Tr}\{\hat{\rho}_0[\boldsymbol{\gamma}]\,\hat{O}\}. \tag{3.51}$$

□

In order to be useful in practice, the formulation of FT-LDFT requires a functional from which the eq-SPDM can be obtained by means of a variational principle. We will construct this functional by a constrained-search method, which is very similar to the one discussed in Section 3.1.2. This will allow us to bypass all problems related to the representability of eq-SPDMs. To this aim, for a given temperature T we introduce the functional

$$G[\boldsymbol{\gamma}] = \min_{\hat{\rho} \to \boldsymbol{\gamma}} \text{Tr}\left\{\hat{\rho}\left(\hat{W} + \frac{1}{\beta}\log\hat{\rho}\right)\right\}, \tag{3.52}$$

where the notation $\hat{\rho} \to \boldsymbol{\gamma}$ indicates the minimization with respect to all density matrices $\hat{\rho} \in \mathcal{P}$ which yield the given SPDM $\boldsymbol{\gamma}$ by means of Eq. (3.42). This means, the functional $G[\boldsymbol{\gamma}]$ is defined on the set of all SPDMs which, via Eq. (3.42), can be associated with *some* density matrix $\hat{\rho} \in \mathcal{P}$. This type of SPDM is called *ensemble representable*, and we denote the set of all ensemble-representable SPDMs by $\boldsymbol{\Gamma}_\text{e}$. One can show (see for example Ref. [103]) that any hermitian matrix $\gamma_{ji\sigma}^* = \gamma_{ij\sigma}$ with eigenvalues $0 \le \eta_{k\sigma} \le 1$ for all $k\sigma$ belongs to the set $\boldsymbol{\Gamma}_\text{e}$ of ensemble-representable SPDMs.[4] The functional (3.52) is valid for arbitrary non-negative particle numbers $N = \sum_{i\sigma} \gamma_{ii\sigma}$ and is universal in the sense that it does not depend on the hopping matrix $\boldsymbol{t}$, which characterizes the system under study. It depends on the temperature T and on the set of interaction integrals $W_{ijkl}^{\sigma\sigma'}$. Furthermore, it depends on the Fock-space under consideration, since the density operators $\hat{\rho}$ in the minimization of Eq. (3.52) are operators in the given Fock space.

Using the functional $G[\boldsymbol{\gamma}]$ defined in Eq. (3.52), we can now introduce the grand-potential SPDM functional

$$\Omega[\boldsymbol{\gamma}] = \sum_{ij\sigma}\left(t_{ij\sigma} - \delta_{ij}\,\mu_\sigma\right)\gamma_{ij\sigma} + G[\boldsymbol{\gamma}], \tag{3.53}$$

---

[4]Therefore, according to Eq. (3.18) the sole distinction between ensemble-representable SPDMs and ensemble N-representable SPDMs is that the eigenvalues $\eta_{k\sigma}$ of an ensemble-representable SPDM must not sum to a given fixed particle number N.

whose minimal value within the set Γ_e of all ensemble representable SPDMs equals the grand potential Ω_0. This can be most easily seen by performing the minimization in the Gibbs variational principle (3.44) in two consecutive steps:

$$
\Omega_0 = \min_{\hat{\rho} \in \mathcal{P}} \mathrm{Tr} \left\{ \hat{\rho} \left(\hat{H} + \frac{1}{\beta} \log \hat{\rho} - \sum_\sigma \mu_\sigma \hat{N}_\sigma \right) \right\} =
$$

$$
= \min_{\boldsymbol{\gamma} \in \Gamma_e} \left[\sum_{ij\sigma} \left(t_{ij\sigma} - \delta_{ij}\,\mu_\sigma \right) \gamma_{ij\sigma} + \min_{\hat{\rho} \to \boldsymbol{\gamma}} \mathrm{Tr} \left\{ \hat{\rho} \left(\hat{W} + \frac{1}{\beta} \log \hat{\rho} \right) \right\} \right] = \quad (3.54)
$$

$$
= \min_{\boldsymbol{\gamma} \in \Gamma_e} \left[\sum_{ij\sigma} \left(t_{ij\sigma} - \delta_{ij}\,\mu_\sigma \right) \gamma_{ij\sigma} + G[\boldsymbol{\gamma}] \right] = \min_{\boldsymbol{\gamma} \in \Gamma_e} \Omega[\boldsymbol{\gamma}] .
$$

Furthermore, from Eq. (3.46) it follows that the density matrix $\hat{\rho}$ which yields the minimum in Eq. (3.54) is the grand-canonical density matrix (3.45) associated with the given hopping matrix $\boldsymbol{t}$, temperature T and chemical potential μ_σ. Consequently, the minimizing SPDM $\boldsymbol{\gamma}$ corresponds to the eq-SPDM.

Let us now perform the minimization in Eq. (3.52) in an explicit manner in order to develop a practical implementation of the functional $G[\boldsymbol{\gamma}]$. To this aim, we seek for the extremes of the Euler-Lagrange functional

$$
\mathcal{L}[\hat{\rho}] = \mathrm{Tr} \left\{ \hat{\rho} \left(\hat{W} + \frac{1}{\beta} \log \hat{\rho} \right) \right\} + \sum_{ij\sigma} \lambda_{ij\sigma} \left(\mathrm{Tr} \left\{ \hat{\rho}\, \hat{c}_{i\sigma}^\dagger \hat{c}_{j\sigma} \right\} - \gamma_{ij\sigma} \right) =
$$

$$
= \mathrm{Tr} \left\{ \hat{\rho} \left(\sum_{ij\sigma} \lambda_{ij\sigma}\, \hat{c}_{i\sigma}^\dagger \hat{c}_{j\sigma} + \hat{W} + \frac{1}{\beta} \log \hat{\rho} \right) \right\} - \sum_{ij\sigma} \lambda_{ij\sigma}\, \gamma_{ij\sigma}
$$

(3.55)

within the set $\mathcal{P}$ of all positive semidefinite density matrices $\hat{\rho}$ with unit trace. Here we have introduced Lagrange multipliers $\lambda_{ij\sigma}$ in order to enforce that the minimizing density matrix $\hat{\rho}$ yields the required SPDM $\boldsymbol{\gamma}$. Apart from an irrelevant constant, the Euler-Lagrange functional (3.55) equals the Gibbs functional (3.43) with vanishing chemical potential $\mu_\sigma = 0$ (the chemical potential can be regarded as absorbed in the parameters $\lambda_{ii\sigma}$) and the effective Hamiltonian

$$
\hat{H}_\lambda = \sum_{ij\sigma} \lambda_{ij\sigma}\, \hat{c}_{i\sigma}^\dagger \hat{c}_{j\sigma} + \hat{W} . \quad (3.56)
$$

Consequently, the minimum of the Euler-Lagrange functional (3.55) within the set $\mathcal{P}$ is attained for the corresponding grand-canonical density matrix

$$
\hat{\rho}_\lambda = \frac{\mathrm{e}^{-\beta \hat{H}_\lambda}}{\mathrm{Tr} \left\{ \mathrm{e}^{-\beta \hat{H}_\lambda} \right\}} . \quad (3.57)
$$

The parameters $\lambda_{ij\sigma}$ in the Hamiltonian (3.56) play the role of effective energy levels ($i = j$) and effective hopping integrals ($i \neq j$), which must be chosen such that the grand-canonical density matrix (3.57) yields the desired SPDM γ. In practice, one usually varies the parameters $\lambda_{ij\sigma}$ systematically in order to scan the whole domain of eq-SPDMs γ. Notice, however, that this procedure requires one to compute the grand-canonical density matrix (3.57), which is usually expressed in terms of the full set of eigenstates and eigenvalues of the effective Hamiltonian $\hat{H}_\lambda$. Therefore, the thus described procedure is in general of the same level of complexity as the initial problem with the Hamiltonian (3.1) and is therefore only applicable to systems which can be solved by analytical or numerical methods.

Mapping to an effective noninteracting system

Similar to the method presented in Section 3.1.3, we would like to map the finite-temperature problem for N interacting particles to the solution of effective single-particle equations. Therefore, let us consider a general noninteracting system described by the Hamiltonian

$$\hat{H}_s = \sum_{ij\sigma} t_{ij\sigma}^s \, \hat{c}_{i\sigma}^\dagger \hat{c}_{j\sigma} \, . \tag{3.58}$$

In the following we will determine the hopping matrix t^s which characterizes the non-interacting system such that it yields the same eq-SPDM γ as the given interacting system. Furthermore, we will introduce the universal functional of the non-interacting Fermion entropy and derive an explicit expression in terms of the natural-orbital occupation numbers $\eta_{k\sigma}$. To this aim, let us first express the creation operator $\hat{c}_{i\sigma}^\dagger$ in terms of the natural-orbital creation operators (3.32)

$$\hat{c}_{i\sigma}^\dagger = \sum_k u_{ik\sigma} \, \hat{b}_{k\sigma}^\dagger \, , \tag{3.59}$$

where the vectors $\boldsymbol{u}_{k\sigma}$ are the orthonormal solutions of the eigenvalue problem

$$\left(t_\sigma^s\right)^\top \boldsymbol{u}_{k\sigma} = \varepsilon_{k\sigma} \, \boldsymbol{u}_{k\sigma} \, . \tag{3.60}$$

Expressed in terms of the natural-orbital creation operators $\hat{b}_{k\sigma}^\dagger$ and the corresponding eigenvalues $\varepsilon_{k\sigma}$, the single-particle Hamiltonian (3.58) assumes diagonal form

$$\hat{H}_s = \sum_{k\sigma} \varepsilon_{k\sigma} \, \hat{b}_{k\sigma}^\dagger \hat{b}_{k\sigma} = \sum_{k\sigma} \varepsilon_{k\sigma} \, \hat{n}_{k\sigma} \, . \tag{3.61}$$

Therefore, at a given temperature T and chemical potential μ_σ, we can express the grand-canonical density matrix of the noninteracting system as

$$\hat{\rho} = \frac{e^{-\beta \sum_{k\sigma} (\varepsilon_{k\sigma} - \mu_\sigma) \hat{n}_{k\sigma}}}{\mathrm{Tr}\left\{e^{-\beta \sum_{k\sigma} (\varepsilon_{k\sigma} - \mu_\sigma) \hat{n}_{k\sigma}}\right\}} \, . \tag{3.62}$$

Consequently, we obtain

$$\text{Tr}\big\{\hat{\rho}\,\hat{b}^{\dagger}_{k\sigma}\hat{b}_{k'\sigma}\big\} = \delta_{kk'}\text{Tr}\big\{\hat{\rho}\,\hat{n}_{k\sigma}\big\} = \frac{\delta_{kk'}}{1 + e^{\beta(\varepsilon_{k\sigma}-\mu_{\sigma})}} \,, \tag{3.63}$$

where we made use of the fact that the equilibrium occupation numbers $\eta_{k\sigma} = \text{Tr}\{\hat{\rho}\,\hat{n}_{k\sigma}\}$ of a noninteracting system follow a Fermi-Dirac distribution. Finally, we obtain the eq-SPDM of the noninteracting system as

$$\gamma_{ij\sigma} = \text{Tr}\big\{\hat{\rho}\,\hat{c}^{\dagger}_{i\sigma}\hat{c}_{j\sigma}\big\} = \sum_{kk'} u_{ik\sigma}\, u^{*}_{jk'\sigma}\text{Tr}\big\{\hat{\rho}\,\hat{b}^{\dagger}_{k\sigma}\hat{b}_{k'\sigma}\big\} = \sum_{k} u_{ik\sigma}\, \eta_{k\sigma}\, u^{*}_{jk\sigma}\,. \tag{3.64}$$

We conclude that the eigenvectors of the eq-SPDM coincide with the eigenvectors $\boldsymbol{u}_{k\sigma}$ of the transposed hopping matrix $\big(\boldsymbol{t}^{s}_{\sigma}\big)^{\top}$ and that its eigenvalues are given by

$$\eta_{k\sigma} = \frac{1}{1 + e^{\beta(\varepsilon_{k\sigma}-\mu_{\sigma})}}\,. \tag{3.65}$$

Clearly, the eq-SPDM (3.64) minimizes the noninteracting grand-potential functional

$$\Omega_{s}[\boldsymbol{\gamma}] = \sum_{ij\sigma}\big(t^{s}_{ij\sigma} - \delta_{ij}\,\mu_{\sigma}\big)\,\gamma_{ij\sigma} + G_{s}[\boldsymbol{\gamma}] \tag{3.66}$$

within the set Γ_{e} of all ensemble representable SPDMs $\boldsymbol{\gamma}$, where

$$G_{s}[\boldsymbol{\gamma}] = -T\,S_{s}[\boldsymbol{\gamma}] = \frac{1}{\beta}\,\min_{\hat{\rho}\to\boldsymbol{\gamma}}\text{Tr}\big\{\hat{\rho}\log\hat{\rho}\big\} \tag{3.67}$$

is, apart of the factor $-T$, the universal entropy functional $S_{s}[\boldsymbol{\gamma}]$ for noninteracting Fermions. In the following we would like to derive an explicit expression for the noninteracting functional $G_{s}[\boldsymbol{\gamma}]$ defined in Eq. (3.67). To this aim we perform the constrained minimization in Eq. (3.67) in a similar manner as in the context of Eqs. (3.55) to (3.57), i. e., by setting $\hat{W} = 0$ in Eq. (3.55), which leads to the minimizing density matrix

$$\hat{\rho}_{\lambda} = \frac{e^{-\beta\hat{H}_{\lambda}}}{\text{Tr}\big\{e^{-\beta\hat{H}_{\lambda}}\big\}} \tag{3.68}$$

with the effective noninteracting Hamiltonian

$$\hat{H}_{\lambda} = \sum_{ij\sigma}\lambda_{ij\sigma}\,\hat{c}^{\dagger}_{i\sigma}\hat{c}_{j\sigma}\,. \tag{3.69}$$

Here, the effective hopping-integrals $\lambda_{ij\sigma}$ must be chosen such that the corresponding grand-canonical density matrix (3.68) yields the desired SPDM via $\gamma_{ij\sigma} = \text{Tr}\{\hat{\rho}_{\lambda}\,\hat{c}^{\dagger}_{i\sigma}\hat{c}_{j\sigma}\}$. Therefore, as discussed in the context of Eq. (3.64), the eigenvectors of the transposed

effective hopping matrix $(\boldsymbol{\lambda}_\sigma)^\top$ must coincide with the eigenvectors of the SPDM $\boldsymbol{\gamma}$. Furthermore, according to Eq. (3.65) the eigenvalues $\varepsilon_{k\sigma}$ of $(\boldsymbol{\lambda}_\sigma)^\top$ must be related to the eigenvalues $\eta_{k\sigma}$ of the given SPDM $\boldsymbol{\gamma}$ by

$$\eta_{k\sigma} = \frac{1}{1 + e^{\beta \varepsilon_{k\sigma}}} \quad \Rightarrow \quad \varepsilon_{k\sigma} = \frac{1}{\beta} \log\left(\frac{1 - \eta_{k\sigma}}{\eta_{k\sigma}}\right). \tag{3.70}$$

Thus, the hopping matrix $\boldsymbol{\lambda} = \{\lambda_{ij\sigma}\}$ which characterizes the effective noninteracting system (3.69) is completely determined in terms of the given SPDM $\boldsymbol{\gamma}$. Using the well known expression for the grand-canonical partition function of noninteracting Fermions

$$Z = \mathrm{Tr}\{e^{-\beta \hat{H}_\lambda}\} = \prod_{k\sigma} \left(1 + e^{-\beta \varepsilon_{k\sigma}}\right) \overset{(3.70)}{=} \prod_{k\sigma} \left(\frac{1}{1 - \eta_{k\sigma}}\right), \tag{3.71}$$

we obtain from Eq. (3.68)

$$\log \hat{\rho}_\lambda = -\beta \hat{H}_\lambda - \log Z = -\beta \hat{H}_\lambda + \sum_{k\sigma} \log(1 - \eta_{k\sigma}), \tag{3.72}$$

and if we use $\mathrm{Tr}\{\hat{\rho}_\lambda \hat{H}_\lambda\} = \sum_{k\sigma} \varepsilon_{k\sigma} \eta_{k\sigma}$ we arrive at the final result

$$\begin{aligned}
G_s[\boldsymbol{\gamma}] &= \frac{1}{\beta} \min_{\hat{\rho} \to \boldsymbol{\gamma}} \mathrm{Tr}\{\hat{\rho} \log \hat{\rho}\} = \frac{1}{\beta} \mathrm{Tr}\{\hat{\rho}_\lambda \log \hat{\rho}_\lambda\} \overset{(3.72)}{=} \\
&= \frac{1}{\beta} \sum_{k\sigma} \left[-\beta \varepsilon_{k\sigma} \eta_{k\sigma} + \log(1 - \eta_{k\sigma})\right] \overset{(3.70)}{=} \\
&= \frac{1}{\beta} \sum_{k\sigma} \left[\eta_{k\sigma} \log \eta_{k\sigma} + (1 - \eta_{k\sigma}) \log(1 - \eta_{k\sigma})\right].
\end{aligned} \tag{3.73}$$

Consequently, the universal functional of the noninteracting Fermion entropy

$$S_s[\boldsymbol{\gamma}] = -k_\mathrm{B} \sum_{k\sigma} \left[\eta_{k\sigma} \log \eta_{k\sigma} + (1 - \eta_{k\sigma}) \log(1 - \eta_{k\sigma})\right] \tag{3.74}$$

is independent of the eigenvectors $\boldsymbol{u}_{k\sigma}$ of the SPDM $\boldsymbol{\gamma}$ and solely depends on its eigenvalues $\eta_{k\sigma}$. The entropy functional $S_s[\boldsymbol{\gamma}]$ given in Eq. (3.74) not only applies to noninteracting Fermions but, more generally, to independent Fermions which, for example, are subject to a mean-field interaction, e. g., the average Coulomb-repulsion between electrons which are distributed with a density $n(\boldsymbol{r})$. Therefore, we will refer to S_s defined in Eq. (3.74) as independent-Fermion entropy (IFE).

Let us now return to the given interacting system described by the general Hamiltonian (3.1), and let us try to establish a connection with the noninteracting system

described by Eq. (3.61). To this aim, we first notice that the eq-SPDM of the interacting system minimizes the corresponding grand-potential functional (3.53), i. e., for the eq-SPDM γ of the interacting system it holds

$$\frac{\partial \Omega[\gamma]}{\partial \gamma_{ij\sigma}} = t_{ij\sigma} - \delta_{ij}\,\mu_\sigma + \frac{\partial G[\gamma]}{\partial \gamma_{ij\sigma}} = 0 \quad \forall ij\sigma\,. \tag{3.75}$$

Let us express the functional $G[\gamma]$ as

$$G[\gamma] = G_s[\gamma] + W_{\mathrm{HF}}[\gamma] + G_c[\gamma]\,, \tag{3.76}$$

where $G_s[\gamma]$ is the noninteracting functional (3.67),

$$W_{\mathrm{HF}}[\gamma] = \sum_{\substack{ijkl \\ \sigma\sigma'}} W_{ijkl}^{\sigma\sigma'}\left(\gamma_{ik\sigma}\,\gamma_{jl\sigma'} - \delta_{\sigma\sigma'}\,\gamma_{il\sigma}\,\gamma_{jk\sigma}\right) \tag{3.77}$$

the interaction-energy functional in Hartree-Fock approximation (see Appendix B), and $G_c[\gamma]$ the correlation contribution to the free energy of interacting electrons with eq-SPDM γ. Thus, $G_c[\gamma]$ includes the contribution to $G[\gamma]$ resulting from the changes in the Coulomb energy and the entropy caused by correlation effects. Using Eq. (3.76), we can rewrite the stationary condition Eq. (3.75) as

$$\frac{\partial \Omega[\gamma]}{\partial \gamma_{ij\sigma}} = t_{ij\sigma}^{s}[\gamma] - \delta_{ij}\,\mu_\sigma + \frac{\partial G_s[\gamma]}{\partial \gamma_{ij\sigma}} = 0 \quad \forall ij\sigma\,, \tag{3.78}$$

where we have introduced the effective single-particle hopping integrals

$$t_{ij\sigma}^{s}[\gamma] = t_{ij\sigma} + \frac{\partial W_{\mathrm{HF}}[\gamma]}{\partial \gamma_{ij\sigma}} + \frac{\partial G_c[\gamma]}{\partial \gamma_{ij\sigma}}\,. \tag{3.79}$$

Equation (3.78) is formally identical to the one obtained for an extremal point of the noninteracting grand-potential functional (3.66). Therefore, we conclude that the auxiliary noninteracting system with the hopping integrals t^s given in Eq. (3.79) yields the same eq-SPDM as the interacting system with the hopping matrix t. Thus, Eqs. (3.60), (3.65), and (3.79) establish a scheme by which the eq-SPDM of a given interacting system can be determined from the solution of effective single-particle equations. Since the hopping integrals (3.79) of the auxiliary noninteracting system depend on the SPDM γ itself, the scheme must be implemented in a self consistent manner:

1. Start from an initial guess for the eq-SPDM γ of the interacting system, for example from the eq-SPDM of the corresponding noninteracting system which is obtained by setting $\hat{W} = 0$.

2. Use the current guess for the eq-SPDM $\boldsymbol{\gamma}$ to compute the effective single-particle hopping integrals (3.79), and solve Eq. (3.60) in order to obtain new eigenvectors $\boldsymbol{u}_{k\sigma}$ and the effective single-particle energy levels $\varepsilon_{k\sigma}$. Subsequently, compute the new natural-orbital occupation numbers $\eta_{k\sigma}$ from Eq. (3.65).

3. Compute the new SPDM $\gamma'_{ij\sigma} = \sum_k u_{ik\sigma}\eta_{k\sigma}u^*_{jk\sigma}$ from the new occupation numbers $\eta_{k\sigma}$ and the new eigenvectors $\boldsymbol{u}_{k\sigma}$.

4. Exit if convergence is achieved, i. e., $\gamma'_{ij\sigma} = \gamma_{ij\sigma} \; \forall ij\sigma$. Otherwise, return to step 2 after having updated $\boldsymbol{\gamma}$ with $\boldsymbol{\gamma}'$.

3.2.2 Canonical ensembles

It is well known that in the thermodynamic or macroscopic limit the particle-number fluctuations in equilibrium are insignificant with respect to the actual number of particles and, consequently, the canonical and grand-canonical ensembles become equivalent. Nevertheless, a canonical-ensemble formulation of FT-LDFT would be most desirable in order to describe physical situations involving systems with a rather small and fixed number of particles, such as atoms, molecules, or small clusters. This can be established in a similar fashion as the grand-canonical formulation of FT-LDFT presented in the previous section.

Connection between the hopping matrix and the eq-SPDM

We consider a system of N interacting particles described by a general Hamiltonian of the form (3.1). As usual, we regard the type of particle interaction specified by the parameters $W^{\sigma\sigma'}_{ijkl}$ as fixed, such that the hopping integrals $t_{ij\sigma}$ define the system under study. We will consider a system which is open with respect to exchange of energy with the environment, where the latter is characterized by a fixed temperature $T > 0$. In order to establish a unique connection between the hopping matrix $\boldsymbol{t}$ and the corresponding eq-SPDM $\boldsymbol{\gamma}$, we make use of the Helmholtz variational principle, which replaces the Gibbs variational principle (3.44) in the present canonical formulation of FT-LDFT. To this aim we consider the functional

$$F[\hat{\rho}] = \mathrm{Tr}_N\left\{\hat{\rho}\left(\hat{H} + \frac{1}{\beta}\log\hat{\rho}\right)\right\} . \tag{3.80}$$

The Helmholtz variational-principle states that the free energy is given by

$$F_0 = \min_{\hat{\rho}\in\mathscr{P}_N} F[\hat{\rho}] = -k_{\mathrm{B}}T\log Z_N \quad \text{with} \quad Z_N = \mathrm{Tr}_N\left\{\mathrm{e}^{-\beta\hat{H}}\right\} . \tag{3.81}$$

Here Z_N is the canonical partition function and the minimization is performed within the set $\mathcal{P}_N$ of all density matrices of the form (3.17), i. e., within the set of all positive semidefinite N-particle density matrices with unit trace representing arbitrary N-particle mixed states. It is easy to verify that the functional (3.80) has a local minimum at the canonical density matrix

$$\hat{\rho}_N = \frac{\mathrm{e}^{-\beta\hat{H}}}{Z_N}, \tag{3.82}$$

which characterizes the canonical N-particle equilibrium state of the system described by the Hamiltonian $\hat{H}$. Furthermore, in Appendix C we demonstrate that the minimum is unique and global within $\mathcal{P}_N$, i. e., that the strict inequality

$$F[\hat{\rho}] > F[\hat{\rho}_N] = F_0, \quad \hat{\rho} \neq \hat{\rho}_N \tag{3.83}$$

holds for any density matrix $\hat{\rho} \in \mathcal{P}_N$ different from $\hat{\rho}_N$. In order to establish a unique connection between the hopping matrix t and the canonical eq-SPDM γ we furthermore need a small

Lemma 3.2. *Consider two Hamiltonians $\hat{H}$ and $\hat{H}'$ with the same set of interaction integrals $W_{ijkl}^{\sigma\sigma'}$, then at a given temperature $T > 0$ the corresponding canonical density matrices $\hat{\rho}_N$ and $\hat{\rho}'_N$ are equal, if and only if, the hopping matrices t and t' differ by an additive scalar matrix, i. e., if $t_{ij\sigma} - t'_{ij\sigma} = c\,\delta_{ij}\,\forall ij\sigma$ with $c \in \mathbb{R}$.*

Proof. Assume that the canonical density matrices $\hat{\rho}_N$ and $\hat{\rho}'_N$ which correspond to the Hamiltonians $\hat{H}$ and $\hat{H}'$ are equal. Then it follows from (3.82)

$$\hat{\rho}_N = \hat{\rho}'_N \quad \Leftrightarrow \quad \hat{H} - \hat{H}' = -\frac{1}{\beta}\left(\log Z_N - \log Z'_N\right) = F_0 - F'_0, \tag{3.84}$$

and consequently the operator

$$\Delta\hat{H} = \hat{H} - \hat{H}' = \sum_{ij\sigma}\left(t_{ij\sigma} - t'_{ij\sigma}\right)\hat{c}_{i\sigma}^{\dagger}\hat{c}_{j\sigma} \tag{3.85}$$

must be equal to the free-energy difference $\Delta F_0 = F_0 - F'_0$ which is a constant. Therefore, $\Delta\hat{H}$ must be proportional to the identity $\mathbb{1}_N = \frac{1}{N}\sum_{i\sigma}\hat{c}_{i\sigma}^{\dagger}\hat{c}_{i\sigma}$ in N-particle Hilbert space, which means that $t_{ij\sigma} - t'_{ij\sigma} = c\,\delta_{ij}\,\forall ij\sigma$ must hold with $c = \Delta F_0/N \in \mathbb{R}$. $\square$

Theorem 3.4. *For any fixed particle number N and temperature $T > 0$, the hopping matrix t of the interacting N-particle system described by the Hamiltonian (3.1) is (besides of an additive scalar matrix) a functional of the canonical eq-SPDM γ.*

Proof. Assume there would be *another* hopping matrix t' which differs from t by more than an additive scalar matrix but, nevertheless, for the given particle number N and temperature $T > 0$ leads to the *same* canonical eq-SPDM γ as the hopping matrix t. If $\hat{H}'$ and $\hat{\rho}'_N$ denote the Hamiltonian and canonical density matrix of the system with the hopping matrix t', the corresponding free energy is given by

$$F'_0 = \sum_{ij\sigma} t'_{ij\sigma}\, \gamma_{ij\sigma} + \mathrm{Tr}_N\left\{\hat{\rho}'_N \left(\hat{W} + \frac{1}{\beta} \log \hat{\rho}'_N\right)\right\}. \tag{3.86}$$

Since the hopping matrices t and t' differ by more than an additive scalar matrix, it follows from Lemma 3.2 that the corresponding canonical density matrices $\hat{\rho}_N$ and $\hat{\rho}'_N$ must be different as well. Thus, from the minimal principle (3.83) it follows that

$$F_0 < F[\hat{\rho}'_N] = \mathrm{Tr}_N\left\{\hat{\rho}'_N \left(\hat{H} + \frac{1}{\beta} \log \hat{\rho}'_N\right)\right\} = F'_0 + \sum_{ij\sigma}\left(t_{ij\sigma} - t'_{ij\sigma}\right) \gamma_{ij\sigma}. \tag{3.87}$$

By interchanging primed and unprimed quantities one obtains

$$F'_0 < F_0 + \sum_{ij\sigma}\left(t'_{ij\sigma} - t_{ij\sigma}\right) \gamma_{ij\sigma}. \tag{3.88}$$

Adding Eqs. (3.87) and (3.88) the contradiction

$$F_0 + F'_0 < F'_0 + F_0 \tag{3.89}$$

is obtained. This proves that two hopping matrices t and t' which differ by more than an additive scalar matrix cannot lead to the same canonical eq-SPDM γ for a given particle number N and temperature $T > 0$. One concludes that t is (besides of an additive real constant) a functional of γ. □

In contrast to the grand-canonical formulation of FT-LDFT, where Theorem 3.3 establishes a unique connection between the grand-canonical eq-SPDM and the hopping matrix t, the canonical eq-SPDM determines the hopping matrix t only up to an additive scalar matrix. Such a scalar matrix is, however, without physical relevance, since it corresponds to a uniform shift of all single-particle energy levels which can be absorbed in the chemical potential or, equivalently, compensated for by choosing the reference point of the energy scale appropriately. Thus, from a physical point of view we can regard the hopping matrix t as uniquely determined by the canonical eq-SPDM. Furthermore, since the hopping matrix characterizes the system under study, the canonical eq-SPDM γ determines the full Hamiltonian $\hat{H}$ such that all physical properties derived from it must be functionals of the eq-SPDM as well. This applies in particular to the canonical density-matrix (3.82), which immediately proves the important

Corollary 3.5. *For any fixed particle number N and temperature $T > 0$, the canonical density-matrix $\hat{\rho}_N$ of the interacting N-particle system described by the Hamiltonian (3.1) is a functional of the canonical eq-SPDM $\boldsymbol{\gamma}$.*

It is obvious that the converse statement is also true, namely that the canonical eq-SPDM $\gamma_{ij\sigma} = \text{Tr}_N\{\hat{\rho}_N \, \hat{c}_{i\sigma}^\dagger \hat{c}_{j\sigma}\}$ is uniquely determined by the canonical density matrix $\hat{\rho}_N$. This establishes a bijective map between the set of the canonical density-matrices and the corresponding set of the canonical eq-SPDMs. A further important consequence of Theorem 3.4 is

Corollary 3.6. *For a fixed particle number N and temperature $T > 0$, the canonical equilibrium average-value of any observable $\hat{O}$ is a functional of the canonical eq-SPDM $\boldsymbol{\gamma}$.*

Proof. From Corollary 3.5 we know that the canonical density matrix $\hat{\rho}_N = \hat{\rho}_N[\boldsymbol{\gamma}]$ is a functional of the canonical eq-SPDM $\boldsymbol{\gamma}$. Therefore, the canonical equilibrium average value of any observable $\hat{O}$ can be obtained from the canonical eq-SPDM as

$$O[\boldsymbol{\gamma}] = \text{Tr}_N\{\hat{\rho}_N[\boldsymbol{\gamma}]\,\hat{O}\}. \tag{3.90}$$

$\square$

Similar to the grand-canonical formulation of FT-LDFT presented in Section 3.2.1, the canonical formulation must rely on a functional from which the eq-SPDM can be obtained by means of a variational principle. Again, we will construct this functional by a constrained search method, which allows us to bypass all problems related to the representability of canonical eq-SPDMs. To this aim, for a given particle number N and temperature T we introduce the functional

$$G_N[\boldsymbol{\gamma}] = \min_{\hat{\rho}\to\boldsymbol{\gamma}} \text{Tr}_N\left\{\hat{\rho}\left(\hat{W} + \frac{1}{\beta}\log\hat{\rho}\right)\right\}, \tag{3.91}$$

where the notation $\hat{\rho} \to \boldsymbol{\gamma}$ indicates the minimization with respect to all density matrices $\hat{\rho} \in \mathcal{P}_N$ which yield the given SPDM by means of $\gamma_{ij\sigma} = \text{Tr}_N\{\hat{\rho}\,\hat{c}_{i\sigma}^\dagger \hat{c}_{j\sigma}\}$. Despite their formal similarity, the functional (3.91) does not coincide with its grand-canonical analog $G[\boldsymbol{\gamma}]$ defined in Eq. (3.52). First, $G_N[\boldsymbol{\gamma}]$ is defined on the set of all ensemble N-representable SPDMs $\boldsymbol{\gamma} \in \Gamma_e(N)$ satisfying the conditions (3.18), while $G[\boldsymbol{\gamma}]$ is defined on the larger set Γ_e formed by the ensemble representable SPDMs which are only constrained by the first condition in Eq. (3.18). Furthermore, even on the common subset $\Gamma_e(N) \subset \Gamma_e$ the functional $G_N[\boldsymbol{\gamma}]$ is just an upper bound for $G[\boldsymbol{\gamma}]$, i. e.,

$$G_N[\boldsymbol{\gamma}] \geq G[\boldsymbol{\gamma}] \quad \text{for} \quad \boldsymbol{\gamma} \in \Gamma_e(N), \tag{3.92}$$

since $G[\gamma]$ is obtained from the minimization with respect all density matrices $\hat{\rho} \in \mathcal{P}$ describing mixed-states with arbitrary particle number, while $G_N[\gamma]$ is obtained from the minimization with respect to the subset $\mathcal{P}_N \subset \mathcal{P}$ formed by all N-particle mixed-states.

A similarity between the functional $G_N[\gamma]$ and its grand-canonical analog (3.52) is, however, its universal character in the sense that it does not depend on the hopping integrals $t_{ij\sigma}$ which characterize the system under study. It depends on the particle number N, on the temperature T, and on the set of interaction integrals $W_{ijkl}^{\sigma\sigma'}$. Furthermore, it depends on the N-particle Hilbert space under consideration, since the density operators $\hat{\rho}$ in the minimization of Eq. (3.91) are operators within this Hilbert space.

Using the functional $G_N[\gamma]$ defined in Eq. (3.91), we can now introduce the free energy functional

$$F[\gamma] = \sum_{ij\sigma} t_{ij\sigma}\, \gamma_{ij\sigma} + G_N[\gamma], \qquad (3.93)$$

whose minimal value within the set $\Gamma_{\mathrm{e}}(N)$ of all ensemble N-representable SPDMs equals the free energy F_0. This can be most easily seen by performing the minimization in the Helmholtz variational-principle (3.81) in two consecutive steps:

$$F_0 = \min_{\hat{\rho}\in\mathcal{P}_N} \mathrm{Tr}_N\left\{\hat{\rho}\left(\hat{H} + \frac{1}{\beta}\log\hat{\rho}\right)\right\} =$$

$$= \min_{\gamma\in\Gamma_{\mathrm{e}}(N)} \left[\sum_{ij\sigma} t_{ij\sigma}\,\gamma_{ij\sigma} + \min_{\hat{\rho}\to\gamma} \mathrm{Tr}_N\left\{\hat{\rho}\left(\hat{W} + \frac{1}{\beta}\log\hat{\rho}\right)\right\}\right] = \qquad (3.94)$$

$$= \min_{\gamma\in\Gamma_{\mathrm{e}}(N)} \left[\sum_{ij\sigma} t_{ij\sigma}\,\gamma_{ij\sigma} + G_N[\gamma]\right] = \min_{\gamma\in\Gamma_{\mathrm{e}}(N)} F[\gamma].$$

Furthermore, from Eq. (3.83) it follows that the density matrix $\hat{\rho}$ which yields the minimum in Eq. (3.94) must be the canonical density-matrix (3.82) associated with the given hopping matrix t, particle number N, and temperature T. Consequently, the minimizing SPDM γ corresponds to the canonical eq-SPDM.

In order to develop a practical implementation of the functional $G_N[\gamma]$, let us perform the minimization in Eq. (3.91) in an explicit manner. To this aim we seek for the extremes of the Euler-Lagrange functional

$$\mathcal{L}_N[\hat{\rho}] = \mathrm{Tr}_N\left\{\hat{\rho}\left(\hat{W} + \frac{1}{\beta}\log\hat{\rho}\right)\right\} + \sum_{ij\sigma}\lambda_{ij\sigma}\left(\mathrm{Tr}_N\left\{\hat{\rho}\,\hat{c}_{i\sigma}^{\dagger}\hat{c}_{j\sigma}\right\} - \gamma_{ij\sigma}\right) =$$

$$\qquad (3.95)$$

$$= \mathrm{Tr}_N\left\{\hat{\rho}\left(\sum_{ij\sigma}\lambda_{ij\sigma}\,\hat{c}_{i\sigma}^{\dagger}\hat{c}_{j\sigma} + \hat{W} + \frac{1}{\beta}\log\hat{\rho}\right)\right\} - \sum_{ij\sigma}\lambda_{ij\sigma}\,\gamma_{ij\sigma}$$

within the set $\mathcal{P}_N$ of all positive semidefinite N-particle density matrices $\hat{\rho}$ with unit trace. As usual, we have introduced Lagrange multipliers $\lambda_{ij\sigma}$ in order to enforce that the minimizing density matrix $\hat{\rho}$ yields the required SPDM γ. Apart from an irrelevant constant, the Euler-Lagrange functional (3.95) equals the Helmholtz functional (3.80) with the effective Hamiltonian

$$\hat{H}_\lambda = \sum_{ij\sigma} \lambda_{ij\sigma}\, \hat{c}_{i\sigma}^\dagger \hat{c}_{j\sigma} + \hat{W}\,. \tag{3.96}$$

Consequently, the minimum of the Euler-Lagrange functional (3.95) within the set $\mathcal{P}_N$ is attained for the corresponding canonical density matrix

$$\hat{\rho}_\lambda = \frac{e^{-\beta \hat{H}_\lambda}}{\mathrm{Tr}_N\{e^{-\beta \hat{H}_\lambda}\}}\,. \tag{3.97}$$

The parameters $\lambda_{ij\sigma}$ in the Hamiltonian (3.96) play the role of effective energy levels ($i = j$) and effective hopping integrals ($i \neq j$), which must be chosen such that the canonical density matrix (3.97) yields the required SPDM via $\gamma_{ij\sigma} = \mathrm{Tr}_N\{\hat{\rho}_\lambda\, \hat{c}_{i\sigma}^\dagger \hat{c}_{j\sigma}\}$. In practice, one usually varies the parameters $\lambda_{ij\sigma}$ systematically in order to scan the whole domain of canonical eq-SPDMs. Like in the previously considered grand-canonical case, this procedure requires one to compute the canonical density matrix (3.97), which is usually expressed in terms of the N-particle eigenstates and eigenvalues of the effective Hamiltonian $\hat{H}_\lambda$. The thus described procedure is therefore in general of the same level of complexity as the initial problem with the Hamiltonian (3.1) and is therefore only applicable to systems which can be solved by analytical or numerical methods.

Mapping to an effective noninteracting system

The mapping between a given interacting N-particle system and a noninteracting system having the same canonical eq-SPDM can be established in a similar fashion as in the previous grand-canonical formulation of FT-LDFT. To this aim, we seek for a noninteracting system described by the general single-particle Hamiltonian

$$\hat{H}_s = \sum_{ij\sigma} t_{ij\sigma}^s\, \hat{c}_{i\sigma}^\dagger \hat{c}_{j\sigma} = \sum_{k\sigma} \varepsilon_{k\sigma}\, \hat{n}_{k\sigma} \tag{3.98}$$

which yields the same canonical eq-SPDM γ as the given interacting system. Here, $\hat{n}_{k\sigma} = \hat{b}_{k\sigma}^\dagger \hat{b}_{k\sigma}$ is the number operator for the natural orbital $k\sigma$ defined in Eqs. (3.59) and (3.60), and $\varepsilon_{k\sigma}$ is the corresponding orbital energy. The canonical density matrix of the noninteracting system described by the Hamiltonian (3.98) is given by

$$\hat{\rho}_N = \frac{e^{-\beta \sum_{k\sigma} \varepsilon_{k\sigma} \hat{n}_{k\sigma}}}{\mathrm{Tr}_N\{e^{-\beta \sum_{k\sigma} \varepsilon_{k\sigma} \hat{n}_{k\sigma}}\}}\,, \tag{3.99}$$

and consequently it holds

$$\mathrm{Tr}_N\{\hat{\rho}_N\,\hat{b}^\dagger_{k\sigma}\,\hat{b}_{k'\sigma}\} = \delta_{kk'}\mathrm{Tr}_N\{\hat{\rho}_N\,\hat{n}_{k\sigma}\} = \delta_{kk'}\,\eta_{k\sigma}\,, \tag{3.100}$$

where $\eta_{k\sigma} = \mathrm{Tr}_N\{\hat{\rho}_N\,\hat{n}_{k\sigma}\}$ is the canonical equilibrium occupation-number of the natural orbital $k\sigma$. Analog to Eq. (3.64), we obtain the canonical eq-SPDM of the noninteracting system described by the Hamiltonian (3.98) as

$$\gamma_{ij\sigma} = \sum_k u_{ik\sigma}\,\eta_{k\sigma}\,u^*_{jk\sigma}\,. \tag{3.101}$$

We conclude that the eigenvalues $\eta_{k\sigma} \in [0,1]$ of the canonical eq-SPDM correspond to the canonical equilibrium occupation numbers of the natural orbitals, and its eigenvectors $\boldsymbol{u}_{k\sigma}$ coincide with the eigenvectors of the transposed hopping matrix $\left(\boldsymbol{t}^s_\sigma\right)^\top$ [see Eq. (3.60)]. Clearly, the SPDM (3.101) minimizes the noninteracting free-energy functional

$$F_s[\boldsymbol{\gamma}] = \sum_{ij\sigma} t^s_{ij\sigma}\,\gamma_{ij\sigma} + G_s[\boldsymbol{\gamma};N] \tag{3.102}$$

within the set $\Gamma_e(N)$ of all ensemble N-representable SPDMs $\boldsymbol{\gamma}$, where

$$G_s[\boldsymbol{\gamma};N] = -T\,S_s[\boldsymbol{\gamma};N] = \frac{1}{\beta}\min_{\hat{\rho}\to\boldsymbol{\gamma}}\mathrm{Tr}_N\{\hat{\rho}\,\log\hat{\rho}\} \tag{3.103}$$

is, apart of the factor $-T$, the universal entropy functional $S_s[\boldsymbol{\gamma};N]$ for N noninteracting Fermions. In contrast to its grand-canonical analog (3.74), no general explicit expression is available for the functional $S_s[\boldsymbol{\gamma};N]$.

Let us now try to establish a connection between the given interacting system described by the general Hamiltonian (3.1) and the noninteracting system described by Eq. (3.98). Clearly, the canonical eq-SPDM of the interacting system minimizes the corresponding free-energy functional (3.93), i. e., for the canonical eq-SPDM $\boldsymbol{\gamma}$ of the interacting system it must hold

$$\frac{\partial F[\boldsymbol{\gamma}]}{\partial \gamma_{ij\sigma}} = t_{ij\sigma} + \frac{\partial G_N[\boldsymbol{\gamma}]}{\partial \gamma_{ij\sigma}} = 0 \quad \forall ij\sigma\,. \tag{3.104}$$

Let us express the functional $G_N[\boldsymbol{\gamma}]$ as

$$G_N[\boldsymbol{\gamma}] = G_s[\boldsymbol{\gamma};N] + W_{\mathrm{HF}}[\boldsymbol{\gamma};N] + G_c[\boldsymbol{\gamma};N]\,, \tag{3.105}$$

where $G_s[\boldsymbol{\gamma};N]$ is the noninteracting functional (3.103), $W_{\mathrm{HF}}[\boldsymbol{\gamma};N]$ the interaction-energy functional in Hartree-Fock approximation, and $G_c[\boldsymbol{\gamma};N]$ the correlation contribution to the free energy of N interacting Fermions. Here, the interaction-energy functional in Hartree-Fock approximation is given by $W_{\mathrm{HF}}[\boldsymbol{\gamma};N] = \mathrm{Tr}_N\{\hat{\rho}_N[\boldsymbol{\gamma}]\,\hat{W}\}$,

where $\hat{\rho}_N[\boldsymbol{\gamma}]$ is the canonical density matrix of the unique noninteracting system whose canonical eq-SPDM equals $\boldsymbol{\gamma}$. Notice, however, that the explicit expression (B.10) for the interaction energy in Hartree-Fock approximation, derived in Appendix B, is not valid for $W_{\mathrm{HF}}[\boldsymbol{\gamma}; N]$, since $\hat{\rho}_N[\boldsymbol{\gamma}]$ does not describe an uncorrelated mixed-state (see Appendix B).

Using Eq. (3.105), we can rewrite the stationary condition Eq. (3.104) as

$$\frac{\partial F[\boldsymbol{\gamma}]}{\partial \gamma_{ij\sigma}} = t^s_{ij\sigma}[\boldsymbol{\gamma}] + \frac{\partial G_s[\boldsymbol{\gamma}; N]}{\partial \gamma_{ij\sigma}} = 0 \quad \forall ij\sigma \,, \tag{3.106}$$

where we have introduced the effective single-particle hopping integrals

$$t^s_{ij\sigma}[\boldsymbol{\gamma}] = t_{ij\sigma} + \frac{\partial W_{\mathrm{HF}}[\boldsymbol{\gamma}; N]}{\partial \gamma_{ij\sigma}} + \frac{\partial G_c[\boldsymbol{\gamma}; N]}{\partial \gamma_{ij\sigma}} \,. \tag{3.107}$$

Equation (3.106) is formally identical to the condition one would obtain for an extremal point of the noninteracting free-energy functional (3.102). Therefore, we conclude that the auxiliary noninteracting system with the hopping integrals $\boldsymbol{t}^s$ given in Eq. (3.107) yields the same canonical eq-SPDM as the interacting system with the hopping matrix $\boldsymbol{t}$. Thus, Eqs. (3.60), (3.99), and (3.107) establish a scheme from which the canonical eq-SPDM of a given interacting system can be determined by the solution of effective single-particle equations. Since the hopping integrals (3.107) of the auxiliary noninteracting system depend on the SPDM $\boldsymbol{\gamma}$ itself, the scheme must be solved in a selfconsistent manner:

1. Start from an initial guess for the canonical eq-SPDM $\boldsymbol{\gamma}$ of the interacting system, for example from the canonical eq-SPDM of the corresponding noninteracting system which is obtained by setting $\hat{W} = 0$.

2. Use the current guess for the canonical eq-SPDM $\boldsymbol{\gamma}$ to compute the effective single-particle hopping integrals (3.107), and solve Eq. (3.60) in order to obtain new eigenvectors $\boldsymbol{u}_{k\sigma}$ and the effective single-particle energy levels $\varepsilon_{k\sigma}$. Subsequently, compute the new natural-orbital occupation numbers $\eta_{k\sigma} = \mathrm{Tr}_N\{\hat{\rho}_N \hat{n}_{k\sigma}\}$, where $\hat{\rho}_N$ is the canonical density matrix (3.99) of the effective noninteracting system.

3. Compute the new SPDM $\gamma'_{ij\sigma} = \sum_k u_{ik\sigma}\eta_{k\sigma}u^*_{jk\sigma}$ from the new occupation numbers $\eta_{k\sigma}$ and the new eigenvectors $\boldsymbol{u}_{k\sigma}$.

4. Exit if convergence is achieved, i. e., $\gamma'_{ij\sigma} = \gamma_{ij\sigma} \; \forall ij\sigma$. Otherwise, return to step 2 after having updated $\boldsymbol{\gamma}$ with $\boldsymbol{\gamma}'$.

Exploiting the links between ground-state correlations and the independent-Fermion entropy

<div style="text-align:right">**4**</div>

In the past decades a large number of studies have been devoted to the problem of electron correlations by applying the methods of density functional theory (DFT) to lattice models [1, 69–87]. Indeed, taking into account the universality of DFT and its efficiency in various complex *ab-initio* calculations, it is physically reasonable to expect that DFT combined with a suitable ansatz for the kinetic- and interaction-energy functionals should be a valuable approach for correlated lattice models. Early studies have been devoted to the band-gap problem in semiconductors [69–71] and have addressed the importance of the off-diagonal elements of the density matrix in the description of strong correlation effects [72]. Density-matrix functionals for the Anderson and Hubbard models have been successfully applied [73, 75] and even some time-dependent approaches have been proposed [76]. In the context of this thesis we focus on the lattice density functional theory (LDFT) formulated in Chapter 3, which considers the single-particle density matrix (SPDM) γ as central variable of the many-body problem.

Several important lattice models of strongly interacting electrons have been addressed within the framework of LDFT. This includes the single-impurity Anderson model [81–83] as well as the Hubbard model with homogeneous and inhomogeneous local potentials, dimerized chains, attractive pairing interactions, and inhomogeneous local repulsions [77–80, 83–87]. The basic idea behind the functionals proposed in previous approaches is to adopt a real-space perspective, and to take advantage of scaling properties of the interaction energy W as a function of the bond order $\gamma_{12\sigma}$, which measures the degree of charge fluctuations between nearest neighbors (NNs). The actual dependence of W on $\gamma_{12\sigma}$ can then be inferred from the exact solution of a reference system, such as the two-site problem (dimer), or some other exactly solvable system. By doing so, the dependence of W on the remaining SPDM elements $\gamma_{ij\sigma}$ has been absorbed in the Levy-Lieb minimization (see Section 3.1.2), which is possible whenever lattice models with hoppings only between NNs are considered, since the kinetic energy K depends only on $\gamma_{12\sigma}$ in this case such that the dependence of W on

---

other SPDM elements is irrelevant for the minimization of the energy $E = T + W$. While the restriction to NN hoppings and SPDM elements is a useful simplification, it also brings about some profound limitations. Indeed, these approaches can only yield the ground-state values of the diagonal and NN elements of the SPDM. This means that more complex observables, whose functional dependence $O[\gamma]$ involves all SPDM elements, as well as physical situations requiring interatomic hoppings beyond NNs, remain out of scope. Therefore, the domain of applicability of these previous approaches in the framework of LDFT remained somewhat limited. It should be furthermore noted that the interaction-energy functional $W[\gamma]$ forfeits its universal character if its dependence on most of the SPDM elements is absorbed in the Levy-Lieb minimization procedure. Consequently, taking into account the dependence of W on the complete SPDM γ is both desirable and necessary in order to leverage the full universality of LDFT. In fact, an approach based on the full SPDM would allow us to investigate the distance dependence of $\gamma_{ij\sigma}$ and thus the long-range electron mobility, which is most interesting in the context of strong electron correlations, even if the actual hybridizations are short-ranged as it is usually the case in narrow-band systems. In this way it should be possible to investigate how electron localization develops in real space as the Coulomb-repulsion strength increases.

Keeping these motivations and challenges in mind, we devote the present chapter to the development of an interaction-energy functional $W[\gamma]$ for the Hubbard model which takes into account its dependence on the full SPDM. To this aim, we will adopt a delocalized $\mathbf{k}$-space perspective and focus on homogeneous periodic systems. First, we investigate the dependence of W on the eigenvalues $\eta_{\mathbf{k}\sigma}$ of the SPDM, which represent the spin-dependent occupation numbers of the natural orbitals. Second, we will derive a simple, yet very effective approximation to $W[\gamma]$ by exploiting certain analogies between electron correlations in the ground state and the entropy of independent fermions having the occupation numbers $\eta_{\mathbf{k}\sigma}$. Finally, we apply our new functional to finite and infinite lattices in 1–3 dimensions as well as to the limit of infinite dimensions. We will consider a variety of interesting physical situations, including spin-polarized systems, correlated Fermions subject to an attractive interaction, and we will study systems with arbitrary electron density exhibiting Luttinger-liquid behavior.

4.1 Reciprocal-space approximation to $W[\gamma]$

In order to derive an approximation to the interaction-energy functional $W[\gamma]$ which takes into account the dependence of W on the full SPDM γ, we will adopt a $\mathbf{k}$-space

perspective and focus on the homogeneous and periodic single-band Hubbard model

$$\hat{H} = \hat{K} + \hat{W} = \sum_{ij\sigma} t_{ij}\, \hat{c}_{i\sigma}^{\dagger} \hat{c}_{j\sigma} + U \sum_i \hat{n}_{i\uparrow}\hat{n}_{i\downarrow}\,. \qquad (4.1)$$

In the usual notation, t_{ij} stands for the hopping integral between atoms or lattice sites at the positions $\boldsymbol{R}_i$ and $\boldsymbol{R}_j$, and U for the local Coulomb-repulsion strength. Due to the translational symmetry of the underlying lattice, the elements of the corresponding ground-state single-particle density matrix (gs-SPDM) $\gamma_{ij\sigma}$ depend only on the vector $\boldsymbol{R}_i - \boldsymbol{R}_j$ connecting the lattice sites i and j, such that we can write

$$\gamma_{ij\sigma} = \gamma_{\sigma}(\boldsymbol{R}_i - \boldsymbol{R}_j) = \frac{1}{N_a} \sum_{\boldsymbol{k}\in\mathrm{BZ}} \eta_{\boldsymbol{k}\sigma}\, \mathrm{e}^{-i\boldsymbol{k}\cdot(\boldsymbol{R}_i - \boldsymbol{R}_j)}\,, \qquad (4.2)$$

where we have introduced the Fourier transform $\eta_{\boldsymbol{k}\sigma}$ of the gs-SPDM. More generally, Eq. (4.2) holds for any SPDM that is consistent with the translational symmetry of the underlying lattice. Comparing Eqs. (3.24) and (4.2) we infer the eigenvectors

$$u_{i\boldsymbol{k}\sigma} = \frac{1}{\sqrt{N_a}}\, \mathrm{e}^{-i\boldsymbol{k}\cdot\boldsymbol{R}_i} \qquad (4.3)$$

of the SPDM as well as the corresponding eigenvalues

$$\eta_{\boldsymbol{k}\sigma} = \sum_{i=1}^{N_a} \gamma_{\sigma}(\boldsymbol{R}_i)\, \mathrm{e}^{i\boldsymbol{k}\cdot\boldsymbol{R}_i}\,. \qquad (4.4)$$

Consequently, any SPDM that is consistent with the translational symmetry of the given lattice structure is fully characterized by its eigenvalues $\eta_{\boldsymbol{k}\sigma} = \langle \hat{b}_{\boldsymbol{k}\sigma}^{\dagger} \hat{b}_{\boldsymbol{k}\sigma} \rangle$, which represent the average occupation numbers of the corresponding Bloch-states

$$\hat{b}_{\boldsymbol{k}\sigma}^{\dagger} = \frac{1}{\sqrt{N_a}} \sum_i \mathrm{e}^{i\boldsymbol{k}\cdot\boldsymbol{R}_i}\, \hat{c}_{i\sigma}^{\dagger}\,. \qquad (4.5)$$

If we focus on the Hubbard model on a given periodic lattice structure and are interested in the ground-state properties, we can restrict our considerations to the SPDMs which are consistent with translational symmetry. In this case, we can regard the SPDM functional of any physical observable $O = O[\eta]$ as functional of the occupation numbers $\boldsymbol{\eta} = \{\eta_{\boldsymbol{k}\sigma}\}$ alone, since they characterize the corresponding translational symmetric SPDM. This applies in particular to the functionals $K[\eta]$, $W[\eta]$, and $E[\eta]$ of the kinetic, interaction, and total energy. For example, the kinetic-energy functional expressed in terms of the occupation numbers $\eta_{\boldsymbol{k}\sigma}$ is given by

$$K[\eta] = \sum_{\boldsymbol{k}\sigma} \varepsilon_{\boldsymbol{k}}\, \eta_{\boldsymbol{k}\sigma}\,, \qquad (4.6)$$

where

$$\varepsilon_{\boldsymbol{k}} = \sum_{i=1}^{N_a} t(R_i) \cos(\boldsymbol{k} \cdot \boldsymbol{R}_i) \tag{4.7}$$

is the single-particle dispersion relation. Here we made use of the fact that the hopping integrals $t_{ij} = t(R_{ij})$ between the local orbitals at the sites i and j depend only on the mutual distance $R_{ij} = |\boldsymbol{R}_i - \boldsymbol{R}_j|$ due to the translational symmetry.

In order to derive a physically sound approximation to the interaction-energy functional $W[\boldsymbol{\eta}]$, it is very useful to consider two important limiting cases. The first one concerns idempotent SPDMs, i. e., $\boldsymbol{\gamma}^2 = \boldsymbol{\gamma}$, which implies $\eta_{\boldsymbol{k}\sigma} \in \{0, 1\}$ for all $\boldsymbol{k}\sigma$. The corresponding many-particle state is the single Slater determinant made of the occupied Bloch states which are defined in Eq. (4.5). The associated interaction energy W is equal to

$$W_{\mathrm{HF}} = U \sum_i \gamma_{ii\uparrow}\gamma_{ii\downarrow} = U N_a\, n_\uparrow n_\downarrow\,, \tag{4.8}$$

where we have used that $\gamma_{ii\sigma} = n_\sigma = N_\sigma/N_a$ for $i = 1, \ldots, N_a$ [see Eq. (B.10) in Appendix B]. The second important limiting case concerns scalar SPDMs, i. e., $\boldsymbol{\gamma}_\sigma = \mathbb{1} n_\sigma$, which implies that the corresponding occupation numbers $\eta_{\boldsymbol{k}\sigma} = n_\sigma$ are independent of $\boldsymbol{k}$. This situation describes a fully localized state since $\gamma_{ij\sigma} = 0$ for all $i \neq j$. The associated ground-state interaction energy is given by

$$W_\infty = U D_\infty\,, \quad \text{where} \quad D_\infty = \begin{cases} 0 & \text{if } N \leq N_a \\ N - N_a & \text{if } N > N_a \end{cases} \tag{4.9}$$

is the minimal number of double occupations for N localized electrons distributed among the N_a orbitals. Any physically sound approximation to the interaction-energy functional $W[\boldsymbol{\eta}]$ should be able to reproduce these two important limiting cases, i. e., the results (4.8) and (4.9) for idempotent and scalar SPDMs.

In this context it is useful to consider the independent-Fermion entropy (IFE)[1]

$$S[\boldsymbol{\eta}] = -k_{\mathrm{B}} \sum_{\boldsymbol{k}\sigma} \left[\eta_{\boldsymbol{k}\sigma} \log \eta_{\boldsymbol{k}\sigma} + (1 - \eta_{\boldsymbol{k}\sigma}) \log(1 - \eta_{\boldsymbol{k}\sigma}) \right], \tag{4.10}$$

representing the entropy of an arbitrary occupation-number distribution $\boldsymbol{\eta} \in [0, 1]^{2N_a}$. It is easy to verify that $S[\boldsymbol{\eta}]$ assumes its minimal value $S = 0$ if $\eta_{\boldsymbol{k}\sigma} \in \{0, 1\}$ for all $\boldsymbol{k}\sigma$,

---

[1]Notice that the inclusion of the Boltzmann constant k_{B} in Eq. (4.10) is arbitrary and that it could be dropped as in the usual mathematical definition of the entropy of a probability distribution [104]. Here we shall keep it in order to facilitate some physical interpretations. It is, however, important to keep in mind that this chapter, and in particular the functionals derived and applied in it, are aimed towards the description of *ground-state* properties exclusively. The utility of the IFE defined in Eq. (4.10) and the corresponding finite-temperature analog results from the fact that the entropy of the occupation-number distribution $\{\eta_{\boldsymbol{k}\sigma}\}$ is the quantity which best characterizes its diversity.

and that its maximum under the constraint $N_\sigma = \sum_k \eta_{k\sigma}$ is attained when $\eta_{k\sigma} = N_\sigma/N_a = n_\sigma$ for all $\boldsymbol{k}\sigma$. In the important case of a half-filled band, i. e., $n_\uparrow + n_\downarrow = 1$, the maximum of the IFE is given by

$$S_\infty = -2N_a k_B \left[n_\uparrow \log(n_\uparrow) + n_\downarrow \log(n_\downarrow) \right] . \tag{4.11}$$

Notice that the IFE (4.10) assumes its extremes for idempotent and scalar SPDMs, just as the interaction energy W. This suggests to use $S[\boldsymbol{\eta}]$ as a measure of the degree of electronic correlations, in terms of which the functional dependence of $W[\boldsymbol{\gamma}]$ could be effectively approximated.

In order to assess the actual connection between the IFE (4.10) and the interaction energy W in the ground state of the half-filled Hubbard model, we have performed exact numerical Lanczos diagonalizations for a number of lattice structures and system sizes. A variety of ground-state occupation-number distributions $\{\eta_{k\sigma}\}$ has been obtained by scaling the hopping integrals in the Hubbard-model Hamiltonian (4.1) from $t_{ij} = 0$ to $t_{ij} \gg U$. In this way, the complete range $0 \le S \le S_\infty$ of the IFE has been scanned. Our results, presented in Fig. 4.1, show a remarkable one-to-one correspondence between W and S, which is approximately independent of the size and dimension of the system under consideration if it is properly scaled by the maximum values W_{HF} and S_∞. It is, however, important to notice that the results shown in Fig. 4.1 suggest a relation between W and S only for the ground state, i. e., for the case of *ground-state representable* occupation-number distributions $\{\eta_{k\sigma}\}$. For the more general case of occupation-number distributions which are not ground-state representable, i. e., which are not associated to any ground state of the model under consideration, there is no one-to-one relation between the IFE S and the interaction energy W, as we will demonstrate in the following. To this aim, let us assume there would be a one-to-one correspondence between W and S for arbitrary occupation-number distributions which are only constrained by the ensemble-representability condition $0 \le \eta_{k\sigma} \le 1 \ \forall \boldsymbol{k}\sigma$. This means, we assume that the interaction-energy functional

$$W[\boldsymbol{\eta}] = W(S[\boldsymbol{\eta}]) \tag{4.12}$$

can be expressed as an ordinary function of the IFE defined in Eq. (4.10). In order to obtain the ground-state energy E_0 and the ground-state occupation numbers for a given number N_σ of electrons with spin polarization σ, we have to minimize the energy functional

$$E[\boldsymbol{\eta}] = \sum_{k\sigma} \varepsilon_k \, \eta_{k\sigma} + W(S[\boldsymbol{\eta}]) \tag{4.13}$$

within the domain of the ensemble-representable occupation-number distributions which correspond to the given particle number. To this aim, we seek for the extremes
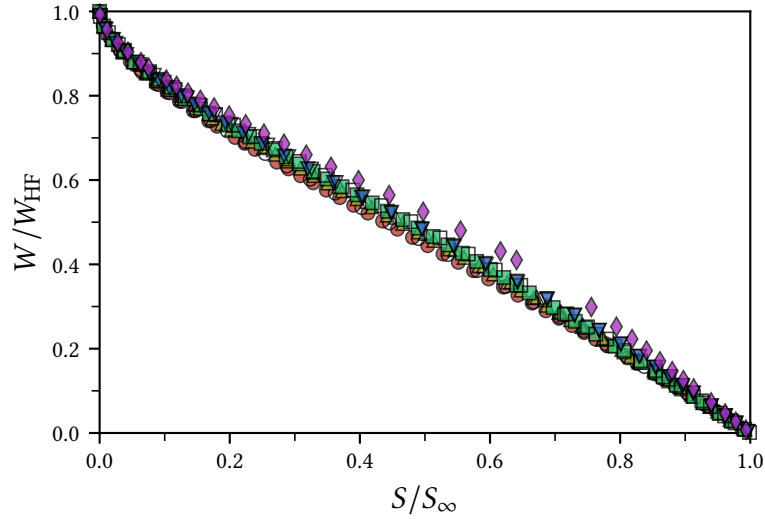
Figure 4.1: Relation between the interaction energy W and the IFE S in the ground state of the half-filled Hubbard model, as obtained from exact numerical Lanczos diagonalizations for a number of different periodic lattice structures. Results are shown for finite 1D rings having $N_a = 6$ (circles), $N_a = 10$ (upright triangles) and $N_a = 14$ (squares) lattice sites, as well as for 2D square-lattices having $N_a = 2{\times}4$ (downright triangles) and $N_a = 3{\times}4$ (diamonds) lattice sites. The solid symbols correspond to the Hubbard model with only NN hopping t, while the open symbols represent results where also second-NN hoppings $t_2 = t/2$ are taken into account. Adapted from Müller *et al.* [1], ©2018 American Physical Society.

of the corresponding Euler-Lagrange functional

$$\mathcal{L} = E[\boldsymbol{\eta}] + \sum_{\sigma} \mu_{\sigma} \left(N_{\sigma} - \sum_{k} \eta_{k\sigma} \right), \tag{4.14}$$

where the Lagrange multipliers μ_{σ} enforce the given number $N_{\sigma} = \sum_{k} \eta_{k\sigma}$ of spin-σ electrons. At an extreme of the Euler-Lagrange functional (4.14) one has

$$\frac{\partial \mathcal{L}}{\partial \eta_{k\sigma}} = \frac{\partial E[\boldsymbol{\eta}]}{\partial \eta_{k\sigma}} - \mu_{\sigma} = \varepsilon_{k} - \mu_{\sigma} + \frac{\partial W}{\partial S} \frac{\partial S[\boldsymbol{\eta}]}{\partial \eta_{k\sigma}} = 0 \quad \forall k\sigma. \tag{4.15}$$

Introducing the effective temperature $T_{\text{eff}} = -\partial W / \partial S$ and using Eq. (4.10), it follows that

$$\eta_{k\sigma} = \frac{1}{1 + e^{\beta_{\text{eff}}(\varepsilon_{k} - \mu_{\sigma})}} \quad \text{with} \quad \beta_{\text{eff}} = \frac{1}{k_{\text{B}} T_{\text{eff}}} . \tag{4.16}$$

This means that our initial assumption (4.12) leads to the conclusion that the ground-state occupation-number distribution $\{\eta_{k\sigma}\}$ of the Hubbard model follows a Fermi-Dirac distribution with an effective temperature $T_{\text{eff}} = -\partial W / \partial S$ which only depends

on U and N_σ. This conclusion, however, contradicts the fact that the occupation numbers in the ground state of the Hubbard model follow a Luttinger-liquid or a Fermi-liquid like distribution (see for example Refs. [105–107]) exhibiting a singularity at the Fermi surface $k = k_F$ which does not occur in the Fermi-Dirac distribution (4.16). Therefore, our initial assumption (4.12) must have been wrong, which means that there is in general no one-to-one connection between the IFE S and the interaction energy W for arbitrary ensemble-representable occupation-number distributions $\{\eta_{k\sigma}\}$. Notice, however, that a very accurate description of the occupation-number distribution $\{\eta_{k\sigma}\}$ is not necessarily needed in order to obtain accurate values for the most relevant observables derived from them, since most observables (such as the kinetic energy or the average number of double occupations) involve an average over all k. Furthermore, a detailed analysis of numerous exact numerical results for the ground-state occupation-number distribution of the Hubbard model on various lattice structures shows the following:

1. Equation (4.12) is valid if *ground-state representable* distributions η are considered. Therefore, combined with a sound approximation to the set of ground-state representable distributions η, Eq. (4.12) is a very promising starting point towards a flexible LDFT approach for the ground state of the Hubbard model.

2. For the half-filled band case the Fermi-Dirac distribution (4.16) yields a sound approximation to the actual ground-state occupation-number distribution. This means, the assumption that Eq. (4.12) holds for arbitrary ensemble representable occupation-number distributions introduces only small errors in the ground-state occupation numbers if one focuses on a half-filled band.

In the following Sections 4.2 to 4.5 we demonstrate that Eq. (4.12) in combination with a very simple approximation to the function $W(S)$ already provides a surprisingly accurate account for the ground-state properties of the half-filled Hubbard model, particularly in the challenging case of strong electronic correlations. Furthermore, in Section 4.6 we combine Eq. (4.12) with a family of functions $\eta_\sigma(k)$ exhibiting a Luttinger-like power-law singularity at the Fermi level, since this type of singularity is expected in the ground-state momentum distribution of the 1D Hubbard model away from half band-filling. In this way we leave the regime of a half-filled band and explore how the electronic correlations are modified as the electron density changes.

4.2 Finite systems in one and two dimensions

For the following applications to the half-filled Hubbard model we assume that Eq. (4.12) holds for arbitrary ensemble-representable occupation-number distributions $\{\eta_{k\sigma}\}$. On the basis of the numerical results shown in Fig. 4.1, we propose to

approximate the corresponding function $W(S)$ by the simple linear relation

$$W(S) = W_{\text{HF}} \left(1 - \frac{S}{S_\infty} \right).$$

(4.17)

Here, W_{HF} is the Hartree-Fock (HF) interaction energy (4.8) and S_∞ the upper bound for the IFE given by Eq. (4.11). Notice that $W(S)$ yields the exact interaction energy in the localized limit (where $S = S_\infty$ and $W = 0$ for $n = 1$), as well as in the uncorrelated limit when ground-state degeneracies are absent (where $S = 0$ and $W = W_{\text{HF}}$). Substituting Eq. (4.17) into Eq. (4.13) we obtain the energy functional

$$
\begin{aligned}
E[\boldsymbol{\eta}] &= \sum_{k\sigma} \varepsilon_k \, \eta_{k\sigma} + U N_a \, n_\uparrow n_\downarrow \left(1 - \frac{S[\boldsymbol{\eta}]}{S_\infty} \right) = \\
&= \sum_{k\sigma} \varepsilon_k \, \eta_{k\sigma} + W_{\text{HF}} - T_{\text{eff}} \, S[\boldsymbol{\eta}] \,,
\end{aligned}
$$

(4.18)

with the effective temperature $T_{\text{eff}} = -\partial W / \partial S = W_{\text{HF}} / S_\infty$. Consequently, in the present linear ansatz for $W(S)$, the correlation energy $W_c = W - W_{\text{HF}}$ of the interacting problem is approximated by the entropy contribution $-T_{\text{eff}} S$ to the Helmholtz free energy of an auxiliary noninteracting system at an effective finite temperature T_{eff} which is proportional to the Coulomb interaction strength U. Thus, fractional occupation numbers $0 < \eta_{k\sigma} < 1$ are obtained in the ground state of all interacting systems, i. e., for any $U > 0$.

4.2.1 One-dimensional rings

Figure 4.2 shows results for several ground-state properties of the Hubbard model on a ring with $N_a = 14$ sites and $N_\uparrow = N_\downarrow = 7$ electrons as functions of the Coulomb-interaction strength U/t. These results were obtained by LDFT in combination with the linear IFE-approximation (4.17) to the interaction energy W, and we compare them with exact numerical Lanczos diagonalizations [108]. In Fig. 4.2 (a) one observes that the proposed linear ansatz for W reproduces the ground-state energy E_0 very accurately for all U/t. The relative difference between LDFT and the exact results are always less than 1.1%. In particular, in the strongly correlated limit we obtain $E_0/N_a = -\alpha t^2/U$ with $\alpha_{\text{IFE}} = 2.77$, while the exact proportionality factor is $\alpha_{\text{ex}} = 2.79$. This demonstrates the ability of LDFT combined with the linear IFE-ansatz (4.17) to account for the Heisenberg limit of the Hubbard model, where the energies associated with spin and charge degrees of freedom are widely separated (see Section 2.3.2). Moreover, it is important to remark that the accuracy of E_0 is not the consequence of a significant compensation of errors. Indeed, as shown in Fig. 4.2 (b), very good results are obtained also for the average number of double occupations D
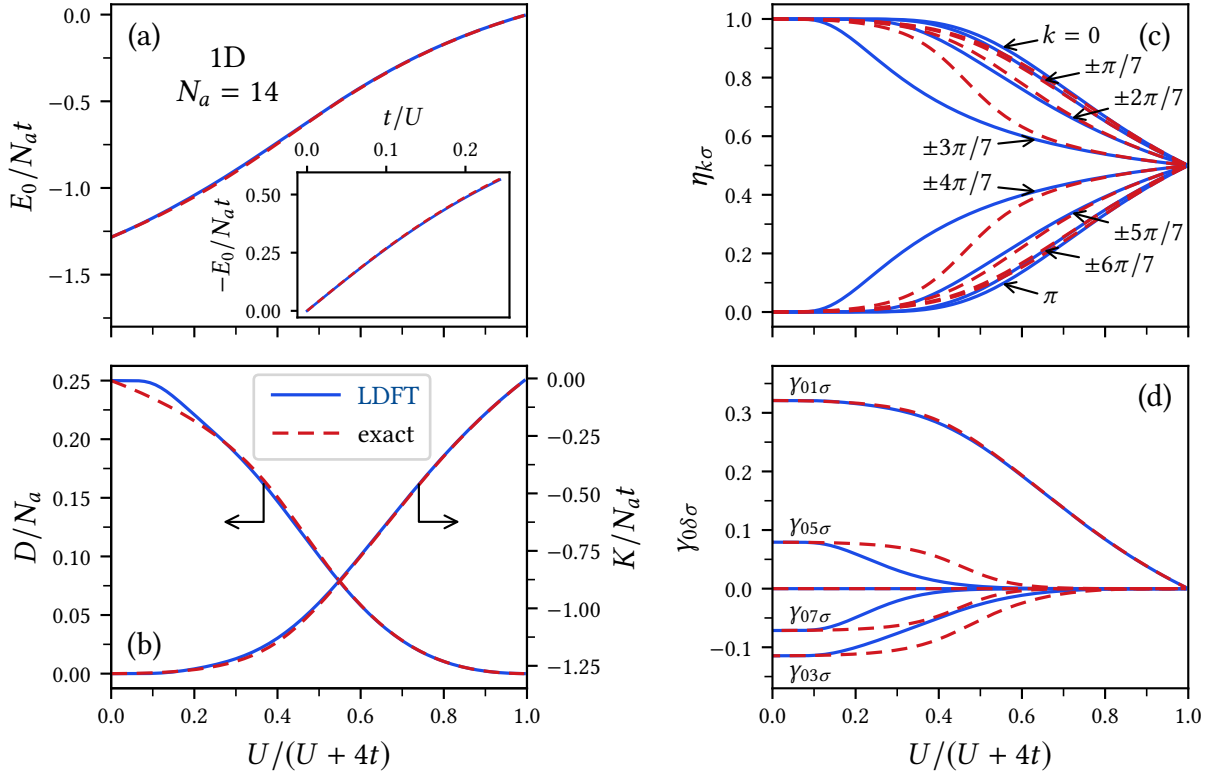
Figure 4.2: Ground-state properties of the 1D Hubbard model on a ring having $N_a = 14$ sites and $N_\uparrow = N_\downarrow = 7$ electrons as functions of the Coulomb-repulsion strength U/t. Results of LDFT combined with the linear IFE-approximation (4.17) to the interaction-energy functional (blue full curves) are compared with exact numerical Lanczos diagonalizations (red dashed curves): (a) ground-state energy E_0, (b) average number of double occupations D and kinetic energy K, (c) natural-orbital occupation numbers $\eta_{k\uparrow} = \eta_{k\downarrow}$, and (d) gs-SPDM elements $\gamma_{0\delta\uparrow} = \gamma_{0\delta\downarrow}$ between site $i = 0$ and its δth-NN. The inset in subfigure (a) highlights the strongly-correlated Heisenberg limit ($U \gg t$) where $E_0 \propto t^2/U$. Adapted from Müller *et al.* [1], ©2018 American Physical Society.

and the kinetic energy K. Only for very weak interactions ($U/t \lesssim 1$) the LDFT approximation overestimates D slightly by remaining too close to $D_{\mathrm{HF}} = N_a/4$. This is a consequence of inaccuracies in our approximation to $W[\boldsymbol{\eta}]$ for nearly integer values of $\eta_{k\sigma}$ which, for the most part, can be ascribed to the deviations from linearity in $W(S)$ for small S, as already observed in the context of Fig. 4.1. In fact, by adapting the function $W(S)$ for small values of S one obtains improved results for the double occupations D at small values of U/t. In any case, these small inaccuracies in the double occupations do not affect the ground-state energy E_0 significantly. In fact, for weak interactions ($U/t \lesssim 1$) the kinetic energy K dominates, which is always very accurately reproduced by the linear IFE-approximation.

In addition to the kinetic and Coulomb energies, it is interesting to investigate the influence of electronic correlations on the ground-state density matrix $\boldsymbol{\gamma}^0$ which minimizes the energy functional $E[\boldsymbol{\gamma}]$. A first insight from a k-space perspective is given in Fig. 4.2 (c), where the ground-state occupation numbers $\eta_{k\sigma}$ are shown as functions of the Coulomb-repulsion strength U/t. We find eight distinct values for the occupation numbers $\eta_{k\sigma}$, which correspond to the wave numbers $k = 0$, $k = \pm\nu\pi/7$ with $\nu = 1$–6 and $k = \pi$, as implied by time-inversion symmetry (i.e., $\eta_{k\sigma} = \eta_{-k\sigma}$ $\forall k$). Taking into account Eq. (4.16) and the fact that the k-dependence of the single-particle spectrum ε_k respects the point-group symmetry of the lattice, it is easy to verify that the $\eta_{k\sigma}$ derived from any IFE approximation of the form (4.12) always satisfy the local symmetry properties of the model under consideration.

Another fundamental property of the average Bloch-state occupation numbers observed in the absence of ground-state degeneracies in the unpolarized half-filled Hubbard model is the sum rule

$$\eta_{k\sigma} + \eta_{k+q,\sigma} = 1, \tag{4.19}$$

where the wave vector $\boldsymbol{q}$ satisfies $\varepsilon_{k+q} = -\varepsilon_k$ for all $\boldsymbol{k} \in$ BZ. From Eq. (2.15) one finds $q = \pi$ for a one-dimensional lattice with NN hopping and $\boldsymbol{q} = \sum_{i=1}^d \boldsymbol{b}_i/2$ in the general case of a d dimensional lattice, where $\boldsymbol{b}_i$ denotes the elementary vectors of the reciprocal lattice. In order to prove Eq. (4.19) let us consider the unitary electron-hole transformation

$$\hat{U} : \hat{c}^\dagger_{k\sigma} \rightarrow \hat{c}_{k+q,\sigma} \quad \forall \boldsymbol{k}\sigma. \tag{4.20}$$

Expressing the operator $\hat{D} = \sum_i \hat{n}_{i\uparrow}\hat{n}_{i\downarrow}$ in terms of the Bloch states (2.13)

$$\hat{D} = \frac{1}{N_a} \sum_{k_1,k_2,Q \in \mathrm{BZ}} \hat{c}^\dagger_{k_1+Q,\uparrow} \hat{c}_{k_1\uparrow} \hat{c}^\dagger_{k_2-Q,\downarrow} \hat{c}_{k_2\downarrow}, \tag{4.21}$$

and using that $\varepsilon_{k+q} = -\varepsilon_k$ for all $\boldsymbol{k} \in$ BZ, it is straight forward to verify that the Hubbard-model Hamiltonian $\hat{H} = \sum_{k\sigma} \varepsilon_k \hat{n}_{k\sigma} + U\hat{D}$ transforms to

$$\hat{H}' = \hat{U}^\dagger \hat{H} \hat{U} = \hat{H} - W_{\mathrm{HF}}, \tag{4.22}$$

where $W_{\text{HF}} = UN_\uparrow N_\downarrow / N_a$ is the HF interaction energy (4.8). Since W_{HF} is just a constant if the number N_σ of spin-σ electrons is kept fixed, it follows that $\hat{H}$ is (besides of this irrelevant constant) invariant upon the electron-hole transformation (4.20). Consequently, if $|\Psi\rangle$ is one of the eigenstates of $\hat{H}$ with energy E and N_σ spin-σ electrons, then the transformed state $|\Psi'\rangle = \hat{U}|\Psi\rangle$ is also an eigenstate of $\hat{H}$ with energy $E' = E - W_{\text{HF}}$ and $N'_\sigma = N_a - N_\sigma$ spin-σ electrons. One readily concludes that $|\Psi'_0\rangle = \hat{U}|\Psi_0\rangle$ must be the ground state for $N'_\sigma = N_a - N_\sigma$ spin-σ electrons if $|\Psi_0\rangle$ is the ground state for N_σ electrons with spin σ. Consequently, in the absence of ground-state degeneracies for $N_\uparrow = N_\downarrow = N_a/2$ we must have $|\Psi_0\rangle = |\Psi'_0\rangle = \hat{U}|\Psi_0\rangle$, such that

$$\eta_{k\sigma} = \langle\Psi_0|\hat{c}^\dagger_{k\sigma}\hat{c}_{k\sigma}|\Psi_0\rangle = \langle\Psi_0|\hat{U}^\dagger\hat{c}^\dagger_{k\sigma}\hat{c}_{k\sigma}\hat{U}|\Psi_0\rangle =$$

$$= \langle\Psi_0|1 - \hat{c}^\dagger_{k+q,\sigma}\hat{c}_{k+q,\sigma}|\Psi_0\rangle = 1 - \eta_{k+q,\sigma} \,. \tag{4.23}$$

This proves the sum rule (4.19). In the present context it is important to note that any IFE approximation of the form (4.12) satisfies this sum rule for $N_\uparrow = N_\downarrow = N_a/2$, since Eq. (4.16) combined with $\mu_\uparrow = \mu_\downarrow = 0$ and $\varepsilon_{k+q} = -\varepsilon_k$ implies Eq. (4.19).

The comparison between the exact and approximate results, shown in Fig. 4.2 (c), leads to the conclusion that the linear IFE-approximation reproduces the occupation numbers $\eta_{k\sigma}$ of the finite half-filled 1D Hubbard model quite accurately in the whole range from weak to strong Coulomb interactions. For very weak interactions $U/t \ll 1$ one obtains the expected behavior $\eta_{k\sigma} \simeq 1$ for $|k| \leq \pi/2$ and $\eta_{k\sigma} \simeq 0$ otherwise. The gradual suppression of charge fluctuations with increasing values of U/t is reflected by the decreasing (increasing) occupations of the Bloch states having lower (higher) energies. Thus, $\eta_{k\sigma}$ decreases (increases) for $|k| < \pi/2$ ($|k| > \pi/2$) until in the strongly correlated limit $\eta_{k\sigma} = 1/2$ is reached for all $k\sigma$. The only significant deviations between the exact and approximate results is observed for $|k| = 3\pi/7$ ($|k| = 4\pi/7$), where $\eta_{k\sigma}$ is underestimated (overestimated) for intermediate values of U/t. Since these values of k are those closest to the Fermi surface $|k_F| = \pi/2$, we conclude that the linear IFE-approximation overestimates the excitation of electrons across the Fermi level $\varepsilon_F = 0$. This is a consequence of the rather small slope $\partial\eta_{k\sigma}/\partial\varepsilon_k$ of the Fermi function (4.16) in the vicinity of the Fermi energy, when compared with the exact occupation-number distribution. In fact, the ground-state occupation-number distribution of the infinite Hubbard chain is expected to exhibit the typical power-law singularity of a Luttinger liquid, which leads to a divergence in the derivative $\partial\eta_\sigma(k)/\partial k$ at the Fermi level [98]. Notice that the Fermi-Dirac distribution (4.16), which is an immediate consequence of the IFE approximation (4.12), can never reproduce this subtle behavior.

In Eqs. (4.2) and (4.4) we have already seen that the occupation numbers $\eta_{k\sigma}$ and the SPDM $\boldsymbol{\gamma}$ are related by a Fourier transformation. Since we are concerned with lattices

having translational and rotational symmetry, the elements $\gamma_{ij\sigma} = \gamma_\sigma(|\boldsymbol{R}_i - \boldsymbol{R}_j|)$ of the gs-SPDM depend solely on the distance between the lattice sites i and j. Therefore, it is sufficient to consider the matrix elements $\gamma_{0\delta\sigma}$ corresponding to a given lattice site $i = 0$ and its δth NN. Before analyzing the results shown in Fig. 4.2 (d), one should notice that in the absence of ground-state degeneracies in the unpolarized half-filled Hubbard model one has $\gamma_{ij\sigma} = 0$ for lattice sites $i \neq j$ belonging to the same sublattice. This property is closely related to the above discussed electron-hole symmetry of the Hubbard-model. In fact, by expressing the SPDM as Fourier transform of the Bloch-state occupation numbers

$$\gamma_{ij\sigma} = \frac{1}{N_a} \sum_{\boldsymbol{k} \in \mathrm{BZ}} \eta_{\boldsymbol{k}\sigma} \, \mathrm{e}^{-\mathrm{i}\boldsymbol{k}\cdot(\boldsymbol{R}_i - \boldsymbol{R}_j)} \tag{4.24}$$

and using the sum rule (4.19), one obtains

$$\gamma_{ij\sigma} \left(1 + \mathrm{e}^{-\mathrm{i}\boldsymbol{q}\cdot(\boldsymbol{R}_i - \boldsymbol{R}_j)} \right) = \delta_{ij} . \tag{4.25}$$

Here $\boldsymbol{q} = \sum_i \boldsymbol{b}_i/2$, and from the orthogonality relation $\boldsymbol{a}_i \cdot \boldsymbol{b}_j = 2\pi \delta_{ij}$ between the elementary real and reciprocal lattice vectors it follows $\boldsymbol{q} \cdot \boldsymbol{R} = M\pi$ with $M = \sum_{i=1}^d n_i \in \mathbb{Z}$ for any lattice vector $\boldsymbol{R} = \sum_{i=1}^d n_i \boldsymbol{a}_i$. Finally, if the lattice is bipartite and the sites $i \neq j$ belong to the same sublattice, we have $\boldsymbol{q} \cdot (\boldsymbol{R}_i - \boldsymbol{R}_j) = M\pi$ with M even, such that Eq. (4.25) implies $\gamma_{ij\sigma} = 0$. Since any approximation of the form (4.12) satisfies the sum rule (4.19) for $N_\uparrow = N_\downarrow = N_a/2$, one concludes that this property is exactly reproduced within the IFE approximation.

In Fig. 4.2 (d) results are shown for the gs-SPDM elements $\gamma_{0\delta\sigma}$. As already discussed, we have $\gamma_{0\delta\sigma} = 0$ for even δ since in the one-dimensional chain the corresponding lattice sites belong to the same sublattice as the site $i = 0$. The LDFT results for the remaining four non-vanishing elements $\gamma_{0\delta\sigma}$ with δ odd are in good qualitative agreement to the exact ones. Both weakly- and strongly-correlated limits ($U/t \lesssim 1$ and $U/t \gtrsim 10$) are very accurately reproduced for all SPDM elements. Moreover, $\gamma_{01\sigma}$, which corresponds to NNs and is proportional to the kinetic energy in the considered NN-hopping model, is obtained with remarkable accuracy for all values of U/t. This is consistent with the very good accuracy of the calculated kinetic energy shown in Fig. 4.2 (b). However, for intermediate values of U/t our approximation underestimates the delocalization of the electrons beyond NNs (i. e., $\gamma_{0\delta\sigma}$ with $\delta = 3, 5, 7$). For example, for $U/t = 4$ the LDFT approximation to $|\gamma_{03\sigma}|$ is about 50% smaller than the exact result, while $\gamma_{05\sigma}$ and $\gamma_{07\sigma}$ nearly vanish. The discrepancies in $\gamma_{0\delta\sigma}$ for $\delta = 3, 5, 7$ seem more severe than what one might have expected on the basis of the results for its Fourier transform $\eta_{\boldsymbol{k}\sigma}$. As already discussed in the context of Fig. 4.2 (c), the approximate values for $\eta_{\boldsymbol{k}\sigma}$ are quite accurate except for $k = \pm 3\pi/7$ and $k = \pm 4\pi/7$. To sum up, we conclude that the correlation-induced localization of the electrons is quite well reproduced qualitatively. However, the degree of the localization is overestimated.

4.2.2 Two-dimensional square lattice

Figure 4.3 shows results for the ground-state properties of the half-filled 2D Hubbard model on a 4×4 square cluster with periodic boundary conditions ($N_\uparrow = N_\downarrow = 8$). The comparison with exact Lanczos diagonalizations shows that in two dimensions the accuracy of LDFT in the linear IFE-approximation (4.17) is similar to the above discussed 1D case. In particular, the ground-state energy E_0 shown in Fig. 4.3 (a) is accurately reproduced for all values of U/t. In the strongly correlated limit we find $E_0/N_a = -\alpha t^2/U$ which correctly reproduces the behavior of localized Heisenberg spins (see Section 2.3.2). Quantitatively, we obtain $\alpha_{\mathrm{IFE}} = 5.55$ which is only 13% larger than the exact value $\alpha_{\mathrm{ex}} = 4.81$ deduced from the Lanczos diagonalizations. For intermediate values of U/t we find that the binding energy $|E_0|$ is somewhat overestimated. The main reason for this is an overestimation of the kinetic-energy gain $|K|$, which turns out to be slightly less accurate than in the 1D case [compare Figs. 4.2 (b) and 4.3 (b)]. Also the average number of ground-state double occupations D is mostly very well reproduced within the linear IFE-approximation, as can be seen in Fig. 4.3 (b). Still, for $U/t \lesssim 2$ we find that D is significantly underestimated. This is the reason for the slight underestimation of $\partial E_0/\partial U$ in the weakly correlated limit ($U/t \lesssim 2$), although the quantitative impact of D on E_0 is weak for small values of U/t.

Notice that for $U/t \to 0$ both the exact and LDFT results for D are smaller than the HF value $D_{\mathrm{HF}} = N_a/4$. This is a consequence of the fact that the single-particle spectrum of the finite 4×4 cluster is degenerate at the Fermi level $\varepsilon_F = 0$. As a result, the Bloch states having $\varepsilon_k = \varepsilon_F = 0$ can be partially occupied in order to reduce the average number of double occupations even in the limit of vanishing interaction energy $U/t \to 0$. In fact, there are six Bloch states at the Fermi level ε_F, which correspond to the wave vectors $\boldsymbol{k} = (\pm\pi/2, \pm\pi/2)$, $(\pi, 0)$ and $(0, \pi)$. These states are occupied by six electrons for $U/t \to 0$ and the remaining 10 electrons occupy the states having $\boldsymbol{k} = (0, 0)$, $(\pm\pi/2, 0)$ and $(0, \pm\pi/2)$. As shown in Fig. 4.3 (c), LDFT yields $\eta_{k\sigma} = 1/2$ for all $\boldsymbol{k}$ at the Fermi level, irrespectively of the Coulomb interaction strength U/t, in agreement with the exact diagonalizations. Furthermore, both exact and LDFT computations yield the same occupation numbers $\eta_{k\sigma} = \eta_{k'\sigma}$ for Bloch states having $\varepsilon_k = \varepsilon_{k'}$. This is consistent with the general result (4.16), stating that the $\boldsymbol{k}$-dependence of the occupation numbers $\eta_{k\sigma}$ obtained from any IFE approximation is determined by the single-particle spectrum ε_k. Nevertheless, the simple linear IFE-approximation (4.17) happens to be unable to accurately reproduce the double occupations D of the weakly-interacting finite Hubbard model in the presence of essential degeneracies, i.e., in the case that the degenerate ground-states are coupled by the action of $\hat{D}$ in the limit $U/t \to 0$. Notice, however, that Eq. (4.21) implies $\langle \Psi_0^{(i)} | \hat{D} | \Psi_0^{(j)} \rangle \in \{0, \pm 1/N_a\}$ for two noninteracting ground states, i.e., for two differ-

Figure 4.3: Ground-state properties of the 2D Hubbard model on a 4×4 square lattice with $N_\uparrow = N_\downarrow = 8$ electrons and periodic boundary conditions as functions of the Coulomb-repulsion strength U/t. Results of LDFT combined with the linear IFE-approximation (4.17) to the interaction-energy functional (blue full curves) are compared with exact numerical Lanczos diagonalizations (red crosses): (a) ground-state energy E_0, (b) average number of double occupations D and kinetic energy K, (c) natural-orbital occupation numbers $\eta_{k\uparrow} = \eta_{k\downarrow}$, and (d) gs-SPDM elements $\gamma_{0\delta\uparrow} = \gamma_{0\delta\downarrow}$ between site $i = 0$ and its δth NN, as illustrated in the inset. The inset in subfigure (a) highlights the strongly-correlated Heisenberg limit ($U \gg t$) where $E_0 \propto t^2/U$. Adapted from Müller *et al.* [1], ©2018 American Physical Society.

ent Slater determinants in the occupied Bloch states ($\langle\Psi_0^{(i)}|\Psi_0^{(j)}\rangle = 0$). Consequently, the effect of a finite degeneracy at the Fermi level vanishes in the thermodynamic limit $N_a \to \infty$. It is for this reason that in Fig. 4.1 we have focused on systems not exhibiting this kind of finite-size degeneracy, since otherwise our inferred approximation (4.17) would have been plagued by spurious finite-size effects. In fact, in Section 4.3 we will demonstrate that the ground-state observables of the infinite Hubbard chain derived from the present IFE approximation are almost indistinguishable from the exact Lieb-Wu solution. Moreover, we will show that very accurate results are obtained for infinite lattices in higher dimensions as well.

As in the one-dimensional case, the occupation numbers $\eta_{k\sigma}$ of the Bloch states with energies below (above) the Fermi level $\varepsilon_F = 0$ decrease (increase) with increasing U/t, starting from $\eta_{k\sigma} = 1$ ($\eta_{k\sigma} = 0$) in the uncorrelated limit ($U/t = 0$) until $\eta_{k\sigma} = 1/2$ is reached for all k in the strongly correlated limit ($U/t \to \infty$). Figure 4.3 (c) shows that the occupation numbers $\eta_{k\sigma}$ obtained within the linear IFE-approximation are remarkably accurate for all $k\sigma$ in the complete range from weak to strong interactions. Furthermore, our approximation respects all point-group symmetries of $\eta_{k\sigma}$ in the reciprocal lattice, since these are inherited from the dispersion relation ε_k.

Results for the gs-SPDM elements $\gamma_{ij\sigma}$ as functions of U/t are presented in Fig. 4.3 (d). Due to the symmetry of the lattice one only needs to consider the matrix elements $\gamma_{0\delta\sigma}$ between an arbitrary lattice site $i = 0$ and its δth NN, as illustrated in the inset of Fig. 4.3 (d). Electron-hole symmetry implies that $\gamma_{0\delta\sigma} = 0$ for $\delta = 2, 3, 5$, since the corresponding sites belong to the same sublattice as the site $i = 0$. This holds, since the 2D square lattice is bipartite and the ground state of the 4×4 cluster with $N_\uparrow = N_\downarrow = 8$ is non-degenerate. The LDFT results for the remaining non-vanishing gs-SPDM elements $\gamma_{01\sigma}$ and $\gamma_{04\sigma}$ follow closely the exact numerical values for all U/t. In particular, the correlation-induced localization of the electrons is very accurately reproduced. Remarkably, the results for $\gamma_{0\delta\sigma}$ are significantly more accurate than in the case of the 1D chain [see Fig. 4.2 (d)], at least for the relatively short distances which can be explored within a finite cluster.

4.2.3 Triangular lattice

In order to explore magnetically frustrated systems, we consider a 4×4 cluster of the 2D triangular lattice with $N_\uparrow = N_\downarrow = 8$ and periodic boundary conditions. Figure 4.4 shows results for several ground-state properties obtained in the framework of LDFT with the linear IFE-approximation (4.17). The comparison with exact numerical Lanczos diagonalizations shows that the ground-state energy E_0 is fairly well reproduced in the whole interaction range from weak to strong correlations. The binding energy $|E_0|$ is overestimated, especially for intermediate interaction strength U/t, where
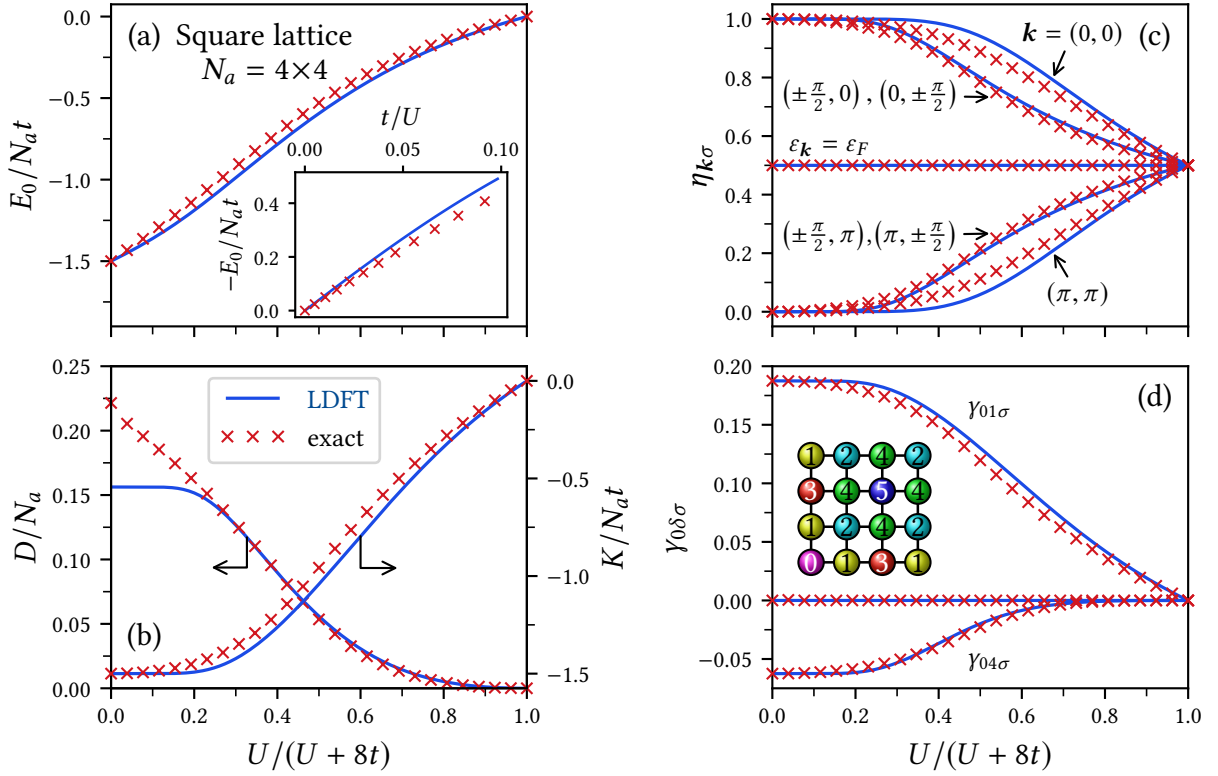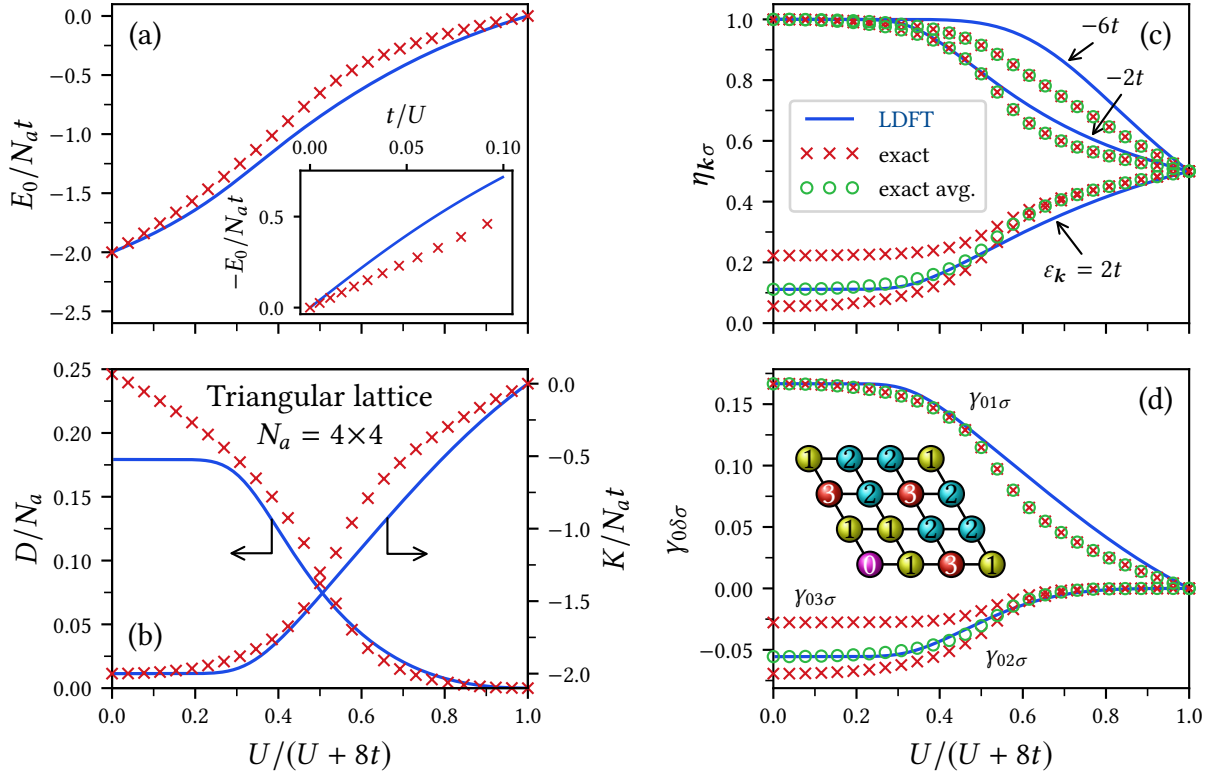
Figure 4.4: Ground-state properties of the 2D Hubbard model on a 4×4 cluster of the triangular lattice with $N_\uparrow = N_\downarrow = 8$ electrons and periodic boundary conditions as functions of the Coulomb repulsion strength U/t. Results of LDFT combined with the linear IFE-approximation (4.17) to the interaction-energy functional (blue full curves) are compared with exact numerical Lanczos diagonalizations (red crosses): (a) ground-state energy E_0, (b) average number of double occupations D and kinetic energy K, (c) natural-orbital occupation numbers $\eta_{k\uparrow} = \eta_{k\downarrow}$, and (d) gs-SPDM elements $\gamma_{0\delta\uparrow} = \gamma_{0\delta\downarrow}$ between site $i = 0$ and its δth NN, as illustrated in the inset. The inset in subfigure (a) highlights the strongly-correlated Heisenberg limit ($U \gg t$) where $E_0 \propto t^2/U$. The open circles in subfigures (c) and (d) are obtained by averaging the exact occupation numbers which belong to Bloch states having the same energy ε_k. Adapted from Müller *et al.* [1], ©2018 American Physical Society.

the maximum deviation $E_0^{\mathrm{ex}} - E_0^{\mathrm{IFE}} = 0.22 N_a t$ is observed for $U/t = 9.33$. In the strongly-correlated Heisenberg limit, the energy relation $E_0 = -\alpha t^2/U$ is correctly reproduced, although the corresponding slope $\alpha_{\mathrm{IFE}} = 8.32$ is significantly larger than the exact value $\alpha_{\mathrm{ex}} = 5.14$ inferred from the Lanczos diagonalizations.

The LDFT results for the average number of double occupations D shown in Fig. 4.4 (b) follow the exact ones fairly close, except for $U/t \lesssim 4$ where D is underestimated by up to 27% in the uncorrelated limit $U/t = 0$. This is probably a consequence of the ninefold degeneracy of ε_k at the Fermi level of the 4×4 cluster, which is occupied by only two electrons. Under these circumstances the linear IFE-approximation overestimates the ability of the finite many-body system to take advantage of the degeneracies in order reduce the double occupations. Nevertheless, this underestimation of D has little impact on the ground-state energy E_0, since U/t is relatively small and the kinetic energy K, which is fairly well approximated, dominates. A similar behavior has already been discovered in the context of the finite 4×4 square cluster (see Fig. 4.3).

The Bloch states of the triangular 4×4 cluster with $N_\uparrow = N_\downarrow = 8$ can be classified in two groups: those at the Fermi level having $\varepsilon_k = \varepsilon_F = 2t$ and those below the Fermi level ε_F. In the uncorrelated limit $U/t = 0$, the Bloch states having $\varepsilon_k < \varepsilon_F$ are fully occupied ($\eta_{k\sigma} = 1$) and the ninefold degenerate Fermi level is occupied by only two electrons with opposite spin polarization. As shown in Fig. 4.4 (c), the exact diagonalizations do not yield a uniform occupation of all Bloch states having $\varepsilon_k = \varepsilon_F$, as one might naively expect. In fact, the exact occupation numbers of the Bloch states at the Fermi level deviate from the value $\eta_{k\sigma} = 1/9$ predicted by any IFE approximation of the form (4.12). This behavior is a subtle finite-size electron-correlation effect, by which the system manages to completely suppress the local Coulomb interaction between the two electrons at the Fermi level, already for arbitrary small values of U/t. Concerning the dependence of $\eta_{k\sigma}$ on the Coulomb-repulsion strength U/t, we observe a qualitatively similar behavior as in the previously considered bipartite lattices: the occupation numbers of the Bloch states with $\varepsilon_k < \varepsilon_F$ ($\varepsilon_k = \varepsilon_F$) decrease (increase) from their initial value $\eta_{k\sigma} = 1$ ($\eta_{k\sigma} \sim 1/9$) for $U/t = 0$, until $\eta_{k\sigma} = 1/2$ is reached for all k in the limit $U/t \to \infty$. The present IFE approximation correctly reproduces the overall trend in $\eta_{k\sigma}$ as a function of U/t, however, for $U/t \gtrsim 8$ it somewhat overestimates (underestimates) $\eta_{k\sigma}$ when $\varepsilon_k < \varepsilon_F$ ($\varepsilon_k = \varepsilon_F$). Although the IFE approximation cannot resolve the differences in the occupation numbers $\eta_{k\sigma}$ belonging to Bloch states having $\varepsilon_k = \varepsilon_F$, the occupation numbers $\eta_{k\sigma}$ predicted by the linear IFE-approximation compare well with the exact ones if the latter are averaged among the Bloch states having the same energy ε_k. These averaged exact $\eta_{k\sigma}$ are indicated by the green circles in Fig. 4.4 (c). It should be also noted, as already discussed in the context of the finite square lattice, that the anomalies due to degeneracies at the Fermi level of the single-particle spectrum become progressively irrelevant as the

system size increases. Therefore, one expects that the accuracy of the occupation numbers $\eta_{k\sigma}$ should improve in the thermodynamic limit.

The gs-SPDM elements $\gamma_{0\delta\sigma}$ between a lattice site $i = 0$ and its δth NN are shown in Fig. 4.4 (d). One observes a good qualitative agreement between the present approximation and the exact numerical results. The most significant deviations are observed for small values of U/t, where the differences between $\gamma_{02\sigma}$ and $\gamma_{03\sigma}$ cannot be resolved. This is a consequence of the fact that the IFE approximation does not account for the subtle finite-size correlation effects responsible for the selective occupation of the Bloch states having $\varepsilon_k = \varepsilon_F$. Nevertheless, the gs-SPDM elements $\gamma_{0\delta\sigma}$ obtained from the averaged exact $\eta_{k\sigma}$ agree fairly well to the approximate results, as indicated by the green circles in Fig. 4.4 (d). In summary, by comparing Figs. 4.3 and 4.4, one may conclude that the overall accuracy of the present IFE approximation for magnetically frustrated non-bipartite lattices, such as the triangular lattice, is comparable to, though in general somewhat inferior than in the case of bipartite lattices.

4.3 Infinite periodic lattices

Having tested the linear IFE-approximation (4.17) on finite one- and two-dimensional clusters, we will now focus on the half-filled Hubbard model on infinite periodic lattices. To be explicit, we focus on d-dimensional hypercubic lattices with NN hopping $t_d = t/\sqrt{d}$, such that the corresponding single-particle dispersion relation (2.15) is given by

$$\varepsilon_k = -\frac{2t}{\sqrt{d}} \sum_{\alpha=1}^{d} \cos(k_\alpha), \qquad (4.26)$$

where $k_\alpha \in (-\pi, \pi]$ are the components of the wave vector $k \in$ BZ. Notice that the hopping integrals $t_d \propto 1/\sqrt{d}$ have been scaled, in order to ensure that the second moment

$$w_2 = \int_{-\infty}^{\infty} \varepsilon^2 \rho(\varepsilon) \, d\varepsilon = 2dt_d^2 = 2t^2 \qquad (4.27)$$

of the single-particle density of states (DOS) per atom and spin

$$\rho(\varepsilon) = \frac{1}{(2\pi)^d} \int_{BZ} \delta(\varepsilon - \varepsilon_k) \, dk \qquad (4.28)$$

is independent of the lattice dimension d. This allows us to compare results for different dimensions on the same footing, and to explore the limit of infinite dimensions.

In order to apply our present linear IFE-approximation to infinite periodic lattices, it is convenient to express the kinetic energy K and the IFE S in terms of the single-

particle DOS $\rho(\varepsilon)$ defined in Eq. (4.28):

$$\frac{K}{N_a} = \sum_\sigma \int_{-\infty}^{\infty} \varepsilon \, \eta_\sigma(\varepsilon) \, \rho(\varepsilon) \, \mathrm{d}\varepsilon \tag{4.29}$$

and

$$\frac{S}{N_a} = -k_\mathrm{B} \sum_\sigma \int_{-\infty}^{\infty} \left[\eta_\sigma(\varepsilon) \log \left(\eta_\sigma(\varepsilon) \right) + \left(1 - \eta_\sigma(\varepsilon) \right) \log \left(1 - \eta_\sigma(\varepsilon) \right) \right] \rho(\varepsilon) \, \mathrm{d}\varepsilon \,. \tag{4.30}$$

Here, the spin-resolved occupation number of a Bloch-state with energy ε is, according to Eq. (4.16), given by

$$\eta_\sigma(\varepsilon) = \frac{1}{1 + e^{\beta_\mathrm{eff}(\varepsilon - \mu_\sigma)}} \quad \text{with} \quad \beta_\mathrm{eff} = \frac{1}{k_\mathrm{B} T_\mathrm{eff}} \,. \tag{4.31}$$

The effective temperature $T_\mathrm{eff} = W_\mathrm{HF}/S_\infty$ is independent of the IFE S within our present linear approximation, and the chemical potential μ_σ for spin-σ electrons is determined by the usual condtion

$$n_\sigma = \frac{N_\sigma}{N_a} = \int_{-\infty}^{\infty} \eta_\sigma(\varepsilon) \, \rho(\varepsilon) \, \mathrm{d}\varepsilon \,. \tag{4.32}$$

From Eq. (4.29) one readily obtains the ground-state kinetic energy K, by using the ground-state occupation-number distribution (4.31) and the well-known expression

$$\rho(\varepsilon) = \frac{1}{\pi} \int_0^{\infty} \cos(\lambda \varepsilon) \, J_0^d(2t_d \lambda) \, \mathrm{d}\lambda \tag{4.33}$$

for the single-particle DOS of hypercubic lattices in d dimensions, where

$$J_0(x) = \frac{1}{\pi} \int_0^{\pi} \cos(x \sin y) \, \mathrm{d}y \tag{4.34}$$

is the zero-order Bessel function of the first kind. Furthermore, from Eq. (4.30) one obtains the ground-state IFE S and, in turn, the ground-state interaction energy W from the linear approximation (4.17). For the moment we restrict ourselves to paramagnetic systems having $n_\uparrow = n_\downarrow = 1/2$. In this case we have $W_\mathrm{HF} = U N_a/4$ and $S_\infty = 2N_a \log 2$ according to Eqs. (4.8) and (4.11), and thus $T_\mathrm{eff} = U/(8 \log 2)$. Spin-polarized systems are considered in Section 4.4.

In Fig. 4.5 we show results for the ground-state kinetic, Coulomb and total energies of the half-filled Hubbard model on hypercubic lattices in $d = 1$–3 dimensions and in the limit $d \to \infty$. For the 1D case one observes that the ground-state energy E_0 obtained within the linear IFE-approximation is nearly indistinguishable from the exact
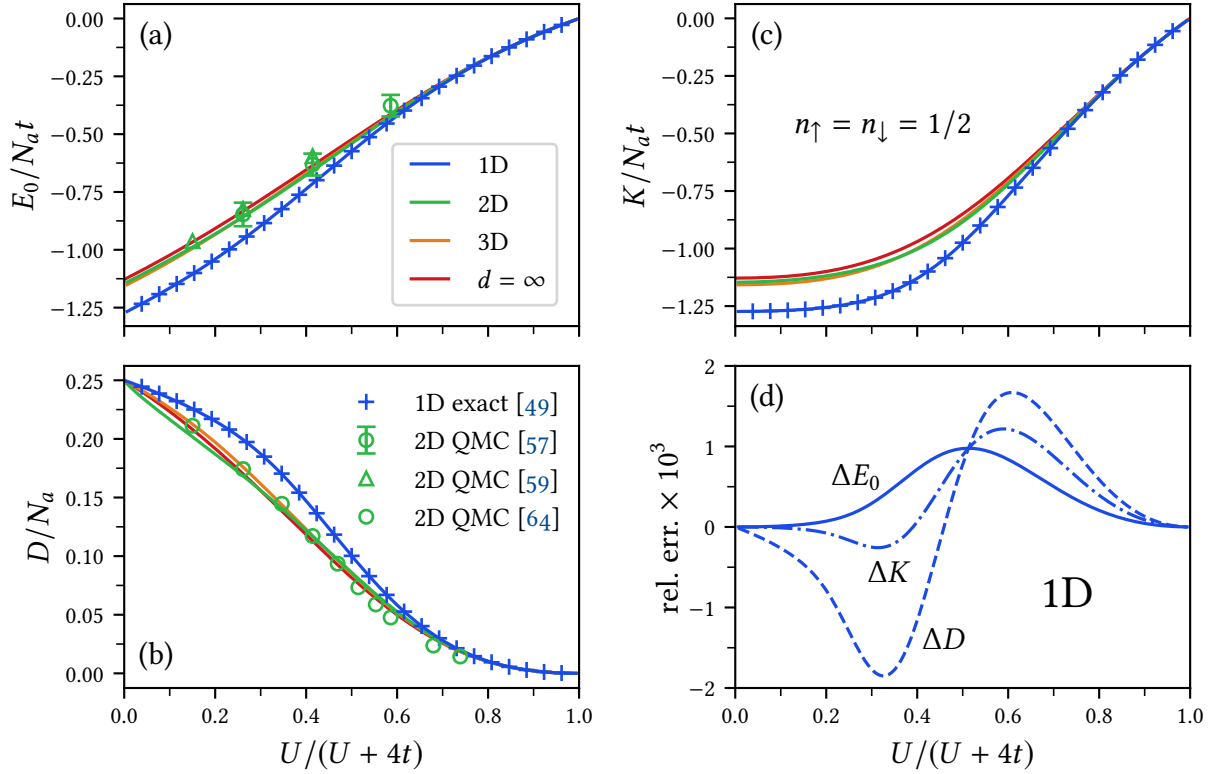
Figure 4.5: Ground-state properties of the half-filled Hubbard model on hypercubic lattices in $d = 1$–3 dimensions and $d \rightarrow \infty$ as functions of the Coulomb-repulsion strength U/t. Results are shown for the (a) ground-state energy E_0, (b) average number of double occupations D, and (c) kinetic energy K. The full curves were obtained by LDFT in combination with the linear IFE-approximation (4.17). The symbols correspond either to the exact Bethe-ansatz solution for the 1D Hubbard model [49] (blue crosses) or to numerical quantum Monte Carlo simulations for the 2D Hubbard model [57, 59, 64] (green open circles and triangles). For each dimension d the NN hopping-integral t_d is scaled as $t_d = t/\sqrt{d}$, such that the second moment $w_2 = 2dt_d^2$ of the single-particle DOS is independent of d. Subfigure (d) shows the relative difference $\Delta X = (X^{\mathrm{IFE}} - X^{\mathrm{ex}})/X^{\mathrm{ex}}$ between the exact Bethe-ansatz solution and the linear IFE-approximation, where X stands respectively for the ground-state energy E_0, the kinetic energy K and the average number of double occupations D in the one-dimensional Hubbard model. Adapted from Müller *et al.* [1], ©2018 American Physical Society.

Bethe-ansatz solution [49]. In fact, the relative difference $\Delta E_0 = (E_0^{\text{IFE}} - E_0^{\text{ex}})/E_0^{\text{ex}}$ between the exact ground-state energy and the IFE approximation is always smaller than 0.1%, as shown in Fig. 4.5 (d). In particular, the exact asymptotic behavior $E_0 = -4N_a \log(2) t^2/U$ in the strongly correlated Heisenberg limit is recovered, as discussed in more detail in Appendix E.1. It is most remarkable that the simple linear approximation, relating W and S, is able to reproduce the exact energy of localized spins in the strongly correlated limit of the 1D Hubbard model. Notice moreover, that the linear IFE-approximation yields highly accurate ground-state averages, even though the occupation numbers $\eta_\sigma(k)$ do not follow the Luttinger-liquid behavior that is expected for the ground state of the one-dimensional Hubbard model [98]. Most likely, the precise form of the occupation-number distribution in the vicinity of the Fermi level ε_F, although crucial for the excitations and the low-temperature behavior, has little influence on the total energy of the system.

We like to point out that the remarkable accuracy of the ground-state energy in 1D, obtained from LDFT and the linear IFE-approximation, is not the result of a significant compensation of errors. In fact, also the kinetic energy K and the double occupations D are almost indistinguishable from the exact results for all U/t. This is quantified in Fig. 4.5 (d), where the relative errors of the kinetic and total energies as well as the double occupations are shown. For example, the largest relative error $\Delta D = 0.17\%$ in the double occupations is only slightly higher than the largest relative errors $\Delta K = 0.12\%$ and $\Delta E_0 = 0.10\%$ in the kinetic and total energies.

No exact solution is available for the half-filled Hubbard model on the 2D square lattice. However, since the low-lying excitations in the strongly correlated limit are described by the antiferromagnetic (AFM) spin-1/2 Heisenberg model (2.52) with coupling constant $J = 2t^2/U$, one can infer the value of α in the strong-coupling limit $E_0/N_a = -\alpha t^2/U$ of the ground-state energy from accurate quantum Monte Carlo (QMC) simulations for the 2D Heisenberg model. As discussed in more detail in Appendix E.1, one obtains $\alpha_{\text{IFE}} = 8 \log 2 \approx 5.55$ within the linear IFE-approximation, while $\alpha_{\text{QMC}} = 4.68$ is inferred from QMC simulations [109]. This means, although the linear IFE-approximation correctly reproduces the dependence $E_0 \propto t^2/U$ in the strongly-correlated limit, the actual binding energy is overestimated by about 18%. For finite values of U/t we find a very good agreement between our results and the far more demanding QMC simulations for the 2D Hubbard model reported in Refs. [57, 59, 64]. This applies to the ground-state energy E_0 shown in Fig. 4.5 (a), as well as to the average number of double occupations D presented in Fig. 4.5 (b). Like in the case of the one-dimensional chain, our approximation tends to slightly underestimate the double occupations for weak to intermediate interaction strength ($U/t \lesssim 4$) and to overestimate it to some extend when strong interactions are considered. We conclude that not only the ground-state energy of the Hubbard model on the 2D square lattice, but also the more subtle double occupations are accurately repro-

duced within the linear IFE-approximation.

Concerning the dependence on the dimension d of the hypercubic lattice, we find a surprisingly fast convergence to the limit of infinite dimensions once the NN hoppings are scaled as $t_d = t/\sqrt{d}$ in order to keep the second moment $w_2 = 2dt_d^2 = 2t^2$ of the single-particle DOS independent of the lattice dimension. This not only applies to the total ground-state energy but also to the kinetic and Coulomb energies, which suggests that, within the linear IFE-approximation, the most important dependence of E_0, K, and D on the lattice dimension is concealed in the variance of the single-particle spectrum. Only in 1D and for $U/t \lesssim 10$ the deviations from the common trend are significant. Most notably, we obtain a universal behavior of E_0, K and D for all d in the limit of strong correlations ($U/t \gtrsim 10$). For example, the ground-state energy is obtained as $E_0 = -4d \log(2) t_d^2/U = -4 \log(2) t^2/U$ in the strongly-correlated Heisenberg limit (see Appendix E.1). This, however, contrasts with accurate QMC simulations and exact diagonalizations on finite square clusters, which do not show such a simple scaling between the ground-state energies of the 1D and 2D Heisenberg models [109–112]. In fact, on the basis of these results for the Heisenberg model one infers, after proper scaling of the hopping integrals $t_d = t/\sqrt{d}$, that the ratio between the ground-state energies of the strongly correlated 1D and 2D Hubbard models is approximately $E_0^{1D}/E_0^{2D} = 1.185$. This also suggests that the convergence to the limit of infinite dimensions is probably slower than predicted by the linear IFE-approximation.

In Fig. 4.6 we show results for the SPDM elements $\gamma_{0\delta\sigma}$ between a site $i = 0$ and its δth NN in the ground state of the half-filled 1D Hubbard model ($n_\uparrow = n_\downarrow = 1/2$). For even values of δ the electron-hole symmetry implies $\gamma_{0\delta\sigma} = 0$, since the corresponding lattice sites belong to the same sublattice as the site $i = 0$ [see the discussion in the context of Eq. (4.25)]. Figure 4.6 (a) shows how $|\gamma_{0\delta\sigma}|$ decreases with increasing U/t, as charge fluctuations are suppressed in order to reduce the average number of double occupations. Notice that the long-range charge fluctuations (larger values of δ) are suppressed faster with increasing U/t than the short-range ones. This applies in particular to $\gamma_{01\sigma}$, which corresponds to the charge fluctuation between NNs, and which decreases much slower than the long-range fluctuations ($\delta \geq 3$). Most notably, in the strongly-correlated Heisenberg limit we have $K \propto t^2/U$, such that $\gamma_{01\sigma}$ decreases proportional to t/U, while the long-range charge fluctuations $|\gamma_{0\delta\sigma}|$ with odd $\delta \geq 3$ fall off exponentially for large values of U/t. Notice that, to the best of our knowledge, the exact values of $\gamma_{0\delta\sigma}$ with $\delta > 1$ cannot be inferred from the Bethe-ansatz solution for the infinite Hubbard chain [49].

A different perspective is adopted in Fig. 4.6 (b), and $\gamma_{0\delta\sigma}$ is shown as a function of δ for representative values of U/t. In the noninteracting limit ($U/t = 0$) the exact result

$$\gamma_{0\delta\sigma} = \frac{1}{2\pi} \int_{-\pi/2}^{\pi/2} e^{-ik\delta} \, dk = \frac{\sin(\delta\pi/2)}{\delta\pi} \tag{4.35}$$
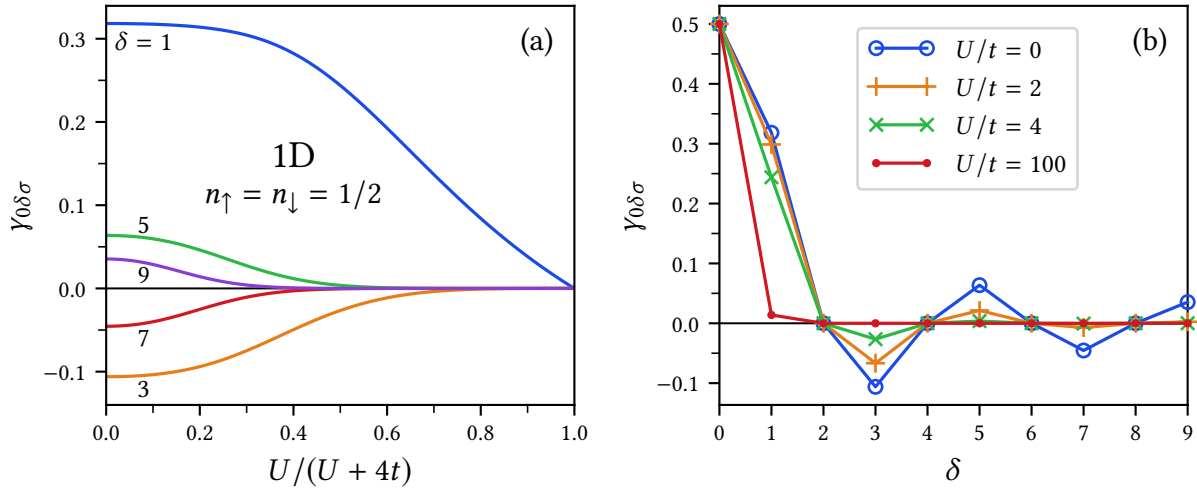
Figure 4.6: Single-particle density matrix elements $\gamma_{0\delta\uparrow} = \gamma_{0\delta\downarrow}$ between a lattice site $i = 0$ and its δth NN in the ground state of the half-filled 1D Hubbard model, as obtained by the linear IFE-approximation. In (a), $\gamma_{0\delta\sigma}$ is shown as a function of the Coulomb-repulsion strength U/t. In (b), $\gamma_{0\delta\sigma}$ is shown as a function of the distance δ for representative values of U/t. Electron-hole symmetry implies $\gamma_{0\delta\sigma} = 0$ for even $\delta > 0$. Adapted from Müller *et al.* [1], ©2018 American Physical Society.

is obviously obtained, since for vanishing interaction strength only the low-lying Bloch states are occupied, i.e., $\eta_\sigma(k) = 1$ for $|k| < \pi/2$ and $\eta_\sigma(k) = 0$ else. Thus, $\gamma_{0\delta\sigma}$ vanishes for even values of $\delta > 0$, and for odd δ it decreases in absolute value as δ increases. Notice that $|\gamma_{0\delta\sigma}|$ with odd δ decreases like $1/\delta$ in the noninteracting limit, and with increasing values of U/t the decrease becomes much more rapid. Consequently, the oscillations in $\gamma_{0\delta\sigma}$ are rapidly flattened as U/t increases, indicating the suppression of charge fluctuations and the progressive onset of localization.

In order to investigate non-bipartite lattices, which may show different kinds of correlations, and in order to address the problem of magnetic frustrations in infinite lattices, we consider the half-filled Hubbard model on the infinite 2D triangular lattice. In Fig. 4.7 results are shown for the ground-state energy E_0, the kinetic energy K and the average number of double occupations D, as obtained from LDFT with the linear IFE-approximation to the interaction-energy functional $W[\boldsymbol{\eta}]$. One observes that the dependence on U/t is qualitatively similar to the one obtained from exact diagonalizations of the Hubbard model on a 4×4 cluster from the triangular lattice with periodic boundary conditions. In the weakly correlated limit the IFE approximation recovers the HF average number of double occupations $D_{HF} = 1/4$. In contrast to the finite systems considered in the previous section, there are no issues related to degeneracies at the Fermi-level in the thermodynamic limit, as already discussed in
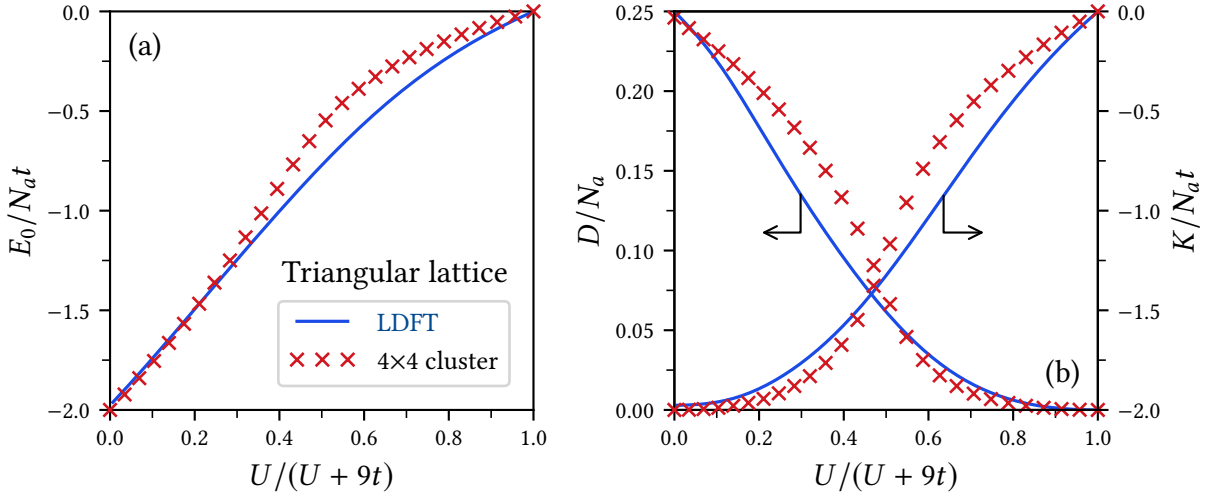
Figure 4.7: Ground-state properties of the half-filled Hubbard model on the infinite 2D triangular lattice as functions of the Coulomb-repulsion strength U/t: (a) total energy E_0 and (b) average number of double occupations D and kinetic energy K. The full curves are obtained by LDFT in combination with the linear IFE-approximation (4.17), while the crosses correspond to the exact diagonalization of a finite 4×4 cluster with periodic boundary conditions. Adapted from Müller *et al.* [1], ©2018 American Physical Society.

Section 4.2.2. Furthermore, the correct qualitative behavior $E_0/N_a = -\alpha t^2/U$ is obtained in the strongly correlated Heisenberg limit, with $\alpha_{\text{IFE}} = 8.62$. This result can be compared with numerical estimates based on the extrapolation of finite-cluster diagonalizations for the Heisenberg model, from which one infers $\alpha_{\text{ex}} = 7.41$ [113]. Notice that the relative error in α is only about 16% and therefore significantly smaller than in the case of the finite triangular 4×4 cluster discussed in Section 4.2.3.

Summarizing this section, we have shown that LDFT in combination with the linear IFE-approximation (4.17) yields the ground-state properties of the half-filled Hubbard model on infinite lattices with very good accuracy, as demonstrated by comparison with available exact results or QMC simulations [49, 57, 59, 64]. Most remarkably, not only the ground-state energy E_0 of the one-dimensional Hubbard chain, but also the more subtle average number of double occupations D and the kinetic energy K are reproduced almost exactly in the complete range from weak to strong interactions. Furthermore, our results are exact in the strongly-correlated Heisenberg limit of the one-dimensional chain, and qualitatively correct results are obtained in higher dimensions with fairly accurate values for the coefficient α of the ground-state energy $E_0/N_a = -\alpha t^2/U$. Also results for the dependence of $\gamma_{0\delta\sigma}$ on the distance δ and the Coulomb-repulsion strength U/t have been obtained for the one-dimensional Hubbard chain, which are not accessible by the exact Bethe-ansatz solution [49]. These

results show how charge fluctuations decrease with the distance between the lattice sites and, how increasing Coulomb interactions give rise to a gradual suppression of the electronic motion. We have also shown that the scope of the linear IFE-approximation is not limited to bipartite lattices. In fact, the results obtained for the magnetically frustrated triangular lattice are in good qualitative agreement with exact diagonalizations on finite clusters, as well as with the exact results in the strongly correlated Heisenberg limit [113]. Regarding the dependence on the coordination number of the underlying lattice, we may conclude that the accuracy of the linear IFE-approximation tends to worsen as the coordination number increases. Thus, the 1D lattice is described more precisely than the 2D square lattice, which in turn is described more precisely than the 2D triangular lattice. Furthermore, comparing the results presented in this section with the ones of Section 4.2, one may conclude that the accuracy of the linear IFE-approximation tends to improve as the system size increases, which is true for both the weakly and strongly correlated regimes. This might indicate that the statistical analog underlying the IFE approximation is more suitable for infinite systems having continuous single-particle spectra.

4.4 Spin-polarized systems

In order to investigate the ground-state properties of the Hubbard model as a function of the spin polarization, we minimize the energy functional $E[\boldsymbol{\eta}]$ under the constraint of fixed $n_\uparrow - n_\downarrow = 2S_z/\hbar N_a$. In Fig. 4.8 we present results for the total, kinetic and Coulomb energies of the half-filled 1D Hubbard model as functions of S_z. As expected, the minimum energy is always attained for $S_z = 0$, since the ground state has total spin $S = 0$ for all U/t [49]. The polarization energy $\Delta E(S_z) = E(S_z) - E(0)$ results from the interplay between the kinetic-energy increase and the Coulomb-energy decrease [see Figs. 4.8 (b) and 4.8 (c)] as the occupations $\eta_{k\sigma}$ of the antibonding ($\varepsilon_k > 0$) majority-spin Bloch states increase at the expense of decreasing occupations of the minority-spin bonding Bloch states ($\varepsilon_k < 0$). Double occupations are progressively suppressed as $|S_z|$ increases, since the probability of finding two electrons with opposite spin-polarization at the same site decreases. In the extreme case of the fully-polarized state (i.e., $|S_z| = \hbar N_a/2$), all lattice sites are occupied by one majority-spin electron and therefore both, local double occupations and interatomic charge fluctuations, are fully suppressed. This implies vanishing total, kinetic, and Coulomb energies for all values of U/t (see Fig. 4.8). The maximum polarization energy $\Delta E(S_z = \hbar N_a/2) = -E(S_z = 0)$, i.e., the energy difference between the fully-polarized and unpolarized states, decreases with increasing Coulomb-repulsion strength U/t and tends to zero in the strongly correlated limit $U/t \to \infty$ since the ground-state energy $E_0 = E(S_z = 0)$ is a monotonic increasing function of U/t. Fur-
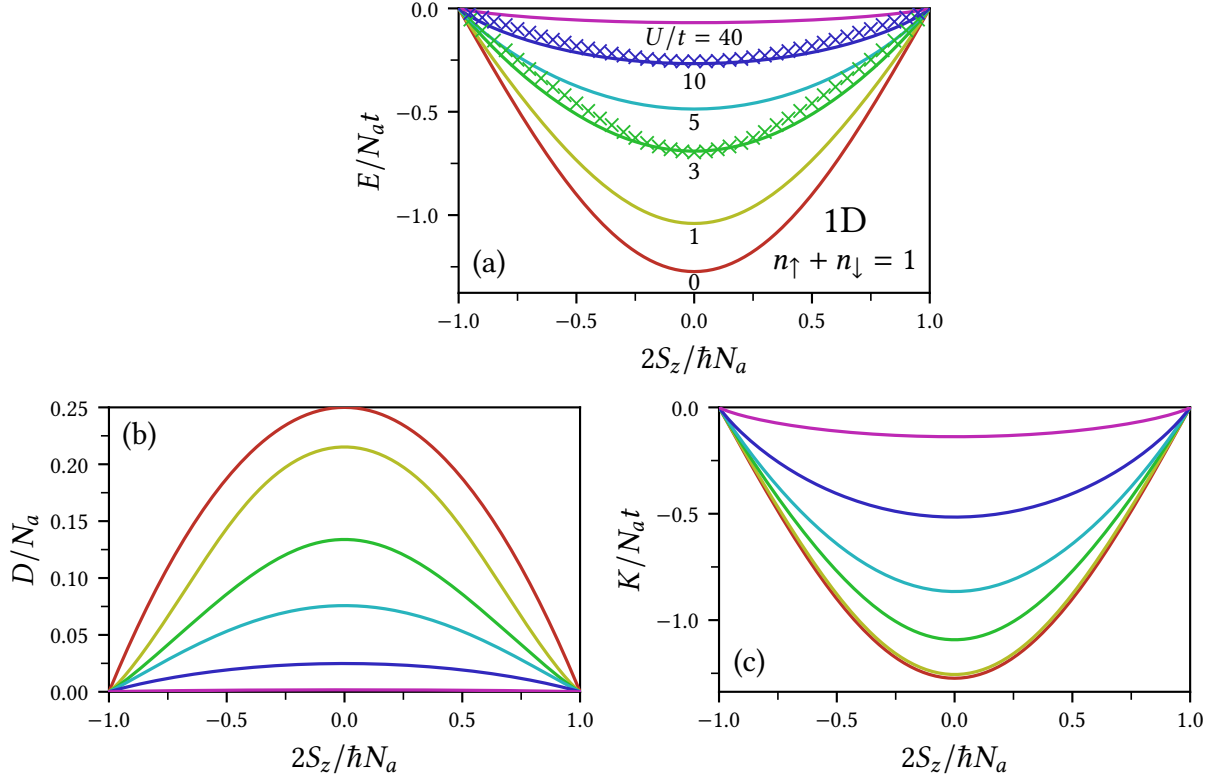
Figure 4.8: Ground-state properties of the one-dimensional half-filled Hubbard model as functions of the spin polarization per atom $n_\uparrow - n_\downarrow = 2S_z/\hbar N_a$ for representative values of the Coulomb-repulsion strength U/t: (a) total energy E, (b) average number of double occupations D, and (c) kinetic energy K. The curves were obtained by LDFT in the linear IFE-approximation, while the crosses in (a) for $U/t = 3$ and 10 are results taken from Ref. [50]. Adapted from Müller *et al.* [1], ©2018 American Physical Society.

thermore, the fact that $\Delta E(S_z) = 0$ for all S_z when $U/t \to \infty$ signals that the energy of the system becomes independent of the total spin S in the strongly-correlated limit, as the effective Heisenberg exchange-coupling constant $J \propto t^2/U$ between NN-spins tends to zero.

In order to assess the accuracy of the present linear IFE-approximation, we compare in Fig. 4.8 (a) our results for $E(S_z)$ with the corresponding results taken from Ref. [50], which are based on the Bethe-ansatz solution and are exact in the unpolarized limit $S_z \to 0$. One observes an overall satisfactory agreement between the two approaches for the two available values of the Coulomb-repulsion strength $U/t = 3$ and 10. Notice, however, that the linear IFE-approximation tends to underestimate the curvature of $E(S_z)$ in the vicinity of $S_z = 0$, which anticipates an overestimation
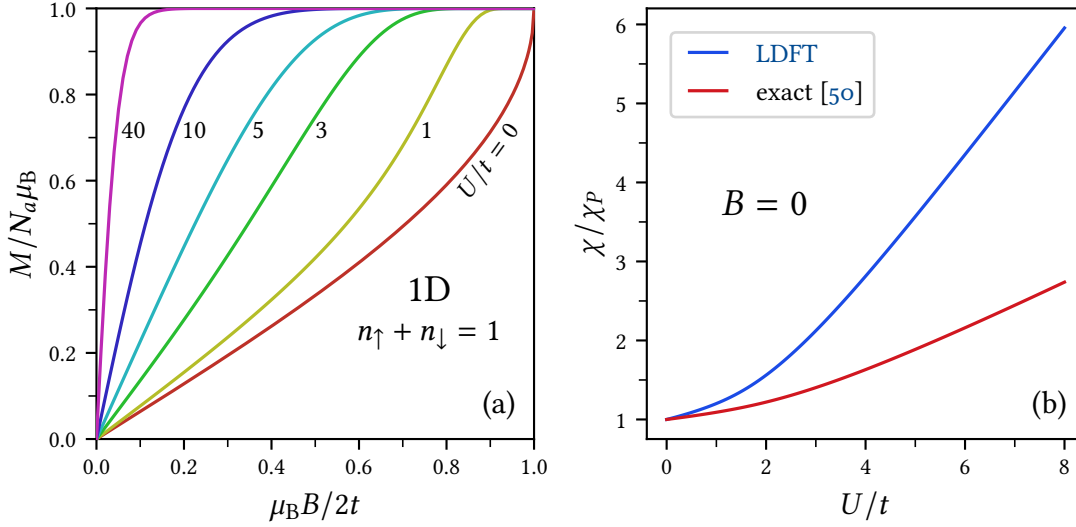
Figure 4.9: (a) Ground-state magnetization $M = -2\mu_B S_z/\hbar$ of the one-dimensional half-filled Hubbard model as a function of the applied magnetic-field strength B. Results of LDFT combined with the linear IFE-approximation are shown for representative values of the Coulomb-repulsion strength U/t. (b) Zero-field magnetic susceptibility χ in units of the uncorrelated Pauli susceptibility $\chi_P = \mu_B^2 N_a/\pi t$ as a function of the Coulomb-repulsion strength U/t. The blue curve corresponds to the linear IFE-approximation, while the red curve shows exact result taken from Ref. [50]. Adapted from Müller *et al.* [1], ©2018 American Physical Society.

of the zero-field magnetic susceptibility χ.

In order to obtain the ground-state magnetization $M = -g_e \mu_B S_z/\hbar$ in the presence of a uniform external magnetic field $\boldsymbol{B} = B\,\hat{\boldsymbol{e}}_z$, we use our previous results for $E(S_z)$ and simply minimize $E_B(S_z) = E(S_z) + g_e \mu_B B S_z/\hbar$ with respect to S_z. Here, μ_B is the Bohr magneton, and g_e the Landé factor, for which it suffices to take $g_e \approx 2$ in the following. In Fig. 4.9 (a) we present results for the ground-state magnetization M of the half-filled one-dimensional Hubbard model as a function of the external magnetic field-strength B for some representative values of the Coulomb-repulsion strength U/t. These results were obtained by LDFT in the linear IFE-approximation. As expected, the magnetization M increases monotonously with increasing field-strength B, until saturation, i. e., $M = N_a \mu_B$, is reached. The magnetization and also its slope $\chi = \partial M/\partial B$ at $B = 0$ are increasing functions of U/t. Consequently, the critical field-strength B_c for which the magnetization saturates decreases with increasing Coulomb-repulsion strength U/t. The critical field-strength is therefore bounded above by the value $\mu_B B_c = 2t$ derived from the magnetization curve

$$\frac{M}{N_a\,\mu_B} = 1 - \frac{2}{\pi}\arccos\left(\frac{\mu_B B}{2t}\right) \qquad (4.36)$$

of the noninteracting half-filled Hubbard chain. The more rapid increase of M and the corresponding lowering of the critical field-strength B_c with increasing values of U/t can be understood by recalling that the energy difference $\Delta E(S_z = \hbar N_a/2)$ between the fully-polarized and the unpolarized states, which represents the band-width for spin-excitations, decreases with U/t.

The zero-field magnetic susceptibility χ can be directly related to the curvature α of the ground-state energy $E(S_z)$ in the vicinity of $S_z = 0$. In fact, from $\Delta E(S_z) = \alpha S_z^2/\hbar^2 N_a + O(S_z^4)$ one readily obtains $\chi = 2\mu_B^2 N_a/\alpha$. In Fig. 4.9 (b) we compare the zero-field susceptibility χ obtained in the linear IFE-approximation with Takahashi's exact results for the half-filled one-dimensional Hubbard model [50]. In the noninteracting limit ($U/t = 0$) our approximation correctly reproduces the well known Pauli susceptibility $\chi_P = 2\mu_B^2 N_a \rho(\varepsilon_F)$, where $\rho(\varepsilon_F) = 1/(2\pi t)$ is the single-particle DOS per spin (4.28) of the Hubbard chain at the Fermi-level $\varepsilon_F = 0$. Furthermore, the IFE approximation explains qualitatively the increase of χ with increasing Coulomb repulsion strength, as the electrons start to localize and the band width of spin excitations narrows. Moreover, the IFE approximation reproduces qualitatively the linear increase of χ in the strongly-correlated limit. However, the corresponding asymptotic behavior $\chi \simeq (\pi \chi_P/4)(U/t)$ (see Appendix E.2) differs from the exact asymptotic result $\chi \simeq (\chi_P/\pi)(U/t)$ derived from the Bethe-ansatz solution [50]. Consequently, our approximation overestimates the zero-field magnetic susceptibility by a factor $\pi^2/4 \approx 2.5$ in the strongly-correlated regime. This is consistent with the previously observed underestimation of the curvature of $E(S_z)$ in the vicinity of $S_z = 0$ [see Fig. 4.8 (a)].

4.5 Attractive interactions

The study of electronic pairing, which leads to superconductivity, remains a major challenge in solid-state physics. In this context, an alternative approach to the famous theory of Bardeen, Cooper, and Schrieffer (BCS) [114] is to consider the Hubbard model (4.1) with local attractive interactions, i.e., with $U < 0$. Clearly, these two approaches to the problem of electronic pairing in metals are vastly different. The effective attractive interactions in the BCS theory have an off-diagonal scattering character, are mediated by phonons, and the spatial extension of the resulting Cooper pair is quite large. In contrast, the interactions in the attractive Hubbard model are strictly local, since they only affect electrons occupying the same lattice site. It is because of these profound differences that the investigation of the physical properties of the attractive Hubbard model are of considerable interest in order to examine the consequences of electronic pairing in solids from a complementary perspective. The attractive Hubbard model has already been addressed in the framework of LDFT

by Saubanère and Pastor [86], who used a simple but very effective scaling approximation to the interaction-energy functional $W[\gamma]$, which is based on exact results for the Hubbard dimer ($N_a = 2$). In this way it was possible to obtain very accurate ground-state observables for the case of bipartite lattices in 1–3 dimensions having homogeneous and alternating local energy levels.

It is the purpose of this section to investigate the attractive Hubbard model from a delocalized k-space perspective by generalizing the IFE approximation to the case of attractive interactions. A rather straight-forward approach towards this goal would be to exploit the electron-hole transformation discussed in the context of Eq. (2.39), which maps the attractive model on a bipartite lattice to a (generally spin-polarized) repulsive model, and to subsequently apply the well-established IFE approximation (4.17) to the resulting repulsive Hubbard model with $N_a - N_\downarrow$ down-spins. Notice, however, that this approach would be restricted to the case of bipartite lattices. Our goal is to derive a physically sound approximation to attractive correlations from an independent perspective in a general way, which is not restricted to bipartite lattice structures. Nevertheless, the existence of a mapping between the attractive and repulsive Hubbard models suggests that the correlations caused by attractive and repulsive interactions are deeply related. Indeed, with increasing interaction-strength $|U|/t$ the fermions tend to localize for attractive as well as for repulsive interactions. However, the physical nature of the localization is quite different. Repulsive interactions lead to the formation and stabilization of local magnetic moments, whereas attractive interactions tend to suppress the local moments and stabilize localized fermion pairs with opposite spin polarization. In spite of these differences, we can expect that the competition between delocalization, driven by the hybridizations, and localization, resulting from the interactions between the particles, is quite similar in the repulsive and attractive cases. This encourages us to use the IFE defined in Eq. (4.10) as an effective measure for the degree of the correlations between the particles also in the case of attractive interactions. In order to verify that the IFE is indeed a measure for the correlations caused by attractive interactions, and to quantify its relation to the interaction energy W, we have performed exact numerical Lanczos diagonalizations for the ground state of the half-filled attractive Hubbard model on multiple lattice structures. To this aim, we have varied the hopping integrals from $t_{ij} = 0$ to $t_{ij} \gg |U|$ in order to scan the complete range of possible values $0 \leq S \leq S_\infty$ of the IFE. In Fig. 4.10 the interaction energy W is scaled between the uncorrelated HF-limit $W_{\mathrm{HF}} = UN_\uparrow N_\downarrow / N_a$ and the strongly-correlated limit $W_\infty = UD_\infty$, where $D_\infty = \min\{N_\uparrow, N_\downarrow\}$ is the maximum number of double occupations. The results presented in Fig. 4.10 show a remarkable one-to-one correspondence between W and S, which, after proper scaling with respect to the extreme values W_{HF}, W_∞, and S_∞, becomes approximately independent of the size and dimension of the system under consideration. This one-to-one correspondence between W and S could thus be exploited in order to derive broadly applicable
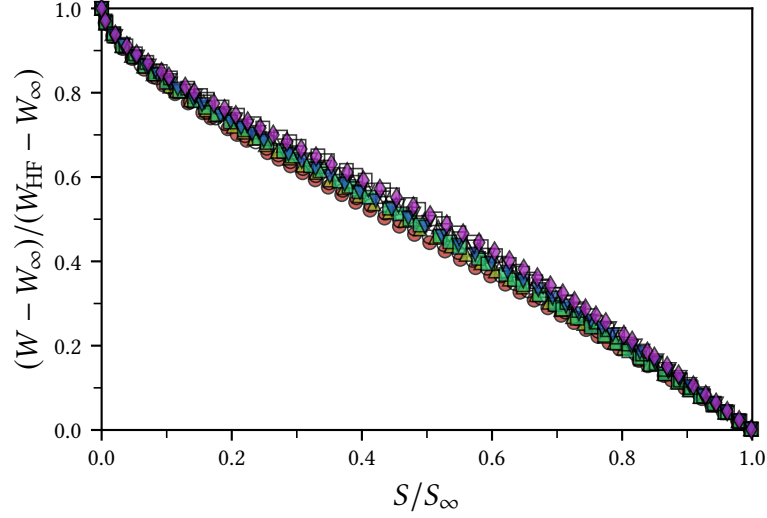
Figure 4.10: Relation between the interaction energy W and the IFE S in the ground state of the half-filled attractive Hubbard model, as obtained from exact numerical Lanczos diagonalizations for a number of different periodic lattice structures. Results are shown for finite 1D rings having $N_a = 6$ (circles), $N_a = 10$ (upright triangles) and $N_a = 14$ (squares) lattice sites, as well as for 2D square-lattices having $N_a = 2 \times 4$ (downright triangles) and $N_a = 3 \times 4$ (diamonds) lattice sites. The solid symbols correspond to the Hubbard model with only NN hopping t, while the open symbols represent results for the non-bipartite case where second-NN hoppings $t_2 = t/2$ are included.

approximations to the interaction-energy functional $W[\boldsymbol{\eta}]$. In the case of a bipartite lattice it is straight forward to derive the relation $W^{(a)} - W_\infty = W^{(r)}$ between the interaction energy in the ground state of the attractive and repulsive Hubbard models, by applying the electron-hole transformation discussed in the context of Eq. (2.39) to the majority spins. Therefore, in the case of bipartite lattices, the scaled ground-state interaction energy shown in Fig. 4.10 follows the exact same dependence as a function of S as the scaled interaction energy in the ground state of the previously considered repulsive Hubbard model (see Fig. 4.1). Notice, however, that Fig. 4.10 also includes results for non-bipartite lattices, such as the periodic 3×4 square-lattice cluster and all lattices with second-NN hoppings. This shows that the common, approximately linear one-to-one relation between the (scaled) interaction energy W and the IFE S is not restricted to the bipartite case, but instead also holds for more general systems. Therefore, we propose to generalize our previous approximation to the interaction-energy functional $W[\boldsymbol{\eta}]$ of the Hubbard model in terms of the IFE $S[\boldsymbol{\eta}]$ as

$$\frac{W[\boldsymbol{\eta}] - W_\infty}{W_{\mathrm{HF}} - W_\infty} = f\left(\frac{S[\boldsymbol{\eta}]}{S_\infty}\right), \tag{4.37}$$

where the function $f : [0,1] \rightarrow [0,1]$ accounts for the common relation between the properly scaled interaction energy W and the IFE S in the attractive and repulsive cases, shown in Figs. 4.1 and 4.10. Furthermore, $W_{\mathrm{HF}} = U N_\uparrow N_\downarrow / N_a$ refers to the uncorrelated HF interaction-energy and

$$W_\infty = U D_\infty \quad \text{with} \quad D_\infty = \begin{cases} \min\{N_\uparrow, N_\downarrow\} & \text{for } U < 0 \\ \max\{N - N_a, 0\} & \text{for } U > 0 \end{cases} \tag{4.38}$$

to the interaction energy in the strongly correlated limit ($|U|/t \rightarrow \infty$). Notice that Eq. (4.37) applies to the Hubbard model with *both* attractive and repulsive interactions, and thus the notion *generalized* IFE-approximation is justified. Since Eq. (4.37) approximates $W[\boldsymbol{\eta}]$ in terms of $S[\boldsymbol{\eta}]$, the consequences of the approximation (4.12) also apply to Eq. (4.37) and thus also to the case of attractive interactions. This applies in particular to the result (4.16) which states that ground-state occupation-numbers $\eta_{k\sigma}$ follow a Fermi-Dirac distribution with an effective U-dependent temperature $T_{\mathrm{eff}} = -\partial W / \partial S$.

Before we apply the generalized IFE-approximation (4.37) to the attractive Hubbard model on finite clusters, it is useful to analyze its relation to the electron-hole transformation (2.39) which maps between attractive and repulsive interactions. It turns out that the relations between the attractive and repulsive models on bipartite lattices are not reproduced for arbitrary particle numbers N_σ. Only for $N_\downarrow = N_a/2$, i.e., if the number of down-spins is conserved under the electron-hole transformation, one can easily show that the generalized IFE-approximation (4.37) correctly reproduces the relations $K^{(a)} = K^{(r)}$ and $W^{(a)} + |U|N_\uparrow = W^{(r)}$ between the kinetic and interaction energies of the attractive and repulsive Hubbard models on bipartite lattices. Notice, however, that the generalized IFE-approximation predicts these relations independent of the lattice structure, i.e., also for non-bipartite lattices. Furthermore, for $N_\downarrow = N_a/2$ it is easy to verify that the generalized IFE-approximation yields the same gs-SPDM $\boldsymbol{\gamma}^{(a)} = \boldsymbol{\gamma}^{(r)}$ for the attractive and repulsive Hubbard models on a bipartite lattice, while the electron-hole transformation implies that $\gamma_{ij\downarrow}^{(a)} = \pm\gamma_{ij\downarrow}^{(r)}$ for $i \neq j$, where the negative sign applies if the sites i and j belong to the same sublattice and the positive otherwise. Consequently, the generalized IFE-approximation fails to reproduce the sign-change of those SPDM elements that do not contribute to the kinetic energy of the Hubbard model on a bipartite lattice. These SPDM elements are non-vanishing in general, however, in the special case where the ground state for $N_\uparrow = N_\downarrow = N_a/2$ is non-degenerate they vanish altogether (see Section 4.2.1). In this case the predictions of the generalized IFE-approximation (4.37) are consistent with the implications of the electron-hole transformation.

In order to apply the generalized IFE-approximation to the attractive Hubbard model on finite lattices, we follow the route taken in the repulsive case and propose to approximate the function f in Eq. (4.37) by the linear relation $f(x) = 1 - x$, such
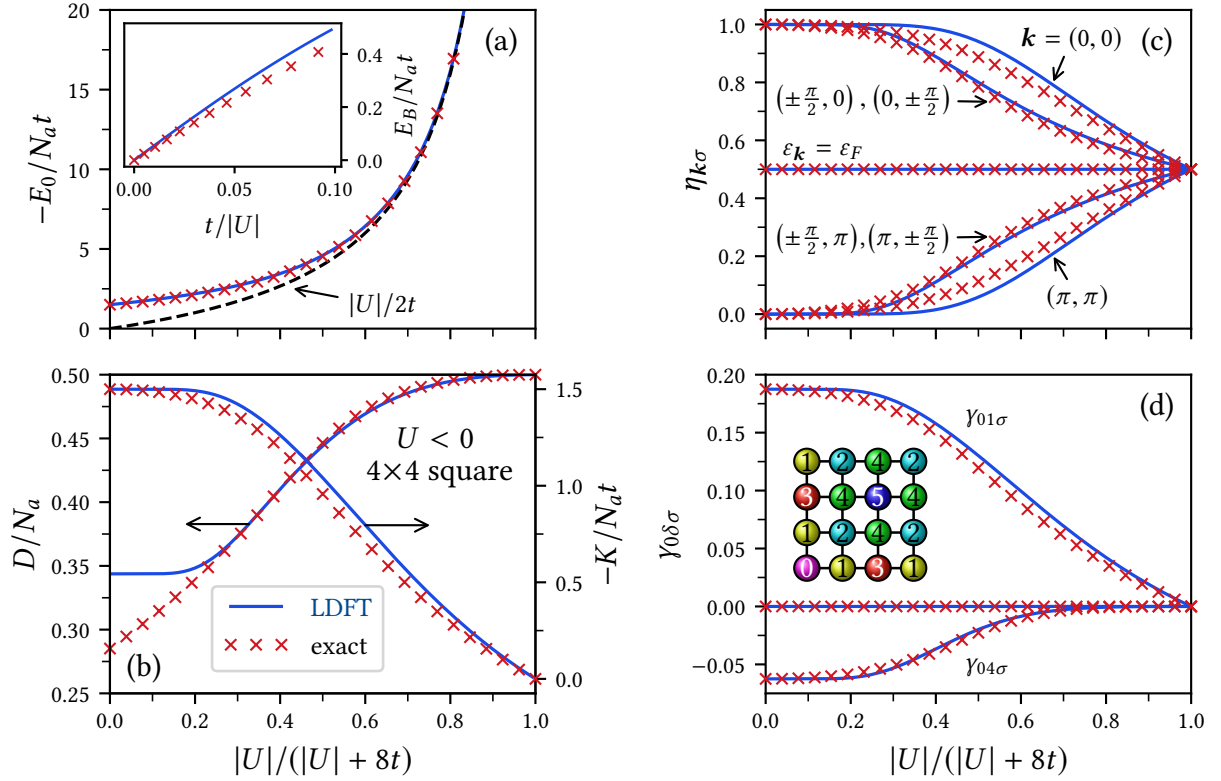
Figure 4.11: Ground-state properties of the attractive 2D Hubbard model on a 4×4 square lattice cluster with $N_\uparrow = N_\downarrow = 8$ and periodic boundary conditions as functions of the attraction strength $|U|/t$. Results of LDFT combined with the generalized linear IFE-approximation (4.39) (blue full curves) are compared with exact numerical Lanczos diagonalizations (red crosses): (a) ground-state energy E_0, (b) average number of double occupations D and kinetic energy K, (c) natural-orbital occupation numbers $\eta_{\bm{k}\uparrow} = \eta_{\bm{k}\downarrow}$, and (d) gs-SPDM elements $\gamma_{0\delta\uparrow} = \gamma_{0\delta\downarrow}$ between site $i = 0$ and its δth NN, as illustrated in the inset. The inset in subfigure (a) shows the binding energy $E_B = W_\infty - E_0$ in the strongly-correlated limit ($|U| \gg t$).

that the generalized IFE-approximation becomes

$$W[\boldsymbol{\eta}] = W_{\mathrm{HF}} + (W_\infty - W_{\mathrm{HF}}) \frac{S[\boldsymbol{\eta}]}{S_\infty} \,. \tag{4.39}$$

In the repulsive case with $N \le N_a$, i.e., $W_\infty = 0$, this coincides with the linear IFE-approximation (4.17) discussed in the previous sections. In Fig. 4.11 we show results for the ground-state properties of the half-filled attractive 2D Hubbard model on a 4×4 square-lattice cluster with periodic boundary conditions and $N_\uparrow = N_\downarrow = 8$. The comparison with exact Lanczos diagonalizations shows that the quality of LDFT in combination with the generalized IFE-approximation (4.39) is as good as in the repulsive case considered in Section 4.2.2. This is not surprising, since the 4×4 cluster with NN hopping is bipartite, and for $N_\uparrow = N_\downarrow = N_a/2$ the generalized IFE-approximation reproduces the relations between the attractive and repulsive Hubbard models inferred from the electron-hole transformation (2.39). Also in this case, where the attractive and repulsive models are connected by an electron-hole transformation, it is very interesting to take a closer look at the ground-state properties of the attractive Hubbard model and to investigate the differences and similarities to the previously considered repulsive case.

Figure 4.11 (a) demonstrates that the ground-state energy E_0 of the attractive Hubbard model is accurately reproduced by the linear IFE-approximation in the complete range of the interaction strength $|U|/t$. In contrast to the repulsive case, we find a monotonously decreasing ground-state energy as the attraction strength $|U|/t$ increases, since the pair-binding energy of the condensing fermions overcompensates the increase in kinetic energy caused by the gradual fermionic localization. Most notably, in the strongly correlated limit $|U|/t \rightarrow \infty$ the pair-binding energy of the condensing fermions dominates and gives rise to a diverging ground-state energy $E_0 \simeq W_\infty = -|U|N_a/2$. Notice that first order hopping processes are prohibited in the strongly-correlated limit, since they would break a strongly bound fermion pair. The fermions can, however, lower their kinetic energy $K \propto t^2/U$ by second order (virtual) hopping processes which break and subsequently reassemble a local fermion pair. Thus, one can expect that the binding energy $E_B = W_\infty - E_0$ behaves like $E_B = \alpha t^2/|U|$ with $\alpha > 0$ in the strongly correlated limit [see the inset in Fig. 4.11 (a)]. In fact, one infers $-E_B = E_0 + |U|D_\infty = E_0^{(r)}$ from the electron-hole transformation (2.39), i.e., the binding energy resulting from the virtual hopping processes coincides with the negative ground-state energy $E_0^{(r)}$ of the repulsive model. Thus, the generalized linear IFE-approximation reproduces the binding energy $E_B = \alpha t^2/|U|$ in the strongly correlated limit of the attractive Hubbard model qualitatively correct, with a coefficient $\alpha_{\mathrm{IFE}} = 5.55$ which is only 13% larger than the exact value $\alpha_{\mathrm{ex}} = 4.81$ for the 4×4 square-cluster. These results are consistent with the ones for the repulsive Hubbard model on the 4×4 square-cluster discussed in Section 4.2.2.

Besides some discrepancies for $|U|/t < 2$, which are the result of degeneracies at the Fermi-level, we find in Fig. 4.11 (b) that also the average number D of ground-state double occupations is very well reproduced by the generalized linear IFE-approximation. As expected, we find increasing values of the double occupations D as the fermionic attraction strength $|U|/t$ increases, which is due to the formation of local fermion-pairs, until the maximum possible value $D_\infty = N_a/2$ is attained in the limit $|U|/t \to \infty$. The increase of the average number D of double occupations with increasing inter-action strength $|U|/t$ is accompanied with an increase of the kinetic energy K, since the fermions condense into localized pairs and one-fermion hopping processes are gradually suppressed as the interaction energy starts to overcompensate the binding energy generated by the fermionic motion. Clearly, in the strongly correlated limit a fully localized state is attained and the kinetic energy vanishes like $K \propto t^2/U$, since first-order hopping processes would break the local strongly bound fermion-pairs.

The dependence of the gs-SPDM elements $\gamma_{ij\sigma}$ on the interaction strength $|U|/t$ is shown in Fig. 4.11 (d). Due to the symmetry of the underlying lattice it is suffi-cient to focus on the matrix elements $\gamma_{0\delta\sigma}$ corresponding to some lattice site $i = 0$ and its δth NN, as illustrated in the inset. The non-vanishing SPDM elements $\gamma_{01\sigma}$ and $\gamma_{04\sigma}$ display the typical correlation-induced suppression of the charge fluctua-tions as $|U|/t$ increases and the fermions condense into localized pairs. Like in the previous case of repulsive interactions, the long-range charge fluctuations $|\gamma_{04\sigma}|$ are suppressed faster than the fluctuations $\gamma_{01\sigma}$ between NNs. In fact, the dependence of the gs-SPDM elements $\gamma_{0\delta\sigma}$ on the strength $|U|/t$ of the attractive interaction coin-cides with the one in the previously considered repulsive case. This is a result of the electron-hole symmetry (2.39), which implies that the gs-SPDM of the attractive and repulsive Hubbard models on bipartite lattices with $N_\uparrow = N_\downarrow = N_a/2$ coincide if the ground state is non-degenerate. This implication is exactly reproduced by the gener-alized linear IFE-approximation (4.39), such that the results for the gs-SPDM shown in Fig. 4.11 (d) coincide with the ones of Fig. 4.3 (d) which accounts for repulsive inter-actions. Clearly, since the gs-SPDM of the attractive and repulsive Hubbard models coincide, the same must be true for its eigenvalues, i. e., for the Bloch-state occupation numbers $\eta_{k\sigma}$, which are shown in Fig. 4.11 (c). The fact that the occupation numbers and gs-SPDM elements of the attractive and repulsive Hubbard models coincide on a bipartite lattice with $N_\uparrow = N_\downarrow = N_a/2$ is a manifestation of the deep underlying rela-tion between the correlation induced localization caused by attractive and repulsive interactions in half-filled band systems.

In order to investigate situations where the ground-state properties of the repul-sive and attractive Hubbard models are not related by an electron-hole transforma-tion, we have to go beyond bipartite lattices. This can be achieved by considering essentially non-bipartite structures, such as the 2D triangular lattice, or by includ-ing hoppings beyond first-NNs. In order to address the second option we have com-
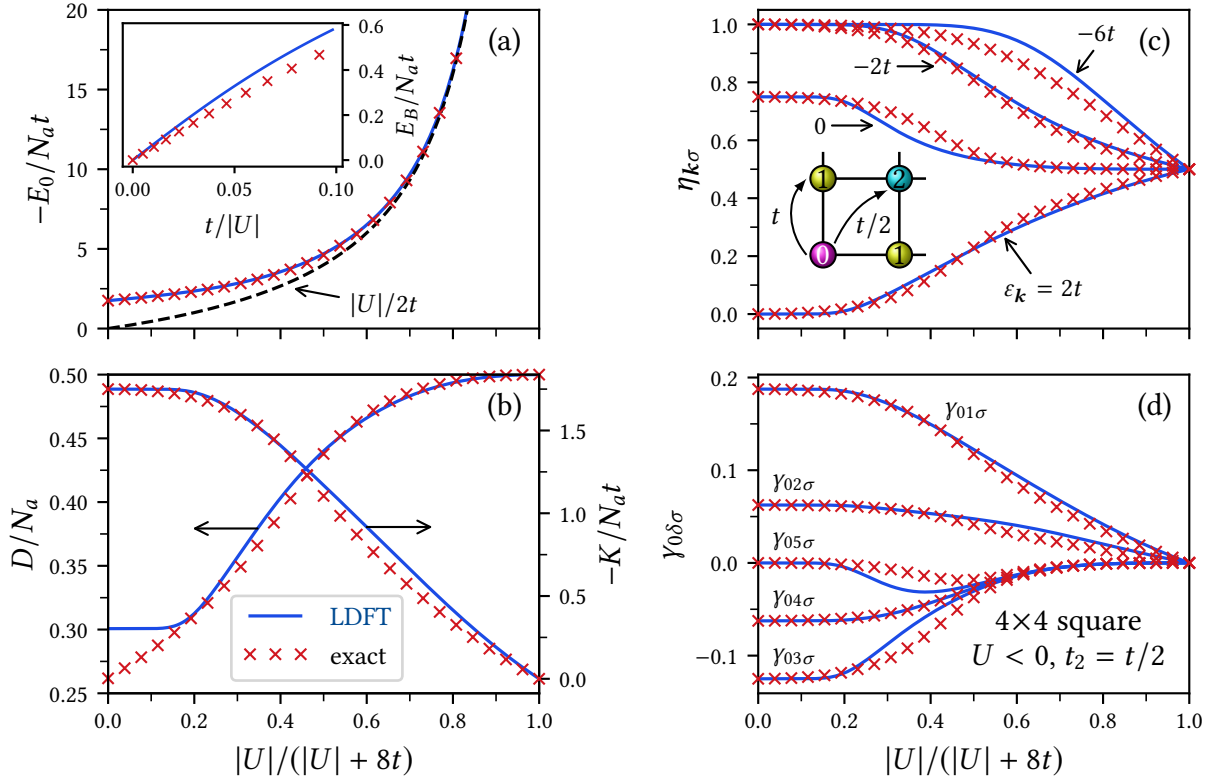
Figure 4.12: Ground-state properties of the attractive 2D Hubbard model with second-NN hopping $t_2 = t/2$ [as illustrated in subfigure (c)] on a 4×4 square lattice with $N_\uparrow = N_\downarrow = 8$ and periodic boundary conditions as functions of the attraction strength $|U|/t$. Results of LDFT combined with the generalized linear IFE-approximation (4.39) (blue full curves) are compared with exact numerical Lanczos diagonalizations (red crosses): (a) ground-state energy E_0, (b) average number of double occupations D and kinetic energy K, (c) natural-orbital occupation numbers $\eta_{k\uparrow} = \eta_{k\downarrow}$, and (d) gs-SPDM elements $\gamma_{0\delta\uparrow} = \gamma_{0\delta\downarrow}$ between site $i = 0$ and its δth NN, as illustrated in the inset of Fig. 4.11 (d). The inset in subfigure (a) shows the binding energy $E_B = W_\infty - E_0$ in the strongly-correlated limit ($|U| \gg t$).

puted the ground-state properties of the half-filled attractive 2D Hubbard model on a 4×4 square-lattice with second-NN hopping $t_2 = t/2$ and $N_\uparrow = N_\downarrow = 8$. The ground-state energy E_0 shown in Fig. 4.12 (a) is very accurately reproduced by the generalized linear IFE-approximation (4.39) in the complete range from weak to strong attractions. This is most remarkable, especially in the range of intermediate interactions ($1 \lesssim |U|/t \lesssim 10$), since the interplay between delocalization driven by hybridizations and localization due to the formation of local fermion-pairs is far from trivial within this regime. Moreover, the asymptotic behavior of the ground-state energy $E_0 \simeq -|U|N_a/2$ in the strongly correlated limit $|U|/t \to \infty$ is exactly obtained within the linear IFE-approximation. The qualitative behaviour $E_B = \alpha t^2/|U|$ of the binding energy in the strongly-correlated regime is also correctly reproduced, with a coefficient $\alpha_{\text{IFE}} = 6.93$ which is about 18.5% larger than the exact value $\alpha_{\text{ex}} = 5.65$ deduced from the Lanczos calculations [see the inset in Fig. 4.12 (a)]. We conclude that the generalized IFE-approximation overestimates the binding energy in the strongly correlated limit slightly more if second-NN hoppings are included, when compared to the previous case where only hoppings between first-NN were implied. The dependence of the average number of ground-state double occupations D and the kinetic energy K on the interaction strength $|U|/t$, shown in Fig. 4.12 (b), is very similar to the previously considered case where only NN-hoppings were involved [see Fig. 4.11 (b)]. However, the inclusion of second-NN hopping allows the system to increase the absolute kinetic energy $|K|$ by about 16.7% in the weakly correlated regime and, at the same time, to reduce the average number of double occupations D by about 8.2% [compare Figs. 4.11 (b) and 4.12 (b)]. The kinetic-energy gain in the weakly-correlated regime, resulting from the inclusion of second-NN hoppings, is exactly reproduced within the linear IFE-approximation, while the average number of double occupations display the typical discrepancies resulting from degeneracies of the Fermi level. Nevertheless, the linear IFE-approximation predicts a decrease of the average number of double occupations by about 12.5% in the weakly-correlated regime due to the inclusion of second-NN hoppings, which is in qualitative agreement with the 8.2% decrease found in the exact results. Moreover, the discrepancies in D essentially disappear for $|U|/t \gtrsim 2$.

Regarding the dependence of the Bloch-state occupation numbers $\eta_{k\sigma}$ on the interaction strength $|U|/t$, shown in Fig. 4.12 (c), we find the typical decrease (increase) of $\eta_{k\sigma}$ for Bloch states having $\varepsilon_k < \varepsilon_F$ ($\varepsilon_k > \varepsilon_F$) as the interaction strength $|U|/t$ increases, which reflects the localization of the fermions. As in the repulsive case, a homogeneous occupation of all Bloch states, i. e., $\eta_{k\sigma} = 1/2$ for all k, is attained in the strongly correlated limit $|U|/t \to \infty$. In contrast to the case which involves only hoppings between NNs, we find decreasing values of the occupation numbers $\eta_{k\sigma}$ also for the Bloch states having $\varepsilon_k = \varepsilon_F = 0$. This is a consequence of the qualitative changes in the single-particle spectrum ε_k resulting from the inclusion of second-NN hoppings.

They lead to a fourfold degenerate Fermi level which is occupied by six fermions in the noninteracting limit $|U|/t \rightarrow 0$, such that $\eta_{k\sigma} = 3/4$ for $\sigma = \uparrow, \downarrow$ and all four Bloch states having $\varepsilon_k = \varepsilon_F$. As shown in Fig. 4.12 (c), the occupation numbers $\eta_{k\sigma}$ obtained from the generalized linear IFE-approximation (4.39) are very accurate in the complete interaction range from weak to strong correlations. Only the occupation of the lowest-lying Bloch state $[k = (0,0)]$ having $\varepsilon_k = -6t$ is slightly overestimated for intermediate $|U|/t$, which results in an overestimation of the absolute kinetic energy $|K|$ in this range. For example, at $|U|/t = 15$ the average occupation-number of the lowest-lying Bloch state is overestimated by 8.7%, which corresponds to an overestimation of $|K|$ by about 17%.

The gs-SPDM elements $\gamma_{0\delta\sigma}$ corresponding to a lattice-site $i = 0$ and its δth NN are shown in Fig. 4.12 (d). The hoppings between second NNs lift the electron-hole symmetry discussed in the context of Eq. (4.25), and as a result the matrix elements $\gamma_{0\delta\sigma}$ with $\delta = 2, 3$ and 5, which correspond to sites within the same sublattice in the absence of second-NN hoppings, are no longer identically zero. An interesting non-monotonous behaviour of $\gamma_{05\sigma}$ is observed, which is qualitatively reproduced, although somewhat exaggerated, by the generalized linear IFE-approximation. The non-monotonous $|U|/t$ dependence of $\gamma_{05\sigma}$ indicates that the second-NN hoppings enhance a charge transfer beyond 4th-NNs at intermediate interaction strength, which optimizes the kinetic energy and, at the same time, lowers the interaction energy due to the formation of local fermion-pairs, i e., due to an increase of the average number of double occupations D.

As an example of an essentially non-bipartite lattice (i. e., a lattice which is non-bipartite even if only NN hoppings are taken into account), we consider in Fig. 4.13 the 4×4 triangular lattice with periodic boundary conditions and $N_\uparrow = N_\downarrow = 8$. The comparison with exact numerical Lanczos diagonalizations in Fig. 4.13 (a) shows that the ground-state energy E_0 is again very accurately obtained within the generalized linear IFE-approximation in the complete range from weak to strong interactions. Also the qualitative behaviour $E_B = \alpha t^2/|U|$ of the binding energy in the strongly-correlated limit is correctly reproduced, and the corresponding coefficient $\alpha_{\text{IFE}} = 8.32$ is about 19% larger than the exact value $\alpha_{\text{ex}} = 6.73$ deduced from the Lanczos calculations [see the inset in Fig. 4.13 (a)]. We conclude that the strongly attracting limit on the 4×4 triangular-cluster is much better reproduced than the corresponding repulsive case, where the coefficient α is overestimated by 38% (see Section 4.2.3).

The average number of double occupations D and the kinetic energy K are shown in Fig. 4.13 (b), and a very similar dependence on $|U|/t$ as in the previously considered attractive models is observed, which is in general very well reproduced by the present IFE approximation. Only in the weakly interacting regime $|U|/t \lesssim 3$ we find the already observed significant overestimation of the double occupations D, which is known to be a consequence of the degeneracies in the single-particle spectrum at the
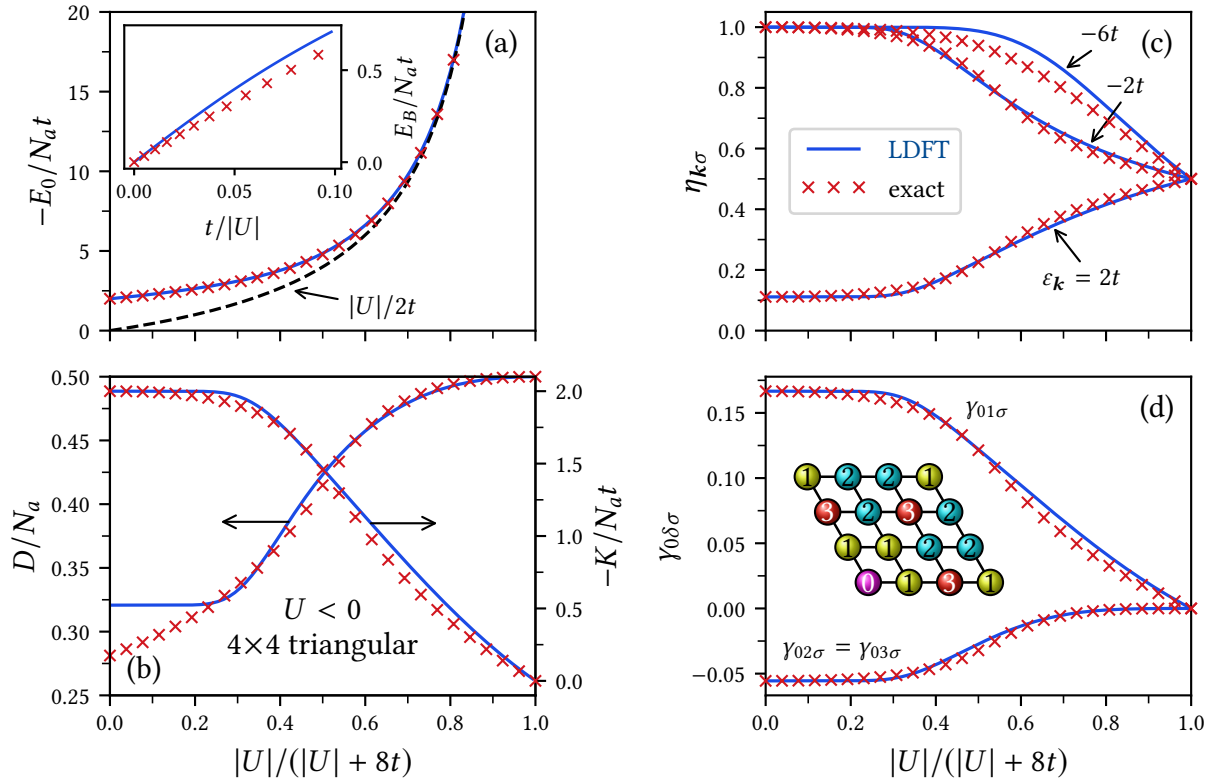
Figure 4.13: Ground-state properties of the attractive 2D Hubbard model on a 4×4 cluster of the triangular lattice with $N_\uparrow = N_\downarrow = 8$ and periodic boundary conditions as functions of the attraction strength $|U|/t$. Results of LDFT combined with the generalized linear IFE-approximation (4.39) (blue full curves) are compared with exact numerical Lanczos diagonalizations (red crosses): (a) ground-state energy E_0, (b) average number of double occupations D and kinetic energy K, (c) natural-orbital occupation numbers $\eta_{\boldsymbol{k}\uparrow} = \eta_{\boldsymbol{k}\downarrow}$, and (d) gs-SPDM elements $\gamma_{0\delta\uparrow} = \gamma_{0\delta\downarrow}$ between site $i = 0$ and its δth NN, as illustrated in the inset. The inset in subfigure (a) shows the binding energy $E_B = W_\infty - E_0$ in the strongly-correlated limit ($|U| \gg t$).

Fermi level.

Regarding the Bloch-state occupation numbers $\eta_{k\sigma}$, shown in Fig. 4.13 (c), one observes the familiar fermionic localization as $|U|/t$ increases: decreasing (increasing) occupations $\eta_{k\sigma}$ for Bloch states having $\varepsilon_k < \varepsilon_F$ ($\varepsilon_k > \varepsilon_F$), starting from $\eta_{k\sigma} = 1$ ($\eta_{k\sigma} = 0$) in the noninteracting limit, until $\eta_{k\sigma} = 1/2$ is reached for all $k\sigma$ in the strongly correlated limit. Concerning the occupation numbers $\eta_{k\sigma}$ of the Bloch states having $\varepsilon_k = \varepsilon_F = 2t$, we find $\eta_{k\sigma} = 1/9$ for $|U|/t \to 0$, since the nine-fold degenerate Fermi-level is occupied by two fermions with opposite spin directions.

A very interesting difference to the previously considered repulsive case is the fact that all Bloch states having $\varepsilon_k = \varepsilon_F = 2t$ are equally occupied in the complete range from weak to strong interactions, while they split into two groups if repulsive interactions are considered [see the exact numerical Lanczos results shown in Fig. 4.4 (c)]. As already discussed in Section 4.2.3, this splitting of the Fermi-level occupation numbers in the repulsive case is a subtle finite-size effect, by which the local Hubbard interaction between the two electrons at the Fermi level is completely suppressed. Clearly, such a suppression of the mutual interaction between the two electrons at the Fermi level would be energetically unfavorable in the present attractive case, and thus the Fermi-level occupation numbers do not split. Figure 4.13 (c) shows that the generalized IFE-approximation (4.39) reproduces the Bloch-state occupation numbers $\eta_{k\sigma}$ quite accurately in the complete range from weak to strong interactions. Only the occupation of the lowest-lying Bloch state [$k = (0,0)$] having $\varepsilon_k = -6t$ is slightly overestimated for intermediate values of the interaction strength $|U|/t$. It is worth noting that for $N_\uparrow = N_\downarrow = N_a/2$ the generalized IFE-approximation always yields the same occupation numbers for attractive and repulsive interactions, although the exact $\eta_{k\sigma}$ might be different if non-bipartite lattices are considered. Comparing Figs. 4.4 (c) and 4.13 (c), one concludes that the LDFT results are more accurate in the attractive case. This is not only due to the absence of the finite-size splitting of the Fermi-level occupation numbers in the attractive case, but also due to the higher accuracy of $\eta_{k\sigma}$ for $\varepsilon_k < \varepsilon_F$ and intermediate values of the interaction strength. The very good accuracy of $\eta_{k\sigma}$ also implies accurate results for the gs-SPDM elements $\gamma_{0\delta\sigma}$, as seen in Fig. 4.13 (d). In the considered attractive case we find $\gamma_{02\sigma} = \gamma_{03\sigma}$ in contrast to the repulsive case, where $\gamma_{02\sigma} \neq \gamma_{03\sigma}$ due to the finite-size correlations which manage to suppress the interaction of the two fermions at the Fermi level. Since this type of correlation is not at all favorable in the attractive case, we find $\gamma_{02\sigma} = \gamma_{03\sigma}$, as predicted by the generalized linear IFE-approximation (4.39).

In summary, the results presented in this section show that an appropriate generalization of the linear IFE-approximation allows us to extend the scope of LDFT to the ground-state properties of the half-filled attractive Hubbard model. This is not only true for bipartite lattices, where such an extension can be formally inferred from the electron-hole transformation (2.39) which maps between the attractive and repulsive

models, but also in more general situations involving non-bipartite structures or hoppings beyond first-NNs. We therefore conclude that the IFE (4.10) is a suitable measure of the degree of fermionic correlations in the Hubbard model for both attractive and repulsive interactions.

4.6 Arbitrary filling and Luttinger-liquid behavior

The focus of the previous sections has been on the ground-state properties of the half-filled Hubbard model, which corresponds to the highest carrier density and is therefore particularly interesting for the study of many-particle correlation effects. Developing accurate interaction-energy functionals for the general case of arbitrary band-filling $n = N/N_a$ poses a number of new challenges. For example, the ground-state kinetic energy K of the Hubbard model does in general not vanish in the strongly correlated limit $U/t \to \infty$ if $n \neq 1$, due to the ability of the electrons or holes to avoid each other completely in a correlated motion, for instance, by adopting a fully polarized state. Consequently, away from half band-filling the strongly-correlated ground state is no longer fully localized, and the gs-SPDM γ is thus no longer scalar. Non-vanishing off diagonal elements $\gamma_{ij\sigma}$ ($i \neq j$) and kinetic energy imply that the Bloch-state occupation numbers $\eta_{k\sigma}$ are no longer homogeneous in the strongly-correlated limit. Therefore, the strongly-correlated IFE S_∞, one of the essential scaling parameters in the linear IFE-approximation (4.17), is no longer easy to obtain in the general case of arbitrary band filling. Furthermore, it is not obvious a priori that the one-to-one correspondence between the ground-state interaction energy W and the IFE S persists for arbitrary values of the band filling n, and if so, one has to expect that the relation between W and S depends on the electron density n. In particular, the simple linear approximation to $W(S)$ employed in the previous sections could be useless for low values of the carrier density, i. e., if the density of the electrons or holes is low.

In order to investigate how the interaction energy W, the IFE S, and the electron density n relate to each other, we have performed exact numerical Lanczos diagonalizations of the Hubbard model on a number of finite periodic lattice structures having different sizes and numbers of electrons. The hopping integrals have been varied from $t_{ij} = 0$ to $t_{ij} \gg U$ in order to scan the complete range $0 \leq S \leq S_\infty$ of the IFE. Our results are shown in Fig. 4.14 (a), where we have scaled the interaction energy by its uncorrelated HF value $W_{\mathrm{HF}} = U N_\uparrow N_\downarrow / N_a$ and the IFE by its maximal value S_∞ attained in the strongly-correlated limit $U/t \to \infty$. The results demonstrate that a one-to-one connection between W and S in the ground state of the Hubbard model exists not only at half band-filling, but also in the more general case of arbitrary electron densities. Notice, however, that the precise form of the connection between W and S depends on n. In fact, the interaction energy W decreases more rapidly with increasing S if the
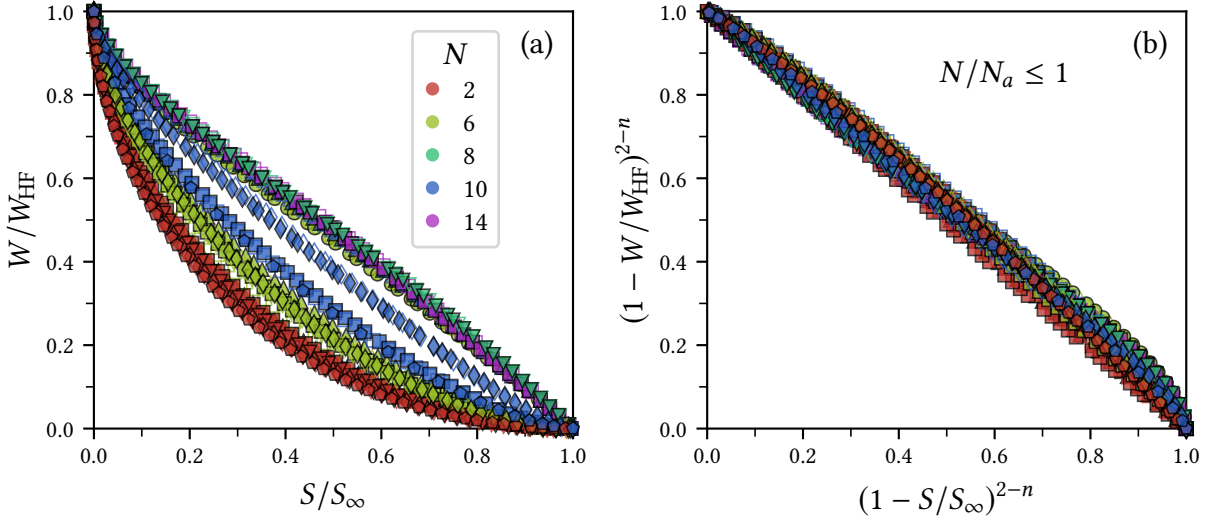
Figure 4.14: Relation between the interaction energy W and the IFE S in the ground state of the Hubbard model with different electron densities $n = N/N_a$. The results are obtained by exact numerical Lanczos diagonalizations for a number of periodic lattice structures and different numbers of electrons N, as indicated in subfigure (a). We have scaled the interaction energy by its uncorrelated HF value $W_{HF} = UN_\uparrow N_\downarrow/N_a$ and the IFE by its maximum value S_∞ attained in the strongly-correlated limit $U/t \to \infty$. Results are shown for finite 1D rings having $N_a = 6$ (circles), $N_a = 10$ (upright triangles) and $N_a = 14$ (squares) lattice sites, as well as for 2D square-lattices having $N_a = 2\times4$ (downright triangles), $N_a = 3\times4$ (diamonds) and $N_a = 4\times4$ (pentagons) lattice sites. Solid symbols correspond to the Hubbard model with only NN hopping t, while open symbols represent results where also second-NN hopping $t_2 = t/2$ is present. Subfigures (a) and (b) show the same data, however different scales are used in (b) in order to highlight the scaling properties of the relation between W and S as the electron density changes.

electron density is low, which reflects the fact that double occupations are more effectively suppressed by the correlated motion of the electrons when the carrier density is lower. Our numerical results show that for very low electron densities the relation between the interaction energy W and the IFE S follows approximately the circle equation

$$(1 - w)^2 + (1 - s)^2 = 1 \quad \text{for} \quad n \to 0, \tag{4.40}$$

where $w = W/W_{HF}$ and $s = S/S_\infty$. On the other hand, at half band-filling ($n = 1$) the relation between W and S is approximately linear, i. e., $w = 1 - s$, which implies

$$(1 - w) + (1 - s) = 1 \quad \text{for} \quad n = 1. \tag{4.41}$$

For intermediate values $0 < n < 1$ of the electron density the relation between W and S in the ground state of the Hubbard model passes smoothly from the low-density

extreme (4.40) to the linear behavior (4.41) at half-band filling. Therefore, in order to cast relation between W and S in a simple form for all $n \leq 1$, we propose to interpolate between the two extremes (4.40) and (4.41) as follows

$$(1 - w)^{2-n} + (1 - s)^{2-n} = 1 \, , \quad 0 < n \leq 1 \, . \tag{4.42}$$

In fact, as shown in Fig. 4.14 (b), we find an almost linear relation between $(1 - w)^{2-n}$ and $(1 - s)^{2-n}$, which is approximately independent not only of the size and dimension of the lattice structure under consideration but also of the band filling n, which is most important for the desired extension of the IFE approximation. The largest deviations from the common linear trend observed in Fig. 4.14 (b) are found at half band-filling ($n = 1$), for which Eq. (4.42) reduces to the linear IFE-approximation $w = 1 - s$, which has already proven to be very successful in the applications to the half-filled Hubbard model discussed in the previous sections. One concludes that Eq. (4.42) is a very promising generalization of the IFE approximation to the regime of arbitrary electron densities in the range $0 < n \leq 1$. To be explicit, we propose to approximate the interaction-energy functional $W[\boldsymbol{\eta}]$ of the Hubbard model with $0 \leq n \leq 1$ in terms of the IFE $S[\boldsymbol{\eta}]$ as

$$\frac{W[\boldsymbol{\eta}]}{W_{\mathrm{HF}}} = \begin{cases} 1 - \left[1 - \left(1 - \frac{S[\boldsymbol{\eta}]}{S_\infty}\right)^{2-n}\right]^{\frac{1}{2-n}} & \text{if } S[\boldsymbol{\eta}] \leq S_\infty \\ 0 & \text{else.} \end{cases} \tag{4.43}$$

Electron densities above half band-filling ($n > 1$) are easily handled by replacing electrons with holes, which corresponds to replacing n by $2-n$ and W by $W - U(N - N_a)$ in Eq. (4.43).[2]

Since Eq. (4.43) approximates $W[\boldsymbol{\eta}]$ in terms of the IFE S, all the conclusions drawn in relation with Eq. (4.12) remain valid for the energy functional $E[\boldsymbol{\eta}] = K[\boldsymbol{\eta}] + W[\boldsymbol{\eta}]$ obtained from Eq. (4.43). This applies in particular to the result (4.16), which states that the ground-state occupation numbers $\eta_{k\sigma}$ follow a Fermi-Dirac distribution with an effective temperature $T_{\mathrm{eff}} = -\partial W / \partial S$ which depends on the Coulomb-repulsion strength U and the electron density n. This contrasts, however, with several well-established results, which state that the one-dimensional Hubbard model behaves like a Luttinger liquid away from half band-filling [115, 116], whose momentum distribution exhibits a typical power-law singularity

$$\eta(k) - \eta(k_F) \sim \mathrm{sign}(k_F - k) \, |k - k_F|^\alpha \tag{4.44}$$

---

[2]Notice that the IFE $S[\boldsymbol{\eta}]$ and thus $W[\boldsymbol{\eta}]$ as given in Eq. (4.43) are invariant with respect to the additional implication $\eta_{k\sigma} \to 1 - \eta_{k\sigma} \, \forall \boldsymbol{k}\sigma$ of the electron-hole transformation.

in the vicinity of the Fermi level. Moreover, in higher dimensions the Hubbard model is a Fermi liquid, having a characteristic step-like singularity in the momentum distribution at the Fermi surface [117]. Clearly, these kind of singularities in the momentum distribution are not obtained in the framework of any IFE approximation to the interaction-energy functional, since the ground-state occupation numbers always follow a Fermi-Dirac distribution.

Notice that the Fermi-Dirac distribution (4.16) is the result of any IFE approximation, if the minimization of the corresponding energy functional $E[\eta_\sigma(\boldsymbol{k})]$ is restricted only by the ensemble-representability condition $0 \leq \eta_\sigma(\boldsymbol{k}) \leq 1 \; \forall \boldsymbol{k}\sigma$. In order to enforce a ground-state occupation-number distribution which displays the typical Luttinger- or Fermi-liquid characteristics, one could restrict the minimization of the energy functional $E[\eta_\sigma(\boldsymbol{k})]$ to a suitable set of trial functions $\{\eta_\sigma(\boldsymbol{k})\}$ which exhibit the corresponding type of singularity. In the following we would like to derive a family of functions which display a typical Luttinger-like power-law singularity at the Fermi-level and are thus suitable to describe the ground-state occupation-number distribution of the 1D Hubbard model away from half band-filling. In the subsequent applications we will investigate whether or not the restriction of the energy functional $E[\eta_\sigma(\boldsymbol{k})]$ to this set of Luttinger-like distributions leads to a significant improvement of the resulting ground-state observables.

In order to obtain a family of Luttinger-like distributions we follow the ideas of Koch and Goedecker [118]. They derived an excellent approximation for the ground-state occupation-number distribution of the half-filled 1D Hubbard model by assuming that the electronic localization, driven by the Coulomb interaction, can be associated to an exponential decay $\gamma_{0\delta\sigma} = \gamma_{0\delta\sigma}^{(0)} \, e^{-\alpha|\delta|}$ of the gs-SPDM elements. Here, $\gamma_{0\delta\sigma}^{(0)} = \sin(\delta\pi/2)/(\delta\pi)$ refers to the elements of the noninteracting gs-SPDM corresponding to a given lattice site $i = 0$ and its δth NN [see Eq. (4.35)], and $\alpha \geq 0$ is a decay constant which depends on the interaction strength. Similarly, away from half band-filling Koch and Goedecker [118] proposed to associate the localization of the electrons to a power-law decay of the gs-SPDM elements

$$\gamma_{0\delta\sigma} = \gamma_{0\delta\sigma}^{(0)} \, |\delta + 1|^{-\alpha} \quad \text{with} \quad \gamma_{0\delta\sigma}^{(0)} = \frac{\sin(k_{F\sigma}\delta)}{\pi\delta} \,, \tag{4.45}$$

where $k_{F\sigma} = \pi n_\sigma$ refers to the Fermi wave-number for spin-σ electrons. The corresponding occupation-number distribution

$$\eta_\sigma(k) = \sum_{\delta=-\infty}^{\infty} \gamma_{0|\delta|\sigma} \, e^{ik\delta} = \frac{k_{F\sigma}}{\pi} + \frac{2}{\pi} \sum_{\delta=1}^{\infty} \frac{\sin(k_{F\sigma}\delta)}{\delta} \, (\delta + 1)^{-\alpha} \cos(k\delta) \tag{4.46}$$

has a Luttinger-like power-law singularity with exponent α at $k = k_{F\sigma}$. The distribution (4.46) is shown in Fig. 4.15 for different values of the decay parameter α and
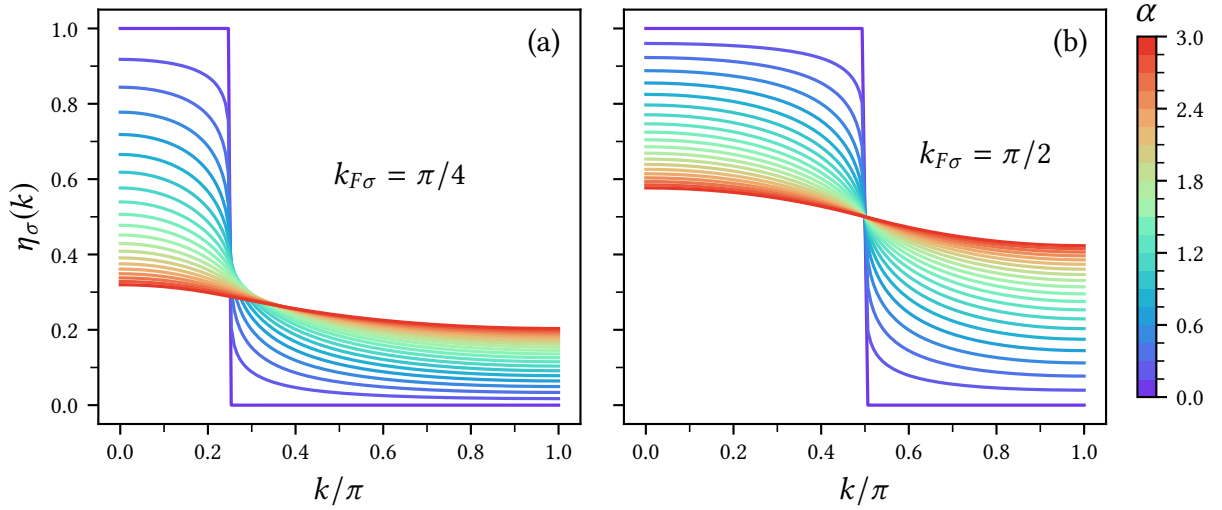
Figure 4.15: Occupation-number distribution (4.46) showing a Luttinger-like power-law singularity at the Fermi wave-number $k_{F\sigma} = \pi n_\sigma$ for different values of the decay parameter α, as indicated by the color scale on the right.

the Fermi wave-number $k_{F\sigma}$. As a result of the singularity at $k_{F\sigma}$, we find in Fig. 4.15 a sharp decay of the distribution $\eta_\sigma(k)$ at the Fermi level if $\alpha < 1$, while for $\alpha > 1$ a finite slope is found in the vicinity of $k_{F\sigma}$. Notice that this behaviour is qualitatively different from a Fermi-Dirac distribution, which has a finite slope at the Fermi level for any positive temperature.

Before we are able to apply the IFE approximation (4.43) to the ground-state problem of the Hubbard model on periodic lattice structures with band filling $n \leq 1$, we need to know the value S_∞ of the IFE in the strongly-correlated ground state. This is not an easy task a priori, since S_∞ is obtained from the occupation-number distribution $\eta_{k\sigma}$ which yields the minimum kinetic energy under the constraint of vanishing double occupations $D = 0$. In practice, it is therefore often necessary to introduce approximations to S_∞. In the framework of the IFE approximation one can start from a physically sound approximation for the strongly-correlated ground-state energy $E_0^\infty(n)$, which is purely kinetic for $n \leq 1$, and tune the parameter x which determines[3] the occupation-number distribution $\eta_\sigma(\mathbf{k}; x)$, i. e., $x = T_{\text{eff}}$ for the Fermi-Dirac distribution (4.16) and $x = \alpha$ for the Luttinger-like distribution (4.46), such that

$$E_0^\infty(n) = \frac{N_a}{(2\pi)^d} \sum_\sigma \int_{\text{BZ}} \varepsilon(\mathbf{k}) \, \eta_\sigma(\mathbf{k}; x) \, \mathrm{d}\mathbf{k} \, . \tag{4.47}$$

From the occupation-number distribution $\eta_\sigma(\mathbf{k}; x)$ one finally obtains an approximate

---

[3] Apart from the chemical potential μ_σ or the Fermi wave-number $k_{F\sigma}$, which are determined by n_σ.

value for the IFE S_∞ in the strongly-correlated ground state by means of Eq. (4.10). Thus, the problem of finding an approximation to S_∞ is replaced by the problem to approximate the strongly-correlated ground-state energy $E_0^\infty(n)$. To this aim, one can consider the lowest-lying fully polarized ferromagnetic (FM) state, since it fulfills the fundamental constraint of vanishing double occupations $D = 0$. Even though the energy $E_{FP}(n)$ of the lowest-lying fully polarized state is in general just an upper bound for the strongly-correlated ground-state energy $E_0^\infty(n)$, it has been found to yield a good first approximation [77, 78]. Moreover, it has been shown that the lowest-lying fully polarized state is always a ground state of the strongly-correlated Hubbard model if there is exactly one hole ($N = N_a - 1$) [52, 53], and in the case of the infinite one-dimensional chain, the strongly-correlated ground-state energy (2.36) coincides with the energy of the lowest-lying fully polarized state for arbitrary electron densities n. To sum up, we propose to approximate the IFE S_∞ in the strongly-correlated ground state of the Hubbard model in the following manner:

1. Approximate the strongly-correlated ground-state energy by the energy of the lowest-lying fully polarized state

$$\frac{E_{FP}(n)}{N_a} = \int_{-\infty}^{\mu(n)} \varepsilon \, \rho(\varepsilon) \, d\varepsilon \, , \tag{4.48}$$

where $0 < n \leq 1$ is the band-filling and $\rho(\varepsilon)$ the single-particle DOS per spin given by Eq. (4.28). Accordingly, the chemical potential $\mu(n)$ fulfills the condition

$$n = \int_{-\infty}^{\mu(n)} \rho(\varepsilon) \, d\varepsilon \, . \tag{4.49}$$

2. Determine the effective temperature T_{eff} in the Fermi-Dirac distribution (4.31) such that the corresponding kinetic energy equals the energy (4.48) of the lowest-lying fully polarized state, i. e., such that

$$\frac{E_{FP}(n)}{N_a} = \sum_\sigma \int_{-\infty}^{\infty} \varepsilon \, \eta_\sigma(\varepsilon; T_{eff}) \, \rho(\varepsilon) \, d\varepsilon \, . \tag{4.50}$$

If one considers Luttinger-like occupation-number distributions of the form (4.46) for the 1D Hubbard model, one instead determines the decay constant α in a similar manner.

3. Once the effective temperature T_{eff} or decay constant α has been determined, it is straight forward to calculate S_∞ as the IFE (4.30) of the corresponding occupation-number distribution.

4.6.1 The infinite Hubbard chain

Having a sound approximation to the IFE S_∞ in the strongly-correlated ground state, we are now in a position to apply our approximation (4.43) in order to determine the ground-state properties of the Hubbard model with arbitrary electron density by minimizing the corresponding energy functional $E[\boldsymbol{\eta}] = K[\boldsymbol{\eta}] + W[\boldsymbol{\eta}]$. In Fig. 4.16 we present our results for the ground-state energy E_0 and the average number of double occupations D of the infinite 1D Hubbard chain and compare them with the exact Bethe-ansatz solution [49]. The LDFT results were obtained either by a minimization of the energy functional which is restricted to the Luttinger-like distributions (4.46), or by a minimization involving arbitrary momentum-distributions $\eta_\sigma(k)$ which are only restricted by the ensemble-representability condition $0 \le \eta_\sigma(k) \le 1$ and the given electron density $\int_{-\pi}^{\pi} \eta_\sigma(k)\,dk = n\pi$ for $\sigma = \uparrow, \downarrow$. As already discussed in the context of Eq. (4.16), the latter leads to a Fermi-Dirac momentum-distribution. Figs. 4.16 (a) and (c) show that both methods yield very accurate results for the ground-state energy E_0 in the whole range of electron densities, starting from an empty band $n = 0$ up to half band-filling $n = 1$, and for all values of the Coulomb-repulsion strength U/t. In this context it is important to recall that the LDFT functional recovers the exact ground-state energy in both the noninteracting ($U/t = 0$) and strongly correlated ($U/t \to \infty$) limits of the 1D Hubbard model for arbitrary values of the electron density $0 < n \le 1$, which are given by Eqs. (2.20) and (2.36).

For low densities ($n \lesssim 0.2$) the differences between the ground-state energies obtained from Luttinger and Fermi-Dirac momentum-distributions are marginal, and the almost linear increase of the binding-energy $|E_0|$ is perfectly reproduced in both cases. For intermediate values of the electron density ($0.2 \le n \le 0.8$) we find that the binding energy is slightly overestimated by the global minimum of the LDFT energy functional, while the restriction to the Luttinger-like distributions leads to a slight underestimation. Nevertheless, the minimization with respect to Luttinger-like distributions generally yields somewhat more accurate ground-state energies in this density range. For example, for $U/t = 4$ the restriction to Luttinger-like distributions leads to a maximal deviation from the exact ground-state energy of only 1.9% at $n = 0.75$, while the global minimization yields a maximal error of 3.5% at $n = 0.58$. The trend changes, however, as we approach half band-filling, and for $n > 0.8$ we find that the global minimization of the LDFT energy functional leads to errors in the ground-state energy which are always smaller than 2.0%, while the restriction to Luttinger-like distributions introduces errors up to 4.4%. This is consistent with our observation in Section 4.3 that the linear IFE-approximation reproduces the ground-state properties of the half-filled infinite Hubbard chain with astonishing accuracy for all values of the Coulomb-repulsion strength U/t.

Similar conclusions can be drawn from Fig. 4.16 (c), where the ground-state en-
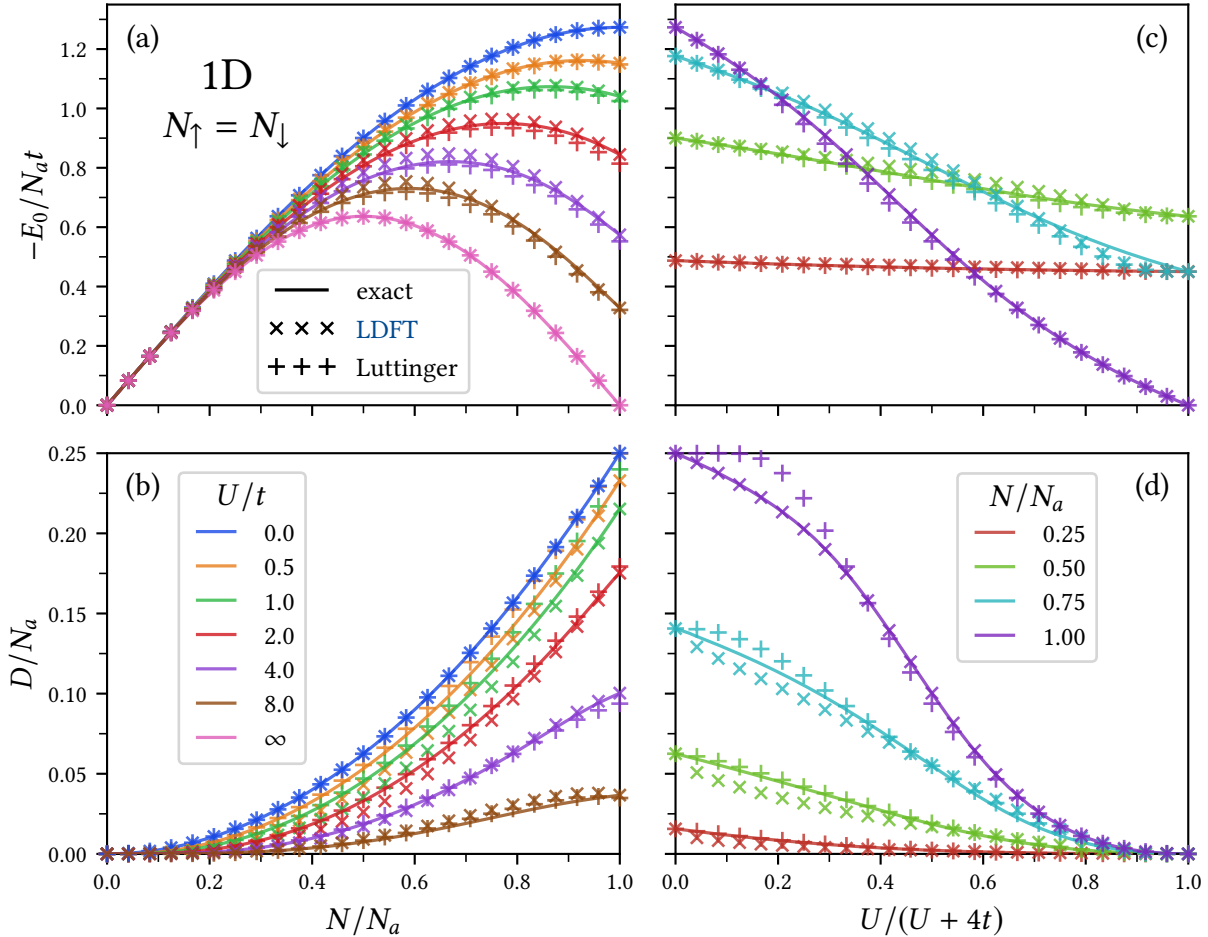
Figure 4.16: Ground-state properties of the one-dimensional Hubbard model with different electron densities. Results are shown for (a) the ground-state energy E_0 and (b) the average number of double occupations D as functions of the electron density N/N_a for representative values of U/t, as indicated in (b). The solid curves correspond to the exact Bethe-ansatz solution [49], while the crosses are the results of LDFT in combination with the IFE approximation (4.43). The plus symbols indicate results obtained by restricting the minimization of the LDFT energy-functional to the Luttinger-like momentum distributions (4.46). Similarly, subfigures (c) and (d) show results for the ground-state energy E_0 and the average number of double-occupations D as functions of the Coulomb-repulsion strength U/t for the electron densities N/N_a indicated in (d).

ergy E_0 is shown as a function of the Coulomb-repulsion strength U/t for representative values of the electron density. For rather small values of the electron density, i. e., for $n = 0.25$ and 0.5, the ground-state energy is only slightly affected by the strength of the Coulomb repulsion, since the electrons are able to avoid each other very effectively in a correlated motion throughout the lattice. For low densities and intermediate values of the Coulomb-repulsion strength ($1 \lesssim U/t \lesssim 10$) we obtain somewhat more accurate results by restricting the minimization to the Luttinger-like distributions. For very low or large values of U/t the differences between both methods become marginal. For $n = 0.75$ the absolute deviations from the exact solution are found to be almost the same for the ground-state energy obtained from both global and restricted minimizations. Notice, however, that the global minimum overestimates the binding energy, while the restricted minimization leads to an underestimation of the latter. Finally, for $n = 1$ the ground-state energy obtained from the global minimum of the LDFT energy functional is far more accurate than its restricted counterpart. As already discussed in Section 4.3 the error in the ground-state energy obtained from the global minimum is always smaller than 0.1% in the whole range from weak to strong coupling, while the restriction to Luttinger-like distributions leads to errors of up to 4.1%.

Concerning the dependence of the average number of double occupations D on the electron density $n = N/N_a$ and the Coulomb-repulsion strength U/t in Figs. 4.16 (b) and (d), we find that the exact results obtained from the Bethe-ansatz solution are qualitatively very well reproduced by LDFT in combination with the IFE approximation (4.43). In the noninteracting ($U/t = 0$) and strongly correlated ($U/t \rightarrow \infty$) limits the corresponding exact values of the double occupations $D/N_a = n^2/4$ and $D = 0$ are reproduced within LDFT. For intermediate to large values of the Coulomb-repulsion strength ($U/t \gtrsim 2$) one obtains more accurate double occupations from the minimization with respect to Luttinger-like momentum distributions, especially in the range of intermediate electron densities ($0.2 \lesssim n \lesssim 0.8$). For example, at $U/t = 2$ the relative error in the double occupations obtained from Luttinger-like momentum distributions is always below 2.7%, while errors up to 21% are found when the energy functional is minimized globally. In contrast, when the interactions are weak ($U/t \lesssim 2$), the Luttinger-like momentum distributions lead to a severe overestimation of the double occupations near half band-filling. This is best seen in Fig. 4.16 (d), where the double occupations obtained from the restricted minimization for $n = 1$ remain approximately constant for weak interactions ($U/t \lesssim 1$), whereas the global minimization reproduces the double occupations of the half-filled Hubbard chain with astonishing accuracy in the whole range from weak to strong interactions. These findings —namely that the Fermi-Dirac momentum distributions obtained from the global minimization yield more accurate results in the vicinity of half band-filling, while Luttinger-like distributions are preferable if intermediate electron densities are considered— is in

good qualitative agreement with the fact that the one-dimensional Hubbard model is a Luttinger liquid only if the band is *not* half filled [116].

4.6.2 The two-dimensional Hubbard model

In order to go beyond the domain of integrable models, we have applied the IFE approximation (4.43) to the infinite square lattice with NN hopping. Figure 4.17 shows our results for the ground-state energy E_0 and the average number of double occupations D obtained by minimizing the LDFT energy functional with respect to arbitrary ensemble representable occupation-number distributions $\eta_\sigma(\boldsymbol{k})$ which yield the given electron density N/N_a. Figures 4.17 (a) and (c) show that the dependence of the ground-state energy E_0 on the electron density N/N_a and the Coulomb-repulsion strength is qualitatively very similar to the previously discussed infinite 1D Hubbard chain. The proposed LDFT functional reproduces the exact value of the ground-state energy in the noninteracting limit ($U/t = 0$). In the strongly correlated limit ($U/t \to \infty$), the energy of the lowest-lying fully polarized state (4.48) is obtained, which is expected to slightly overestimate the strongly-correlated ground-state energy. The ground-state energy obtained in the framework of LDFT agrees fairly well with numerical QMC simulations for the Hubbard model on 12×12 and 8×8 square-lattice clusters [57, 59]. This applies to the complete range of electron densities, starting from low densities up to the half-filled band. However, the comparison with QMC simulations suggests that the present IFE approximation slightly overestimates the binding energy $|E_0|$.

In Figs. 4.17 (b) and (d) we show results for the average number of ground-state double occupations D. The comparison with numerical QMC simulations reported in Refs. [57, 59, 64] demonstrates that LDFT in combination with the interaction-energy functional (4.43) reproduces the ground-state double occupations D fairly well as a function of the electron density N/N_a and the Coulomb-repulsion strength U/t in the complete range of parameters. Nevertheless, for weak to intermediate interaction strength ($1 \lesssim U/t \lesssim 4$) the increase of double occupations with increasing electron density seems to be somewhat underestimated by our approximation. Notice, however, that the more recent results reported by Varney *et al.* [64] suggest a less severe underestimation of the double occupations than the previous QMC calculations of Hirsch [57] and Moreo *et al.* [59].

Before closing this section, we like to investigate how the ground-state momentum-distribution $\eta_\sigma(\boldsymbol{k})$ depends on the electron density $n = N/N_a$ and the Coulomb repulsion strength U/t. To this aim we compare in Fig. 4.18 the momentum distribution obtained within our present IFE approximation to the results of QMC simulations [59, 64]. In Figs. 4.18 (a) and (b) the ground-state momentum distribution is shown for the path in the first Brillouin zone (BZ) which crosses the Fermi surface
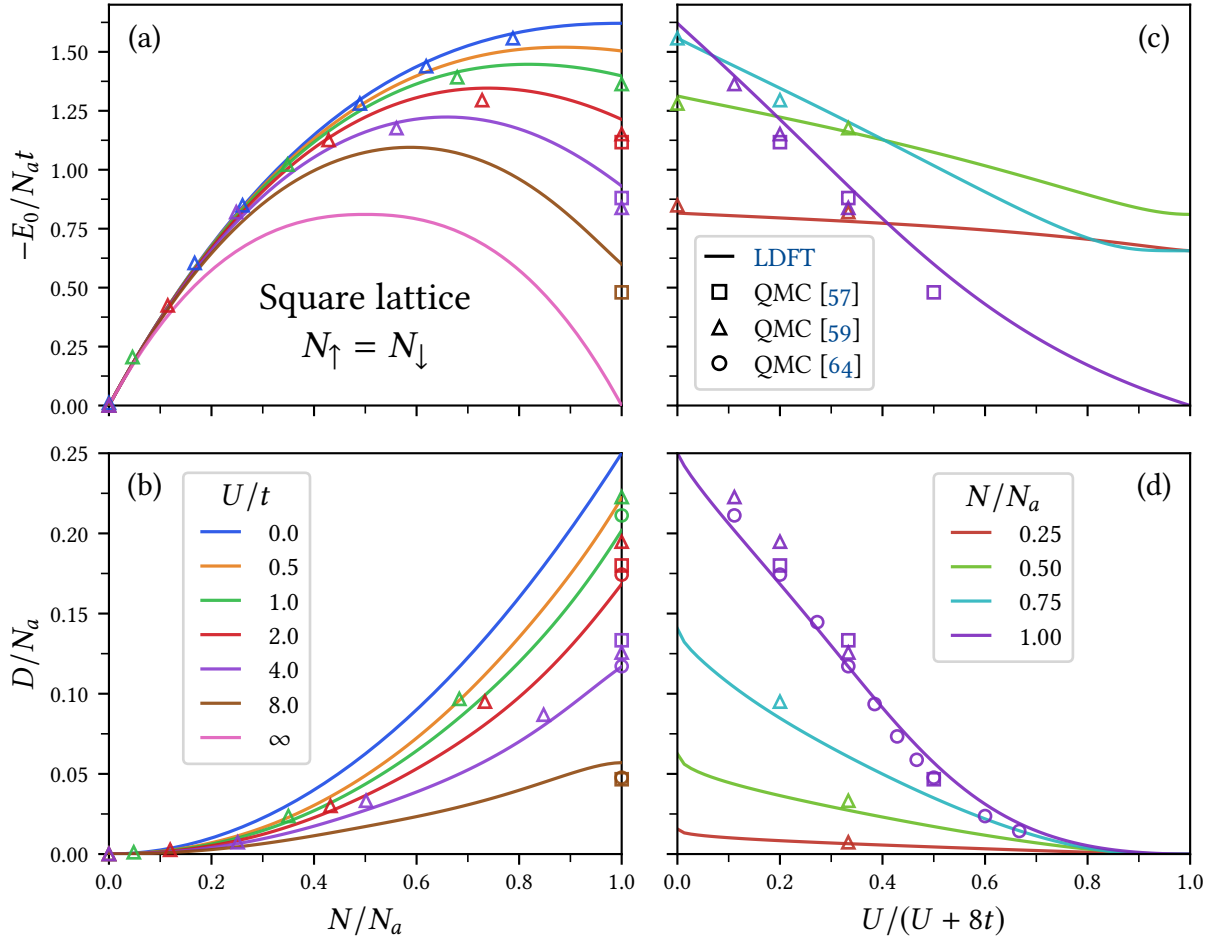
Figure 4.17: Ground-state properties of the Hubbard model on the 2D square lattice with different electron densities. Results are shown for (a) the ground-state energy E_0 and (b) the average number of double occupations D as functions of the electron density N/N_a for different values of U/t, as indicated in (b). The solid curves correspond to LDFT in combination with the IFE approximation (4.43), while the open symbols are the results of numerical QMC simulations [57, 59, 64]. In (c) and (d) similar results are shown for the ground-state energy E_0 and average number of double-occupations D as functions of the Coulomb-repulsion strength U/t for the electron densities N/N_a indicated in (d).
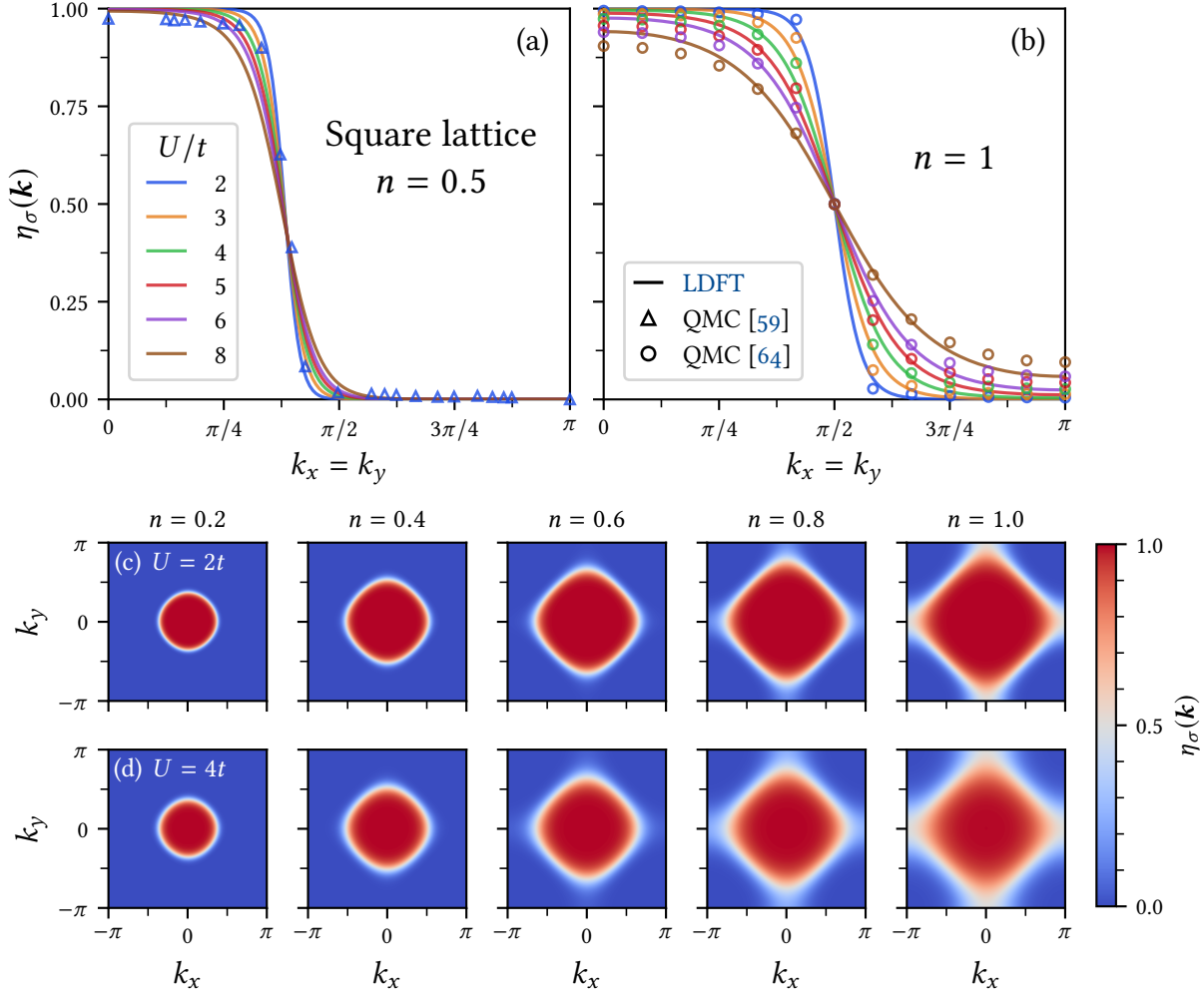
Figure 4.18: Momentum distribution $\eta_\uparrow(\boldsymbol{k}) = \eta_\downarrow(\boldsymbol{k})$ in the ground state of the Hubbard model on the 2D square-lattice with different electron densities $n = N/N_a$ and Coulomb-repulsion strengths U/t. Results are shown for the path in the BZ which crosses the Fermi surface along the diagonal $k_x = k_y$ for (a) quarter ($n = 0.5$) and (b) half band-filling ($n = 1$) at different values of U/t. The solid lines correspond to LDFT in combination with the interaction-energy functional (4.43), while the open symbols indicate results obtained from numerical QMC simulations [59, 64]. The color contour-plots show the LDFT momentum distribution in the complete BZ for electron densities ranging from $n = 0.2$ to 1.0 for weak [$U/t = 2$, row (c)] and intermediate [$U/t = 4$, row (d)] Coulomb-repulsion strength.

along the diagonal $k_x = k_y$. Different values of the Coulomb-repulsion strength U/t are considered for quarter band-filling ($n = 0.5$) as well as for half band-filling ($n = 1$). The rather sharp Fermi surface found for weak interactions ($U/t \lesssim 2$) broadens considerably as the Coulomb-repulsion strength increases. Notice that this broadening is particularly pronounced near half band-filling ($n = 1$), where the carrier density is maximal. Indeed, for low or intermediate densities the electrons are able to avoid each other very effectively, without much impact on their kinetic- or binding-energy. The momentum distribution obtained within our IFE approximation is in good agreement with the available results of QMC simulations. In particular, the broadening of the Fermi surface is very well reproduced in the case of half band-filling. The IFE approximation slightly overestimates the occupation numbers of the low-lying Bloch states having $k_x = k_y \lesssim 3\pi/8$, while the occupation numbers of the states with $k_x = k_y \gtrsim 5\pi/8$ are underestimated by the same amount. This is consistent with the overestimation of the binding energy $|E_0|$ already discussed in the context of Fig. 4.17. In any case, it is worth noting that our results are remarkably accurate despite of the fact that the 2D Hubbard model is expected to be a Fermi liquid, having a step-like singularity in the momentum distribution at the Fermi surface, a behavior which cannot be reproduced by the continuous Fermi-Dirac distribution predicted by our present IFE approximation.

In the lower part of Fig. 4.18 we visualize the momentum distribution obtained from the IFE approximation in the complete BZ by means of color density-plots for different values of the Coulomb-repulsion strength U/t and the electron density $0.2 \leq n \leq 1$. The plots in row (c) display the momentum distribution for a relatively weak interaction $U/t = 2$, while the plots in row (d) show similar results for intermediate interaction strength $U/t = 4$. Our results compare very well with similar ones obtained from QMC simulations [64]. One observes how changes in the electron density n cause a deformation of the Fermi surface, starting from a circular shape for low densities to the rotated square in the case of half band-filling. Moreover, the broadening of the Fermi surface with increasing electron density, which is a distinctive sign of electronic correlations, is clearly visible. A qualitatively similar broadening of the Fermi surface is also observed when the electronic correlations are enhanced by increasing Coulomb-repulsions U/t, as can be seen by comparing the plots in rows (c) and (d) for a given electron density n.

4.7 Summary

We have developed new practical methods to tackle the ground-state problem of the homogeneous Hubbard model on periodic lattice structures in the framework of LDFT. Our approach is based on a delocalized $\boldsymbol{k}$-space perspective, which exploits a

newly discovered connection between the interaction energy W in the ground state of the model and the IFE S of the corresponding Bloch-state occupation-number distribution $\eta_{k\sigma}$. This has opened up a completely new perspective to the ground-state problem by taking into account the dependence of the central interaction-energy functional $W[\gamma]$ on all elements of the SPDM γ, and led to an approximation which leverages the full universality of LDFT.

An almost linear connection between W and S has been discovered in exact numerical results for the ground state of the half-filled Hubbard model, which led us to approximate the interaction-energy functional $W[\eta] = W(S[\eta])$ in terms of a simple linear function of the IFE $S[\eta]$. Subsequent applications to the half-filled Hubbard model on finite and infinite lattices in $d = 1-3$ dimensions as well as in the limit $d \rightarrow \infty$ have demonstrated the predictive power of our method. In fact, within our approximation it was possible to reproduce the ground-state properties in all considered situations with very good accuracy in the complete range from weak to strong Coulomb interactions. This applies in particular to the subtle strongly-correlated Heisenberg limit $U/t \rightarrow \infty$, where the linear IFE-approximation exactly reproduces the asymptotic behaviour of the ground-state energy $E_0 = -\alpha t^2/U$ expected for localized Heisenberg spins. Most notably, the ground-state properties of the infinite 1D Hubbard chain derived from the linear IFE-approximation are almost indistinguishable from the exact Bethe-ansatz solution [49]. In higher dimensions, the linear IFE-approximation has proven to be very accurate as well, and the corresponding ground-state observables agree well with available QMC simulations and exact diagonalizations. Moreover, the spin-polarized Hubbard model has been studied in the framework of the linear IFE-approximation. In this way we have obtained the magnetization curve and the zero-field magnetic susceptibility of the infinite 1D Hubbard chain.

In order to study physical situations involving attractive interactions between the fermions, giving rise to electronic pairing, we have considered the half-filled Hubbard model with negative coupling constant $U < 0$. Also in this case an almost linear connection between W and S has been discovered in exact numerical results for the ground state. This encouraged us to propose a generalized formulation of the linear IFE-approximation to the interaction-energy functional $W[\eta]$, which treats attractive and repulsive interactions on the same footing. Subsequent applications to the half-filled attractive Hubbard model on finite bipartite and non-bipartite lattices in two dimensions have proven that the IFE approximation is able to account for the correlations caused by attractive interactions, and very accurate results have been obtained for the most important ground-state observables in the complete range from weak to strong interactions.

Our final challenge has been to go beyond half band-filling and to address the problem of arbitrary electron densities. The evaluation of exact numerical results for the ground state of the Hubbard model on various lattice structures with different elec-

tron densities has shown that a unique relation between W and S exists even in this more general case. However, the connection between W and S has been found to be strongly affected by the electron density n. Nevertheless, by an interpolation between the low-density limit $n \rightarrow 0$ and the half-filled band case $n = 1$ it was possible to derive a physically sound extension of the IFE approximation, which applies to arbitrary electron densities. Applications to the one- and two-dimensional Hubbard model have shown that the ground-state observables of the Hubbard model are reproduced very accurately within this approximation to $W[\gamma]$ in the complete range from low electron density up to half band-filling for all values of the Coulomb-repulsion strength. We have also studied the implications of qualitative changes in the occupation-number distribution $\eta_\sigma(k)$ near the Fermi level. To this aim we have focused on the 1D Hubbard chain and we have restricted the minimization of the LDFT energy functional $E[\eta_\sigma(k)]$ to a class of functions $\eta_\sigma(k)$ exhibiting a typical power-law singularity at the Fermi-level, which is characteristic for Luttinger liquids, such as the 1D Hubbard model away from half band-filling. The corresponding results have shown that Luttinger-like distributions are preferable if low electron densities are concerned, however, in the vicinity of a half filled band ($0.8 \lesssim n \leq 1$) the Fermi-Dirac distributions obtained from the unconstrained minimization of the energy functional within the IFE approximation lead to significantly more accurate results. We have also studied the ground-state occupation-number distribution $\eta_\sigma(\boldsymbol{k})$ of the 2D Hubbard model on the square lattice in the framework of the IFE approximation. Our results agree surprisingly well with accurate QMC simulations, and the typical broadening of the Fermi surface, as the electron density and Coulomb-repulsion strength increases, has been very well reproduced.

Thermodynamic equilibrium and the separation of spin and charge excitations

<div style="text-align:right">5</div>

One of the major shortcomings of present-day density functional theory (DFT) is the lack of effective approaches which account for correlated electrons in thermodynamic equilibrium at finite temperatures. Therefore, a large number of fundamental many-body effects which give rise to important new temperature scales cannot be addressed within the framework of DFT. Examples include phase transitions in magnetic or superconducting materials, the Kondo-screening, or metal-insulator transitions, which appear at specific temperatures, such as the Curie or Néel ordering temperatures in ferromagnets and antiferromagnets, or the Kondo temperature for magnetic impurities in metals. It is therefore most desirable to develop practical finite-temperature approximations in the framework of DFT, which would extend the scope of DFT and open the path to these crucial many-body effects.

It is therefore the aim of the present chapter to approach this problem from the perspective of lattice models for interacting electrons, and to extend the scope of practical applications of lattice density functional theory (LDFT) to the regime of the thermodynamic equilibrium at finite temperatures $T > 0$. To this aim, we will focus on the Hubbard model and exploit the scaling properties of the functional $G_c[\gamma]$ which accounts for the correlation contribution to the free energy. In this way we derive a simple, yet very effective approximation to the central grand-potential functional $\Omega[\gamma]$. Previous works in the framework of LDFT have employed similar scaling properties of the interaction-energy functional $W[\gamma]$ in order to address the ground-state problem of the homogeneous and inhomogeneous Hubbard models [83–87], as well as the single-impurity Anderson model [81–83].

In order to derive the approximate finite-temperature functionals, we focus on homogeneous and periodic systems with hoppings only between nearest neighbors (NNs), which enables us to reduce the complexity of the central grand-potential functional $\Omega[\gamma]$ considerably. These simplifications allow us to investigate the nontrivial correlation contribution $G_c[\gamma]$ to the free-energy functional in an explicit manner, and the scaling properties discovered in this context will lead us to propose a very efficient approximation. The variational principle of Gibbs in combination with this scaling approximation enables us to explore the equilibrium properties of the Hubbard model in 1–3 dimensions and to derive the temperature dependence of important

observables such as the kinetic and interaction energies, the entropy S and the specific heat C_V.

Most notably, we will demonstrate that the scaling approximation is able to reproduce the physical effects resulting from the separation of spin and charge degrees of freedom in the strongly correlated limit ($U \gg t$) of the Hubbard model. In the half-filled band case this fundamental fingerprint of strong electronic correlations manifests itself through the appearance of two distinct peaks in the specific heat C_V, which are caused respectively by low-lying spin excitations and higher-energy charge excitations, the latter being caused by the onset of electronic motion throughout the lattice and the associated fluctuations of the Coulomb energy. Moreover, we will apply our scaling approximation to the case of a less than half-filled band in order to study the changes in the equilibrium properties caused by variations in the electronic density. Finally, we will consider spin-polarized systems in order to investigate the physical properties of strongly-interacting electron systems in the presence of external magnetic fields.

5.1 Reduced density-matrix functionals

In Section 3.2 we have already developed the formalism of finite-temperature lattice density functional theory (FT-LDFT), which accounts for the thermodynamic equilibrium in the canonical and grand-canonical ensembles. In a grand-canonical ensemble with a given temperature $T > 0$ and chemical potentials μ_σ for electrons with spin polarization σ, the functional $\Omega[\gamma]$ defined by Eqs. (3.52) and (3.53) incorporates Gibbs' variational principle (3.54) and thus gives access to the equilibrium single-particle density matrix (eq-SPDM) γ^{eq}. Subsequently, once the eq-SPDM is known, the equilibrium average value of any physical observable can be obtained in principle by virtue of Corollary 3.4. It is important to keep in mind that the functional (3.53) of the grand-potential $\Omega[\gamma]$ involves the functional $G[\gamma]$, defined in Eq. (3.52), which includes the contributions of the Coulomb energy and the entropy to the free energy. An explicit exact expression for $G[\gamma]$ is, however, unknown at present. Consequently, the main challenge in practical applications of FT-LDFT is the development of physically sound approximations to $G[\gamma]$. In order to address this fundamental problem, we focus on the homogeneous single-band Hubbard model with NN hopping

$$\hat{H} = \hat{K} + \hat{W} = -t \sum_{\langle i,j \rangle \sigma} \hat{c}^\dagger_{i\sigma} \hat{c}_{j\sigma} + U \sum_i \hat{n}_{i\uparrow} \hat{n}_{i\downarrow} \,, \tag{5.1}$$

where $\langle i, j \rangle$ indicates the summation over all NN lattice sites, $t > 0$ is the NN hopping integral, and U the local Coulomb repulsion strength. The rotational and translational symmetry of the lattices to be considered in the following (e. g., the linear chain, the

2D square and triangular lattices or hypercubic lattices in d dimensions) implies that the elements

$$\gamma_{ij\sigma}^{\text{eq}} = \gamma_{\sigma}^{\text{eq}}(|\mathbf{R}_i - \mathbf{R}_j|) \tag{5.2}$$

of the eq-SPDM depend only on the distance $|\mathbf{R}_i - \mathbf{R}_j|$ between the corresponding lattice sites i and j. Consequently, we may restrict ourselves to the subset of the ensemble representable single-particle density matrices (SPDMs) $\boldsymbol{\gamma}$ which fulfill the symmetry constraint (5.2). In this case we have $\gamma_{ii\sigma} = \gamma_{11\sigma}$ for all diagonal elements $i = 1, \ldots, N_a$ of the spin-dependent SPDM, which represent the local density $n_\sigma = N_\sigma/N_a$ of spin-σ electrons, and $\gamma_{ij\sigma} = \gamma_{12\sigma}$ for all i, j corresponding to NNs. If we furthermore focus on the unpolarized case, i. e., $\mu_\uparrow = \mu_\downarrow = \mu$, the grand-potential functional (3.53) of the Hubbard model (5.1) takes the form

$$\Omega[\boldsymbol{\gamma}] = G[\boldsymbol{\gamma}] - N_a \left(tz\,\gamma_{12} + \mu\,\gamma_{11} \right), \tag{5.3}$$

where N_a is the number of sites, z is the coordination number, and we have introduced $\gamma_{11} = \sum_\sigma \gamma_{11\sigma}$ and $\gamma_{12} = \sum_\sigma \gamma_{12\sigma}$. Physically, $\gamma_{11} = N/N_a$ represents the electron density and γ_{12} the degree of charge fluctuations or hybridization between NNs. Notice that, as long as only NN hoppings are taken into account (i. e., $t_{ij} = 0$ for i, j beyond NNs), the dependence of $\Omega[\boldsymbol{\gamma}]$ on all SPDM elements other than γ_{11} and γ_{12} appears only through the interaction and entropy functional $G[\boldsymbol{\gamma}]$. Consequently, we can absorb all SPDM elements other than γ_{11} and γ_{12} in the Levy-Lieb (LL) minimization procedure (3.52) and define the reduced functional

$$G[\gamma_{11}, \gamma_{12}] = \min_{\hat{\rho} \to \{\gamma_{11}, \gamma_{12}\}} \text{Tr}\left\{\hat{\rho}\left(U \sum_i \hat{n}_{i\uparrow}\hat{n}_{i\downarrow} + \frac{1}{\beta}\log\hat{\rho}\right)\right\}. \tag{5.4}$$

Here, the notation $\hat{\rho} \to \{\gamma_{11}, \gamma_{12}\}$ indicates that the minimization is performed within the set formed by the positive semidefinite density matrices $\hat{\rho} \in \mathcal{P}$ with unit trace, satisfying

$$\sum_\sigma \text{Tr}\left\{\hat{\rho}\,\hat{c}_{i\sigma}^\dagger\hat{c}_{i\sigma}\right\} = \gamma_{11} \quad \text{for} \quad i = 1, \ldots, N_a \tag{5.5a}$$

and

$$\sum_\sigma \text{Tr}\left\{\hat{\rho}\,\hat{c}_{i\sigma}^\dagger\hat{c}_{j\sigma}\right\} = \gamma_{12} \quad \forall i, j \in \text{NNs}. \tag{5.5b}$$

The reduced functional (5.4) has a universal character in the sense that it does not depend on the chemical potential μ and the NN hopping-integral t. It depends on the underlying Fock-space, which is determined by the number of lattice sites N_a, on the temperature T, the Coulomb-repulsion strength U, and, in contrast to $G[\boldsymbol{\gamma}]$, also on the topology of the lattice structure under consideration. The dependence on the lattice structure is introduced by the constraint (5.5b), requiring that all SPDM elements γ_{ij}

which correspond to NNs must equal γ_{12}. Clearly, since this constraint makes explicit reference to the NNs, it is not transferable between lattice structures having different local topologies.

The restriction to homogeneous systems with hoppings only between NNs introduces a remarkable simplification: Given any explicit approximation to the reduced functional $G[\gamma_{11}, \gamma_{12}]$, the grand-potential Ω_0 is easily accessible as the minimum of the corresponding functional

$$\Omega[\gamma_{11}, \gamma_{12}] = G[\gamma_{11}, \gamma_{12}] - N_a \left(tz\, \gamma_{12} + \mu\, \gamma_{11} \right). \tag{5.6}$$

The minimizing values γ_{11}^{eq} and γ_{12}^{eq} directly yield the local electron density $n = \gamma_{11}^{\text{eq}}$ and the kinetic energy $K/N_a = -tz\, \gamma_{12}^{\text{eq}}$ in thermodynamic equilibrium, and additional equilibrium averages can be obtained from corresponding derivatives of the grand potential Ω_0. Clearly, the minimization of the reduced grand-potential functional (5.6) must be restricted to the corresponding domain of definition, which is given by the set X_e containing all tuples $(\gamma_{11}, \gamma_{12})$ that can be associated with a density matrix $\hat{\rho} \in \mathcal{P}$ satisfying Eq. (5.5). Therefore, before we derive explicit approximations to the functional (5.4), it is important to explore the domain X_e and to characterize its boundaries.

5.1.1 Domain of ensemble representability

In order to identify the domain of definition X_e of the reduced functionals (5.4) and (5.6), it is sufficient to focus on ensemble representable SPDMs which fulfill the constraint (5.2), since we are concerned with periodic lattices having translational and rotational symmetry. Under these circumstances, the constraints (5.5) on the SPDM elements, i. e., $\gamma_{ii} = \gamma_{11}$ for $i = 1, \ldots, N_a$ and $\gamma_{ij} = \gamma_{12}$ for all i, j corresponding to NNs, are automatically satisfied for all $(\gamma_{11}, \gamma_{12}) \in X_e$. Furthermore, the translational symmetry implies that the natural orbitals are the Bloch states of the lattice structure under consideration. Thus, we can express the spin-resolved SPDM elements $\gamma_{ij\sigma}$ in terms of the eigenvalues or Bloch-state occupation numbers $\eta_{k\sigma}$ as (see Section 4.1)

$$\gamma_{ij\sigma} = \gamma_\sigma(R_i - R_j) = \frac{1}{N_a} \sum_{k \in \text{BZ}} \eta_{k\sigma}\, e^{-ik \cdot (R_i - R_j)}, \tag{5.7}$$

where the summation runs over the wavevectors in the first Brillouin zone (BZ). Since the eigenvalues of ensemble representable SPDMs are bounded by $0 \leq \eta_{k\sigma} \leq 1\ \forall k\sigma$ (see Section 3.2.1), the domain of representability can be identified as follows. The diagonal elements

$$\gamma_{ii\sigma} = \frac{1}{N_a} \sum_{k \in \text{BZ}} \eta_{k\sigma} \tag{5.8}$$

are bounded by $0 \leq \gamma_{ii\sigma} \leq 1$, which is simply a consequence of Pauli's exclusion principle. This implies that $\gamma_{11} = \sum_\sigma \gamma_{11\sigma}$ satisfies $0 \leq \gamma_{11} \leq 2$. For the case of the NN SPDM-element $\gamma_{12\sigma}$, we recall that the invariance with respect to the discrete rotations in the point group of the lattice implies $\gamma_{ij\sigma} = \gamma_{12\sigma}$ for all i, j belonging to NNs. Thus,

$$\gamma_{12\sigma} = \frac{1}{z} \sum_{\Delta \in \mathrm{NN}} \gamma_\sigma(\Delta) = \frac{1}{N_a z} \sum_{k \in \mathrm{BZ}} \omega_k \, \eta_{k\sigma} \,, \tag{5.9}$$

where $\Delta \in \mathrm{NN}$ indicates the unique vectors connecting a given lattice site to its z NNs. In Eq. (5.9) we have introduced the numbers

$$\omega_k = \sum_{\Delta \in \mathrm{NN}} \cos(k \cdot \Delta)\,, \tag{5.10}$$

which coincide with the Bloch-state energies (2.15) of the single-band Hubbard model when the NN-hopping integral is set to $t = -1$, and play the role of the energy levels in an effective single-particle problem. Therefore, we will refer to ω_k as "effective" Bloch-state energies, regardless of the fact that they are dimensionless numbers. Notice that Eqs. (5.9) and (5.10) are a simple consequence of the relation between $\gamma_{12\sigma}$ and the spin-resolved kinetic energy $K_\sigma / N_a = -tz\,\gamma_{12\sigma}$ in periodic single-band systems with NN hopping. Equation (5.9) shows that for any number $N_\sigma = N_a\,\gamma_{11\sigma}$ of spin-σ electrons, the upper (lower) bound of $\gamma_{12\sigma}$ is attained when the Bloch states with the highest (lowest) ω_k are occupied ($\eta_{k\sigma} = 1$) while all other Bloch states are unoccupied ($\eta_{k\sigma} = 0$). Therefore, in order to determine the boundaries on $\gamma_{12\sigma}$, it is save to assume that the Bloch-state occupation numbers $\eta_{k\sigma} = \eta_\sigma(\omega_k)$ are determined by the corresponding effective energies ω_k, and by introducing

$$\rho(\omega) = \frac{1}{N_a} \sum_{k \in \mathrm{BZ}} \delta(\omega - \omega_k) \tag{5.11}$$

we can thus rewrite Eqs. (5.8) and (5.9) as

$$\gamma_{11\sigma} = \int_{-\infty}^{\infty} \eta_\sigma(\omega)\,\rho(\omega)\,\mathrm{d}\omega \quad \text{and} \quad \gamma_{12\sigma} = \frac{1}{z} \int_{-\infty}^{\infty} \omega\,\eta_\sigma(\omega)\,\rho(\omega)\,\mathrm{d}\omega \,. \tag{5.12}$$

Clearly, $\rho(\omega)$ defined in Eq. (5.11) is simply the density of states (DOS) of the tight-binding Hamiltonian

$$\hat{H}_{\mathrm{tb}} = \sum_{\langle i,j \rangle} \hat{c}_i^\dagger \hat{c}_j \,, \tag{5.13}$$

whose single-particle eigenvalues coincide with ω_k given in Eq. (5.10). In particular, in the unpolarized case $\gamma_\uparrow = \gamma_\downarrow$ the upper and lower bounds on $\gamma_{12} = \sum_\sigma \gamma_{12\sigma}$ are given by

$$\gamma_{12}^{\max} = \frac{2}{z} \int_{\mu_{\max}}^{\infty} \omega\,\rho(\omega)\,\mathrm{d}\omega \quad \text{and} \quad \gamma_{12}^{\min} = \frac{2}{z} \int_{-\infty}^{\mu_{\min}} \omega\,\rho(\omega)\,\mathrm{d}\omega \,, \tag{5.14}$$
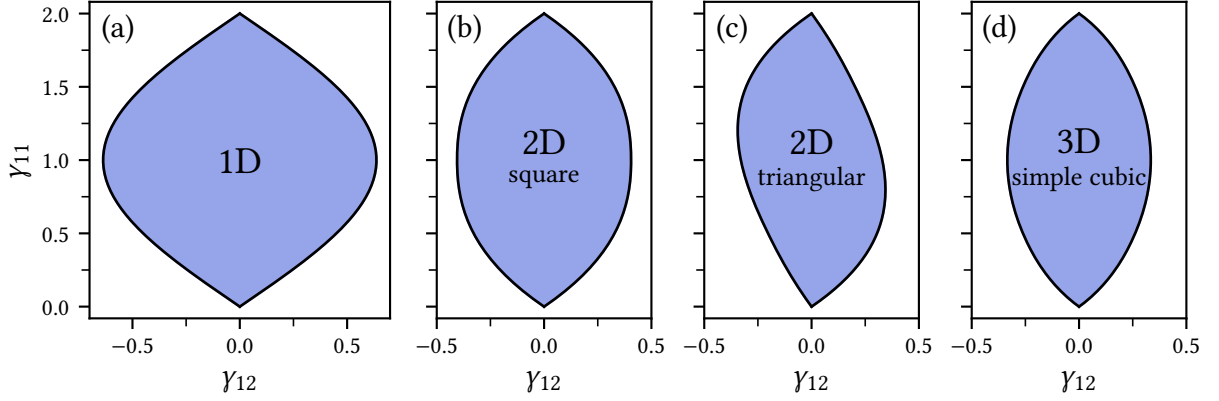
Figure 5.1: Domain X_e of ensemble representable $(\gamma_{11}, \gamma_{12})$ for different lattice structures. The results correspond to unpolarized SPDMs $(\boldsymbol{\gamma}_\uparrow = \boldsymbol{\gamma}_\downarrow)$ of the periodic (a) 1D chain, (b) square lattice, (c) triangular lattice, and (d) simple-cubic lattice.

where μ_{min} and μ_{max} are associated with the electron density $n = \gamma_{11}$ by the condition

$$\frac{\gamma_{11}}{2} = \int_{\mu_{max}}^{\infty} \rho(\omega)\,\mathrm{d}\omega = \int_{-\infty}^{\mu_{min}} \rho(\omega)\,\mathrm{d}\omega \,. \tag{5.15}$$

In Fig. 5.1 the domain X_e formed by the ensemble representable values of γ_{11} and γ_{12} is shown for a number of representative lattice structures. We have focused on the unpolarized case and used Eqs. (5.14) and (5.15) in order to determine the boundaries on γ_{12} as a function of the electron density in the complete range $0 \leq \gamma_{11} \leq 2$. For bipartite lattice structures we find domains which are symmetric with respect to $\gamma_{12} = 0$, i. e., $\gamma_{12}^{min}(\gamma_{11}) = -\gamma_{12}^{max}(\gamma_{11})$. This symmetry is readily understood by recalling that for bipartite lattices the tight-binding Hamiltonian (5.13) simply changes sign upon the unitary transformation which replaces $\hat{c}_i^\dagger \rightarrow \pm\hat{c}_i^\dagger$, where the positive sign applies to the sites i within one of the two sublattices and the negative to the others. In this case, the spectrum of $\hat{H}_{tb}$ and thus the DOS (5.11) is symmetric with respect to $\omega = 0$, which implies $\gamma_{12}^{min} = -\gamma_{12}^{max}$ according to Eq. (5.14). This symmetry does not apply to non-bipartite lattice structures as, for example, the triangular lattice shown in Fig. 5.1 (c). Nevertheless, the upper and lower boundaries on γ_{12} are always linked by the relation $\gamma_{12}^{min}(\gamma_{11}) = -\gamma_{12}^{max}(2 - \gamma_{11})$, which follows from a similar argument by using the fact that the tight-binding Hamiltonian (5.13) changes sign upon electron-hole transformation. We conclude that the knowledge of only one of the bounds on γ_{12}, upper or lower, for all electron densities $0 \leq \gamma_{11} \leq 2$ suffices in order to characterize the domain of ensemble representability. Moreover, in the case of bipartite lattice structures, the additional symmetry $\gamma_{12}^{min} = -\gamma_{12}^{max}$ implies that it suffices to consider the

upper or lower boundary on γ_{12} for electron densities up to half band-filling, i. e., in the range $0 \le \gamma_{11} \le 1$.

5.1.2 Functionals for uncorrelated mixed-states

An important class $\mathcal{P}_s$ of many-particle states is formed by the uncorrelated mixed-states, which are particularly relevant for the thermodynamic equilibrium in the non-interacting limit $U/t \to 0$ and in the limit of high temperatures $T/U \to \infty$ (see Appendix B). Therefore, it is instructive to consider the restriction of the functional (5.4) to the set of uncorrelated mixed-states, which is given by

$$G_s[\gamma_{11}, \gamma_{12}] = \min_{\hat{\rho}_s \to \{\gamma_{11}, \gamma_{12}\}} \mathrm{Tr}\left\{\hat{\rho}_s \left(U \sum_i \hat{n}_{i\uparrow}\hat{n}_{i\downarrow} + \frac{1}{\beta} \log \hat{\rho}_s\right)\right\}, \qquad (5.16)$$

where $\hat{\rho}_s \to \{\gamma_{11}, \gamma_{12}\}$ indicates the minimization with respect to all uncorrelated mixed-states $\hat{\rho}_s \in \mathcal{P}_s$ which satisfy the conditions (5.5). If we focus on the unpolarized case $\gamma_\uparrow = \gamma_\downarrow$, the interaction energy $W = U \sum_i \mathrm{Tr}\{\hat{\rho}_s\, \hat{n}_{i\uparrow}\hat{n}_{i\downarrow}\}$ in any uncorrelated mixed-state which meets these requirements is given by (see Appendix B)

$$W_{\mathrm{HF}}[\gamma_{11}] = U N_a \frac{\gamma_{11}^2}{4}. \qquad (5.17)$$

Consequently, only the entropy contribution to G_s needs to be minimized in Eq. (5.16). Thus, we can write

$$G_s[\gamma_{11}, \gamma_{12}] = W_{\mathrm{HF}}[\gamma_{11}] - T\, S_s[\gamma_{11}, \gamma_{12}], \qquad (5.18)$$

where we have introduced the reduced form

$$S_s[\gamma_{11}, \gamma_{12}] = -k_{\mathrm{B}} \min_{\hat{\rho} \to \{\gamma_{11}, \gamma_{12}\}} \mathrm{Tr}\{\hat{\rho} \log \hat{\rho}\} \qquad (5.19)$$

of the universal independent-Fermion entropy (IFE) functional (3.74). Notice that in Eq. (5.19) it is not necessary to restrict the minimization to the subspace $\mathcal{P}_s$, since the minimizing $\hat{\rho}$ always represents an uncorrelated mixed state. This is readily seen by considering the corresponding Euler-Lagrange functional

$$\mathcal{L}[\hat{\rho}] = \mathrm{Tr}\{\hat{\rho} \log \hat{\rho}\} + \lambda \sum_{\langle i,j \rangle} \left(\mathrm{Tr}\left\{\hat{\rho} \sum_\sigma \hat{c}_{i\sigma}^\dagger \hat{c}_{j\sigma}\right\} - \gamma_{12}\right) - \nu \sum_{i=1}^{N_a} \left(\mathrm{Tr}\left\{\hat{\rho} \sum_\sigma \hat{n}_{i\sigma}\right\} - \gamma_{11}\right)$$

$$= \mathrm{Tr}\left\{\hat{\rho} \left(\lambda \sum_{\langle i,j \rangle \sigma} \hat{c}_{i\sigma}^\dagger \hat{c}_{j\sigma} + \log \hat{\rho} - \nu \hat{N}\right)\right\} + N_a \left(\nu \gamma_{11} - \lambda z \gamma_{12}\right), \qquad (5.20)$$

where $\hat{N} = \sum_{i\sigma} \hat{n}_{i\sigma}$ and the Lagrange multipliers λ and ν enforce that the minimizing $\hat{\rho}$ satisfies the conditions (5.5). Apart from irrelevant constants, the functional (5.20) is of the Gibbs form (3.43) and thus the minimum within the set $\mathcal{P}$ of all positive semidefinite density matrices $\hat{\rho}$ with unit trace is taken for

$$\hat{\rho}_s = \frac{e^{-\beta_s\,(\hat{H}_s - \mu_s \hat{N})}}{\mathrm{Tr}\left\{e^{-\beta_s\,(\hat{H}_s - \mu_s \hat{N})}\right\}}\,, \tag{5.21}$$

where $\beta_s = \lambda$ and $\mu_s = \nu/\lambda$ can be interpreted as effective inverse temperature and chemical potential, and

$$\hat{H}_s = \sum_{\langle i,j\rangle\sigma} \hat{c}_{i\sigma}^{\dagger}\hat{c}_{j\sigma} \tag{5.22}$$

is the Hamiltonian of an auxiliary noninteracting system. We conclude that $\hat{\rho}_s$ describes an uncorrelated mixed-state, since it is the grand-canonical density matrix of a noninteracting system (see Appendix B).

Following the argument which led to the explicit expression (3.74) for the IFE functional, we conclude that

$$S_s[\gamma_{11}, \gamma_{12}] = -k_B \sum_{k\sigma} \left[\eta_{k\sigma} \log \eta_{k\sigma} + (1 - \eta_{k\sigma}) \log(1 - \eta_{k\sigma}) \right], \tag{5.23}$$

where

$$\eta_{k\uparrow} = \eta_{k\downarrow} = \frac{1}{1 + e^{\beta_s\,(\omega_k - \mu_s)}} \tag{5.24}$$

are the occupation numbers of the Bloch-states with the effective energies ω_k given in Eq. (5.10). Equation (5.24) implies that, for a given effective temperature and chemical potential, the occupation numbers $\eta_{k\sigma} = \eta_\sigma(\omega_k)$ depend solely on the corresponding Bloch-state energy ω_k. Therefore, we can express the reduced IFE-functional (5.23) in terms of the tight-binding DOS (5.11) as

$$S_s[\gamma_{11}, \gamma_{12}] = -k_B N_a \sum_\sigma \int_{-\infty}^{\infty} \left[\eta_\sigma(\omega) \log\big(\eta_\sigma(\omega)\big) + \big(1 - \eta_\sigma(\omega)\big) \log\big(1 - \eta_\sigma(\omega)\big) \right] \rho(\omega)\, d\omega\,. \tag{5.25}$$

In practice, one calculates the Bloch-state occupation numbers (5.24) for given values of the effective inverse temperature β_s and the effective chemical potential μ_s, and uses Eq. (5.12) in order to compute $\gamma_{11} = \sum_\sigma \gamma_{11\sigma}$ and $\gamma_{12} = \sum_\sigma \gamma_{12\sigma}$, as well as Eq. (5.25) in order to obtain the corresponding IFE S_s. Subsequently, one varies β_s and μ_s systematically in order to scan the complete domain of ensemble representability.

In Fig. 5.2 results are shown for the reduced IFE-functional $S_s[\gamma_{11}, \gamma_{12}]$ corresponding to different periodic lattice structures. For the bipartite lattice structures considered it is sufficient to focus on the partial domain $0 \leq \gamma_{11} \leq 1$ and $\gamma_{12} \geq 0$. Indeed,
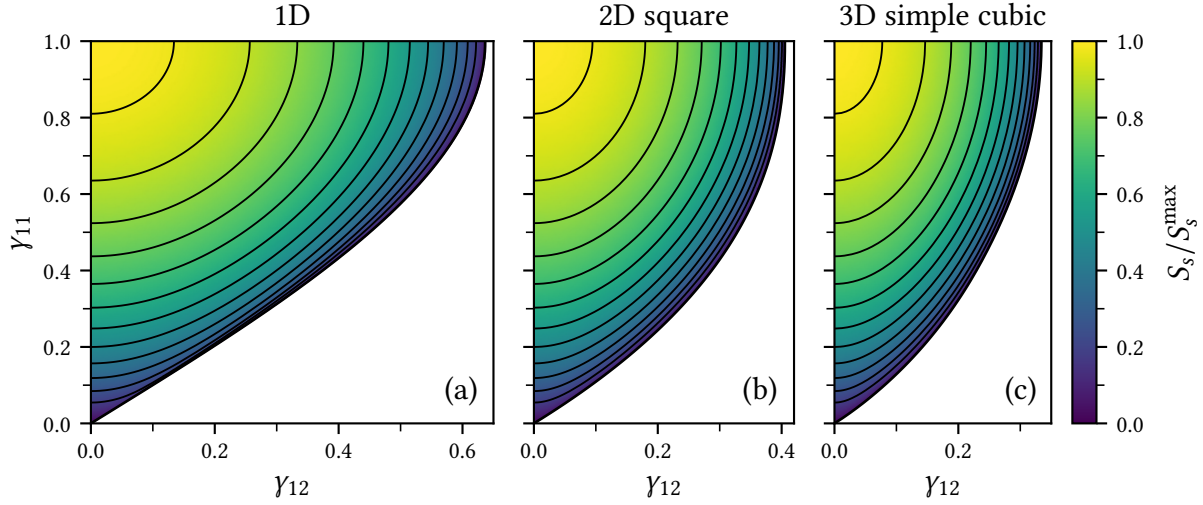
Figure 5.2: Reduced IFE-functional $S_s[\gamma_{11}, \gamma_{12}]$ for different bipartite lattice structures. Color contour-plots are shown for the periodic (a) one-dimensional chain, (b) square lattice, and (c) simple cubic lattice. The color scale for S_s is indicated on the right, where $S_s^{\max} = k_B N_a \log 4$ refers to the structure-independent global maximum of S_s, which is attained in the localized limit $\gamma_{12} = 0$ at half band-filling $\gamma_{11} = 1$. Contour lines are drawn at equidistant values of S_s in order to display its functional dependence more clearly.

changing the sign of the effective temperature in Eq. (5.24) leads to $\eta_{k\sigma} \rightarrow 1 - \eta_{k\sigma}$, which leaves the IFE (5.23) invariant but changes the sign of γ_{12}, which follows from Eq. (5.12) if the DOS $\rho(\omega)$ is an even function. Thus, one readily concludes that $S_s[\gamma_{11}, \gamma_{12}] = S_s[\gamma_{11}, -\gamma_{12}]$ if the underlying lattice structure is bipartite. Furthermore, the fact that the auxiliary Hamiltonian (5.22) changes sign upon electron-hole transformation implies that $S_s[\gamma_{11}, \gamma_{12}] = S_s[2 - \gamma_{11}, -\gamma_{12}]$. As already discussed in Section 5.1.1, the upper bound on γ_{12} is attained when the Bloch states with the highest effective energies ω_k are occupied ($\eta_{k\sigma} = 1$) while all other Bloch-states are unoccupied ($\eta_{k\sigma} = 0$). Consequently, S_s vanishes on the complete delocalized boundary ($\gamma_{12} = \gamma_{12}^{\max}$), and for a given electron density γ_{11} the IFE increases monotonously as the degree of NN charge fluctuations γ_{12} decreases, until the localized limit $\gamma_{12} = 0$ is reached. According to Eq. (5.12) the localized limit $\gamma_{12} = 0$ corresponds to homogeneous occupations $\eta_{k\sigma} = \gamma_{11}/2$ for all $k\sigma$. In this case the IFE (5.23) assumes its maximal value

$$S_s^{\max}(\gamma_{11}) = k_B N_a [\log 4 - (2 - \gamma_{11}) \log(2 - \gamma_{11}) - \gamma_{11} \log \gamma_{11}] \tag{5.26}$$

for the given electron density. Notice that this maximal value is independent of the lattice structure under consideration.

5.2 Scaling approximation for correlation effects

Having discussed the case of uncorrelated mixed-states and derived the exact functional dependence of the corresponding functional $G_s[\gamma_{11}, \gamma_{12}]$ which comprises the interaction energy and entropy of independent Fermions, we will now focus on the effects caused by electronic correlations. To this aim it is helpful to express the functional (5.4) in the form

$$G[\gamma_{11}, \gamma_{12}] = G_s[\gamma_{11}, \gamma_{12}] + G_c[\gamma_{11}, \gamma_{12}], \tag{5.27}$$

where $G_c[\gamma_{11}, \gamma_{12}]$ takes into account all contributions to the free energy which are the result of electronic correlations. In order to investigate the functional $G_c[\gamma_{11}, \gamma_{12}]$ in detail, one first needs to derive a practical implementation of the functional $G[\gamma_{11}, \gamma_{12}]$ defined in Eq. (5.4), which is possible by performing the corresponding minimization in an explicit manner. To this aim, let us consider the corresponding Euler-Lagrange functional

$$\mathcal{L}[\hat{\rho}] = \mathrm{Tr}\left\{\hat{\rho}\left(U \sum_i \hat{n}_{i\uparrow}\hat{n}_{i\downarrow} + \frac{1}{\beta}\log\hat{\rho}\right)\right\} + \lambda \sum_{\langle i,j\rangle}\left(\mathrm{Tr}\left\{\hat{\rho}\sum_\sigma \hat{c}_{i\sigma}^\dagger \hat{c}_{j\sigma}\right\} - \gamma_{12}\right)$$

$$- \mu \sum_{i=1}^{N_a}\left(\mathrm{Tr}\left\{\hat{\rho}\sum_\sigma \hat{n}_{i\sigma}\right\} - \gamma_{11}\right) \tag{5.28}$$

$$= \mathrm{Tr}\left\{\hat{\rho}\left(\lambda \sum_{\langle i,j\rangle\sigma} \hat{c}_{i\sigma}^\dagger \hat{c}_{j\sigma} + U \sum_i \hat{n}_{i\uparrow}\hat{n}_{i\downarrow} + \frac{1}{\beta}\log\hat{\rho} - \mu\hat{N}\right)\right\} + N_a\left(\mu\gamma_{11} - \lambda z\gamma_{12}\right),$$

where the Lagrange multipliers λ and μ enforce that the minimizing density matrix $\hat{\rho}$ satisfies the conditions (5.5). Apart from an irrelevant additive constant, the functional (5.28) is of the Gibbs form (3.43) and thus its minimum within the set $\mathcal{P}$ of all positive semidefinite density matrices $\hat{\rho}$ with unit trace is taken for

$$\hat{\rho}_0 = \frac{\mathrm{e}^{-\beta\,(\hat{H}_{\mathrm{aux}}-\mu\hat{N})}}{\mathrm{Tr}\left\{\mathrm{e}^{-\beta\,(\hat{H}_{\mathrm{aux}}-\mu\hat{N})}\right\}}, \tag{5.29}$$

where μ is identified as the chemical potential of the system described by the auxiliary Hamiltonian

$$\hat{H}_{\mathrm{aux}} = \lambda \sum_{\langle i,j\rangle\sigma} \hat{c}_{i\sigma}^\dagger \hat{c}_{j\sigma} + U \sum_i \hat{n}_{i\uparrow}\hat{n}_{i\downarrow}. \tag{5.30}$$

Clearly, the range of practical applications of this approach is limited, since it requires one to compute the grand-canonical density matrix $\hat{\rho}_0$ for the auxiliary Hamiltonian (5.30), which has the same level of complexity as the initial problem defined by

the Hubbard-model Hamiltonian (5.1). Therefore, applications of the thus described method are restricted to systems which are either soluble by exact analytical methods or which are sufficiently small in order to allow for an exact numerical calculation of the complete many-body spectrum. In these cases, one computes the grand-canonical density matrix (5.29) for given values of the effective NN hopping-integral λ and chemical potential μ, obtains the equilibrium electron density γ_{11} and the degree of NN charge fluctuations γ_{12} as

$$\gamma_{ij} = \sum_{\sigma} \text{Tr} \left\{ \hat{\rho}_0 \, \hat{c}_{i\sigma}^{\dagger} \hat{c}_{j\sigma} \right\}, \tag{5.31}$$

and the corresponding interaction- and entropy-contribution to the free energy is given by

$$G[\gamma_{11}, \gamma_{12}] = \text{Tr} \left\{ \hat{\rho}_0 \left(U \sum_i \hat{n}_{i\uparrow} \hat{n}_{i\downarrow} + \frac{1}{\beta} \log \hat{\rho} \right) \right\}. \tag{5.32}$$

Subtracting the uncorrelated part $G_s[\gamma_{11}, \gamma_{12}]$ finally yields the correlation contribution $G_c[\gamma_{11}, \gamma_{12}]$ to the free energy. Varying the effective NN hopping-integral λ and chemical potential μ systematically allows us to scan the complete domain X_e of ensemble representability (see also Fig. 5.1). Alternatively, one may focus on a fixed electron density γ_{11} by solving the eigenvalue problem for the auxiliary Hamiltonian (5.30) and determining μ such that the desired density is obtained. Varying the effective NN hopping-integral λ systematically then yields the functional dependence $G_c[\gamma_{12}]$ in the complete range of representable γ_{12} for the given electron density.

In Fig. 5.3 we focus on the case of a half-filled band ($\gamma_{11} = 1$) and present results for the correlation contribution $G_c[\gamma_{12}]$ to the free energy of the 1D Hubbard model on finite rings having $N_a = 2$–7 sites as well as for the infinite chain. Notice that G/U and thus also G_c/U depends only on the ratio U/k_BT and not on the Coulomb-repulsion strength U and the temperature T individually [see Eq. (5.32)]. Thus, in Figs. 5.3 (a)–(c) we plot G_c/U against γ_{12} for different ratios U/k_BT. Furthermore, we focus on the sector $0 \leq \gamma_{12} \leq \gamma_{12}^0$, where $\gamma_{12}^0 = \gamma_{12}^{\max}$ refers to the upper bound on the NN charge fluctuation [see Eq. (5.14)]. The correlation functionals $G_c[\gamma_{12}]$ of the finite rings were obtained from exact numerical diagonalizations of the auxiliary Hubbard-model Hamiltonian (5.30), while the results for the infinite Hubbard chain were obtained from the exact finite-temperature solution of Jüttner, Klümper, and Suzuki [56]. In Fig. 5.3 one observes $G_c \leq 0$ in the complete range of representable γ_{12}, which is expected, since the correlated motion of the electrons necessarily yields a reduction of the free energy. Furthermore, $|G_c|$ increases monotonously with decreasing γ_{12}, which reflects the fact that strong correlations in the electronic motion, aimed at the reduction of the average Coulomb energy, are accompanied with a significant suppression of the charge fluctuations. Concerning the dependence on the temperature and the Coulomb-repulsion strength, we find that $|G_c|/U$ increases with the
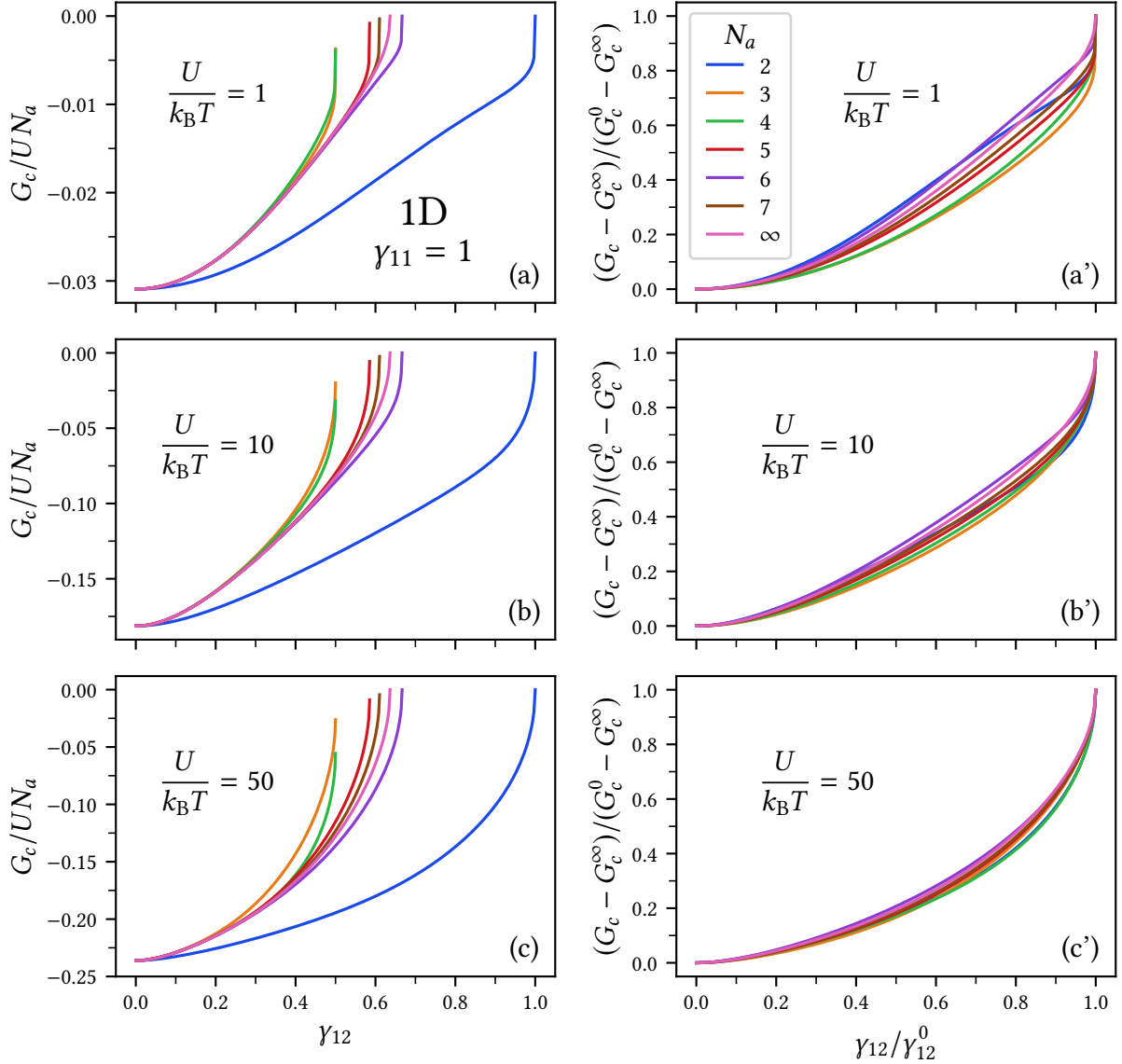
Figure 5.3: Correlation contribution $G_c[\gamma_{11}, \gamma_{12}]$ to the free-energy functional of the one-dimensional Hubbard model at half band-filling ($\gamma_{11} = 1$). Results are shown for finite rings having $N_a = 2$–7 sites as well as for the infinite chain with different ratios $U/k_\mathrm{B}T$ between the Coulomb-repulsion strength U and the temperature T. Subfigures in the right column [(a')–(c')] show the same data as their counterparts on the left [(a)–(c)], however, in the right column the values of G_c and the domain of representable γ_{12} are scaled to a common range by using the system-dependent upper bound γ_{12}^0 on the degree of NN charge fluctuations as well as the correlation contributions G_c^∞ and G_c^0 in the localized ($\gamma_{12} = 0$) and delocalized ($\gamma_{12} = \gamma_{12}^0$) limits.

ratio $U/k_\mathrm{B}T$. Clearly, in the uncorrelated or high-temperature limit $U/k_\mathrm{B}T \to 0$, the Coulomb energy has negligible impact in the minimization (5.4) which determines the functional dependence of $G[\gamma_{11}, \gamma_{12}]$. Therefore, the minimizing density matrix $\hat{\rho}_s$ must be the one which yields the maximum entropy for the given γ_{11} and γ_{12}. This implies $G[\gamma_{11}, \gamma_{12}] = G_s[\gamma_{11}, \gamma_{12}]$ (see Section 5.1.2), such that the correlation contribution to the free energy vanishes in this limit. On the other hand, the Coulomb energy dominates $G[\gamma_{11}, \gamma_{12}]$ in the strongly-interacting or low temperature limit $U/k_\mathrm{B}T \to \infty$. Thus, the minimization in Eq. (5.4) leads to a strongly-correlated mixed state $\hat{\rho}_\infty$ which, regardless of the entropy loss, yields the minimal average number of double occupations achievable for the given γ_{11} and γ_{12}. This strongly-correlated mixed state $\hat{\rho}_\infty$ is in general very different from the uncorrelated mixed-state $\hat{\rho}_s$ which yields the maximal entropy. Thus, the correlation contribution $|G_c| = |G - G_s|$ increases with $U/k_\mathrm{B}T$ as the underlying mixed-state evolves from $\hat{\rho}_s$ in the uncorrelated limit to $\hat{\rho}_\infty$ in the strongly-interacting limit.

In Figs. 5.3 (a)–(c) we find a qualitative similar dependence of G_c on the NN charge fluctuation γ_{12} and on the ratio $U/k_\mathrm{B}T$ for all considered systems. The most relevant dependence on the lattice size N_a originates from the system-dependent representability domain, which is characterized by the upper boundary γ_{12}^0 on the degree of NN charge fluctuations. In addition, a rather weak dependence on N_a is introduced by the minimal and maximal values G_c^∞ and G_c^0 of the correlation functional, which are attained, respectively, in the localized ($\gamma_{12} = 0$) and delocalized ($\gamma_{12} = \gamma_{12}^0$) limits. In fact, in Section 5.2.1 we will see that the correlation contribution G_c^∞ to the free energy in the localized limit $\gamma_{12} = 0$ is independent of the lattice structure under consideration, and that it scales with the size of the system such that G_c^∞/N_a depends solely on the electron density γ_{11}, the Coulomb-repulsion strength U, and the temperature T. Furthermore, in Section 5.2.2 we will demonstrate that the non-vanishing, slightly system-dependent values G_c^0 observed in the delocalized limit of some finite clusters [see, for example, the results for $N_a = 3$–5 in Figs. 5.3 (a)–(c)] are due to finite-size effects resulting from degeneracies in the single-particle spectrum. These findings suggest that the functional $G_c[\gamma_{12}]$ could reveal a quasi-universal behaviour if the system-dependent representability domains are scaled to a common range. In order to test this conjecture, we plot in Figs. 5.3 (a')–(c') the relative correlation contribution to the free energy $(G_c - G_c^\infty)/(G_c^0 - G_c^\infty)$ against the relative degree of NN charge fluctuations $\gamma_{12}/\gamma_{12}^0$. In this way, a nearly system-independent behaviour of the scaled $G_c[\gamma_{12}]$ is indeed observed, which is especially true for intermediate to large values of $U/k_\mathrm{B}T$, i. e., in the parameter range where correlation effects play a crucial role. Therefore, it is reasonable to expect that the functional dependence of $G_c[\gamma_{12}]$ can be inferred to a very high level of accuracy from the properly scaled correlation functional of a reference system which can be solved by exact analytical or numerical methods. Consequently, we propose the following scaling approximation for the cor-

relation contribution to the free-energy functional of the half-filled Hubbard model:

$$G_c[\gamma_{12}] = G_c^\infty + \left(G_c^0 - G_c^\infty\right) \frac{G_c^{\mathrm{rf}}\left[\gamma_{12}^{\mathrm{rf}}\right] - G_c^{\mathrm{rf},\infty}}{G_c^{\mathrm{rf},0} - G_c^{\mathrm{rf},\infty}} \quad \text{with} \quad \gamma_{12}^{\mathrm{rf}} = \gamma_{12}\, \frac{\gamma_{12}^{\mathrm{rf},0}}{\gamma_{12}^0}, \tag{5.33}$$

where the upper index "rf" on G_c and γ_{12} refers to the exactly solvable reference system. Notice that the temperature T and the interaction-integrals $W_{ijkl}^{\sigma\sigma'}$ merely play the role of fixed external parameters in the framework of FT-LDFT formulated in Section 3.2. Therefore, we require to consider the reference system in the scaling approximation (5.33) at the temperature T and the Coulomb-repulsion strength U specified by the target system in order to be compliant with the principles of FT-LDFT.

In this context, it is worth mentioning that the accuracy of the scaling approximation (5.33) can be improved by an appropriate choice of the reference system. As already discussed in Section 5.1, the functional (5.4) and thus $G_c[\gamma_{12}]$ depends to some extent on the lattice structure. Therefore, although the scaling properties exploited in Eq. (5.33) take into account most of the dependence of $G_c[\gamma_{12}]$ on the system size N_a, it is clear that the nature of the correlated electronic motion and thus the extent of the correlation effects expressed by G_c also depend on the local topology of the underlying lattice. This is especially true in the regime of small to intermediate values of γ_{12}, where short-ranged charge fluctuations dominate. Therefore, it is advisable to choose a reference system whose local topology matches the one of the system under study. For example, in the case of the 2D square lattice one expects more accurate results by using a finite square-lattice cluster as reference system rather than a 1D ring.

Notice that the scaling approximation (5.33) involves the system-specific correlation contributions G_c^∞ and G_c^0 to the free energy in the localized and delocalized limits. Therefore, it is worthwhile to study the extent of electronic correlations in these crucial limits in detail, before we move on and apply the scaling approximation to the half-filled Hubbard model on 1–3 dimensional periodic lattices.

5.2.1 Correlation effects in the localized limit

The purpose of this section is to determine the correlation contribution G_c^∞ to the free energy in the localized limit $\gamma_{12} = 0$, which enters the approximation (5.33) as an essential scaling parameter. We have already seen that the functional $G[\gamma_{11}, \gamma_{12}]$ can be determined from the solution of the thermodynamic equilibrium problem with the auxiliary Hamiltonian (5.30), and it is clear that a localized thermal-equilibrium state, i. e., $\gamma_{ij} = \sum_\sigma \mathrm{Tr}\left\{\hat{\rho}_0\, \hat{c}_{i\sigma}^\dagger \hat{c}_{j\sigma}\right\} = 0$ for all i, j corresponding to NNs, can only be achieved for $\lambda = 0$. Thus, in order to handle the localized limit, the auxiliary Hamiltonian can be simplified to

$$\hat{H}_{\mathrm{aux}} = U \sum_i \hat{n}_{i\uparrow} \hat{n}_{i\downarrow}. \tag{5.34}$$

Since $\hat{H}_{\text{aux}}$ is a sum of mutually commuting local terms, the corresponding grand-canonical partition function

$$Z = \text{Tr}\left\{e^{-\beta\,(\hat{H}_{\text{aux}}-\Sigma_\sigma\,\mu_\sigma\hat{N}_\sigma)}\right\} = \prod_{i=1}^{N_a}\text{Tr}_i\left\{e^{-\beta\,(U\hat{n}_{i\uparrow}\hat{n}_{i\downarrow}-\Sigma_\sigma\,\mu_\sigma\hat{n}_{i\sigma})}\right\} = Z_1^{N_a} \tag{5.35}$$

can be partitioned into a product of local contributions, where

$$Z_1 = \text{Tr}_1\left\{e^{-\beta\,(U\hat{n}_\uparrow\hat{n}_\downarrow-\Sigma_\sigma\,\mu_\sigma\hat{n}_\sigma)}\right\} = 1 + e^{\beta\mu_\uparrow} + e^{\beta\mu_\downarrow} + e^{\beta(\mu_\uparrow+\mu_\downarrow-U)} \tag{5.36}$$

is the partition function for a single site and Tr_1 denotes the trace in the corresponding four-dimensional singe-site Fock space. In order to be more general, we consider a spin-dependent chemical potential μ_σ, which will turn out to be useful in later applications to spin-polarized systems. From the partition function (5.35), we obtain the grand potential as

$$\Omega_0 = -\frac{1}{\beta}\log Z = -\frac{N_a}{\beta}\log\left(1 + e^{\beta\mu_\uparrow} + e^{\beta\mu_\downarrow} + e^{\beta(\mu_\uparrow+\mu_\downarrow-U)}\right), \tag{5.37}$$

and thus we readily infer the spin-dependent electron density as

$$\gamma_{11\sigma} = \frac{N_\sigma}{N_a} = -\frac{1}{N_a}\frac{\partial\Omega_0}{\partial\mu_\sigma} = 1 - \frac{1 + e^{\beta\mu_{-\sigma}}}{Z_1}. \tag{5.38}$$

Combining Eqs. (5.36) and (5.38), it is straight forward to express the single-site partition function in terms of the spin-dependent electron density

$$Z_1 = \frac{x - (2 - \gamma_{11})(x - 1) + \sqrt{[x - (2 - \gamma_{11})(x - 1)]^2 + 4\,(x - 1)(1 - \gamma_{11\uparrow})(1 - \gamma_{11\downarrow})}}{2\,(1 - \gamma_{11\uparrow})(1 - \gamma_{11\downarrow})}, \tag{5.39}$$

where $x = e^{\beta U}$ and $\gamma_{11} = \Sigma_\sigma\gamma_{11\sigma}$. Furthermore, using Eq. (5.38), we can express the chemical potentials in terms of the spin-dependent electron density as

$$\mu_\sigma = \frac{1}{\beta}\log\left[Z_1\,(1 - \gamma_{11,-\sigma}) - 1\right]. \tag{5.40}$$

Finally, we obtain the contribution (5.32) of the Coulomb energy and the entropy to the free energy in the localized limit as

$$\frac{G^\infty}{N_a} = -\frac{1}{\beta}\log Z_1 + \sum_\sigma\mu_\sigma\gamma_{11\sigma}. \tag{5.41}$$
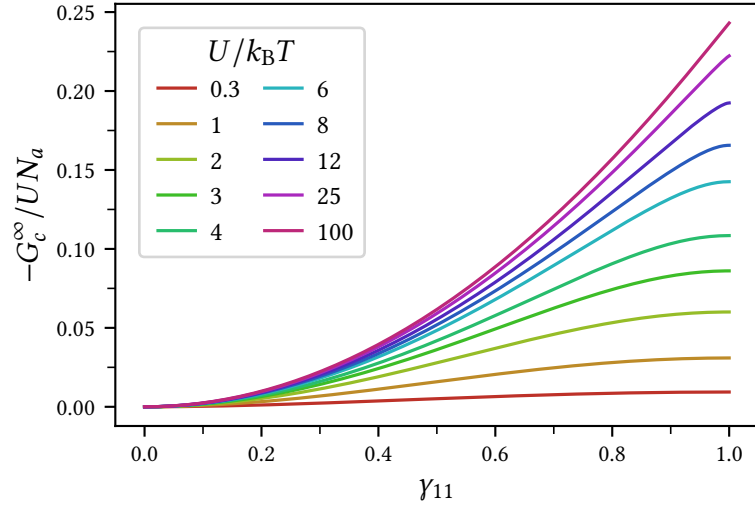
Figure 5.4: Correlation contribution G_c^∞ to the free energy in the localized limit ($\gamma_{12} = 0$) as function of the electron density γ_{11}. Results are shown for unpolarized charge distributions ($\gamma_{11\uparrow} = \gamma_{11\downarrow} = \gamma_{11}/2$) and representative values of the ratio $U/k_\text{B}T$ between the Coulomb-repulsion strength U and the temperature T.

Notice that G^∞/N_a depends only on the spin-dependent electron density $\gamma_{11\sigma}$, the Coulomb-repulsion strength U, and the temperature T, but not on the structure or size of the lattice, since the underlying many-particle state is fully localized.

In order to obtain the correlation contribution $G_c^\infty = G^\infty - G_s^\infty$ to the free energy in the localized limit, we subtract the uncorrelated part $G_s^\infty = W_\text{HF} - T\,S_s^\infty$, where $W_\text{HF} = U N_a\,\gamma_{11\uparrow}\gamma_{11\downarrow}$ is the Hartree-Fock interaction energy (see Appendix B) and S_s^∞ the IFE in the localized limit. In this case, the Bloch-state occupation numbers $\eta_{k\sigma} = \gamma_{11\sigma}\,\forall k$ are independent of the wave-vector k, such that we obtain the corresponding IFE from Eq. (5.23) as

$$S_s^\infty = -k_\text{B}N_a \sum_\sigma \left[\gamma_{11\sigma} \log \gamma_{11\sigma} + (1 - \gamma_{11\sigma}) \log(1 - \gamma_{11\sigma}) \right]. \tag{5.42}$$

Clearly, just like G^∞/N_a, the correlation contribution G_c^∞/N_a to the free energy per lattice site in the localized limit does not depend on the lattice structure and size, but only on the spin-dependent electron density $\gamma_{11\sigma}$, the Coulomb-repulsion strength U, and the temperature T.

In Fig. 5.4 the dependence of G_c^∞ on the electron density γ_{11} is shown for the case of unpolarized charge distributions ($\gamma_{11\uparrow} = \gamma_{11\downarrow} = \gamma_{11}/2$). The results shown account for G_c^∞/U, which depends on the ratio $U/k_\text{B}T$ but not on the Coulomb-repulsion strength U and the temperature T individually. Notice that $|G_c^\infty|$ increases

monotonously with the Coulomb-repulsion strength U and the electron density in the considered range $0 \leq \gamma_{11} \leq 1$, and its maximum is reached the case of a half-filled band ($\gamma_{11} = 1$). Similar observations were already made in the context of Fig. 5.3.

5.2.2 Correlation effects in the delocalized limit

The purpose of this section is to determine the correlation contribution G_c^0 to the free energy in the delocalized limit where the degree of charge fluctuations between NNs is maximal, i. e., $\gamma_{12} = \gamma_{12}^0$. As already discussed in Section 5.1.1, the many-body states which yield $\gamma_{12} = \gamma_{12}^0$ are Slater determinants where the Bloch states with effective energies (5.10) above the chemical potential, i. e., with $\omega_{\bm{k}} > \mu_\sigma$, are fully occupied ($\eta_{\bm{k}\sigma} = 1$) while Bloch states having $\omega_{\bm{k}} < \mu_\sigma$ are unoccupied ($\eta_{\bm{k}\sigma} = 0$). In order to account for the delocalized limit, it is therefore sufficient to work in the truncated Fock-space $\mathcal{H}_0$ spanned by the Slater determinants

$$|\Phi\rangle = \prod_\sigma \prod_{\omega_{\bm{k}}=\mu_\sigma} \left(\hat{c}_{\bm{k}\sigma}^\dagger\right)^{n_{\bm{k}\sigma}} |\Phi_0\rangle \quad \text{with} \quad n_{\bm{k}\sigma} \in \{0,1\}, \tag{5.43}$$

which differ only in the occupation of the usually degenerate lowest occupied energy level $\omega_{F\sigma} = \mu_\sigma$ for spin-σ electrons, which can be regarded as the Fermi level since it marks the boundary between occupied and unoccupied Bloch states. Furthermore, we have introduced the state

$$|\Phi_0\rangle = \prod_\sigma \prod_{\omega_{\bm{k}}>\mu_\sigma} \hat{c}_{\bm{k}\sigma}^\dagger |\text{vac}\rangle, \tag{5.44}$$

which represents the bulk of the Fermi sea. The Fock-space truncation reduces the initially 4^{N_a}-dimensional Fock-space to the $2^{g_{F\uparrow}+g_{F\downarrow}}$-dimensional subspace which is relevant in the delocalized limit. Here, $g_{F\sigma}$ denotes the degeneracy of the Fermi level $\omega_{F\sigma} = \mu_\sigma$ for spin-σ electrons. The Fock-space truncation thus renders the delocalized limit tractable if the degeneracy of the Fermi level is sufficiently low. For a given spin-dependent electron density $\gamma_{11\sigma}$, the contribution of the Coulomb energy and the entropy to the free energy in the delocalized limit is then given by

$$G^0 = \min_{\hat{\rho}\to\{\gamma_{11\uparrow},\gamma_{11\downarrow}\}} \text{Tr}_0\left\{\hat{\rho}\left(U\sum_i \hat{n}_{i\uparrow}\hat{n}_{i\downarrow} + \frac{1}{\beta}\log\hat{\rho}\right)\right\}, \tag{5.45}$$

where Tr_0 denotes the trace in the truncated Fock-space $\mathcal{H}_0$, and $\hat{\rho} \to \{\gamma_{11\uparrow},\gamma_{11\downarrow}\}$ indicates that the minimization is performed with respect to all positive semidefinite density matrices $\hat{\rho} \in \mathcal{P}_0 \subset \mathcal{P}$ having unit trace in $\mathcal{H}_0$, i. e., $\text{Tr}_0\{\hat{\rho}\} = 1$, and yield the desired local spin density $\text{Tr}_0\{\hat{\rho}\,\hat{c}_{i\sigma}^\dagger\hat{c}_{i\sigma}\} = \gamma_{11\sigma}$ for all $i = 1,\ldots,N_a$. Notice that, in contrast to the definition of $G[\gamma_{11},\gamma_{12}]$ in Eq. (5.4), no constraint is needed

in order to enforce $\gamma_{12} = \gamma_{12}^0$, since this condition is granted for all states within the truncated Fock-space $\mathcal{H}_0$. Moreover, it is important to remark that, in contrast to the localized limit discussed in the previous section, G^0 does depend on the lattice structure under consideration, since the truncated Fock-space $\mathcal{H}_0$ is defined in terms of the lattice-specific Bloch states and the corresponding effective energies ω_k [see Eqs. (5.10) and (5.43)].

In order to find the minimum in Eq. (5.45), one considers the corresponding Euler-Lagrange functional $\mathcal{L}[\hat{\rho}]$, which includes Lagrange multipliers in order to enforce that the constraints $\mathrm{Tr}_0\{\hat{\rho}\,\hat{c}_{i\sigma}^\dagger \hat{c}_{i\sigma}\} = \gamma_{11\sigma}$ are satisfied for all $i = 1, \ldots, N_a$. As usual, the Euler-Lagrange functional has the Gibbs form (3.43) and therefore, the minimum within the set $\mathcal{P}_0$ of all positive semidefinite density matrices $\hat{\rho}$ having unit-trace in the truncated Fock-space $\mathcal{H}_0$ is given by

$$\hat{\rho}_0 = \frac{e^{-(u\hat{D}-\sum_\sigma v_\sigma \hat{N}_\sigma)}}{\mathrm{Tr}_0\{e^{-(u\hat{D}-\sum_\sigma v_\sigma \hat{N}_\sigma)}\}}, \tag{5.46}$$

where $\hat{D} = \sum_i \hat{n}_{i\uparrow}\hat{n}_{i\downarrow}$ is the operator counting the local double occupations, $u = U/k_{\mathrm{B}}T$ is the ratio between the Coulomb-repulsion strength and the temperature, and v_σ can be considered as an effective chemical potential for spin-σ electrons. Notice that, in contrast to Eq. (5.35), the partition function in the denominator of Eq. (5.46) can not be separated into a product of local contributions, since the trace is taken in the truncated Fock space. Therefore, one expresses $\hat{D}$ in terms of the Bloch-states (2.13)

$$\hat{D} = \frac{1}{N_a} \sum_{k_1,k_2,q \in \mathrm{BZ}} \hat{c}_{k_1+q,\uparrow}^\dagger \hat{c}_{k_1\uparrow} \hat{c}_{k_2-q,\downarrow}^\dagger \hat{c}_{k_2\downarrow} \tag{5.47}$$

and one constructs the matrix representation $D_{nm} = \langle \Phi_n|\hat{D}|\Phi_m \rangle$ in the truncated Fock space spanned by the Slater determinants (5.43). Since $\hat{D}$ conserves the number N_σ of spin-σ electrons as well as the total momentum $K = \sum_{k\sigma} k\, n_{k\sigma}$, one can diagonalize $\hat{D}$ within each $(N_\uparrow, N_\downarrow, K)$-block separately. Expressing the minimizing density operator (5.46) in terms of the thus obtained eigenvalues D_n and orthonormal eigenstates $|\Psi_n\rangle$, one has

$$\hat{\rho}_0 = \frac{1}{Z_0} \sum_n e^{-(u D_n - \sum_\sigma v_\sigma N_\sigma^{(n)})} |\Psi_n\rangle\langle\Psi_n| \tag{5.48a}$$

with

$$Z_0 = \sum_n e^{-(u D_n - \sum_\sigma v_\sigma N_\sigma^{(n)})}. \tag{5.48b}$$

In this way, we obtain the contribution (5.45) of the Coulomb energy and the entropy to the free energy in the delocalized limit as

$$G^0 = \mathrm{Tr}_0\left\{\hat{\rho}_0\left(U\sum_i \hat{n}_{i\uparrow}\hat{n}_{i\downarrow} + \frac{1}{\beta}\log\hat{\rho}_0\right)\right\} = \sum_n p_n\left(U D_n + \frac{1}{\beta}\log p_n\right), \tag{5.49}$$

where $p_n = e^{-\left(u\, D_n - \sum_\sigma v_\sigma N_\sigma^{(n)}\right)}/Z_0$ is the statistical weight of the eigenstate $|\Psi_n\rangle$.

The correlation contribution G_c^0 is finally obtained by subtracting the uncorrelated portion $G_s^0 = W_{HF} - T\, S_s^0$ from Eq. (5.49). Clearly, a non-vanishing IFE S_s^0 in the delocalized limit can only be the result of a partially filled Fermi level, i. e., $0 < \eta_{k\sigma} = n_{F\sigma} < 1$ for all Bloch states having $\omega_k = \mu_\sigma$, such that

$$S_s^0 = -k_B \sum_\sigma g_{F\sigma} \left[n_{F\sigma} \log n_{F\sigma} + (1 - n_{F\sigma}) \log(1 - n_{F\sigma}) \right]. \tag{5.50}$$

However, the relative degree of degeneracy at the Fermi level

$$\frac{g_{F\sigma}}{N_a} = \lim_{\Delta\omega \to 0} \int_{\mu_\sigma}^{\mu_\sigma + \Delta\omega} \rho(\omega)\, d\omega = \lim_{\Delta\omega \to 0} \rho(\mu_\sigma)\, \Delta\omega \tag{5.51}$$

vanishes if the DOS (5.11) at the Fermi level is finite, which is always the case in the thermodynamic limit $N_a \to \infty$, at least somewhere in an arbitrarily small neighborhood of μ_σ. Therefore, we conclude that $S_s^0/N_a \to 0$ in the thermodynamic limit, as already observed in the context of Fig. 5.2. The fact that $g_{F\sigma}/N_a$ vanishes in the thermodynamic limit means that we can neglect all complications arising from degeneracies at the Fermi level if the system under consideration is sufficiently large. In this case, we can assume that $|\Phi_0\rangle$, given in Eq. (5.44), is the only many-body state which yields the maximum degree $\gamma_{12} = \gamma_{12}^0$ of NN charge fluctuations. Since $|\Phi_0\rangle$ is a single Slater determinant, we have $G^0 = U \langle\Phi_0|\hat{D}|\Phi_0\rangle = W_{HF} = G_s^0$. Therefore, one concludes that the correlation contribution $G_c^0 = G^0 - G_s^0$ to the free energy in the delocalized limit vanishes if sufficiently large systems are considered. For small finite systems, such as the reference systems used in the following applications of the scaling approximation (5.33), we use Eq. (5.49) in order to compute G_c^0 explicitly.

5.3 Infinite periodic lattices

Having introduced the scaling approximation (5.33) for the correlation contribution G_c to the free-energy functional, and discussed the localized and delocalized limits in detail, we are now in a position to apply our method in order to explore the equilibrium properties of the Hubbard model in the framework of FT-LDFT. We will focus on the thermodynamic limit $N_a \to \infty$ at half band-filling ($N/N_a = \gamma_{11} = 1$), and for given NN hopping-integral t, Coulomb-repulsion strength U, and temperature T we minimize the free-energy functional

$$F[\gamma_{12}] = -t N_a z\, \gamma_{12} + G_s[\gamma_{12}] + G_c[\gamma_{12}] \tag{5.52}$$

in the domain of ensemble representable γ_{12}. As usual, $G_s[\gamma_{12}]$ stands for the interaction-energy and entropy functional for uncorrelated mixed-states, given by

Eq. (5.16), and $G_c[\gamma_{12}]$ for the correlation contribution to the free-energy functional obtained from the scaling approximation (5.33) using an appropriate reference system. We treat the reference system in a grand-canonical ensemble formulation at the temperature T and Coulomb-repulsion strength U defined by the target system and choose the chemical potential μ_{rf} of the reference system such that a half-filled band is obtained. The minimization of the functional (5.52) directly yields the free energy F, the degree of NN charge fluctuations γ_{12} and thus the kinetic energy $K = -tN_a z \gamma_{12}$ in thermodynamic equilibrium. Additional equilibrium observables, such as the average number of double occupations D, the entropy S, and the specific heat C_V can be subsequently obtained from appropriate derivatives of the free energy F.

5.3.1 The infinite Hubbard chain

In Fig. 5.5 we present results for several equilibrium properties of the half-filled 1D Hubbard model as functions of the temperature T for representative values of the Coulomb-repulsion strength U/t. These results were obtained from FT-LDFT in combination with the scaling approximation (5.33) for the correlation contribution $G_c[\gamma_{12}]$ to the free-energy functional using a 7-site ring as reference system. The 7-site ring has been chosen, since it is the largest 1D reference system for which the computations within our current implementation of FT-LDFT are feasible. Furthermore, in order to account for long-range correlations a sufficiently large reference system is required, such that one generally expects to obtain more accurate results if a larger reference system is used. Further below we will quantify to which extent the equilibrium properties obtained in the framework of FT-LDFT depend on the choice of the reference system. In order to assess the accuracy of the FT-LDFT results shown in Fig. 5.5, we compare them with the exact finite-temperature solution of the 1D Hubbard model [56]. The free energy F, shown in Fig. 5.5 (a), results directly from the minimization of the free-energy functional (5.52) and the comparison with the corresponding exact analytical solution demonstrates that FT-LDFT is remarkably accurate in the whole range of temperatures T and Coulomb-repulsion strengths U/t. Indeed, the deviation between the exact and FT-LDFT results is smaller than the width of the individual lines on the scale used in Fig. 5.5 (a). The temperature dependence of F is in fact reproduced to such a high level of detail that accurate results are also obtained for its derivatives with respect to the Coulomb-repulsion strength and the temperature. Therefore, we obtain accurate results also for the average number of double occupations $D = \partial F/\partial U$, the entropy $S = -\partial F/\partial T$, and the specific heat $C_V = T \, \partial S/\partial T$, which are shown in Figs. 5.5 (d)–(f).

For the double occupations D, shown in Fig. 5.5 (d), we find a non-vanishing value in the ground state ($T = 0$), which is the result of the competition between electronic delocalization, driven by hybridization, and localization, which reduces the local
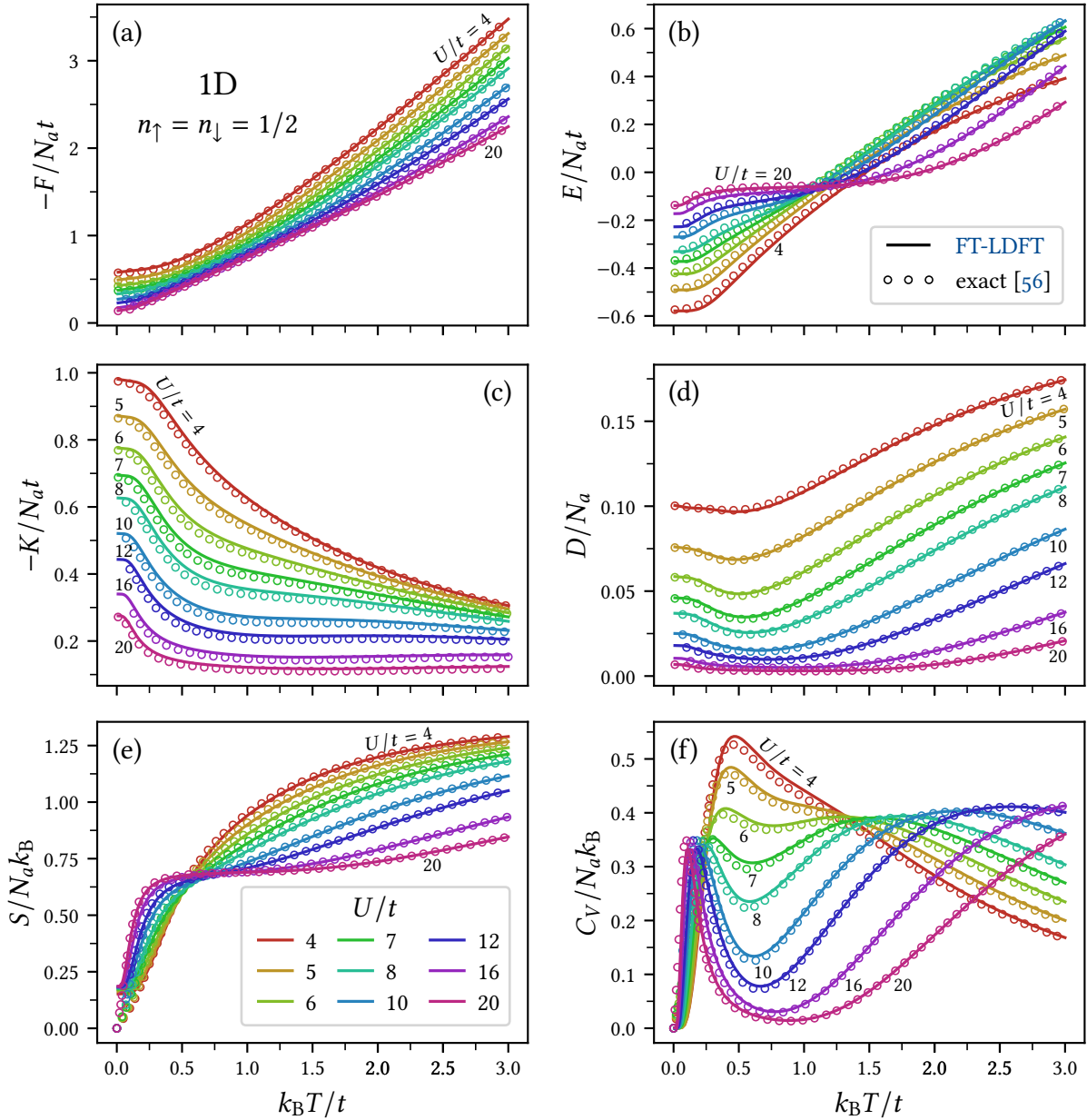
Figure 5.5: Equilibrium properties of the half-filled infinite 1D Hubbard chain as functions of the temperature T for representative values of the Coulomb-repulsion strength U/t. Results obtained by FT-LDFT in combination with the scaling approximation (5.33) using a 7-site ring as reference system (full curves) are compared with the exact solution of Jüttner *et al.* [56] (open circles): (a) free energy F, (b) total energy E, (c) kinetic energy K, (d) average number of double occupations D, (e) entropy S, and (f) specific heat C_V.

Coulomb energy. Thus, the average number of double occupations in the ground state decreases monotonously as the Coulomb-repulsion strength U/t increases. Clearly, the same is also true for any finite temperature, since the creation of double occupations requires more energy, and thus higher temperatures, if the Coulomb repulsions are stronger. Remarkably, the minimum of D is not attained in the ground state, but at a finite temperature which increases slightly with increasing U/t. This effect is caused by low-lying spin excitations from the antiferromagnetic (AFM) ground state which leads to a partial ferromagnetic (FM) alignment of the spins, such that the number of hopping processes permitted by the Pauli principle decreases. As a result, the charge fluctuations which give rise to the binding energy in the ground state are partly suppressed as the temperature increases, which is accompanied by a decrease of the double occupations generated by them. As the temperature increases beyond a critical threshold, charge excitations in the upper Hubbard band give rise to a renewed increase of D and thus to the formation of a minimum at a finite temperature which increases with U/t. Finally, in the high-temperature limit $k_\mathrm{B}T/U \to \infty$ the electronic motion becomes essentially uncorrelated, and thus one has $D = N_a/4$ regardless of the Coulomb-interaction strength ($U \ll k_\mathrm{B}T$). Notice that FT-LDFT reproduces the decrease of the double occupations due to the spin excitations from the AFM ground and the corresponding minimum in D very accurately for all values of the Coulomb-interaction strength U/t. Also the increase of D in the high-temperature regime is very well reproduced. In fact, the relative error $\Delta D = |D_\mathrm{ex} - D_\mathrm{FT\text{-}LDFT}|/D_\mathrm{ex}$ in the double occupations obtained within the framework of FT-LDFT is in average[1] just about 2% and always below 8% in the complete range of parameters shown in Fig. 5.5 (d).

The temperature dependence of the kinetic energy $K = -tN_a z\,\gamma_{12}$, shown in Fig. 5.5 (c), is obtained directly from the minimization of the free-energy functional (5.52). In the ground state we find the minimal value of K, which is the result of the NN charge fluctuations in the AFM ground state. These charge fluctuations are accompanied by double occupations, which have more impact on the energy if the Coulomb repulsions are stronger. Thus, we find a monotonously decreasing kinetic energy in the ground state and also at any finite temperature as U/t increases. As already discussed above, increasing temperatures give rise to the excitation of low-lying collective spin waves from the AFM ground state, causing a partial suppression of the ground-state charge fluctuations, and thus a rather rapid increase of K is observed in the low-temperature regime ($k_\mathrm{B}T \lesssim t/2$). Notice that K increases more rapidly in the low-temperature regime if the Coulomb repulsions are stronger. This is

---

[1] Here and in the following the average error is calculated as the deviation between the results of FT-LDFT and the given benchmark, averaged among the whole dataset. The FT-LDFT results are always distributed equally spaced on the scale shown and the benchmark data are interpolated to the same regular grid in order to compute the errors.

due to the fact that the low-lying spin excitations are described by the AFM Heisenberg model (2.52) with coupling constant $J = 2t^2/U$, and thus the bandwidth of the spin waves narrows as U/t increases. As the temperature further increases, antibonding Bloch-states are progressively excited and finally, in the high-temperature limit $k_B T/t \rightarrow \infty$, bonding and antibonding Bloch-states are equally occupied, resulting in an unbound state with $\gamma_{ij} = 0$ for all $i \neq j$. Thus, the kinetic energy vanishes for all values of $U \ll k_B T$ in this limit. The comparison with the corresponding exact results demonstrates that the increase of the kinetic energy caused by the low-lying spin excitations from the AFM ground state, as well as the transition to an unbound state as the temperature increases is very accurately reproduced within FT-LDFT in the complete range of temperatures and Coulomb-interaction strengths. The relative deviation $\Delta K = |(K_{ex} - K_{FT\text{-}LDFT})/K_{ex}|$ between the kinetic energy obtained from FT-LDFT and the exact solution is in average about 4%, and a maximum deviation of 8% is found for strong coupling $U/t = 20$ at $k_B T = 0.2t$. Clearly, the temperature dependence of the total energy $E = K + UD$, shown in Fig. 5.5 (b), results from the kinetic energy and the double occupations already discussed. Therefore, FT-LDFT yields very accurate results also for the total energy E in the complete range from the ground state to the high-temperature limit and for all values of the Coulomb-interaction strength.

The temperature dependence of the entropy S is shown in Fig. 5.5 (e). We find a rapid increase of the entropy at low temperatures if the Coulomb repulsion is strong ($U/t \gtrsim 10$), which results from the excitation of low-lying collective spin waves from the AFM ground state. A further entropy increase at higher temperatures is the result of charge-transfer excitations from the lower to the upper Hubbard-band, which involves the creation of double occupations. For weaker Coulomb repulsions ($U/t \lesssim 8$), the energy scales of spin and charge excitations have a noticeable overlap, such that a rather continuous increase of the entropy is observed in this case. Notice, however, that FT-LDFT fails to reproduce the linear entropy increase in the regime of very low temperatures ($k_B T \lesssim 0.2t$).[2] This is an artefact of the finite size of the reference system and results from the gap between the ground state and the lowest-lying excited states, as well as from degeneracies of the ground state. However, for $k_B T \gtrsim 0.2t$ the entropy obtained in the framework of FT-LDFT follows the exact analytical result very closely and an average relative deviation of 0.6% is found, which never exceeds 6% for all values of the Coulomb-repulsion strength shown in

---

[2]Notice that the NN hopping integral t in transition metals is typically of the order 0.1–0.5 eV, such that comparable temperatures $T \sim t/k_B = 1000$–6000 K are actually quite large for typical experimental setups. However, here and in the following the term "low temperature" refers to temperatures $k_B T$ which are small when compared to the energy scales specified by the model under consideration, such as the bandwidth $w \sim 4dt$ for a lattice in d dimensions, the Coulomb-repulsion strength U, or the effective exchange-coupling constant $J = 2t^2/U$ which is relevant in the strongly-interacting Heisenberg limit.

Fig. 5.5 (e) as long as $k_{\mathrm{B}}T > 0.2t$.

The specific heat C_V, shown in Fig. 5.5 (f), displays a most interesting temperature dependence. For intermediate Coulomb-repulsion strengths ($U/t \lesssim 5$) we find a broad peak in the specific heat which splits into two separate peaks as U/t increases. The peak appearing at low temperatures corresponds to spin excitations in the lower Hubbard-band, while the one at higher temperatures is caused by charge fluctuations, which give rise to increasing Coulomb interactions. The low-lying spin excitations are governed by the AFM Heisenberg model (2.52) with exchange-coupling constant $J = 2t^2/U$. Therefore, we expect to find the low-temperature peak in the specific heat, which marks the Néel transition from the AFM ground-state to the paramagnetic (PM) phase, at a temperature $k_{\mathrm{B}}T_N \propto t^2/U$ which scales like the effective exchange-coupling constant J with the Coulomb-interaction strength. In fact, in the strong-coupling limit $U/t \to \infty$ we expect to find the low-temperature peak in C_V at the temperature $k_{\mathrm{B}}T_N = J = 2t^2/U$ where the transition between the AFM and PM phases occurs in the one-dimensional spin-1/2 Heisenberg model [119, 120]. Figure 5.6 (a) shows the Néel-transition temperature T_N inferred from the low-temperature peak in the specific heat C_V as a function of the Coulomb-repulsion strength U/t. The comparison with the Néel-transition temperature derived from the exact solution [56] reveals that FT-LDFT in combination with the scaling approximation (5.33) not only reproduces the qualitative behavior $T_N \propto t^2/U$ correctly, but also yields very accurate values for the transition temperature, such that the relative error in T_N is in average about 13% and never exceeds 14.3% for all values shown in Fig. 5.6 (a). Furthermore, the convergence to the asymptotic behaviour $k_{\mathrm{B}}T_N = 2t^2/U$ in the strongly-correlated limit $U/t \to \infty$ is very well reproduced within FT-LDFT.

Another interesting feature of the specific heat is the almost unique high-temperature crossing point of the curves for $U \lesssim 8$, which occurs at $k_{\mathrm{B}}T \simeq 1.4t$. This nearly universal crossing point has attracted much attention in the past [121, 122], since it not only occurs in the Hubbard model but has been also observed experimentally in the specific-heat curves $C_V(T)$ of strongly correlated systems at different pressures. This includes normalfluid ^{3}H as well as heavy-fermion systems such as CeAl$_3$ and UBe$_{13}$ [123–126]. The comparison with the corresponding exact results shown in Fig. 5.5 (f) demonstrates that FT-LDFT reproduces the nearly universal crossing point of the specific-heat curves very accurately for the 1D Hubbard model.

For $U/t \gtrsim 6$ we find a second peak in C_V at high temperatures, which corresponds to charge excitations across the Hubbard gap. In Fig. 5.6 (b) the corresponding charge-excitation temperature T_C, inferred from the position of the high-temperature peak, is shown as a function of the Coulomb-repulsion strength U/t. Since the high-temperature peak in C_V is caused by charge excitations in the upper Hubbard-band, which lead to the creation of double occupations, we expect that the charge-excitation temperature T_C scales linearly with the Coulomb-repulsion strength U. In fact, the
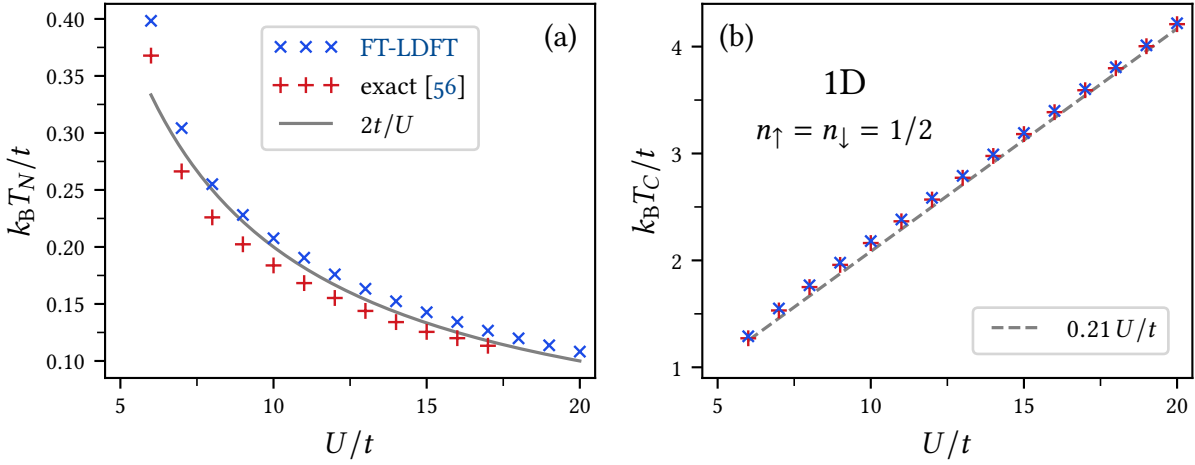
Figure 5.6: (a) Néel-transition temperature T_N and (b) charge-excitation temperature T_C of the half-filled infinite 1D Hubbard chain as functions of the Coulomb-repulsion strength U/t. The critical temperatures are inferred, respectively, from the positions of the low- and high-temperature peaks in the specific heat C_V. Results obtained by FT-LDFT in combination with the scaling approximation (5.33) using a 7-site ring as reference system are indicated by blue crosses, while red plus-symbols correspond to the critical temperatures derived from the exact solution of Jüttner *et al.* [56]. The gray solid line in (a) marks the asymptotic behaviour $k_B T_N = 2t^2/U$ of the Néel-transition temperature in the strongly-correlated limit $U/t \to \infty$, as inferred from the 1D Heisenberg model [119, 120]. The gray dashed line in (b) marks the corresponding strong-correlation asymptote $k_B T_C = 0.21U$ of the charge-excitation temperature, which is derived from the specific heat of the doublons (see Appendix F).

comparison with the temperature T_C derived from the exact finite-temperature solution of the 1D Hubbard-model [56] reveals that FT-LDFT not only yields the expected behavior $T_C \propto U$ but also reproduces the value of T_C almost exactly. The relative error in T_C is in average only 0.6% and never exceeds 1.5% in the complete range of parameters shown in Fig. 5.6 (b). In the strongly-correlated limit $U/t \to \infty$, where the energy scales of spin and charge excitations are widely separated, the dominant contribution to the specific heat at temperatures $k_B T \sim U$ results from the charge fluctuations and the accompanying fluctuations in the average number of double occupations. In this case, we can infer the asymptotic behaviour $k_B T_C = 0.21U$ from the structure-independent specific heat of the doublons, which we have calculated in Appendix F. From Fig. 5.6 (b) we conclude that the charge-excitation temperature T_C of the 1D Hubbard model converges rapidly to the strongly-correlated behavior $k_B T_C = 0.21U$ and that FT-LDFT is able to reproduce this rapid convergence with astonishing accuracy.

It is most remarkable that FT-LDFT in combination with the scaling approximation (5.33) is able to reproduce the gradual separation of spin and charge degrees
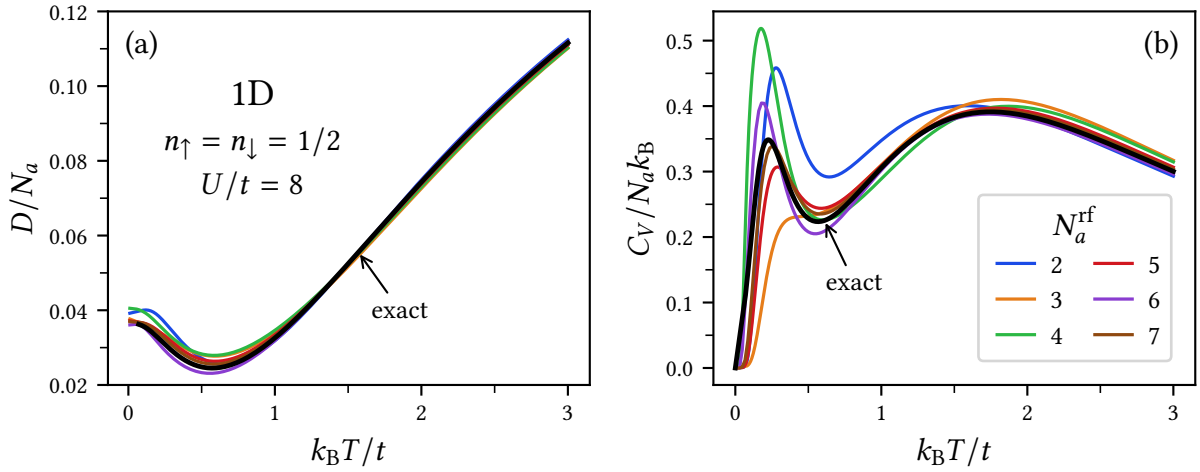
Figure 5.7: Equilibrium properties of the half-filled infinite 1D Hubbard chain with $U/t = 8$ obtained from FT-LDFT in combination with the scaling approximation (5.33) using 1D rings with $N_a^{\mathrm{rf}} = 2$–7 sites as reference systems. Results are shown for the temperature dependence of (a) the average number of double occupations D and (b) the specific heat C_V. The thick black curves mark the corresponding exact results for the infinite 1D Hubbard chain [56].

of freedom as the Coulomb-repulsion strength increases. In fact, this subtle effect of strong electronic correlations has, to our knowledge, not been reproduced in the framework of DFT before, neither on the qualitative and even less on the quantitative level. Clearly, it is one of the major advantages of FT-LDFT in combination with the scaling approximation (5.33) that the approximate functional $G_c[\gamma_{12}]$ is derived from an *interacting* system which already incorporates the effects of electronic correlations, such as the separation of spin and charge degrees of freedom. In contrast, most approximations in conventional DFT are based on the homogeneous electron gas, which does not incorporates most of the crucial effects of electronic correlations.

Before we apply the methods of FT-LDFT to the Hubbard model in two and three dimensions, let us briefly assess the importance of the reference system and investigate how the equilibrium properties obtained from the scaling approximation (5.33) are influenced by the choice of the reference system. To this aim we compare in Fig. 5.7 the average number of double occupations D and the specific heat C_V of the half-filled infinite 1D Hubbard chain with $U/t = 8$ obtained from the scaling approximation (5.33) using 1D rings with $N_a^{\mathrm{rf}} = 2$–7 sites as reference systems. From Fig. 5.7 (a) we conclude that the average number of double occupations depends rather weakly on the choice of the reference system in the whole range from the ground state to the high-temperature limit. As expected, the most noticeable deviations are observed in the low-temperature regime ($k_{\mathrm{B}}T \lesssim t$), where correlation effects play a

crucial role. At higher temperatures, the dependence of D on the choice of the reference system becomes rather negligible and the average number of double occupations of the infinite 1D Hubbard chain is reproduced very accurately. The situation is different in the case of the specific heat C_V shown in Fig. 5.7 (b), where the extent of the low-temperature peak strongly depends on the chosen reference system. This is, however, to be expected, since the specific heat $C_V = -T \, \partial^2 F / \partial T^2$ is a second-order derivative of the free-energy and thus depends sensitively on minor changes of the free-energy functional (5.52) in the vicinity of the minimum. Notice, however, that the Néel-transition temperature T_N is nevertheless fairly well reproduced with a maximal relative error of 28% when a 5-site ring is used as reference system. The only exception to this occurs for $N_a^{\mathrm{rf}} = 3$, where the low-temperature peak in the specific heat degenerates into a shoulder. For higher temperatures ($k_B T \gtrsim t$) we observe a rapid converge to the exact specific heat of the infinite 1D Hubbard chain as the size of the reference system increases, such that the relative error in the charge-excitation temperature T_C never exceeds 6.8% if rings with three or more sites are used as reference systems.

We conclude that FT-LDFT in combination with the scaling approximation (5.33) tends to yield more accurate results as the size of the reference system increases. However, it should be noted that a reference system whose symmetries and local topology matches those of the target system should always be preferred.

5.3.2 The square lattice

In Fig. 5.8 we present results for the equilibrium properties of the half-filled Hubbard model on the 2D square lattice as functions of the temperature T for representative values of the Coulomb-repulsion strength U/t. These results were obtained from FT-LDFT in combination with the scaling approximation (5.33) using a 2×2 square-lattice cluster with periodic boundary conditions as reference system. The periodic 2×2 cluster has been chosen as reference system since its symmetries and its local topology matches those of the infinite square lattice. The larger 2×3 cluster lacks the $\pi/2$ rotational symmetry and the 3×3 cluster is beyond the scope of our current implementation of the scaling approximation.

In order to assess the accuracy of the FT-LDFT results shown in Fig. 5.8, we compare them with quantum Monte Carlo (QMC) simulations for the 2D Hubbard model as well as to numerical linked-cluster expansions (NLCEs) [63, 66]. The total energy E, shown in Fig. 5.8 (a), increases very slowly in the low-temperature regime $k_B T \ll U$ where spin excitations with energies of the order t^2/U dominate. At higher temperatures of the order $k_B T \sim U$ also charge excitations in the upper Hubbard band contribute, which lead to an increase of the average number of double occupations and thus to a rather steep increase of the total energy. The absolute difference between
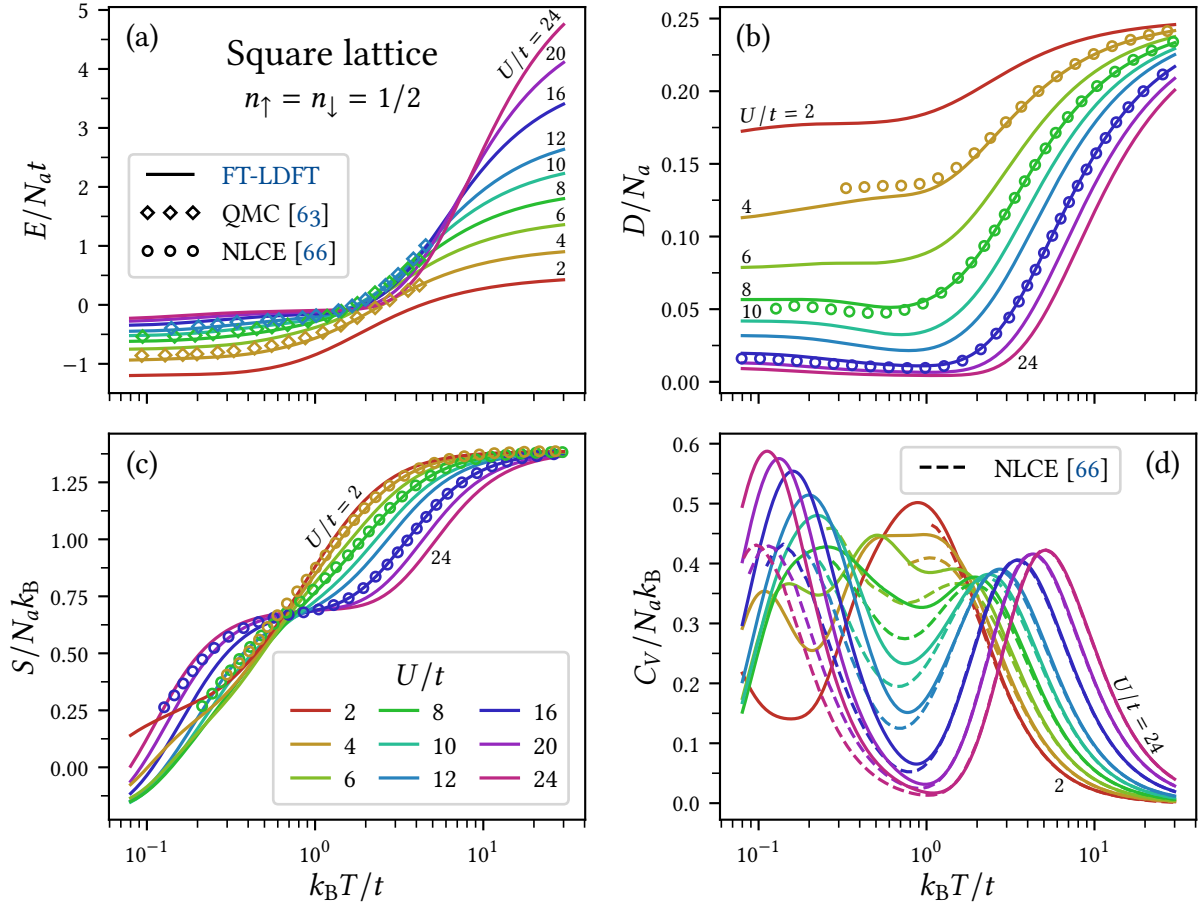
Figure 5.8: Equilibrium properties of the half-filled Hubbard model on the 2D square lattice as functions of the temperature T for representative values of the Coulomb-repulsion strength U/t. Results obtained by FT-LDFT in combination with the scaling approximation (5.33) using a 2×2 square-lattice cluster with periodic boundary conditions as reference system (full curves) are compared with QMC simulations of Duffy and Moreo [63] (diamonds) as well as with the NLCEs reported by Khatami and Rigol [66] (open circles and dashed lines): (a) total energy E, (b) average number of double occupations D, (c) entropy S, and (d) specific heat C_V.

the energy per lattice site E/N_a obtained from FT-LDFT and the QMC simulations reported by Duffy and Moreo [63] is in average about 4% of the NN hopping amplitude t and never exceeds 8.5% of t in the whole range of available data.

Concerning the average number of double occupations D, shown in Fig. 5.8 (b), we find a similar temperature dependence as in the previously considered one-dimensional case. Thus, we find monotonously decreasing values of D as U/t increases in the complete range from the ground state to the high-temperature limit. For intermediate to strong Coulomb-repulsions ($U/t \gtrsim 8$) we observe the formation of a minimum in D at a finite, rather low temperature, which increases slightly with U/t. Like in the previously considered one-dimensional case, this effect is caused by spin excitations from the AFM ground state, which leads to a partial suppression of the ground-state charge fluctuations and the accompanying double occupations. At higher temperatures, charge excitations in the upper Hubbard band give rise to a renewed increase of D, which is more rapid if the Coulomb repulsions are strong. In the case of rather weak Coulomb repulsions ($U/t \lesssim 6$) the energy scales of spin and charge excitations have a noticeable overlap, such that we observe slightly increasing values of D due to charge excisions already in the low-temperature regime ($k_B T \lesssim t$). This also explains the less rapid increase of D in the high-temperature regime ($k_B T \gtrsim 1.5$) observed for rather weak Coulomb repulsions, since in this case a large portion of the charge degrees of freedom unfreezes already at low temperatures. Finally, in the high-temperature limit $k_B T/U \to \infty$ the electronic motion becomes essentially uncorrelated, such that $D = N_a/4$ regardless of the Coulomb-interaction strength. The average number of double occupations D obtained in the framework of FT-LDFT is in overall very good agreement with the corresponding results of NLCEs [66]. The relative difference between the double occupations obtained from both methods is in average about 4.5% but can be as large as 24% if strong Coulomb-repulsions ($U/t = 16$) and temperatures below the charge-excitation threshold ($k_B T \lesssim 2.5t$) are considered. However, these large relative deviations are mainly caused by the small value of D in the strongly-interacting and low-temperature regime, and the absolute difference in D/N_a in fact never exceeds 9.7×10^{-3}.

The entropy S shown in Fig. 5.8 (c) develops the typical plateau as the Coulomb-repulsion strength U/t increases and the Hubbard gap is formed, which separates the low-lying spin excitations from the high-energy charge excitations. The comparison with the NLCEs reported by Khatami and Rigol [66] demonstrates that the formation of the plateau and the overall temperature dependence of the entropy is well reproduced within the framework of FT-LDFT. However, in the low-temperature regime the scaling approximation (5.33) in combination with the selected 2×2 square-lattice cluster as reference system fails to reproduce the temperature dependence of the entropy accurately, and for ($k_B T \lesssim 0.2t$) even slightly negative values of S are obtained. This unphysical behavior in the low-temperature regime results from an overestima-

tion of the entropy loss caused by correlations in the electronic motion. In fact, the comparison with the NLCEs in the low-temperature regime ($k_BT \lesssim t$) reveals that FT-LDFT predicts a too rapid decrease of the entropy as the system is cooled down, which ultimately results in negative values of the entropy. Nevertheless, for sufficiently high temperatures the entropy obtained within the framework of FT-LDFT is in excellent agreement with the corresponding NLCEs and the relative difference between both is in average only 0.4% and never exceeds 2.8% for $k_BT > t$.

Let us now focus on the specific heat shown in Fig. 5.8 (d). The broad peak in C_V which appears at $k_BT \simeq t$ for intermediate Coulomb repulsions ($U/t \lesssim 8$) splits into two well separated peaks as U/t increases. As already discussed in the context of the one-dimensional Hubbard model, the low-temperature peak corresponds to spin excitations in the lower Hubbard band, while the peak at higher temperatures is caused by charge excitations across the Hubbard gap. The formation of the two-peak structure in the specific heat is well reproduced within the framework of FT-LDFT on the qualitative level, however, the comparison with corresponding NLCEs reveals that the low-temperature peak is overestimated by up to 36%. Clearly, this is caused by the tendency of FT-LDFT to overestimate the entropy gain in the low-temperature regime ($k_BT \lesssim t$), as already discussed above. Nevertheless, the temperature T_N at which the low-temperature peak occurs in C_V agrees fairly well with the Néel-transition temperature inferred from NLCEs and QMC simulations, as shown in Fig. 5.9 (a). In fact, the convergence to the theoretical asymptote $T_N = 4J/3 = 8t^2/3U$ inferred from the specific heat of the AFM Heisenberg model (2.52) on the 2D square lattice [127, 128] is accurately reproduced within the framework of FT-LDFT.

For sufficiently high temperatures ($k_BT \gtrsim 1.5t$) we find an excellent agreement between the specific heat obtained from FT-LDFT and NLCEs, and the relative differences are in average as low as 0.13%. Within this temperature range we find the nearly universal crossing point of the specific-heat curves, which appears for $U/t \lesssim 12$ at a temperature $k_BT \simeq 1.75t$, and which is very well reproduced by FT-LDFT. Furthermore, we obtain very accurate results also for the charge-excitation temperature T_C derived from the position of the high-temperature peak in the specific heat. This is shown in Fig. 5.9 (b), where the dependence of T_C on U/t is compared with corresponding results of NLCEs and QMC simulations. If the Coulomb-repulsions are strong ($U/t \gtrsim 10$) the dominant contributions to the high-temperature excitations are due to charge fluctuations and the accompanying increase of the double occupations. The corresponding energies are thus independent of the underlying lattice structure. Therefore, we find in Fig. 5.9 (b) a similar dependence of the charge-excitation temperature T_C on the Coulomb-repulsion strength U/t as in the previously considered one-dimensional case [see Fig. 5.6 (b)] and a rapid convergence to the structure-independent asymptotic behavior $k_BT_C = 0.21U$ is observed (see Appendix F).

Figure 5.9: (a) Néel-transition temperature T_N and (b) charge-excitation temperature T_C of the half-filled Hubbard model on the 2D square lattice as functions of the Coulomb-repulsion strength U/t. The critical temperatures are inferred, respectively, from the positions of the low- and high-temperature peaks in the specific heat C_V. Results obtained by FT-LDFT in combination with the scaling approximation (5.33) using a 2×2 square-lattice cluster with periodic boundary conditions as reference system are indicated by blue crosses, while green circles and red plus-symbols correspond to the critical temperatures obtained from QMC simulations [63] and NLCEs [66]. The gray solid line in (a) marks the asymptotic behaviour $k_B T_N = 8t^2/3U$ of the Néel-transition temperature in the strongly-correlated limit $U/t \rightarrow \infty$, as inferred from the 2D Heisenberg model [127, 128]. The gray dashed line in (b) marks the corresponding strong-correlation asymptote $k_B T_C = 0.21U$ of the charge-excitation temperature, which is derived from the specific heat of the doublons (see Appendix F).

5.3.3 The simple-cubic lattice

Moving on to higher-dimensions, we have applied the methods of FT-LDFT to the half-filled Hubbard model on the 3D simple-cubic lattice. The equilibrium properties shown in Fig. 5.10 were obtained from the minimization of the free-energy functional (5.52) using the scaling approximation (5.33) for the correlation contribution $G_c[\gamma_{12}]$. We have chosen a 2×2×2 simple-cubic cluster with periodic boundary conditions as reference system, which is the smallest system resembling the local topology of the 3D simple-cubic lattice and, at the same time, the largest 3D reference system for which the computations within our current implementation of FT-LDFT are feasible. The equilibrium properties of the 3D Hubbard model obtained by FT-LDFT are in overall excellent agreement with available results of accurate QMC simulations reported by Paiva [65] and Kozik *et al.* [67], as well as with NLCEs performed by Khatami [68]. The energy E, shown in Fig. 5.10 (a), displays a very similar tem-
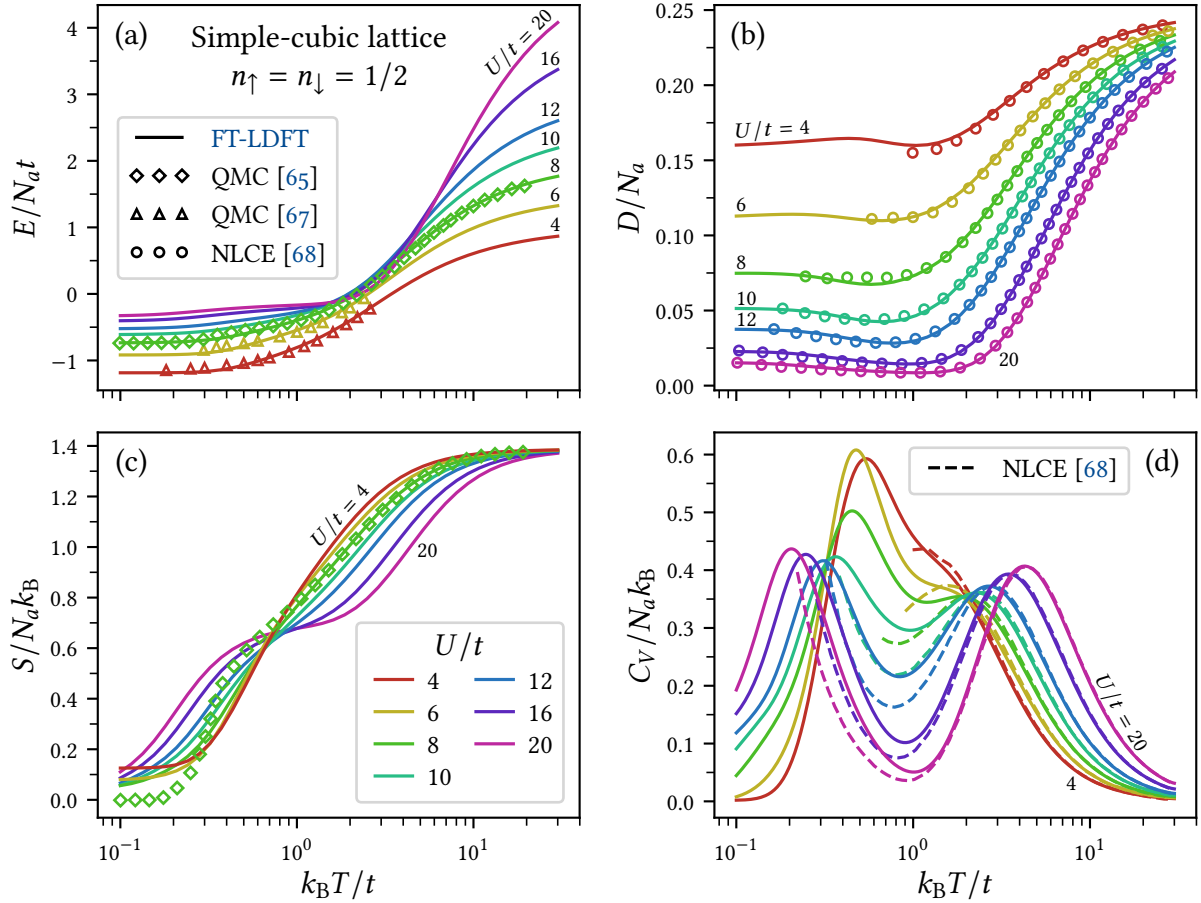
Figure 5.10: Equilibrium properties of the half-filled Hubbard model on the 3D simple-cubic lattice as functions of the temperature T for representative values of the Coulomb-repulsion strength U/t. Results obtained by FT-LDFT in combination with the scaling approximation (5.33) using a 2×2×2 simple-cubic cluster with periodic boundary conditions as reference system (full curves) are compared with QMC simulations of Paiva [65] (diamonds) and Kozik *et al.* [67] (triangles), as well as with the NLCEs reported by Khatami [68] (open circles and dashed lines): (a) total energy E, (b) average number of double occupations D, (c) entropy S, and (d) specific heat C_V.

perature dependence as in the previously considered two-dimensional case. Thus, a slow increase of E is observed in the low temperature regime ($k_\mathrm{B}T \ll U$), where the spin excitations dominate, while a steep increase of the energy is found when temperatures of the order $k_\mathrm{B}T \sim U$ give rise to charge excitations across the Hubbard gap, resulting in the creation of double occupations. Concerning the accuracy of the energy per lattice site E/N_a obtained in the framework of FT-LDFT, we find the absolute deviation from the available QMC simulations [65, 67] in average as low as 3% of the NN hopping amplitude t and no discrepancies larger than 7.5% of t are observed in the whole range of available data.

The temperature dependence of the average double occupancy D, shown in Fig. 5.10 (b), closely resembles the qualitative features already observed in the case of one- and two-dimensional lattices. Thus, we observe that D decreases monotonously with increasing U/t regardless of the temperature, and a minimum is formed at a finite temperature which increases slightly with U/t. Just like in the previously considered low-dimensional cases, the minimum in D is caused by spin excitations from the AFM ground state, which leads to a partial suppression of the ground-state charge fluctuations and the accompanying double occupations. Again, at higher temperatures D increases more rapidly with the temperature if the Coulomb repulsions are strong, until $D = N_a/4$ is attained for all values of U/t in the high-temperature limit $k_\mathrm{B}T/U \to \infty$. The comparison with available results of NLCEs [68] reveals that the temperature dependence of the double occupations in the 3D Hubbard model is very accurately reproduced within FT-LDFT. The relative difference between D obtained from both methods is in average as low as 1.4% and a maximal relative deviation of 10.5% is found at low temperatures and strong Coulomb-repulsions ($k_\mathrm{B}T = 0.3t$, $U/t = 16$). Again, this somewhat large relative deviation is a result of the fact that double occupations are largely suppressed in the regime of low temperatures and strong Coulomb repulsions. In fact, the absolute deviation between the double occupations per lattice site D/N_a obtained from FT-LDFT and NLCEs never exceeds 2.2×10^{-3} for $U \geq 10$ and the largest absolute deviation in D/N_a is found to be 5×10^{-3} in the weak-coupling case ($U/t = 4$) at rather low temperatures $k_\mathrm{B}T \approx t$.

Also the entropy of the 3D Hubbard model, shown in Fig. 5.10 (c), displays a very similar temperature dependence as its counterpart in two dimensions. Thus, we observe the formation of a plateau as the Coulomb-repulsion strength U/t increases, which is due to the increasing Hubbard gap and the resulting separation of the energy scales for spin and charge excitations. The comparison with the results of QMC simulations [65] indicates that the scaling approximation (5.33) in combination with the selected 2×2×2 simple-cubic cluster as reference system again leads to somewhat inaccurate values of the entropy in the low-temperature regime ($k_\mathrm{B}T \lesssim t$). Thus, FT-LDFT predicts a finite entropy in the ground state and for $k_\mathrm{B}T \lesssim 0.2t$ the entropy increases too rapid with the temperature, while for $0.2t \gtrsim k_\mathrm{B}T \gtrsim t$ the increase of S is
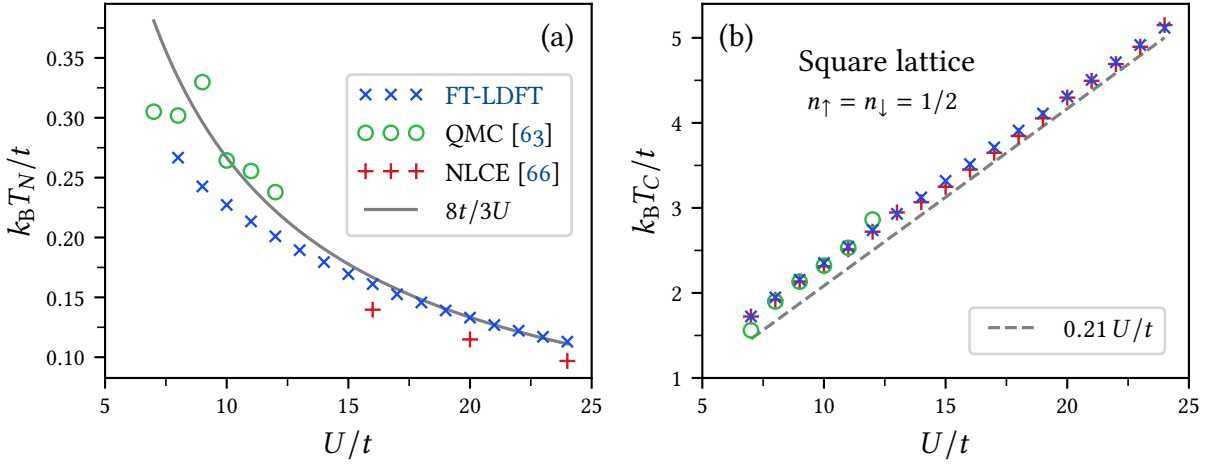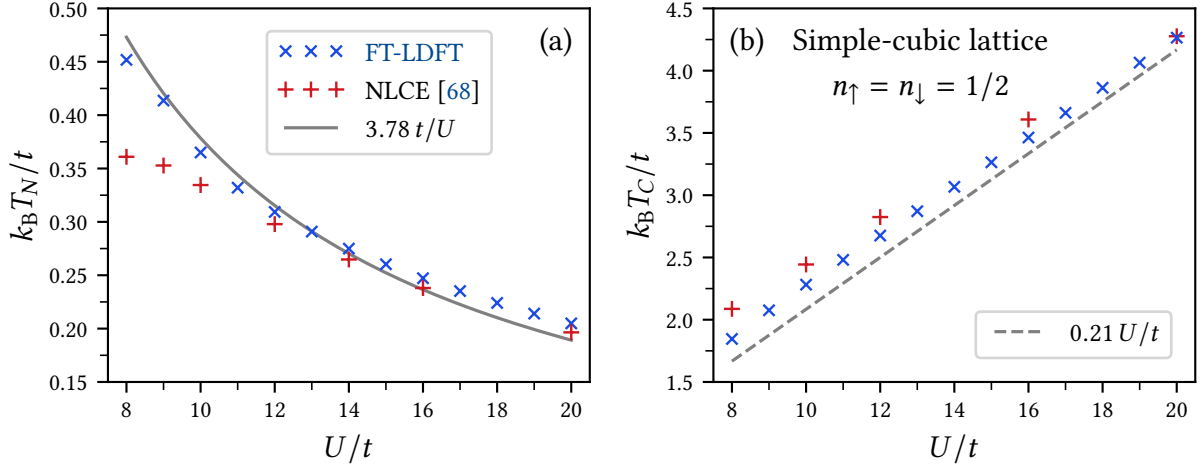
Figure 5.11: (a) Néel-transition temperature T_N and (b) charge-excitation temperature T_C of the half-filled Hubbard model on the 3D simple-cubic lattice as functions of the Coulomb-repulsion strength U/t. The critical temperatures are inferred, respectively, from the positions of the low- and high-temperature peaks in the specific heat C_V. Results obtained by FT-LDFT in combination with the scaling approximation (5.33) using a 2×2×2 simple-cubic cluster with periodic boundary conditions as reference system are indicated by blue crosses, while red plus-symbols correspond to the critical temperatures obtained from NLCEs [68]. The gray solid line in (a) marks the asymptotic behaviour $k_B T_N = 3.78 \, t^2/U$ of the Néel-transition temperature in the strongly-correlated limit $U/t \to \infty$, as inferred from the 3D Heisenberg model [129]. The gray dashed line in (b) marks the corresponding strong-correlation asymptote $k_B T_C = 0.21U$ of the charge-excitation temperature, which is derived from the specific heat of the doublons (see Appendix F).

underestimated. Nevertheless, for sufficiently high temperatures an excellent agreement between the entropy obtained from FT-LDFT and QMC simulations is obtained, and the relative deviation between both is in average as low as 0.3% for $k_B T \geq t$ and never exceeds 1.7% within this temperature range.

The specific heat C_V shown in Fig. 5.10 (d) exhibits the typical behavior caused by the separation of spin and charge degrees of freedom as the Coulomb-repulsion strength U/t increases. Thus, the broad peak which appears at a temperature $k_B T \sim t$ for fairly weak Coulomb-repulsions ($U/t \lesssim 6$) splits into two well separated peaks which correspond to the spin excitations in the lower Hubbard-band and the charge excitations across the Hubbard gap. The comparison with results of NLCEs [68] demonstrates that the formation of the two-peak structure in the specific heat of the 3D Hubbard model is very well reproduced within the framework of FT-LDFT, however some deviations from the NLCEs are observed in the low-temperature regime ($k_B T \lesssim t$). The NLCEs for the 3D Hubbard model do not converge down to

arbitrary low temperatures, such that the corresponding results shown in Fig. 5.10 (d) do not account for the low-temperature peak in C_V. However, since FT-LDFT in combination with the scaling approximation (5.33) and the selected 2×2×2 simple-cubic cluster as reference system underestimates the entropy increase in the temperature range $0.2t \gtrsim k_B T \gtrsim t$, we expect that FT-LDFT underestimates the specific heat $C_V = T \, \partial S / \partial T$ in the vicinity of the low-temperature peak as well. The temperature T_N at which the low-temperature phase transition from the AFM configuration to the PM phase occurs can be inferred from the position of the low-temperature peak in the specific heat. In Fig. 5.11 (a) we compare the Néel-transition temperature T_N obtained from FT-LDFT to corresponding results derived from the AFM structure factor of NLCEs [68]. In the strong-coupling regime ($U/t \gtrsim 12$) the Néel-transition temperature obtained from both methods is in excellent agreement and the mutual relative deviations are less than 4.3%. This implies that the convergence to the expected asymptotic behavior $T_N = 1.89 J = 3.78 \, t^2/U$, inferred from the AFM–PM phase transition in the 3D Heisenberg model [129], is accurately reproduced within FT-LDFT. However, the convergence to the strong-coupling asymptote $T_N = 3.78 \, t^2/U$ appears too rapid in the framework of FT-LDFT, such that T_N it is considerably overestimated for weaker Coulomb-repulsions ($U/t \lesssim 12$) and deviations up to 25% are observed.

For higher temperatures ($k_B T \gtrsim 1.5t$) we find an excellent agreement between the specific heat obtained from FT-LDFT and NLCEs. This implies that the nearly universal crossing point of the specific-heat curves, which appears at $k_B T \simeq 2t$ for $U \lesssim 12$, is accurately reproduced within FT-LDFT. Also the peak at higher temperatures, which corresponds to the charge excitations in the upper Hubbard band, and the corresponding charge-excitation temperature T_C is very well reproduced. From Fig. 5.11 (b) we conclude that the relative deviation between the charge-excitation temperature T_C obtained from FT-LDFT and NLCEs is in average as low as 5.5% and the maximal deviation is found to be 11.6% for $U/t = 8$. Like in the previously considered low-dimensional cases, also the rapid convergence to the structure-independent asymptotic behaviour $k_B T_C = 0.21U$ in the strong-coupling limit is very accurately reproduced (see Appendix F).

5.4 Arbitrary electron densities

Having applied the methods of FT-LDFT to the thermodynamic equilibrium problem of the half-filled Hubbard model in 1–3 dimensions, we would now like to go beyond half band-filling and to generalize our scaling approximation (5.33) such that arbitrary electron densities can be taken into account. The most general approach towards this goal would be to infer the functional dependence $G_c[\gamma_{11}, \gamma_{12}]$ of the correlation contribution to the free energy of a given target system with electron density $n = \gamma_{11}$

from the corresponding, properly scaled functional of some suitable reference system with (possibly different) electron density $n_{\mathrm{rf}} = \gamma_{11}^{\mathrm{rf}}$, i. e.,

$$G_c[\gamma_{11}, \gamma_{12}] = G_c^\infty + \left(G_c^0 - G_c^\infty\right) \frac{G_c^{\mathrm{rf}}\left[\gamma_{11}^{\mathrm{rf}}, \gamma_{12}^{\mathrm{rf}}\right] - G_c^{\mathrm{rf},\infty}}{G_c^{\mathrm{rf},0} - G_c^{\mathrm{rf},\infty}} \quad \text{with} \quad \gamma_{12}^{\mathrm{rf}} = \gamma_{12}^{\mathrm{rf},0} \frac{\gamma_{12}}{\gamma_{12}^0}. \quad (5.53)$$

Here the reference system is treated in a grand-canonical ensemble formulation at the temperature T and Coulomb-repulsion strength U defined by the target system, and the chemical potential μ_{rf} of the reference system is chosen such that the desired electron density $\gamma_{11}^{\mathrm{rf}}$ is obtained. In order to ease the notation we have not indicated the explicit dependence of $G_c^\infty = G_c^\infty(\gamma_{11})$ and $G_c^{\mathrm{rf},\infty} = G_c^{\mathrm{rf},\infty}(\gamma_{11}^{\mathrm{rf}})$, as well as of $\gamma_{12}^0 = \gamma_{12}^0(\gamma_{11})$ and $\gamma_{12}^{\mathrm{rf},0} = \gamma_{12}^{\mathrm{rf},0}(\gamma_{11}^{\mathrm{rf}})$ on the electron density in the target and reference systems (see Sections 5.1.1 and 5.2.1). Notice that also $G_c^0 = G_c^0(\gamma_{11})$ and $G_c^{\mathrm{rf},0} = G_c^{\mathrm{rf},0}(\gamma_{11}^{\mathrm{rf}})$ depends on the respective electron density if the corresponding system is finite (see Section 5.2.2).

The most natural choice in Eq. (5.53) would be to consider a reference system with the same electron density as the target system, i. e., $\gamma_{11} = \gamma_{11}^{\mathrm{rf}}$. However, it turns out to be sometimes favourable to choose the electron density in the reference system slightly different from the one in the target system. In order to understand this point, we consider in Fig. 5.12 the functional dependence of the correlation contribution G_c to the free energy of the one-dimensional Hubbard model for the case of strong Coulomb-repulsions or low temperatures $U/k_{\mathrm{B}}T \to \infty$ and quarter filling ($n = 0.5$). In the previous applications to the half-filled Hubbard model we have already seen that an accurate approximation to G_c is most crucial in the regime of strong Coulomb-repulsions or low temperatures, since correlation effects are most pronounced within this regime. Clearly, in the limit $U/k_{\mathrm{B}}T \to \infty$ depicted in Fig. 5.12, the entropy-contribution to G_c can be neglected, such that the functional dependence of $G_c = U(D - D_{\mathrm{HF}})$, leaving constants aside, coincides with the one of the doublons. Notice in Fig. 5.12 (a) that the overall shape of G_c as a function of γ_{12} is largely affected by the degree of NN charge fluctuations γ_{12}^∞ in the strongly-correlated ground state. This is particularly true for rather low electron densities ($n \lesssim 0.5$). The non-vanishing degree of NN charge fluctuations $\gamma_{12}^\infty > 0$ remaining in the strongly-correlated ground state away from half band-filling ($n < 1$) results from the ability of the electrons to avoid each other very effectively in a correlated motion, such that double occupations can be fully suppressed as long as $\gamma_{12} \leq \gamma_{12}^\infty$. In other words, γ_{12}^∞ is the maximal degree of NN charge fluctuations which is consistent with the requirement of vanishing double occupations $D = 0$. Furthermore, γ_{12}^∞ is directly related to the ground-state energy

$$E^\infty = -t N_a z \, \gamma_{12}^\infty \quad (5.54)$$

in the strongly-correlated limit $U/t \to \infty$ if a not more than half-filled band is considered. We conclude that γ_{12}^∞ is a crucial parameter for the low-temperature physics of
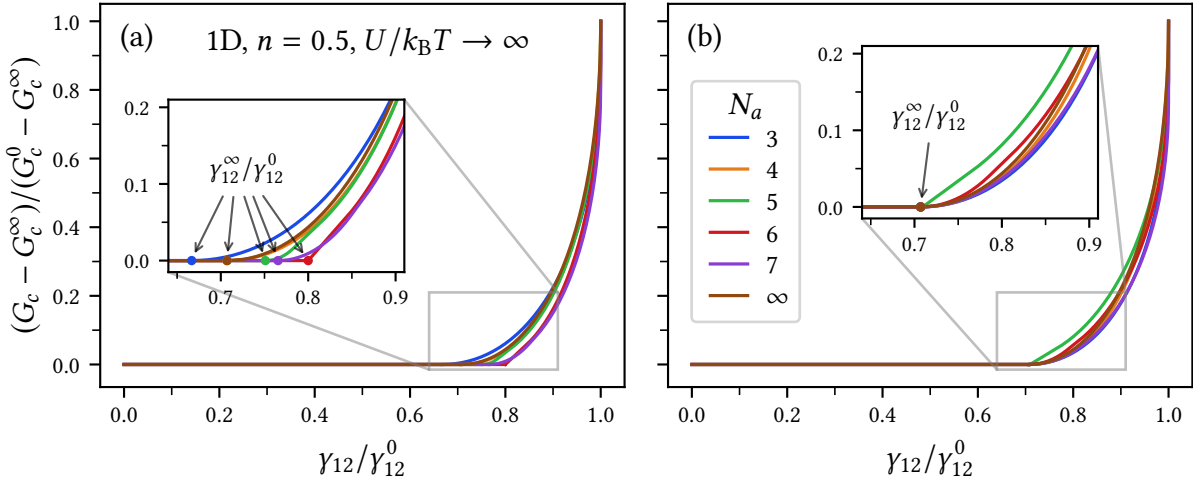
Figure 5.12: (a) Correlation contribution $G_c[\gamma_{11}, \gamma_{12}]$ to the free-energy functional of the one-dimensional Hubbard model for the case of strong Coulomb-repulsions or low temperatures $U/k_B T \to \infty$ and quarter filling ($n = \gamma_{11} = 0.5$). The functionals of finite rings with 3–7 sites as well as of the infinite chain are scaled to a common domain and range, and the inset highlights the region around the relative degree of NN charge fluctuations $\gamma_{12}^\infty/\gamma_{12}^0$ remaining in the strongly-correlated ground state. Subfigure (b) is similar to (a), however the electron density γ_{11} in the finite rings has been slightly adapted such that the relative degree of NN charge fluctuations in the strongly-correlated ground state matches the corresponding value $\gamma_{12}^\infty/\gamma_{12}^0 = 1/\sqrt{2} \approx 0.707$ of the infinite quarter-filled chain.

the Hubbard model away from half band-filling. However, from Fig. 5.12 (a) one concludes that a scaling of the functionals G_c taken from systems with the same electron density does in general not bring the relative degree of NN charge fluctuations $\gamma_{12}^\infty/\gamma_{12}^0$ remaining in the strongly-correlated ground state to a common point. As a consequence, the scaling approximation (5.53) will in general fail to reproduce the ground-state energy (5.54) in the strongly-correlated limit $U/t \to \infty$ if the electron density in the reference system matches the one in the target system, i. e., if $\gamma_{11}^{\mathrm{rf}} = \gamma_{11}$. Therefore, it is in general favourable to choose the electron density $\gamma_{11}^{\mathrm{rf}}$ in the reference system such that the corresponding relative degree of NN charge fluctuations in the strongly-correlated ground state matches the one of the target system, i. e.,

$$\frac{\gamma_{12}^{\mathrm{rf},\infty}(\gamma_{11}^{\mathrm{rf}})}{\gamma_{12}^{\mathrm{rf},0}(\gamma_{11}^{\mathrm{rf}})} = \frac{\gamma_{12}^\infty(\gamma_{11})}{\gamma_{12}^0(\gamma_{11})} \,. \tag{5.55}$$

This situation is depicted in Fig. 5.12 (b), where the band filling of the finite rings having 3–7 sites is chosen according to Eq. (5.55), such that the relative degree of charge fluctuations in the strongly-correlated ground state matches the correspond-
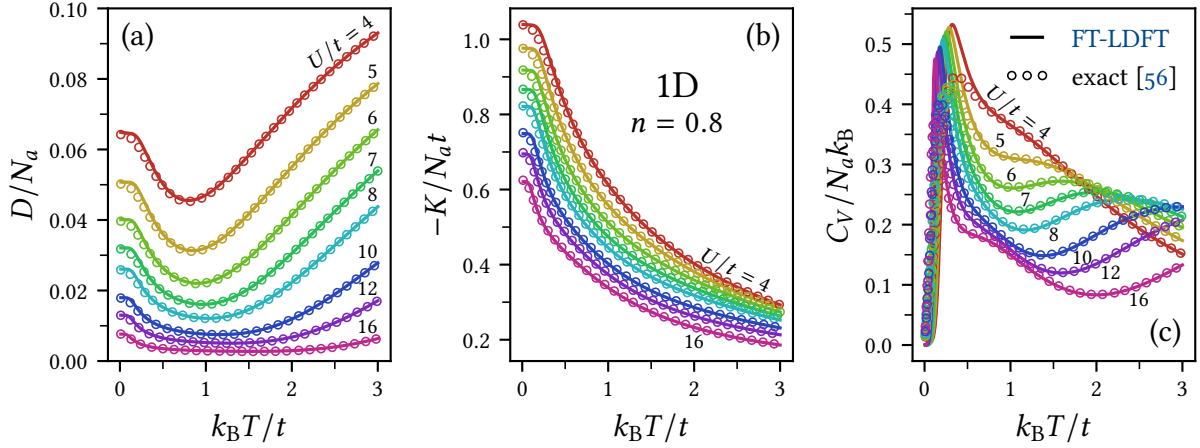
Figure 5.13: Equilibrium properties of the infinite 1D Hubbard chain with electron density $n = 0.8$ as functions of the temperature T for representative values of the Coulomb-repulsion strength U/t. Results obtained by FT-LDFT in combination with the scaling approximation (5.53) using a 7-site ring with electron density $\gamma_{11}^{\text{rf}} = 0.8013$ as reference system (full curves) are compared with the exact solution of Jüttner *et al.* [56] (open circles): (a) average number of double occupations D, (b) kinetic energy K, and (c) specific heat C_V.

ing value $\gamma_{12}^{\infty}/\gamma_{12}^{0} = 1/\sqrt{2}$ of the infinite Hubbard chain with quarter filling ($n = 0.5$). Notice that the choice of the band filling in the reference system according to Eq. (5.55) not only guarantees that the scaling approximation (5.53) reproduces the correct ground-state energy in the strongly-correlated limit (5.54), but in general also leads to a significant improvement of the approximation to G_c in the vicinity of γ_{12}^{∞} [compare the insets in Figs. 5.12 (a) and (b)], which is crucial in the regime of low temperatures or strong Coulomb repulsions. The exact value of the ground-sate energy E^{∞} in the strongly-correlated limit and thus the corresponding degree of NN charge fluctuations γ_{12}^{∞} is, however, unknown in general, such that Eq. (5.55) usually requires some approximations. One possibly is to proceed in a similar fashion as in Section 4.6, and to approximate the strongly-correlated ground state energy $E^{\infty} \approx E_{\text{FP}}$ by the energy (4.48) of the lowest-lying fully polarized state. The resulting approximation $\gamma_{12}^{\infty} \approx -E_{\text{FP}}/(tN_a z)$ is in general a lower bound for the degree of NN charge fluctuations in the strongly-correlated ground state, but matches the exact result $\gamma_{12}^{\infty} = \sin(\pi n)/\pi$ in the case of the infinite Hubbard chain.

Figure 5.13 shows the temperature dependence of several equilibrium average values of the infinite Hubbard chain with electron density $n = 0.8$ for representative values of the Coulomb repulsion strength U/t. The results of FT-LDFT in combination with the scaling approximation (5.53) are compared with the exact solution of Jüttner *et al.* [56]. As reference system we have chosen a 7-site ring with electron

density $\gamma_{11}^{\mathrm{rf}} = 0.8013$, which has been determined from Eq. (5.55) such that the relative degree of NN charge fluctuations in the strongly-correlated ground state of the reference system matches the corresponding value of the infinite chain with electron density $n = 0.8$. Notice that the electron density determined from Eq. (5.55) differs only very slightly from the one in the target system in the present case of a nearly half-filled band. Therefore, the modification of the electron density in the reference system has only marginal impact on the equilibrium averages obtained in the framework of FT-LDFT. In fact, the results obtained when a 7-site ring with electron density $\gamma_{11}^{\mathrm{rf}} = 0.8$ is used as reference system differ by less than the line width from the ones presented in Fig. 5.13. Nevertheless, the differences become substantial if lower electron densities are considered, as we will see further below when the methods of FT-LDFT are applied to the infinite Hubbard chain at quarter filling.

Concerning the average number of double occupations in Fig. 5.13 (a), we find a temperature dependence which is qualitatively very similar to the previously considered case of a half-filled band [compare Fig. 5.5 (d)]. However, in the present case of a less than half-filled band we find noticeable smaller values of D for any given temperature T and Coulomb-repulsion strength U/t, which is a consequence of the fact that the electrons are able to avoid each other very effectively in a correlated motion throughout the lattice. Clearly, this is also reflected in the U-independent high-temperature limit $D = D_{\mathrm{HF}} = 0.16\,N_a$, where the average number of double occupations is 36% smaller than in the previous half-filled band case. We also observe the formation of a pronounced minimum in D at a finite, rather low temperature which increases slightly with U/t. Just like in the half-filled band case we associate this minimum with the tendency of the spins to prefer an AFM alignment in the ground state, since the low-energy physics of the Hubbard model away from half band-filling is described by the t-J model (2.51) with AFM exchange-coupling $J = 2t^2/U > 0$. Low-lying spin excitations give rise to a partial suppression of the ground-state charge fluctuations and the accompanying double occupations, such that we observe decreasing values of D in the low-temperature regime. At higher temperatures, charge excitations in the upper Hubbard band give rise to a renewed increase of D, and thus to the formation of a minimum at a temperature which increases with U/t. The average number of double occupations obtained in the framework of FT-LDFT is in excellent agreement with the exact solution of Jüttner *et al.* [56] in the whole range from the ground state to high temperatures as well as for weak to strong Coulomb repulsions U/t. The relative difference between the exact and FT-LDFT double occupations is in average as low as 1.5% and never exceeds 5.7% in the whole range of temperatures and Coulomb repulsions shown.

In contrast to the double occupations, the temperature dependence of the kinetic energy K, shown in Fig. 5.13 (b), is quite different from the previously considered case of a half-filled bad, at least if strong Coulomb-repulsions ($U/t \gtrsim 8$) are considered

[compare Fig. 5.5 (c)]. Away from half band-filling, the suppression of the kinetic energy in the low-temperature regime as a result of increasing Coulomb repulsions is considerably less pronounced than in the previous case of a half-filled band. Clearly, this is due to the fact that the holes can move freely throughout the lattice without any impact on the Coulomb energy, which ultimately leads to the remaining kinetic energy in the strongly-correlated ground state. The kinetic energy increases with the temperature as antibonding Bloch-states are thermally excited, until bonding and antibonding Bloch-states are equally occupied in the high-temperature limit $k_\mathrm{B}T/t \to \infty$ resulting in a vanishing kinetic energy $K = 0$ for all values of U/t. The comparison with the corresponding exact results demonstrates that the temperature dependence of the kinetic energy of the infinite Hubbard chain with electron density $n = 0.8$ is very accurately reproduced within the framework of FT-LDFT. In fact, the relative error in K is in average as low as 0.7% and no discrepancies larger than 3% are found in the whole range of parameters explored.

Moving on to the specific heat, shown in Fig. 5.13 (c), we find a temperature dependence which is qualitatively similar to the one at half band-filling in the sense that the pronounced peak observed for intermediate Coulomb repulsions ($U/t = 4$) splits into two well separated peaks as U/t increases. However, in contrast to the half-filled band case, the low-temperature peak also includes contributions from charge excitations corresponding to the degrees of freedom of the holes. Thus, in comparison to the previous half-filled band case [see Fig. 5.5 (f)], we observe a more pronounced peak in the low-temperature regime if the Coulomb repulsions are strong ($U/t \gtrsim 6$). However, the comparison with the specific heat obtained from the exact solution shows that the increase of the low-temperature peak due to the admixture of charge excitations is considerably overestimated by FT-LDFT. In fact, the extent of the low-temperature peak in C_V is overestimated by up to 25%. Nevertheless, the temperature at which the low-temperature peak arises in the specific heat is quite accurately reproduced with a relative error of less than 6.4% for $U/t \geq 6$. Furthermore, the specific heat obtained in the framework of FT-LDFT converges to the exact solution as the temperature increases, and for sufficiently high temperatures we find both in excellent agreement. In fact, for $k_\mathrm{B}T \geq 0.6t$ the relative error in C_V is in average as low as 0.5% and never exceeds 2.7% within this temperature range.

In order to investigate the equilibrium properties at rather low electron densities, we present in Fig. 5.14 results for the infinite 1D Hubbard chain at quarter filling ($n = 0.5$). These results were obtained from FT-LDFT in combination with the scaling approximation (5.53) using a 7-site ring as reference system. The electron density in the reference system has been determined from Eq. (5.55) as $\gamma_{11}^{\mathrm{rf}} = 0.556$. In order to illustrate the influence of the electron density in the reference system we also include results obtained by matching the band filling in the reference system to the one in the infinite chain (i. e., $\gamma_{11}^{\mathrm{rf}} = 0.5$). The comparison with the exact solution of
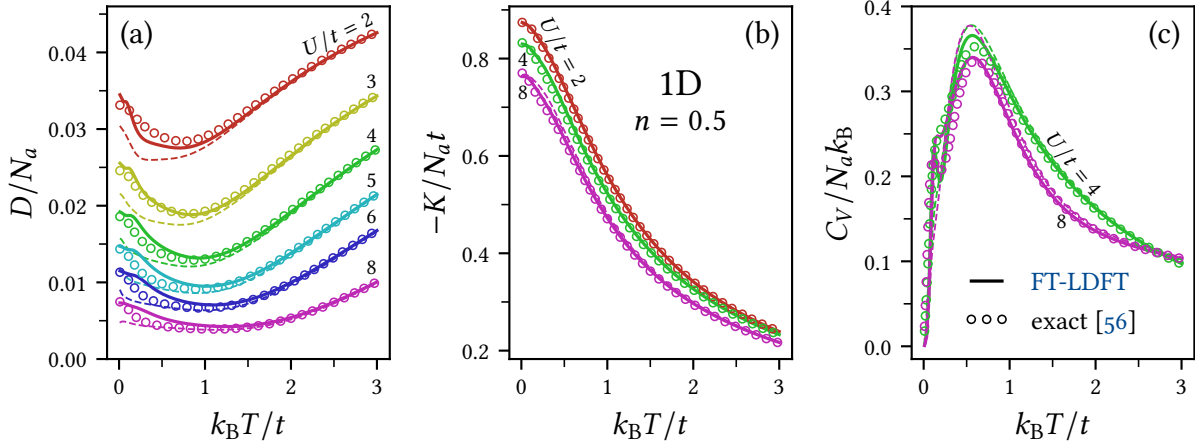
Figure 5.14: Equilibrium properties of the infinite 1D Hubbard chain at quarter band-filling ($n = 0.5$) as functions of the temperature T for representative values of the Coulomb-repulsion strength U/t. Results obtained by FT-LDFT in combination with the scaling approximation (5.53) using a 7-site ring with electron density $\gamma_{11}^{rf} = 0.556$ as reference system (full curves) are compared with the exact solution of Jüttner *et al.* [56] (open circles): (a) average number of double occupations D, (b) kinetic energy K, and (c) specific heat C_V. Results of FT-LDFT obtained by matching the electron density in the 7-site reference system to the one of the infinite chain (i. e., $\gamma_{11}^{rf} = 0.5$) are indicated by thin dashed lines.

Jüttner *et al.* [56] demonstrates that the modification of the electron density according to Eq. (5.55) improves the FT-LDFT results considerably in the low-temperature regime ($k_B T \lesssim t$). Nevertheless, in the present quarter-filled case, FT-LDFT yields slightly less accurate equilibrium averages at low temperatures as in the previously considered cases close to or at half band-filling. The deviations between the exact and FT-LDFT results might be attributed to finite-size effects in the reference system, which are more pronounced if lower electron densities are considered.

Concerning the average number of double occupations D, shown in Fig. 5.14 (a), we find the familiar qualitative behaviour already observed previously. Clearly, as the density decreases the electrons are able to avoid each other more effectively in a correlated motion throughout the lattice. Thus, in the present case of a quarter-filled band, we find noticeable smaller values of D at any given temperature T and Coulomb-repulsion strength U/t than in the previous case $n = 0.8$. This is also reflected in U-independent high-temperature limit $D = D_{HF} = N_a/16$, which is 61% smaller than in the case $n = 0.8$. We also observe the formation of a pronounced minimum at a finite temperature, which we associate with the tendency of the spins to prefer an AFM alignment in the ground state, and the corresponding low-temperature spin excitations. Concerning the accuracy of the average number of double occupations ob-

tained in the framework of FT-LDFT, we find some noticeable deviations of up to 30% from the exact results within the regime of rather low temperatures ($k_BT \lesssim t$). For higher temperatures, the dependence of the doublons is more accurately reproduced with relative errors never exceeding 11% for $k_BT > t$. Since the electrons are able to avoid each other very effectively without much impact on their kinetic energy K in the present case of a rather low density, we observe in Fig. 5.14 (b) a temperature dependence of K which is rather insensitive to variations of the Coulomb-repulsion strength U/t. The comparison with corresponding exact results demonstrates that FT-LDFT reproduces the temperature dependence of the kinetic energy very accurately in the present low-density case. The relative error of K is in average as low as 0.5% and never exceeds 2% in the whole range of data shown.

The specific heat C_V, shown in Fig. 5.14 (c), displays a temperature dependence which is qualitatively very different from the one observed at and close to half band-filling. In the present case of a rather low electron density, the formation of the two-peak structure in C_V as the Coulomb-repulsion strength U/t increases is largely suppressed since the low-lying spin excitations are superimposed by charge excitations corresponding to the holonic motion. We thus observe a single broad maximum, which appears at $k_BT \approx 0.6t$ and is rather insensitive to the value of U/t. However, for sufficiently strong Coulomb repulsions ($U/t = 8$) we still observe a small satellite-peak which appears at a very low temperature ($k_BT \approx 0.1t$) and it is believed to be caused by low-lying spin excitations [56]. The comparison of our results to the specific heat derived from the exact solution shows that the broad peak at $k_BT \approx 0.6t$ is very well reproduced within FT-LDFT. Noticeable deviations are, however, observed in the low-temperature regime ($k_BT \lesssim 0.5t$), such that the small satellite-peak at $k_BT \approx 0.1t$ is not accurately obtained. Nevertheless, for sufficiently high temperatures the specific heat obtained in the framework of FT-LDFT is in excellent agreement with the exact result and the relative error never exceeds 2% for $k_BT \geq t$.

In order to assess the performance of our FT-LDFT approach in higher dimensions, we present in Fig. 5.15 results for the temperature dependence of the doublons D in the Hubbard model on the 2D square lattice and the 3D simple cubic lattice with electron densities ranging from $n = 0.65$ to 1.0. Like in the previous applications to the half-filled Hubbard model, we have chosen a 2×2 square lattice cluster with periodic boundary conditions as reference system in 2D, and a periodic 2×2×2 simple cubic cluster in 3D. In the present applications to the two- and three-dimensional Hubbard model it turns out to be favorable to match the electron density in the reference system to the one in the target system, instead of choosing it according to Eq. (5.55), where we approximate the degree of NN charge fluctuations in the strongly-correlated ground state in terms of the energy E_{FP} of the lowest-lying fully polarized state:

$$\gamma_{12}^{\infty} \approx -\frac{E_{FP}}{tN_a z} \, . \tag{5.56}$$
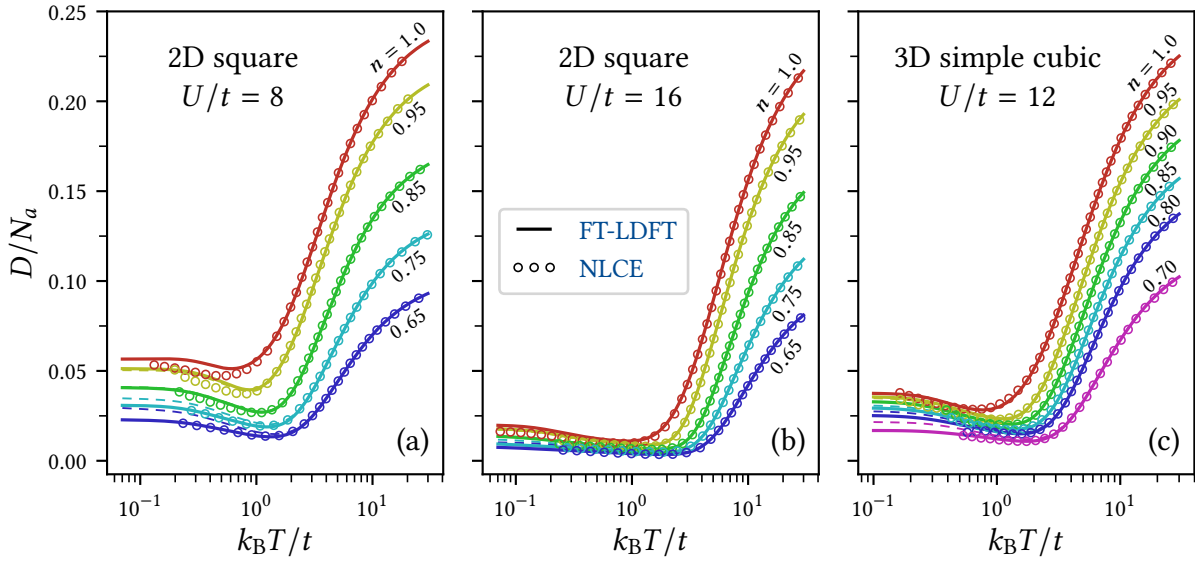
Figure 5.15: Temperature dependence of the doublons D in the Hubbard model on [(a) and (b)] the 2D square lattice and (c) the 3D simple cubic lattice with electron densities ranging from $n = 0.65$ to 1.0. Results obtained by FT-LDFT in combination with the scaling approximation (5.53) are indicated by solid lines, while open circles correspond to NLCEs reported by Khatami *et al.* [68, 130]. FT-LDFT results in 2D were obtained by using a 2×2 square lattice cluster as reference system, while in 3D a 2×2×2 simple cubic cluster has been used. The electron density in the FT-LDFT reference system matches the one in the target system. Results obtained by choosing the electron density in the reference system according to Eq. (5.55) are indicated by thin dashed lines.

This can be attributed to the fact that the approximation (5.56) generally underestimates γ_{12}^{∞}, such that the electron density in the reference system determined from Eqs. (5.55) and (5.56) tends to be too large. Thus, Eq. (5.55) must be combined with a more accurate approximation to γ_{12}^{∞} in order to improve the results of FT-LDFT in two and three dimensions. However, in contrast to the previously considered one-dimensional case, it turns out that the scaling approximation (5.53) yields excellent results in higher dimensions if the electron density in the reference system is chosen to match the one in the target system. Thus, in Fig. 5.15 we observe that the temperature dependence of the doublons in the 2D and 3D Hubbard models is remarkably well reproduced in the complete range of electron densities n and Coulomb-repulsion strengths U/t. This includes the gradual suppression of D as the electron density decreases, which reflects the fact that the electrons are able to avoid each other more effectively if the density is lower. Also the minimum in D, which is a result of low-lying spin excitations, is very accurately reproduced for all electron densities. Notice

that the upturn in D, which leads to the sharp increase of D in the high-temperature regime, occurs at higher temperatures if the electron density is lower. This can be ascribed to the fact that charge excitations have less impact on the double occupations if low electron densities are concerned. The comparison with the NLCEs reported by Khatami *et al.* [68, 130] confirms that FT-LDFT yields highly accurate results for the double occupations and we find relative deviations for the 2D square lattice which are in average as low as 1.8% for $U/t = 8$, as seen in Fig. 5.15 (a), and 3.5% for the strong-coupling case $U/t = 16$ shown in Fig. 5.15 (b). Similarly, for the doublons in the 3D simple-cubic lattice with $U/t = 12$, shown in Fig. 5.15 (c), we find relative deviations which are in average as low as 1.7%. Concerning the dependence on the electron density, we notice that FT-LDFT tends to yield more accurate results if the electron density is lower. Thus, we find no discrepancies larger than 3% for the 2D square lattice with $U/t = 8$ and $n = 0.65$, while at half band-filling ($n = 1$) relative differences of up to 12.6% are observed. Similarly, in the strong-coupling case $U/t = 16$ the maximal deviation for $n = 0.65$ is less than 4%, while close to half band-filling ($n = 0.95$) differences of up to 24% are observed in the low-temperature regime ($k_B T \lesssim t$). However, these large relative deviations are mainly due to the fact that the doublons are largely suppressed in the low-temperature regime if the Coulomb repulsions are strong. In fact, the absolute deviation in D/N_a never exceeds 3.5×10^{-3} for $U/t = 16$. Concerning the 3D simple cubic lattice with $U/t = 12$, the largest relative discrepancy is found to be 11.5% at $k_B T \approx 0.7t$ and $n = 0.8$. Again, the relative deviation might be slightly misleading and thus we notice that the absolute differences in D/N_a never exceed 3.1×10^{-3} in the whole range of data shown in Fig. 5.15 (c).

We conclude that FT-LDFT in combination with the scaling approximation (5.53) and a suitable reference system is able to account very accurately for the modifications in the electronic structure and the resulting changes in the equilibrium observables caused by variations in the electron density. Thus, the crossover from the regime around half band-filling, where the spin-charge separation dominates the strong-coupling physics, to the low-density regime, where low-lying charge excitations associated with the holonic motion lift the separation between spin and charge degrees of freedom, is accurately reproduced within FT-LDFT. Furthermore, the ability of the electrons to reduce double occupations more effectively in a correlated motion as their density decreases is very well reproduced, not only in one spatial dimension but also for lattice structures in 2D and 3D.

5.5 Spin-polarized systems

In order to investigate the physical properties of interacting electron systems in the presence of external magnetic fields, it is desirable to extend the scope of FT-LDFT

to the regime of spin-polarized electron densities. We will focus on the single-band Hubbard model in the presence of an external magnetic field $\boldsymbol{B} = B\,\hat{\boldsymbol{e}}_z$ which couples to the spins by means of a Zeeman term $\hat{H}_S = -\hat{\boldsymbol{\mu}}_S \cdot \boldsymbol{B} = g_e\mu_B B\hat{S}_z$, such that the energy of the system is described by the Hamiltonian

$$\hat{H} = -t \sum_{\langle i,j \rangle \sigma} \hat{c}^\dagger_{i\sigma}\hat{c}_{j\sigma} + \frac{1}{2}\,g_e\mu_B B \sum_i \left(\hat{n}_{i\uparrow} - \hat{n}_{i\downarrow}\right) + U \sum_i \hat{n}_{i\uparrow}\hat{n}_{i\downarrow}\,. \tag{5.57}$$

Here μ_B is the Bohr magneton and g_e the Landé factor for which it suffices to take $g_e \approx 2$ in the following. Since the inclusion of an external magnetic field only breaks the spin-rotational symmetry but not the rotational and translational symmetries in real space, it follows that the eq-SPDM of the system described by the Hamiltonian (5.57) still fulfills the symmetry (5.2). Thus, similar to Eq. (5.3), for a given chemical potential $\mu = (\mu_\uparrow + \mu_\downarrow)/2$ and magnetic field strength $B = (\mu_\downarrow - \mu_\uparrow)/2\mu_B$ we can write the grand-potential functional (3.53) of the Hubbard model (5.57) as

$$\Omega[\boldsymbol{\gamma}] = G[\boldsymbol{\gamma}] - N_a \left[tz\,\gamma_{12} + \mu\left(\gamma_{11\uparrow} + \gamma_{11\downarrow}\right) - \mu_B B\left(\gamma_{11\uparrow} - \gamma_{11\downarrow}\right)\right], \tag{5.58}$$

where N_a is the number of sites and z the coordination number of the lattice. Notice that, as long as only NN hoppings are taken into account (i. e., $t_{ij} = 0$ for i, j beyond NNs), the dependence of $\Omega[\boldsymbol{\gamma}]$ on all SPDM elements other than $\gamma_{11\uparrow}$, $\gamma_{11\downarrow}$ and γ_{12} appears only through the interaction and entropy functional $G[\boldsymbol{\gamma}]$. Therefore, we can absorb all other SPDM elements in the LL minimization procedure (3.52) and define the generalization of the reduced functional (5.4) to the case of spin-polarized electron densities:

$$G[\gamma_{11\uparrow}, \gamma_{11\downarrow}, \gamma_{12}] = \min_{\hat{\rho} \to \{\gamma_{11\uparrow}, \gamma_{11\downarrow}, \gamma_{12}\}} \mathrm{Tr}\left\{\hat{\rho}\left(U \sum_i \hat{n}_{i\uparrow}\hat{n}_{i\downarrow} + \frac{1}{\beta}\log\hat{\rho}\right)\right\}. \tag{5.59}$$

The usual notation $\hat{\rho} \to \{\gamma_{11\uparrow}, \gamma_{11\downarrow}, \gamma_{12}\}$ indicates that the minimization is performed within the set formed by the positive semidefinite density matrices $\hat{\rho} \in \mathcal{P}$ with unit trace, satisfying

$$\mathrm{Tr}\left\{\hat{\rho}\,\hat{c}^\dagger_{i\sigma}\hat{c}_{i\sigma}\right\} = \gamma_{11\sigma} \quad \text{for} \quad \sigma = \uparrow, \downarrow \quad \text{and} \quad i = 1, \dots, N_a \tag{5.60a}$$

and

$$\sum_\sigma \mathrm{Tr}\left\{\hat{\rho}\,\hat{c}^\dagger_{i\sigma}\hat{c}_{j\sigma}\right\} = \gamma_{12} \quad \forall i, j \in \text{NNs}\,. \tag{5.60b}$$

The reduced functional (5.59) has a universal character in the sense that it does not depend on the chemical potential μ, the external magnetic filed strength B, and the NN hopping integral t. Like its unpolarized counterpart (5.4) it depends on the underlying Fock-space, which is determined by the number of lattice sites N_a, on the

temperature T, the Coulomb-repulsion strength U, and on the topology of the lattice structure under consideration.

In the present case of a spin-dependent electron density we will proceed in a similar fashion as in the previously considered unpolarized case in order to derive a practical approximation to the reduced functional (5.59). Thus, we start by exploring the corresponding domain of definition and subsequently we derive the exact functional dependence $G_s[\gamma_{11\uparrow}, \gamma_{11\downarrow}, \gamma_{12}]$ for the important case of uncorrelated mixed-states. Finally, we will propose a scaling approximation for the remaining correlation contribution $G_c = G - G_s$.

5.5.1 Domain of ensemble representability

Building on the preliminary work done in Section 5.1.1, it is straight forward to identify the domain of definition of the reduced functional (5.59). This is the set of all tuples $(\gamma_{11\uparrow}, \gamma_{11\downarrow}, \gamma_{12})$ that can be associated with some density matrix $\hat{\rho} \in \mathcal{P}$ which satisfies Eq. (5.60). In the context of Eq. (5.8) we have already seen that $\gamma_{11\sigma}$ is bound to the interval $[0, 1]$, which is simply a consequence of Pauli's exclusion principle since $\gamma_{11\sigma} = N_\sigma/N_a$ represents the average spin-dependent occupation of the localized Wannier orbitals. Furthermore, adapting the argument which led to Eq. (5.14) to the case of a spin-polarized electron density, we readily obtain the upper and lower bounds on $\gamma_{12} = \sum_\sigma \gamma_{12\sigma}$ as

$$\gamma_{12}^{\max} = \frac{1}{z} \sum_\sigma \int_{\mu_\sigma^{\max}}^\infty \omega\,\rho(\omega)\,\mathrm{d}\omega \quad \text{and} \quad \gamma_{12}^{\min} = \frac{1}{z} \sum_\sigma \int_{-\infty}^{\mu_\sigma^{\min}} \omega\,\rho(\omega)\,\mathrm{d}\omega\,. \tag{5.61}$$

Here, $\rho(\omega)$ is the DOS of the tight-binding Hamiltonian (5.13), and $\mu_\sigma^{\max}$ and $\mu_\sigma^{\min}$ are associated with the spin-dependent electron density $\gamma_{11\sigma}$ by the condition

$$\gamma_{11\sigma} = \int_{\mu_\sigma^{\max}}^\infty \rho(\omega)\,\mathrm{d}\omega = \int_{-\infty}^{\mu_\sigma^{\min}} \rho(\omega)\,\mathrm{d}\omega\,. \tag{5.62}$$

Figure 5.16 shows the domain formed by the set of ensemble representable SPDM elements $\gamma_{11\uparrow}$, $\gamma_{11\downarrow}$, and γ_{12} for the case of bipartite lattice structures in 1–3 dimensions. The boundaries on γ_{12} have been determined from Eqs. (5.61) and (5.62) by varying the spin-dependent electron densities in the complete range of representable values $0 \leq \gamma_{11\sigma} \leq 1$ for $\sigma = \uparrow, \downarrow$. The resulting domains are convex and highly symmetric. The reflection symmetry with respect to the $\gamma_{12} = 0$ plane, i. e., $\gamma_{12}^{\min}(\gamma_{11\uparrow}, \gamma_{11\downarrow}) = -\gamma_{12}^{\max}(\gamma_{11\uparrow}, \gamma_{11\downarrow})$, observed for the bipartite lattice structures in Fig. 5.16, has already been discussed in Section 5.1.1. In the general case, which includes non-bipartite lattice structures, the upper and lower boundaries on γ_{12} are
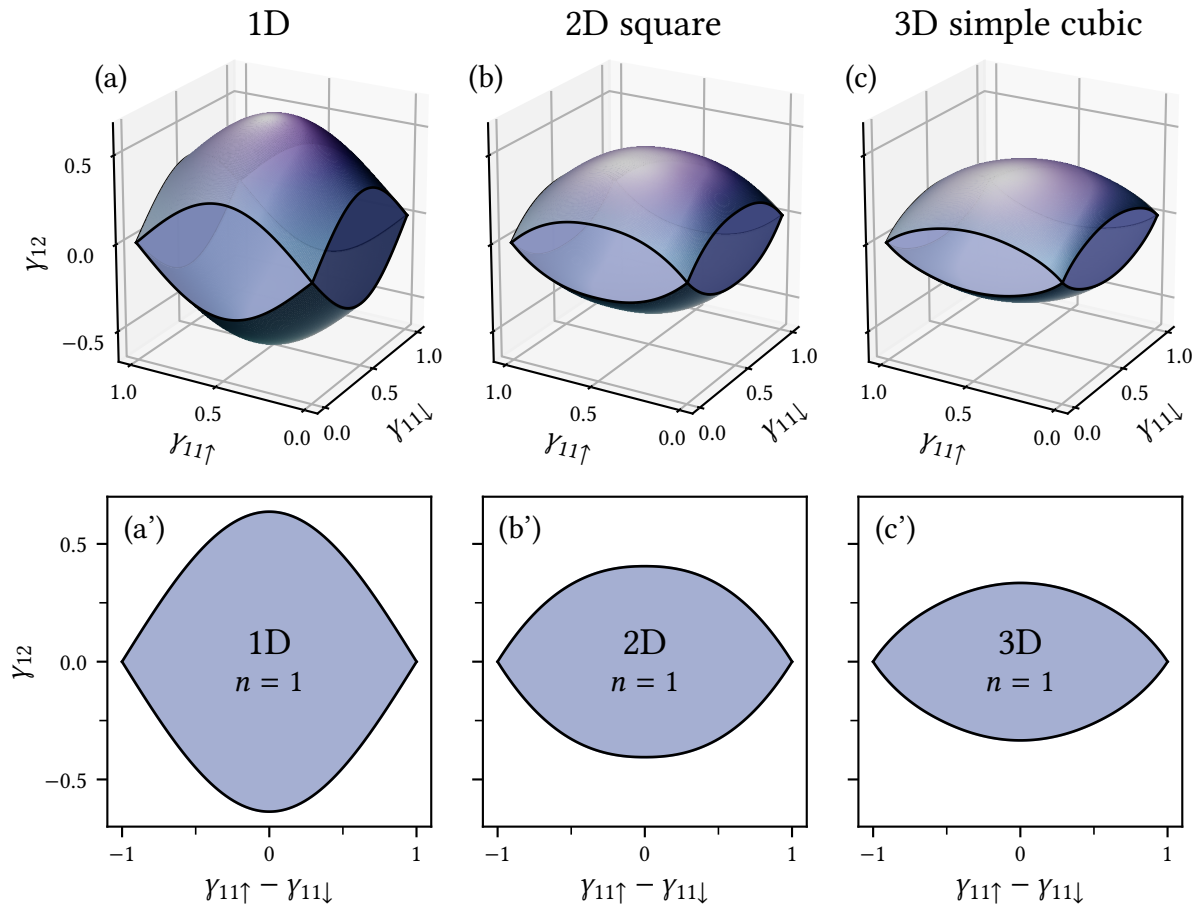
Figure 5.16: Domain formed by the set of ensemble representable SPDM elements $\gamma_{11\uparrow}$, $\gamma_{11\downarrow}$, and γ_{12} for the periodic (a) 1D chain, (b) 2D square lattice, and (c) 3D simple-cubic lattice. Subfigures in the bottom row, indicated by primed letters, show cuts through the corresponding domains at the top along the $n = \gamma_{11\uparrow} + \gamma_{11\downarrow} = 1$ plane, which corresponds to a half-filled band.

related by $\gamma_{12}^{\min}(\gamma_{11\uparrow}, \gamma_{11\downarrow}) = -\gamma_{12}^{\max}(1 - \gamma_{11\uparrow}, 1 - \gamma_{11\downarrow})$, which follows from the fact that the tight-binding Hamiltonian (5.13) changes sign upon the unitary electron-hole transformation $\hat{c}_i^\dagger \rightarrow \hat{c}_i$. A further prominent symmetry of the representability domains results from the fact that the upper and lower boundaries on γ_{12}, given by Eq. (5.61), are additive in the equivalent contributions of the up and down spins. Therefore, the upper and lower boundaries on γ_{12} are invariant upon interchange of the spin-dependent electron densities, i. e., $\gamma_{12}^{\max}(\gamma_{11\uparrow}, \gamma_{11\downarrow}) = \gamma_{12}^{\max}(\gamma_{11\downarrow}, \gamma_{11\uparrow})$ and $\gamma_{12}^{\min}(\gamma_{11\uparrow}, \gamma_{11\downarrow}) = \gamma_{12}^{\min}(\gamma_{11\downarrow}, \gamma_{11\uparrow})$.

In the following we will mainly focus on the important case of a half-filled band and thus, in Figs. 5.16 (a')–(c'), we present cuts through the corresponding domains along the $n = \gamma_{11\uparrow} + \gamma_{11\downarrow} = 1$ plane. The boundaries on γ_{12} within this plane have been determined from Eqs. (5.61) and (5.62) by varying the spin polarization $\gamma_{11\uparrow} - \gamma_{11\downarrow} = 2S_z/\hbar N_a$ in the complete range of representable values $-1 \leq \gamma_{11\uparrow} - \gamma_{11\downarrow} \leq 1$.

5.5.2 Functionals for uncorrelated mixed-states

Following the route we took in order to describe unpolarized systems in the framework of FT-LDFT, we would now like to consider the restriction of the functional (5.59) to the set $\mathcal{P}_s$ formed by the uncorrelated mixed-states (see Appendix B). This means, we consider the functional

$$G_s[\gamma_{11\uparrow}, \gamma_{11\downarrow}, \gamma_{12}] = \min_{\hat{\rho}_s \rightarrow \{\gamma_{11\uparrow}, \gamma_{11\downarrow}, \gamma_{12}\}} \text{Tr}\left\{\hat{\rho}_s \left(U \sum_i \hat{n}_{i\uparrow}\hat{n}_{i\downarrow} + \frac{1}{\beta} \log \hat{\rho}_s\right)\right\}, \qquad (5.63)$$

where $\hat{\rho}_s \rightarrow \{\gamma_{11\uparrow}, \gamma_{11\downarrow}, \gamma_{12}\}$ indicates the minimization with respect to all uncorrelated mixed-states $\hat{\rho}_s \in \mathcal{P}_s$ which satisfy the conditions (5.60). Since the interaction energy $W = U \sum_i \text{Tr}\{\hat{\rho}_s \, \hat{n}_{i\uparrow}\hat{n}_{i\downarrow}\}$ in any uncorrelated mixed-state which meets these requirements is given by (see Appendix B)

$$W_{\text{HF}}[\gamma_{11\uparrow}, \gamma_{11\downarrow}] = U N_a \gamma_{11\uparrow}\gamma_{11\downarrow}, \qquad (5.64)$$

it is sufficient to minimize the entropy contribution to G_s. This means we can write Eq. (5.63) as

$$G_s[\gamma_{11\uparrow}, \gamma_{11\downarrow}, \gamma_{12}] = W_{\text{HF}}[\gamma_{11\uparrow}, \gamma_{11\downarrow}] - T S_s[\gamma_{11\uparrow}, \gamma_{11\downarrow}, \gamma_{12}], \qquad (5.65)$$

where we have introduced the generalization of the reduced IFE-functional (5.19) to the case of spin-polarized electron densities

$$S_s[\gamma_{11\uparrow}, \gamma_{11\downarrow}, \gamma_{12}] = -k_\text{B} \min_{\hat{\rho} \rightarrow \{\gamma_{11\uparrow}, \gamma_{11\downarrow}, \gamma_{12}\}} \text{Tr}\{\hat{\rho} \log \hat{\rho}\}. \qquad (5.66)$$

Like in the previous unpolarized case, it is not necessary to restrict the minimization in Eq. (5.66) to the set $\mathcal{P}_s$, since the minimizing $\hat{\rho}$ always represents an uncorrelated

mixed-state. As usual, the minimization in Eq. (5.66) is carried out by seeking for the extremes of the corresponding Euler-Lagrange functional

$$\mathcal{L}[\hat{\rho}] = \text{Tr}\{\hat{\rho}\log\hat{\rho}\} + \lambda \sum_{\langle i,j\rangle}\left(\text{Tr}\Big\{\hat{\rho}\sum_{\sigma}\hat{c}_{i\sigma}^{\dagger}\hat{c}_{j\sigma}\Big\} - \gamma_{12}\right) - \sum_{i\sigma}\nu_{\sigma}\left(\text{Tr}\{\hat{\rho}\,\hat{n}_{i\sigma}\} - \gamma_{11\sigma}\right)$$

$$= \text{Tr}\left\{\hat{\rho}\left(\lambda\sum_{\langle i,j\rangle\sigma}\hat{c}_{i\sigma}^{\dagger}\hat{c}_{j\sigma} + \log\hat{\rho} - \sum_{\sigma}\nu_{\sigma}\,\hat{N}_{\sigma}\right)\right\} - N_a\left(\lambda z\,\gamma_{12} - \sum_{\sigma}\nu_{\sigma}\gamma_{11\sigma}\right), \quad (5.67)$$

where $\hat{N}_{\sigma} = \sum_i \hat{n}_{i\sigma}$ and the Lagrange multipliers λ and ν_{σ} enforce that the minimizing $\hat{\rho}$ satisfies the conditions (5.60). Following a similar argument which led from Eq. (5.20) to Eq. (5.25), we obtain the reduced IFE-functional (5.66) as

$$S_s[\gamma_{11\uparrow}, \gamma_{11\downarrow}, \gamma_{12}] = -k_{\text{B}}N_a \sum_{\sigma}\int_{-\infty}^{\infty}\Big[\eta_{\sigma}(\omega)\log\big(\eta_{\sigma}(\omega)\big)$$

$$+ \big(1 - \eta_{\sigma}(\omega)\big)\log\big(1 - \eta_{\sigma}(\omega)\big)\Big]\rho(\omega)\,\text{d}\omega, \quad (5.68)$$

where $\rho(\omega)$ is the tight-binding DOS (5.11) and

$$\eta_{\sigma}(\omega) = \frac{1}{1 + e^{\beta_s(\omega - \mu_{s\sigma})}} \quad (5.69)$$

the spin-dependent occupation number of the Bloch state with energy ω at the effective temperature $\beta_s = \lambda$ and the effective chemical potential $\mu_{s\sigma} = \nu_{\sigma}/\lambda$.

In Fig. 5.17 we focus on the case of a half-filled band ($n = \gamma_{11\uparrow} + \gamma_{11\downarrow} = 1$) and present results for the reduced IFE-functional (5.68) on periodic lattice structures in 1–3 dimensions. Since we focus on a fixed electron density, we can express the IFE-functional in terms of the spin polarization $\gamma_{11\uparrow} - \gamma_{11\downarrow} = 2S_z/\hbar N_a$ and the degree of NN charge fluctuations γ_{12}. Furthermore, for the bipartite lattice structures under consideration it is sufficient to focus on the partial domain $\gamma_{12} \geq 0$ and $\gamma_{11\uparrow} \geq \gamma_{11\downarrow}$. The reflection symmetry of S_s with respect to $\gamma_{12} = 0$ has already been discussed in Section 5.1.2. The invariance upon interchange of the spin-dependent electron densities, i.e., $S_s[\gamma_{11\uparrow}, \gamma_{11\downarrow}, \gamma_{12}] = S_s[\gamma_{11\downarrow}, \gamma_{11\uparrow}, \gamma_{12}]$, is evident from the fact that the additive contributions of the up and down spins to the IFE-functional (5.68) are equivalent. The functional dependence of the IFE-functionals shown in Fig. 5.17 is deeply related to the previously considered case of unpolarized electron densities (see Fig. 5.2). Thus, S_s vanishes on the complete delocalized boundary ($\gamma_{12} = \gamma_{12}^{\text{max}}$), since this limit is attained when the Bloch-states with the highest effective energies ω are occupied [$\eta_{\sigma}(\omega) = 1$] while all other Bloch-states are unoccupied [$\eta_{\sigma}(\omega) = 0$]. Starting from the delocalized boundary, the IFE increases monotonously as γ_{12} decreases, until the localized
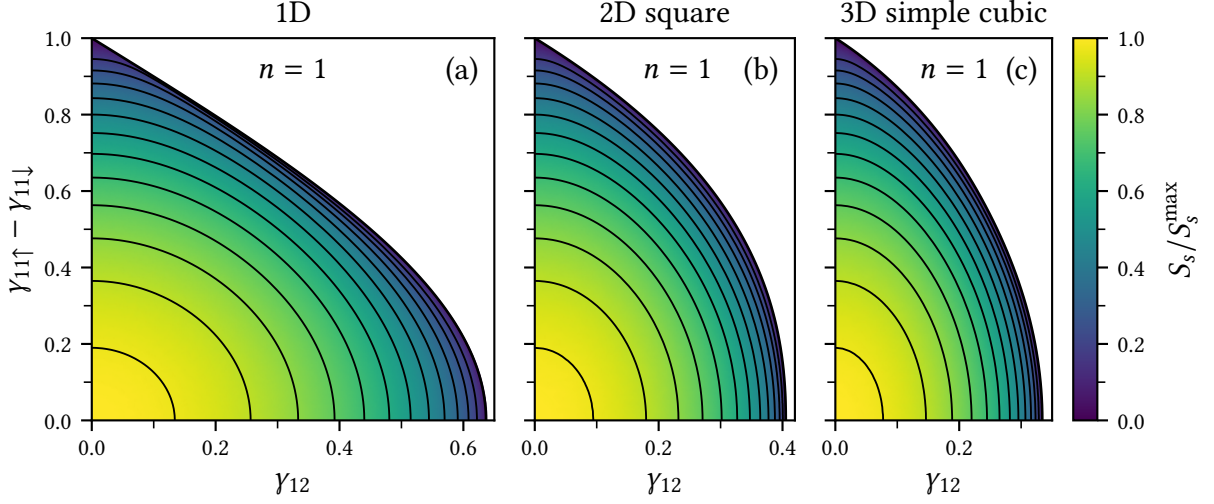
Figure 5.17: Reduced IFE-functional $S_s[\gamma_{11\uparrow}, \gamma_{11\downarrow}, \gamma_{12}]$ for the case of a half-filled band ($n = \gamma_{11\uparrow} + \gamma_{11\downarrow} = 1$) and different bipartite lattice structures. Color contour-plots are shown for the periodic (a) one-dimensional chain, (b) square lattice, and (c) simple cubic lattice. The color scale for S_s is indicated on the right, where $S_s^{\max} = k_B N_a \log 4$ refers to the structure-independent global maximum of S_s, which is attained in the localized limit $\gamma_{12} = 0$ with vanishing spin polarization $\gamma_{11\uparrow} = \gamma_{11\downarrow} = 1/2$. Contour lines are drawn at equidistant values of S_s in order to display its functional dependence more clearly.

limit $\gamma_{12} = 0$ is reached, where S_s assumes its maximum for any given spin-dependent electron density $\gamma_{11\sigma}$. The localized limit $\gamma_{12} = 0$ corresponds to homogeneous occupations $\eta_\sigma(\omega) = \gamma_{11\sigma}$ across the complete Bloch-state spectrum, such that the corresponding structure-independent maximal value of the IFE (5.68) is given by

$$S_s^{\max}(\gamma_{11\uparrow}, \gamma_{11\downarrow}) = -k_B N_a \sum_\sigma \left[\gamma_{11\sigma} \log \gamma_{11\sigma} + (1 - \gamma_{11\sigma}) \log(1 - \gamma_{11\sigma}) \right]. \qquad (5.70)$$

5.5.3 Scaling approximation for correlation effects

Having derived the exact functional dependence $G_s[\gamma_{11\uparrow}, \gamma_{11\downarrow}, \gamma_{12}]$, which represents the interaction-energy and entropy contribution to the free energy of independent Fermions, it remains to account for the contributions resulting from the electronic correlations. We follow the approach taken in Section 5.2 and begin by carrying out the minimization procedure (5.59) in an explicit manner. To this aim we seek for the

extremes of the corresponding Euler-Lagrange functional

$$\mathcal{L}[\hat{\rho}] = \text{Tr}\left\{\hat{\rho}\left(U\sum_i \hat{n}_{i\uparrow}\hat{n}_{i\downarrow} + \frac{1}{\beta}\log\hat{\rho}\right)\right\} + \lambda\sum_{\langle i,j\rangle}\left(\text{Tr}\left\{\hat{\rho}\sum_\sigma \hat{c}^\dagger_{i\sigma}\hat{c}_{j\sigma}\right\} - \gamma_{12}\right)$$

$$- \sum_{i\sigma}\mu_\sigma\left(\text{Tr}\{\hat{\rho}\,\hat{n}_{i\sigma}\} - \gamma_{11\sigma}\right) \tag{5.71}$$

$$= \text{Tr}\left\{\hat{\rho}\left(\hat{H}_{\text{aux}} + \frac{1}{\beta}\log\hat{\rho} - \sum_\sigma\mu_\sigma\hat{N}_\sigma\right)\right\} - N_a\left(\lambda z\,\gamma_{12} - \sum_\sigma\mu_\sigma\gamma_{11\sigma}\right),$$

where $\hat{H}_{\text{aux}}$ is the auxiliary Hamiltonian (5.30) and the Lagrange multipliers λ and μ_σ have been introduced in order to enforce that the minimizing $\hat{\rho}$ satisfies the conditions (5.60). Apart from an irrelevant additive constant, the functional (5.71) is of the Gibbs form (3.43) and thus, the minimum among the set $\mathcal{P}$ of all positive semidefinite density matrices $\hat{\rho}$ with unit trace is taken for the grand-canonical density matrix of the auxiliary Hamiltonian $\hat{H}_{\text{aux}}$, i. e., for

$$\hat{\rho}_0 = \frac{e^{-\beta(\hat{H}_{\text{aux}}-\sum_\sigma\mu_\sigma\hat{N}_\sigma)}}{\text{Tr}\left\{e^{-\beta(\hat{H}_{\text{aux}}-\sum_\sigma\mu_\sigma\hat{N}_\sigma)}\right\}}\,. \tag{5.72}$$

The functional dependence of $G[\gamma_{11\uparrow},\gamma_{11\downarrow},\gamma_{12}]$ can thus be obtained from the solution of the finite-temperature problem with the auxiliary Hamiltonian (5.30), which has the same level of complexity as the initial problem defined by the Hubbard-model Hamiltonian (5.57). Like in the previously considered case of unpolarized electron densities, we conclude that the range of applications of the thus described method is limited to systems which can be solved by either analytical or numerical methods. Nevertheless, it provides us with a practical means to access the exact functional dependence $G[\gamma_{11\uparrow},\gamma_{11\downarrow},\gamma_{12}]$ for a number of relevant systems.

In Fig. 5.18 we focus on the infinite one-dimensional Hubbard chain with a half-filled band ($n=1$) and show results for the nontrivial correlation functional

$$G_c[\gamma_{11\uparrow},\gamma_{11\downarrow},\gamma_{12}] = G[\gamma_{11\uparrow},\gamma_{11\downarrow},\gamma_{12}] - G_s[\gamma_{11\uparrow},\gamma_{11\downarrow},\gamma_{12}]\,. \tag{5.73}$$

The results shown account for different ratios $U/k_\text{B}T$ between the Coulomb-repulsion strength U and the temperature T and were obtained from the exact finite-temperature solution of Jüttner, Klümper, and Suzuki [56]. The infinite chain with NN hopping is bipartite, and thus we have $G_c[\gamma_{11\uparrow},\gamma_{11\downarrow},\gamma_{12}] = G_c[\gamma_{11\uparrow},\gamma_{11\downarrow},-\gamma_{12}]$. Furthermore, from the fact that the auxiliary Hamiltonian (5.30) is invariant with respect to spin flips ($\hat{c}^\dagger_{i\sigma} \to \hat{c}^\dagger_{i,-\sigma}$) we conclude that $G_c[\gamma_{11\uparrow},\gamma_{11\downarrow},\gamma_{12}] = G_c[\gamma_{11\downarrow},\gamma_{11\uparrow},\gamma_{12}]$ must hold in general. Thus, in Fig. 5.18 it is sufficient to focus on the sector having $\gamma_{12} \geq 0$ and $\gamma_{11\uparrow} \geq \gamma_{11\downarrow}$.

Figure 5.18: Correlation contribution $G_c[\gamma_{11\uparrow}, \gamma_{11\downarrow}, \gamma_{12}]$ to the free-energy functional of the infinite spin-polarized Hubbard chain at half band-filling ($n = \gamma_{11\uparrow} + \gamma_{11\downarrow} = 1$). Subfigures in the right column [(a')–(c')] show the functional dependence of G_c for different ratios $U/k_B T$ between the Coulomb-repulsion strength U and the temperature T in the sector having $\gamma_{12} \geq 0$ and $\gamma_{11\uparrow} \geq \gamma_{11\downarrow}$. Subfigures in the left column [(a)–(c)] correspond to the same values of $U/k_B T$ as their counterparts on the right, and show the functional dependence of G_c along cuts with fixed spin polarizations $s_z = \hbar (\gamma_{11\uparrow} - \gamma_{11\downarrow})/2$. The correlation functionals along the cuts with fixed s_z have been scaled to a common range by using the upper bound $\gamma_{12}^0(s_z)$ on the degree of NN charge fluctuations, as well as the correlation contribution $G_c^\infty(s_z)$ to the free energy in the localized limit $\gamma_{12} = 0$.

For a given spin polarization $s_z = S_z/N_a = \hbar\,(\gamma_{11\uparrow} - \gamma_{11\downarrow})/2$ we observe in Fig. 5.18 a qualitatively similar dependence of G_c on the degree of NN charge fluctuations γ_{12} as in the previously considered unpolarized case (see Fig. 5.3). Thus, starting from the localized limit $\gamma_{12} = 0$, where G_c assumes its minimum $G_c = G_c^\infty(s_z)$ for any given spin polarization s_z, we find G_c monotonously increasing with γ_{12}, until $G_c = 0$ is reached on the complete delocalized boundary $\gamma_{12} = \gamma_{12}^0(s_z)$.[3] Here

$$\gamma_{12}^0(s_z) = \frac{2}{\pi}\cos(\pi s_z/\hbar) \tag{5.74}$$

refers to the upper bound on the NN charge fluctuations in the half-filled 1D Hubbard-chain. Regarding the dependence of the correlation contribution to the free energy on the spin polarization s_z, we find that $|G_c|$ decreases with increasing values of $|s_z|$, since the correlated electronic motion is gradually suppressed as the system polarizes. Thus, the global minimum of G_c is attained in the localized limit $\gamma_{12} = 0$ with vanishing spin polarization ($\gamma_{11\uparrow} = \gamma_{11\downarrow} = 1/2$), and it is given by (see Section 5.2.1)

$$\frac{G_c^\infty(0)}{N_a} = \frac{U}{4} - \frac{1}{\beta}\log\!\left(\frac{1 + e^{\beta U/2}}{2}\right). \tag{5.75}$$

Therefore, the correlation contribution to the free energy is bound by $G_c^\infty(0) \le G_c \le 0$, and since the lower boundary $G_c^\infty(0)/U$ is a strictly decreasing function of βU, we conclude that $|G_c|/U$ increases with the ratio $U/k_\mathrm{B}T$. Clearly, this is simply a consequence of the fact that correlation effects are most pronounced in the regime of strong Coulomb repulsions and low temperatures, as already observed in the context of unpolarized spin densities in Section 5.2.
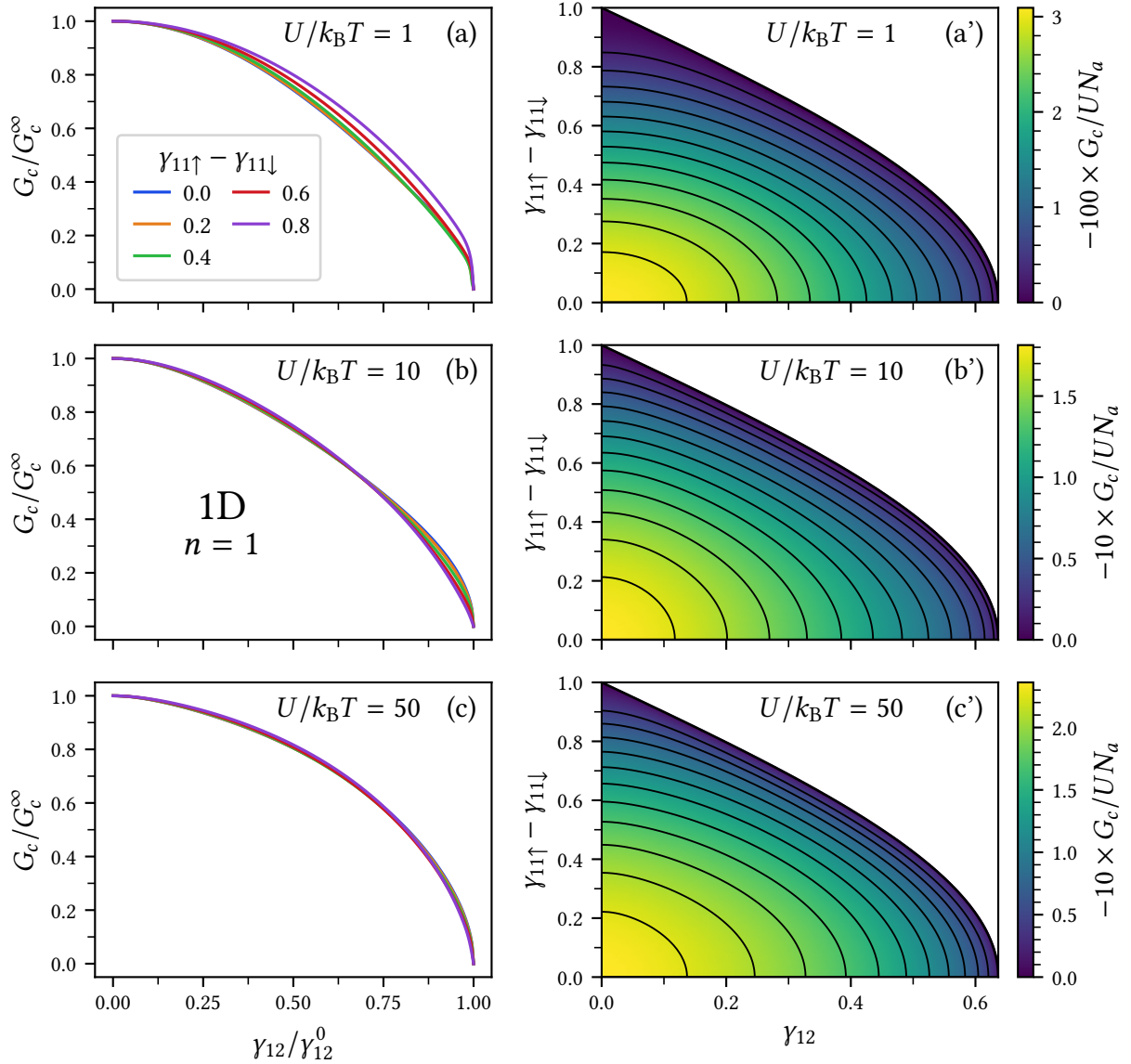
In order to approximate the functional dependence of the correlation contribution $G_c[\gamma_{11\uparrow}, \gamma_{11\downarrow}, \gamma_{12}]$ to the free energy of the half-filled Hubbard model, we aim to extend the scaling approach (5.33) to the regime of spin-polarized electron densities. The most naive generalization would be to focus on a fixed spin polarization $s_z = \hbar\,(\gamma_{11\uparrow} - \gamma_{11\downarrow})/2$, and to extract the dependence of G_c on the degree of NN charge fluctuations γ_{12} from the properly scaled functional of a suitable reference system having the same s_z. However, for the applications we have in mind, involving dynamic variations of the magnetization due to changes in the external magnetic field strength and the temperature, this approach turns out the be inappropriate if small finite reference systems are used, as discussed in more detail in Appendix G. In order to develop a more suitable generalization of the scaling idea, let us now focus on Figs. 5.18 (a)–(c), where the functional dependence of the correlation contribution G_c to the free energy of the infinite half-filled Hubbard chain is shown along cuts through

---

[3]See Sections 5.2.1 and 5.2.2 for a detailed discussion of the correlation effects in the localized and delocalized limits.

the domain which correspond to fixed spin polarizations s_z. When scaled to a common domain and range, using the upper bound $\gamma_{12}^0(s_z)$ on the degree of NN charge fluctuations, given in Eq. (5.74), as well as the correlation contribution $G_c^\infty(s_z)$ in the localized limit $\gamma_{12} = 0$ (see Section 5.2.1), the functional dependence of G_c reveals a remarkable quasi-universal behaviour, which is approximately independent of the spin polarization s_z. This is especially true in the regime of strong Coulomb-repulsions or low temperatures $U \gg k_\mathrm{B}T$, where correlation effects play a crucial role. This quasi-universal behaviour of G_c upon proper scaling suggests that its dependence on the spin polarization is to a great extent concealed in $\gamma_{12}^0(s_z)$ and $G_c^\infty(s_z)$, at least in the present case of the infinite half-filled Hubbard chain. We conclude that the dependence of G_c on γ_{12} could be well approximated for any $-\hbar/2 \le s_z \le \hbar/2$, if it would be known for *some* fixed value of s_z. Building upon the success of the scaling approximation (5.33) to account for the unpolarized case, it is thus most reasonable to focus on $s_z = 0$, and to infer the qualitative dependence of G_c on the degree of NN charge fluctuations γ_{12} from an unpolarized reference system. The only modification of the scaling approximation (5.33) is then to account for the s_z-dependence of the scaling parameters of the infinite target system, i. e., $\gamma_{12}^0 = \gamma_{12}^0(s_z)$, $G_c^\infty = G_c^\infty(s_z)$ and $G_c^0 = 0$. We thus arrive at the following generalization of the scaling approximation (5.33) to the infinite spin-polarized Hubbard model at half band-filling:

$$G_c[s_z, \gamma_{12}] = G_c^\infty(s_z) \frac{G_c^{\mathrm{rf},0} - G_c^{\mathrm{rf}}[\gamma_{12}^{\mathrm{rf}}]}{G_c^{\mathrm{rf},0} - G_c^{\mathrm{rf},\infty}} \quad \text{with} \quad \gamma_{12}^{\mathrm{rf}} = \gamma_{12}^{\mathrm{rf},0} \frac{\gamma_{12}}{\gamma_{12}^0(s_z)} . \tag{5.76}$$

Here the upper index "rf" on G_c and γ_{12} refers to the exactly solvable, half-filled, and unpolarized ($s_z^{\mathrm{rf}} = 0$) reference system. Furthermore, we consider the reference system at the temperature T and the Coulomb-repulsion strength U specified by the target system, in order to be compliant with the principles of FT-LDFT.

5.5.4 Application to the infinite Hubbard chain

Having introduced the scaling approximation for spin-polarized systems (5.76), we are now in a position to apply our method in order to explore the equilibrium properties of the infinite Hubbard chain in the framework of FT-LDFT. To this aim we focus on the half-filled band case ($\gamma_{11\uparrow} + \gamma_{11\downarrow} = 1$), and for given NN hopping integral t, Coulomb-repulsion strength U, temperature T, and magnetic field strength B we minimize the free-energy functional

$$F[s_z, \gamma_{12}] = -tN_a z\, \gamma_{12} + 2N_a\mu_\mathrm{B}B\, \frac{s_z}{\hbar} + G_s[s_z, \gamma_{12}] + G_c[s_z, \gamma_{12}] \tag{5.77}$$

in the domain of ensemble-representable spin polarizations $-\hbar/2 \le s_z \le \hbar/2$ and NN charge fluctuations γ_{12}. As usual, $G_s[s_z, \gamma_{12}]$ stands for the interaction-energy and

entropy functional for uncorrelated mixed-states, given by Eq. (5.63), and $G_c[s_z, \gamma_{12}]$ for the correlation contribution to the free-energy functional obtained from the scaling approximation (5.76) using an appropriate reference system. We treat the unpolarized reference system in a grand-canonical ensemble formulation at the temperature T and Coulomb-repulsion strength U defined by the infinite chain and chose the chemical potential μ_{rf} of the reference system such that a half-filled band is obtained. The minimization of the functional (5.77) directly yields the free energy F, the spin polarization s_z, and the degree of NN charge fluctuations γ_{12} and thus the kinetic energy $K = -tN_a z \, \gamma_{12}$ in thermodynamic equilibrium. Additional equilibrium observables, such as the average number of double occupations D, the entropy S, the specific heat C_V, and the magnetic susceptibility χ can be subsequently obtained from appropriate derivatives of the free energy F.

In Fig. 5.19 we present results for several equilibrium properties of the infinite half-filled Hubbard chain with strong Coulomb repulsion $U/t = 8$ in the presence of an external magnetic field B. The results shown were obtained from FT-LDFT in combination with the scaling approximation (5.76) for the correlation contribution $G_c[s_z, \gamma_{12}]$ to the free energy, using a 7-site ring as reference system. In order to assess the accuracy of the equilibrium properties obtained in the framework of FT-LDFT, we compare them with the exact finite-temperature solution of the infinite 1D Hubbard chain [56].

Let us begin our discussion by considering in Fig. 5.19 (c) the dependence of the magnetization $M = -2\mu_B S_z/\hbar$ on the temperature T and the magnetic field strength B. In the present case of a strong Coulomb repulsion $U/t = 8$, the low-lying spin excitations in the Hubbard model are described by an effective Heisenberg model (2.52) with NN exchange-coupling constant $J = 2t^2/U$. Thus, we expect to find the gradual crossover from the AFM ground state in the absence of an external magnetic field ($B = 0$) to the fully polarized FM ground state at field strengths of the order $\mu_B B \simeq J = t/4$. In fact, for rather weak[4] magnetic fields ($0.2t \leq \mu_B B \leq 0.4t$) we find a partially polarized ground state, while for stronger fields the ground state is fully polarized. The magnetization decreases as low-spin states are thermally excited with increasing temperature, and for sufficiently high temperatures we discover the typical Curie-law $M = C\,B/T$ of a paramagnet with Curie-constant $C \approx \mu_B^2/(2k_B)$ [131]. In fact, for $\mu_B B \geq t/2$, where the ground state of the Hubbard chain is fully polarized, the magnetization curves can be roughly approximated by the well-known relation $M/N = \mu_B \tanh(\mu B/k_B T)$ for N noninteracting spin-1/2 particles with magnetic

---

[4]Notice that the NN hopping integral t in transition metals is typically of the order 0.1–0.5 eV, such that comparable magnetic field strengths $B \sim t/\mu_B = 2000$–9000 T are actually very large for typical experimental setups. However, here and in the following we relate the magnetic field strength $\mu_B B$ to the energy scales specified by the model under consideration, such as the bandwidth $w = 4t$, the Coulomb-repulsion strength U, or the effective exchange-coupling constant $J = 2t^2/U$ which is relevant in the strongly-interacting Heisenberg limit.
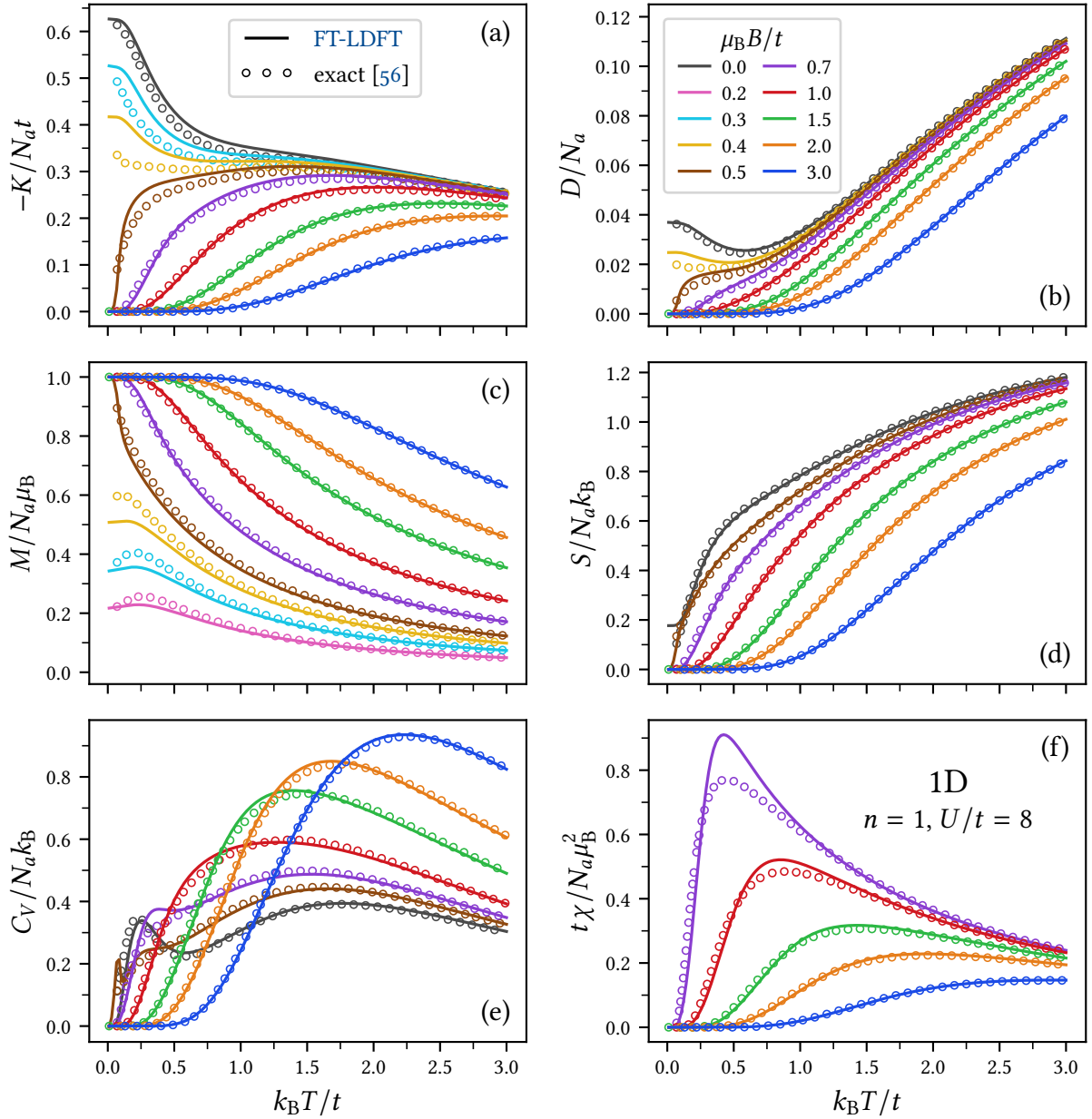
Figure 5.19: Equilibrium properties of the half-filled infinite 1D Hubbard chain as functions of the temperature T for the case of strong Coulomb repulsion $U/t = 8$ and representative values of the external magnetic field strength B. Results obtained by FT-LDFT in combination with the scaling approximation (5.76) using a 7-site ring as reference system (full curves) are compared with the exact solution of Jüttner *et al.* [56] (open circles): (a) kinetic energy K, (b) average number of double occupations D, (c) magnetization $M = -2\mu_B S_z/\hbar$, (d) entropy S, (e) specific heat C_V, and (f) magnetic susceptibility $\chi = \partial M/\partial B$.

moment $\mu = \mu_B/\sqrt{2}$, which is chosen such that the corresponding Curie-constant $C = \mu^2/k_B = \mu_B^2/(2k_B)$ matches the one of the Hubbard chain. The results obtained in the framework of FT-LDFT correctly predict the transition to a fully polarized ground state at $\mu_B B \approx t/2$ and exactly reproduce the high-temperature Curie-law. The magnetization curves obtained within the framework of FT-LDFT show an overall very good quantitative agreement with the corresponding exact analytical results in the complete range of parameters explored. Only in the low-temperature regime ($k_B T \lesssim 0.5t$) with rather weak fields ($\mu_B B \leq 0.4t$) some noticeable deviations are observed. For example, at $\mu_B B = 0.4t$ FT-LDFT underestimates the ground-state magnetization by about 15%. For intermediate and strong fields the FT-LDFT results are in excellent agreement with the exact analytical solution. In fact, for $\mu_B B \geq 0.5t$ the relative error in M is in average as low as 1% and never exceeds 6% within this range.

Concerning the influence of external magnetic fields on the kinetic energy K, shown in Fig. 5.19 (a), we observe that charge fluctuations are gradually suppressed as the magnetic field strength increases. This is a simple consequence of Pauli's exclusion principle, since the spins tend to align in a FM pattern as the external field strength increases, and hopping processes are prohibited if NN sites are occupied by parallel spins. In the extreme case of a fully-polarized state, as found in the ground state for $\mu_B B \geq t/2$, the kinetic energy vanishes completely since the band is half filled. However, at temperatures of the order $k_B T \approx \mu_B B$ low-spin states are thermally excited, opening up the way for NN hopping processes, which give rise to a rapid increase of $|K|$ for intermediate magnetic field strengths ($t/2 \lesssim \mu_B B \lesssim t$). The comparison with the exact analytical solution demonstrates that FT-LDFT is able to reproduce the thus described effects of external magnetic fields on the kinetic energy of the lattice electrons very accurately. However, in the range of rather low temperatures ($k_B T \lesssim t$) and weak to intermediate fields ($\mu_B B \leq t/2$), where the transition from the AFM to the FM ground-state occurs, we find some noticeable deviations between the exact and FT-LDFT results. For example, at $\mu_B B = 0.4$ FT-LDFT overestimates the binding energy $|K|$ in the ground state by about 24%. Nevertheless, for intermediate to strong fields, the agreement between the exact and FT-LDFT results is excellent in the whole range of temperatures considered, such that the error in the kinetic energy per lattice site is in average as low as $2.8t \times 10^{-3}$ for $\mu_B B \geq 0.7t$ and never exceeds $1.5t \times 10^{-2}$ within this range, which is just about 0.4% of the bandwidth $w = 4t$.

Let us now focus on the average number of double occupations D, shown in Fig. 5.19 (b). Starting from the B-independent high-temperature limit $D = N_a/4$, we find a decrease of the doublons upon cooling which is more rapid if strong magnetic fields are applied, since strong fields stabilize a FM alignment of the spins and thus lead to a rapid suppression of D. The typical increase in D upon further cooling in the low-temperature regime ($k_B T \lesssim t/2$), signalling the onset of an AFM configuration if

no magnetic field is applied, is gradually suppressed as the magnetic field strength increases, and for $\mu_B B \geq t/2$ a fully polarized ground state with $D = 0$ is formed. These modifications in the temperature dependence of the doublons, caused by the external magnetic field, are very well reproduced within the framework of FT-LDFT. In fact, the error in the double occupations per lattice site is in average as low as 4.3×10^{-4} and never exceeds 5.6×10^{-3} in the whole range of data shown in Fig. 5.19 (b).

Concerning the influence of external magnetic fields on the temperature dependence of the entropy S, shown in Fig. 5.19 (d), we find the rapid entropy-increase in the low-temperature regime ($k_B T \lesssim t$) gradually suppressed as the magnetic field strength increases. Clearly, for intermediate to strong fields ($\mu_B B \geq t/2$), the spin excitations from the FM ground state and the charge excitations across the Hubbard gap are suppressed until temperatures of the order $k_B T \sim \mu_B B$ are reached. In contrast to the unpolarized case ($B = 0$), where degeneracies in the ground state of the reference system prevent FT-LDFT from reproducing the linear increase of S in the regime of very low temperatures ($k_B T \lesssim 0.2t$), as already discussed in the context of Fig. 5.5, we find that FT-LDFT reproduces the entropy of the infinite Hubbard chain in the presence of intermediate to strong magnetic fields very well also in the low-temperature regime. In fact, for $\mu_B B \geq t/2$ we find errors in the entropy per lattice site (measured in units of k_B) which are in average as low as 3×10^{-3} and never exceed 3×10^{-2} in the complete temperature range shown in Fig. 5.19 (d).

Also the temperature dependence of the specific heat C_V, shown in Fig. 5.19 (e), displays very interesting modifications in the presence of external magnetic fields. If no field is applied ($B = 0$), the specific heat exhibits the typical two-peak structure, where the low-temperature peak at $k_B T \approx 0.23t$ corresponds to the excitation of spin waves from the AFM ground-state, while the peak at higher temperatures ($k_B T \approx 1.75t$) corresponds to charge excitations across the Hubbard gap. As the magnetic field strength increases above values of the order $\mu_B B \sim 2t^2/U = t/4$, an antiferromagnetic alignment of the spins becomes energetically unfavorable and the crossover to a FM ground-state occurs. For intermediate field strengths ($0.5t \lesssim \mu_B B \lesssim 0.7t$) we still observe a low-temperature structure in the specific heat, which is caused by low-lying spin excitations from the FM ground-state. As the field strength exceeds values of $\mu_B B \approx t = U/8$, the low-temperature structure in C_V is suppressed and a single broad peak is formed. Upon further increase of the external magnetic field strength the broad peak in C_V is shifted to higher temperatures, since spin and charge excitations remain suppressed until temperatures of the order $k_B T \sim \mu_B B$ are reached. All of the thus described modifications in the temperature dependence of C_V, caused by variations in the magnetic field strength, are very well reproduced within the framework of FT-LDFT. Only in the low-temperature regime ($k_B T \lesssim 0.7t$) with intermediate fields ($0.5t \leq \mu_B B \leq 0.7t$) we find noticeable deviations from the exact results of up to 20%. For higher temperatures ($k_B T > 0.7t$), the relative error in the specific heat
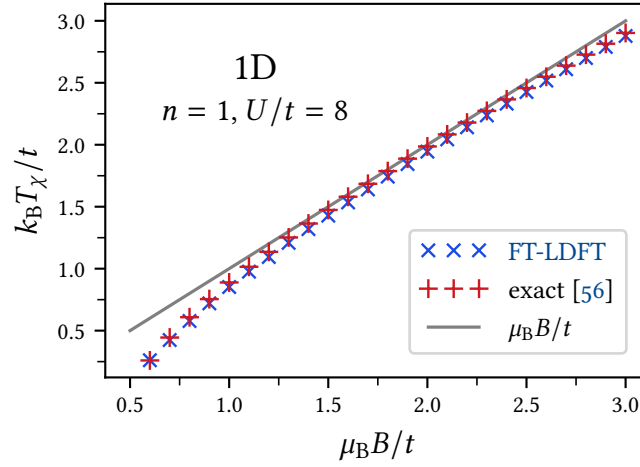
Figure 5.20: Temperature T_χ at which the peak in the magnetic susceptibility of the half-filled Hubbard chain with $U/t = 8$ occurs as a function of the magnetic field strength B. Results obtained by FT-LDFT in combination with the scaling approximation (5.76) using a 7-site ring as reference system are indicated by blue crosses, while red plus symbols correspond to the exact solution of Jüttner *et al.* [56]. The gray solid line marks the asymptotic behavior $k_B T_\chi = \mu_B B$ expected for strong magnetic fields.

obtained from FT-LDFT is in average as low as 1.4% and never exceeds 7% within this range of temperatures for all values of the magnetic field strength.

The temperature dependence of the magnetic susceptibility $\chi = \partial M/\partial B$ of the half-filled Hubbard chain with $U/t = 8$, shown in Fig. 5.19 (f), is very similar to the one of the spin-1/2 Heisenberg chain if intermediate to strong fields ($\mu_B B \geq 0.7t$) are applied [120]. Thus, starting from $T = 0$, where χ vanishes since the ground state is already fully polarized, we find the magnetic susceptibility increasing with the temperature until a pronounced peak at $k_B T_\chi \simeq \mu_B B$ is formed. The temperature T_χ where the peak in χ occurs roughly marks the transition from the fully polarized regime at low temperatures to the Curie-law decay of the magnetization in the high-temperature range. In Fig. 5.20 we show the dependence of the temperature T_χ on the external magnetic field strength, and for sufficiently large values of B the expected behavior $k_B T_\chi = \mu_B B$ is observed. The comparison with the temperature T_χ derived from the exact analytical solution demonstrates that the position of the peak in χ is very well reproduced within the framework of FT-LDFT and the relative error in T_χ is less than 5% in the whole range of parameters explored in Fig. 5.20. However, for intermediate values of the magnetic field strength ($\mu_B B = 0.7t$) FT-LDFT overestimates the peak in χ by about 18%, as seen in Fig. 5.19 (f). Nevertheless, as the temperature increases beyond T_χ, the magnetic susceptibility obtained in the framework of FT-LDFT
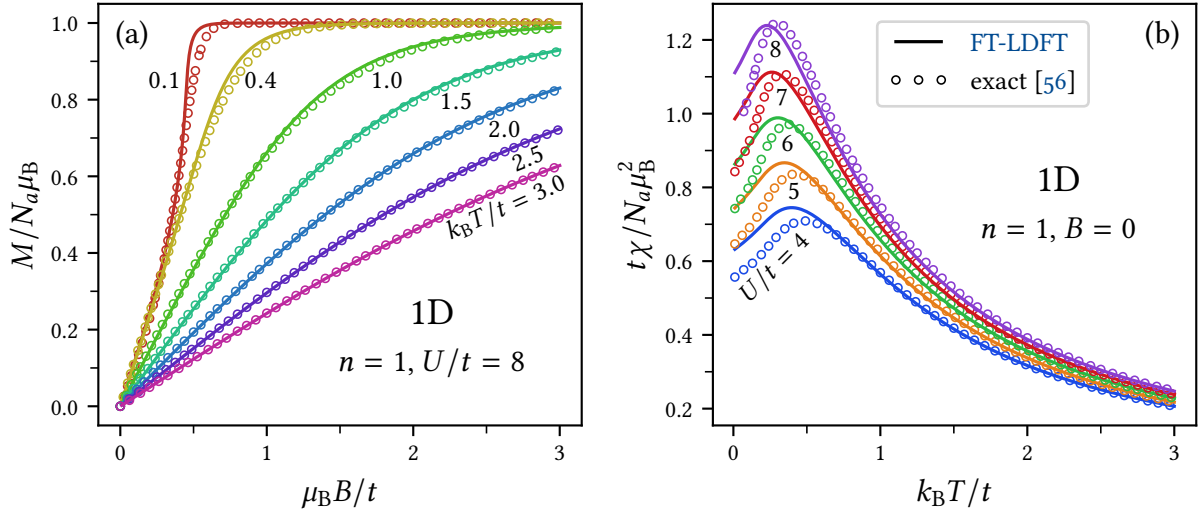
Figure 5.21: (a) Magnetization curve of the infinite half-filled Hubbard chain with $U/t = 8$ for representative values of the temperature T. (b) Zero-field magnetic susceptibility of the half-filled infinite Hubbard chain for representative values of the Coulomb-repulsion strength U/t. The solid lines in both figures mark results obtained by FT-LDFT in combination with the scaling approximation (5.76) using a 6-site ring as reference system, while the exact analytical solution of Jüttner *et al.* [56] is indicated by open circles.

approaches the exact result, and for $k_B T \gtrsim t$ an almost perfect agreement is obtained. The same is true if strong fields ($\mu_B B \geq t$) are considered. Within this range, the absolute error in the magnetic susceptibility per lattice site (measured in units of μ_B^2/t) is in average as low as 4.8×10^{-3} and never exceeds 3.9×10^{-2} for $\mu_B B \geq t$.

In Fig. 5.21 we present results for the magnetization curve $M(B)$ of the infinite half-filled Hubbard chain for representative values of the temperature T, as well as for the temperature dependence of the zero-field magnetic susceptibility χ at different values of the Coulomb-repulsion strength U/t. Results obtained by FT-LDFT in combination with the scaling approximation (5.76) using a 6-site ring as reference system are compared with the exact analytical solution of the Hubbard chain at finite temperatures [56].

The magnetization curves shown in Fig. 5.21 (a) correspond to a fairly strong Coulomb repulsion $U/t = 8$, where the low-lying spin excitations in the Hubbard chain are governed by the spin-1/2 Heisenberg model (2.52) with exchange-coupling constant $J = 2t^2/U$. Thus, at very low temperatures, magnetic field strengths of the order $\mu_B B \simeq J = t/4$ are sufficient in order to destabilize the AFM alignment of the spins, and we expect to observe a gradual crossover to a fully polarized state within this region. In fact, for $k_B T = t/10$ we observe in Fig. 5.21 (a) a rapid increase

of the magnetization in the weak-field regime, and a fully-polarized state is formed for $\mu_B B \gtrsim t/2$. As the temperature increases, low-spin states are thermally excited, giving rise to a gradual suppression of the magnetization if the field strength B is kept fixed. The comparison to the corresponding exact analytical results demonstrates that FT-LDFT reproduces the magnetization curve of the infinite Hubbard chain with astonishing accuracy. Only at very low temperatures ($k_B T = t/10$) we find some noticeable deviations of up to 17% in the weak-field range ($\mu_B B \lesssim t/2$), where the magnetization increases very rapidly. For higher temperatures ($k_B T \geq 0.4t$), the relative error in the magnetization obtained form FT-LDFT is in average as low as 0.6% and never exceeds 5% within the whole range of field strengths considered.

In Fig. 5.21 (b) we show the zero-field magnetic susceptibility of the infinite half-filled Hubbard chain as a function of the temperature for intermediate to strong Coulomb repulsions U/t. Since the low-lying spin excitations in the Hubbard chain have energies of the order $J = 2t^2/U$, we find χ increasing in the low-temperature regime and a pronounced peak is formed at a temperature $k_B T \approx J$. The effective exchange-coupling constant J decreases like $1/U$ with the Coulomb-interaction strength, and thus, the maximum in χ increases approximately proportional to U. For higher temperatures ($k_B T \gtrsim 2t^2/U$), the magnetic susceptibility decreases rather rapidly, and for sufficiently high temperatures the typical Curie-law decay $\chi = C/T$ of a paramagnet is observed. The comparison with the exact analytical solution demonstrates that the temperature dependence of the zero-field susceptibility is overall very accurately reproduced within the framework of FT-LDFT. Only in the low-temperature regime ($k_B T \lesssim t/2$) FT-LDFT tends to overestimate the susceptibility. For example, at $U/t = 7$ FT-LDFT overestimates the magnetic susceptibility in the ground state by 17%. Nevertheless, for sufficiently high temperatures ($k_B T \geq t/2$), the susceptibility obtained in the framework of FT-LDFT is in excellent agreement with the exact analytical solution, and the relative deviations are in average as low as 1.1% and never exceed 4.2% within this range.

5.6 Summary

We have developed practical methods to handle the thermodynamic equilibrium problem of the Hubbard model in the framework of FT-LDFT. Our focus has been on the homogeneous Hubbard model with hoppings only between NNs. In this case we can regard the grand potential $\Omega[\boldsymbol{\gamma}]$ as a functional of the SPDM elements $\gamma_{11\sigma}$ and $\gamma_{12} = \sum_\sigma \gamma_{12\sigma}$ alone, which represent the spin-dependent local electron density and the total degree of charge fluctuations between NNs.

In a first step we have focused on the unpolarized case $\boldsymbol{\gamma}_\uparrow = \boldsymbol{\gamma}_\downarrow$, and we have identified the corresponding domain of definition of the reduced grand-potential func-

tional $\Omega[\gamma_{11}, \gamma_{12}]$. Furthermore, we have derived its exact functional dependence in the subspace formed by the uncorrelated mixed-states. Subsequently, we have focused on the important case of a half-filled band ($\gamma_{11} = 1$), and we have devoted our attention to the nontrivial correlation contribution $G_c = G - G_s$ to the free energy $F = K + G$, where $G_s = W_{\mathrm{HF}} - T S_s$ incorporates the interaction energy and entropy of independent fermions. Exact numerical results have been presented for the functional dependence $G_c[\gamma_{12}]$ of the correlation contribution to the free energy of finite Hubbard rings and the infinite 1D Hubbard chain. Our numerical results have revealed that $G_c[\gamma_{12}]$ only depends weakly on the system size if it is properly scaled between the localized ($\gamma_{12} = 0$) and delocalized ($\gamma_{12} = \gamma_{12}^0$) limits. This quasi-universal behaviour of the scaled functional $G_c[\gamma_{12}]$ led us to propose a scaling approximation, which extracts the functional dependence of G_c along the crossover from the localized to the delocalized limit from a suitable reference system.

The scaling approximation has been applied in order to explore the equilibrium properties of the infinite half-filled Hubbard model by minimizing the corresponding free-energy functional $F[\gamma_{12}] = K[\gamma_{12}] + G_s[\gamma_{12}] + G_c[\gamma_{12}]$ within the set of ensemble representable γ_{12}. In this way, very accurate results have been obtained for the most important equilibrium observables of the half-filled Hubbard model in 1–3 dimensions, such as the energy E, the average number of double occupations D, the entropy S, and the specific heat C_V. In fact, the deviations between the results of the scaling approximation and available exact or accurate numerical results are usually found in the lower one-digit percent range. Noticeable deviations have been observed only in the low-temperature regime ($k_{\mathrm{B}}T \lesssim t$) for observables which are higher-order derivatives of the free energy F, such as the specific heat C_V.

One of the most important results is the fact that our newly developed scaling approximation is able to account for the physical effects caused by the separation of spin and charge degrees of freedom in the strongly-correlated Hubbard model. This effect is most clearly reflected by the temperature dependence of the specific heat C_V, which develops a characteristic two-peak structure as the Coulomb-repulsion strength U/t increases. The low-temperature peak corresponds to collective spin wave excitations from the AFM ground state, which are described by an effective Heisenberg model with exchange-coupling constant $J = 2t^2/U$. The peak which occurs at higher temperatures is caused by charge excitations across the Hubbard gap, which involves the creation of double occupations with energies of the order U. The gradual formation of this two-peak structure in C_V with increasing Coulomb-repulsion strength is very well reproduced within our scaling approximation. Furthermore, the qualitative and quantitative dependence of the temperature $T_N \propto t^2/U$, at which the low-temperature peak arises in C_V and which marks the Néel transition from the AFM to the PM phase, is accurately reproduced. The same is also true for the temperature $T_C \propto U$, which corresponds to the high-temperature peak and marks the onset of charge excitations.

Motivated by the excellent performance of the scaling approximation in the case of the half-filled Hubbard model, we have proposed a very intuitive extension which takes into account the dependence of G_c on the electron density $n = \gamma_{11}$. In this way it was possible to explore the equilibrium properties of the Hubbard model in 1–3 dimensions at various band fillings in the framework of FT-LDFT. The comparison with available exact results, as well as with accurate QMC simulations and NLCEs, has demonstrated that FT-LDFT in combination with the scaling approximation is able to reproduce the dependence of the most important equilibrium observables on the electron density very accurately in the complete range from low to high temperatures and weak to strong Coulomb repulsions.

The final challenge has been the extension of our scaling approximation to the regime of spin-polarized electron densities, in order to investigate the influence of external magnetic fields on the most important equilibrium observables in the framework of FT-LDFT. As a prerequisite, we have identified the domain of definition of the reduced grand-potential functional $\Omega[\gamma_{11\uparrow}, \gamma_{11\downarrow}, \gamma_{12}]$, and we have derived its exact functional dependence for the case of uncorrelated mixed-states. Subsequently, we have focused on the half-filled band case ($\gamma_{11\uparrow} + \gamma_{11\downarrow} = 1$), and we have studied the correlation contribution $G_c[s_z, \gamma_{12}]$ to the free-energy functional of the infinite 1D Hubbard chain. This has led to the remarkable result that $G_c[s_z, \gamma_{12}]$ only depends weakly on the spin polarization $s_z = \hbar(\gamma_{11\uparrow} - \gamma_{11\downarrow})/2$ if it is properly scaled between the localized ($\gamma_{12} = 0$) and delocalized [$\gamma_{12} = \gamma_{12}^0(s_z)$] limits. This led us to propose an approximation, which extracts the functional dependence of $G_c[s_z, \gamma_{12}]$ along the crossover from the localized to the delocalized limit for arbitrary spin polarizations $-\hbar/2 \leq s_z \leq \hbar/2$ from a suitable unpolarized reference system.

Our scaling approximation has been subsequently applied to the half-filled infinite 1D Hubbard chain in the presence of an external magnetic field. In this way we were able to investigate the modifications in the temperature dependence of the most important equilibrium observables caused by variations in the magnetic field strength. This includes the kinetic and Coulomb energies, the magnetization M, the entropy S, the specific heat C_V, and the magnetic susceptibility χ. Only in the region $\mu_B B \lesssim t/2$, where the transition from the AFM ground state to the fully polarized state occurs, some noticeable deviations from the exact results have been observed in the low-temperature regime ($k_B T \lesssim t$). For stronger fields ($t/2 \lesssim \mu_B B \lesssim t$), only higher-order derivatives of the free energy, e. g., the specific heat C_V and the magnetic susceptibility χ, show such discrepancies at low temperatures, while for very strong fields ($\mu_B B \gtrsim t$) an almost perfect agreement with the exact analytical solution has been achieved in the complete range from low to high temperatures. Also the magnetization curves $M(B)$ at different temperatures and the temperature dependence of the zero-field magnetic susceptibility for intermediate to strong Coulomb repulsions have been very accurately reproduced within the framework of FT-LDFT.

Summary and outlook

<div style="text-align: right; font-size: 2em;">6</div>

A density functional theory for lattice models of strongly interacting fermions has been formulated, which applies both to the ground state as well as to the thermodynamic equilibrium at finite temperatures. The finite-temperature formalism represents an important fundamental extension of current lattice density functional theory (LDFT) and has been formulated in two different flavours accounting for canonical and grand-canonical ensembles. In order to pave the way to practical applications of LDFT for the ground state as well as for the finite-temperature case, we have focused on the Hubbard model and developed new approximations to the central functionals $W[\gamma]$ and $G_c[\gamma]$ representing respectively the interaction energy and the correlation contribution to the free energy. Our new functionals have demonstrated their universality in applications to a wide range of physical situations, and very accurate results have been obtained for the most important observables in the ground state as well as in the thermodynamic equilibrium at finite temperatures.

For the ground-state problem in the framework of LDFT we have focused on the homogeneous Hubbard model on periodic lattice structures. We have adopted a delocalized $\boldsymbol{k}$-space perspective and discovered a remarkable one-to-one connection between the interaction energy W in the ground state of the model and the entropy S of the corresponding Bloch-state occupation-number distribution $\eta_{\boldsymbol{k}\sigma}$. This has opened up a completely new perspective to the ground-state problem by taking into account the dependence of the central interaction-energy functional $W[\gamma]$ on all elements of the single-particle density matrix (SPDM) $\boldsymbol{\gamma}$, and led to an approximation which leverages the full universality of LDFT.

The almost linear connection between W and S discovered in exact numerical results for the ground state of the half-filled Hubbard model led us to approximate the interaction-energy functional $W[\boldsymbol{\eta}] = W(S[\boldsymbol{\eta}])$ in terms of a simple linear function of the independent-Fermion entropy (IFE) $S[\boldsymbol{\eta}]$. In order to obtain the ground-state properties of the model, the corresponding energy functional $E[\boldsymbol{\eta}] = K[\boldsymbol{\eta}] + W[\boldsymbol{\eta}]$ has been minimized with respect to $\eta_{\boldsymbol{k}\sigma}$, where $K[\boldsymbol{\eta}] = \sum_{\boldsymbol{k}\sigma} \varepsilon_{\boldsymbol{k}\sigma}\eta_{\boldsymbol{k}\sigma}$ stands for the kinetic-energy functional. In this way, the predictive power of the linear IFE-approximation has been demonstrated in applications to the half-filled Hubbard model on finite and infinite lattices in $d = 1\text{–}3$ dimensions as well as in the limit $d \to \infty$. In fact, within

our approximation it was possible to reproduce the ground-state properties in all considered situations with very good accuracy in the complete range from weak to strong Coulomb interactions. This applies in particular to the subtle strongly-correlated Heisenberg limit $U/t \rightarrow \infty$, where the linear IFE-approximation exactly reproduces the asymptotic behaviour of the ground-state energy $E_0 = -\alpha t^2/U$ expected for localized Heisenberg spins. Most notably, the ground-state properties of the infinite 1D Hubbard chain derived from the linear IFE-approximation are almost indistinguishable from the exact Bethe-ansatz solution [49]. In higher dimensions, the linear IFE-approximation has proven to be very accurate as well, and the corresponding ground-state observables agree well with available quantum Monte Carlo (QMC) simulations and exact diagonalizations. Moreover, the spin-polarized Hubbard model has been studied in the framework of the linear IFE-approximation. In this way we have obtained the magnetization curve and the zero-field magnetic susceptibility of the infinite 1D Hubbard chain.

In order to study physical situations involving attractive interactions between the fermions, giving rise to electronic pairing, we have considered the half-filled Hubbard model with negative coupling constant $U < 0$. Also in this case an almost linear connection between W and S has been discovered in exact numerical results for the ground state. This encouraged us to propose a generalized formulation of the linear IFE-approximation to the interaction-energy functional $W[\boldsymbol{\eta}]$, which treats attractive and repulsive interactions on the same footing. Subsequent applications to the half-filled attractive Hubbard model on finite bipartite and non-bipartite lattices in two dimensions have proven that the IFE-approximation is able to account for the correlations caused by attractive interactions, and very accurate results have been obtained for the most important ground-state observables in the complete range from weak to strong interactions.

We also went beyond half band-filling and addressed the problem of arbitrary electron densities. The evaluation of exact numerical results for the ground state of the Hubbard model on various lattice structures with different electron densities has shown that a unique relation between W and S exists even in this more general case. However, the connection between W and S has been found to be strongly affected by the electron density n. Nevertheless, by an interpolation between the low-density limit $n \rightarrow 0$ and the half-filled band case $n = 1$ it was possible to derive a physically sound extension of the IFE-approximation, which applies to arbitrary electron densities. Applications to the one- and two-dimensional Hubbard model have shown that the ground-state observables of the Hubbard model are reproduced very accurately within this approximation to $W[\boldsymbol{\gamma}]$ in the complete range from low electron density up to half band-filling for all values of the Coulomb-repulsion strength. We have also studied the implications of qualitative changes in the occupation-number distribution $\eta_\sigma(k)$ near the Fermi level. To this aim we have focused on the 1D Hubbard chain

and we have restricted the minimization of the LDFT energy functional $E[\eta_\sigma(k)]$ to a class of functions $\eta_\sigma(k)$ exhibiting a typical power-law singularity at the Fermi-level, which is characteristic for Luttinger liquids, such as the 1D Hubbard model away from half band-filling. The corresponding results have shown that Luttinger-like distributions are preferable if low electron densities are concerned, however, in the vicinity of a half filled band ($0.8 \lesssim n \leq 1$) the Fermi-Dirac distributions obtained from the unconstrained minimization of the energy functional within the IFE-approximation lead to significantly more accurate results. We have also studied the ground-state occupation-number distribution $\eta_\sigma(\boldsymbol{k})$ of the 2D Hubbard model on the square lattice in the framework of the IFE-approximation. Our results agree surprisingly well with accurate QMC simulations, and the typical broadening of the Fermi surface, as the electron density and Coulomb-repulsion strength increases, has been very well reproduced.

After the ground-state properties of the periodic Hubbard model have been explored in the framework of the IFE-approximation, we have devoted our attention to the thermodynamic equilibrium at finite temperatures. Our applications of finite-temperature lattice density functional theory (FT-LDFT) were aimed at the homogeneous Hubbard model with hoppings only between nearest neighbors (NNs). In this case we can regard the grand potential $\Omega[\boldsymbol{\gamma}]$ as a functional of the SPDM elements $\gamma_{11\sigma}$ and $\gamma_{12} = \sum_\sigma \gamma_{12\sigma}$ alone, which represent the spin-dependent local electron density and the total degree of charge fluctuations between NNs.

In a first step we have focused on the unpolarized case $\boldsymbol{\gamma}_\uparrow = \boldsymbol{\gamma}_\downarrow$, and we have identified the corresponding domain of definition of the reduced grand-potential functional $\Omega[\gamma_{11}, \gamma_{12}]$. Furthermore, we have derived its exact functional dependence in the subspace formed by the uncorrelated mixed states. Subsequently, we have focused on the important case of a half-filled band ($\gamma_{11} = 1$), and we have devoted our attention to the nontrivial correlation contribution $G_c = G - G_s$ to the free energy $F = K + G$, where $G_s = W_{\mathrm{HF}} - T S_s$ incorporates the interaction energy and entropy of independent fermions. Exact numerical results have been presented for the functional dependence $G_c[\gamma_{12}]$ of the correlation contribution to the free energy of finite Hubbard rings and the infinite 1D Hubbard chain. Our numerical results have revealed that $G_c[\gamma_{12}]$ only depends weakly on the system size if it is properly scaled between the localized ($\gamma_{12} = 0$) and delocalized ($\gamma_{12} = \gamma_{12}^0$) limits. This quasi-universal behaviour of the scaled functional $G_c[\gamma_{12}]$ led us to propose a scaling approximation, which extracts the functional dependence of G_c along the crossover from the localized to the delocalized limit from a suitable reference system.

The scaling approximation has been applied in order to explore the equilibrium properties of the infinite half-filled Hubbard model by minimizing the corresponding free-energy functional $F[\gamma_{12}] = K[\gamma_{12}] + G_s[\gamma_{12}] + G_c[\gamma_{12}]$ within the set of ensemble-representable γ_{12}. In this way, very accurate results have been obtained for the most

important equilibrium observables of the half-filled Hubbard model in 1–3 dimensions, such as the energy E, the average number of double occupations D, the entropy S, and the specific heat C_V. In fact, the deviations between the results of the scaling approximation and available exact or accurate numerical results are usually found in the lower one-digit percent range. Noticeable deviations have been observed only in the low-temperature regime ($k_\mathrm{B}T \lesssim t$) for observables which are higher-order derivatives of the free energy F, such as the specific heat C_V.

One of the most important results is the fact that our newly developed scaling approximation is able to account for the physical effects caused by the separation of spin and charge degrees of freedom in the strongly-correlated Hubbard model. This effect is most clearly reflected by the temperature dependence of the specific heat C_V, which develops a characteristic two-peak structure as the Coulomb-repulsion strength U/t increases. The low-temperature peak corresponds to collective spin-wave excitations from the antiferromagnetic (AFM) ground state, which are described by an effective Heisenberg model with exchange-coupling constant $J = 2t^2/U$. The peak which occurs at higher temperatures is caused by charge excitations across the Hubbard gap, which involves the creation of double occupations with energies of the order U. The gradual formation of this two-peak structure in C_V with increasing Coulomb-repulsion strength is very well reproduced within our scaling approximation. Furthermore, the qualitative and quantitative dependence of the temperature $T_N \propto t^2/U$, at which the low-temperature peak arises in C_V and which marks the Néel transition from the AFM to the paramagnetic (PM) phase, is accurately reproduced. The same is also true for the temperature $T_C \propto U$, which corresponds to the high-temperature peak and marks the onset of charge excitations.

Motivated by the excellent performance of the scaling approximation in the case of the half-filled Hubbard model, we have proposed a very intuitive extension which takes into account the dependence of G_c on the electron density $n = \gamma_{11}$. In this way it was possible to explore the equilibrium properties of the Hubbard model in 1–3 dimensions at various band fillings in the framework of FT-LDFT. The comparison with available exact results, as well as with accurate QMC simulations and numerical linked-cluster expansions (NLCEs), has demonstrated that FT-LDFT in combination with the scaling approximation is able to reproduce the dependence of the most important equilibrium observables on the electron density very accurately in the complete range from low to high temperatures and weak to strong Coulomb repulsions.

The final challenge has been the extension of our scaling approximation to the regime of spin-polarized electron densities, in order to investigate the influence of external magnetic fields on the most important equilibrium observables in the framework of FT-LDFT. As a prerequisite, we have identified the domain of definition of the reduced grand-potential functional $\Omega[\gamma_{11\uparrow}, \gamma_{11\downarrow}, \gamma_{12}]$, and we have derived its ex-

act functional dependence for the case of uncorrelated mixed-states. Subsequently, we have focused on the half-filled band case ($\gamma_{11\uparrow} + \gamma_{11\downarrow} = 1$), and we have studied the correlation contribution $G_c[s_z, \gamma_{12}]$ to the free-energy functional of the infinite 1D Hubbard chain. This has led to the remarkable result that $G_c[s_z, \gamma_{12}]$ only depends weakly on the spin polarization $s_z = \hbar(\gamma_{11\uparrow} - \gamma_{11\downarrow})/2$ if it is properly scaled between the localized ($\gamma_{12} = 0$) and delocalized [$\gamma_{12} = \gamma_{12}^0(s_z)$] limits. This led us to propose an approximation, which extracts the functional dependence of $G_c[s_z, \gamma_{12}]$ along the crossover from the localized to the delocalized limit for arbitrary spin polarizations $-\hbar/2 \leq s_z \leq \hbar/2$ from a suitable unpolarized reference system.

Our scaling approximation has been subsequently applied to the half-filled infinite 1D Hubbard chain in the presence of an external magnetic field. In this way we were able to investigate the modifications in the temperature dependence of the most important equilibrium observables caused by variations in the magnetic field strength. This includes the kinetic and Coulomb energies, the magnetization M, the entropy S, the specific heat C_V, and the magnetic susceptibility χ. Also the magnetization curves $M(B)$ at different temperatures and the temperature dependence of the zero-field magnetic susceptibility for intermediate to strong Coulomb repulsions have been studied in the framework of FT-LDFT, and the comparison with the exact analytical solution confirms the accuracy of our method.

This work has opened up a new perspective to the ground-state properties of strongly interacting electrons on a lattice in the framework of LDFT by adopting a delocalized k-space perspective which leverages the full universality of the theory. Furthermore, it has extended the scope of the theory to the regime of the thermodynamic equilibrium at finite temperatures by providing a rigorous formulation of FT-LDFT and first applications to the unpolarized Hubbard model at various band fillings, as well as to the case of spin-polarized systems. Future developments in the framework of LDFT could transfer the methods developed in this thesis to other lattice models, such as the single-impurity Anderson or Kondo models, in order to study magnetic impurities in metals and the related Kondo effect. Furthermore, it would be very interesting to investigate if a connection between the entropy S of the Bloch-state occupation-number distribution $\eta_{k\sigma}$ and the correlation contribution G_c to the free energy, similar to the one exploited in our k-space approach for the ground state, could be established also in the case of the thermodynamic equilibrium at finite temperatures. This would provide a new, potentially most effective perspective to practical approximations in the framework of FT-LDFT.

Another fundamental challenge in the framework of LDFT would be to derive practical approximations to the functionals of more general observables, such as the spin- and charge-correlation functions. To this aim one could focus on homogeneous and periodic systems, where all physical observables $O[\eta]$ can be regarded as a functionals of the Bloch-state occupation numbers $\eta_{k\sigma}$ alone. A very promising approach towards

approximate functionals of more general observables would be to employ supervised machine-learning techniques, and to train a model on a large set of data $(O, \boldsymbol{\eta})$ obtained from exactly solvable systems. One of the most important challenges one would face in the framework of such machine-learning approaches is to find suitable extrapolations of the models' predictions to larger systems or to the thermodynamic limit, since the data used in the training phase is usually obtained from the exact numerical solution for small finite clusters. Nevertheless, taking into account the universality of LDFT, such machine-learning methods would be most promising, since robust approximations, especially to the central functionals $W[\boldsymbol{\eta}]$ and $G_c[\boldsymbol{\eta}]$, would provide a unified method which gives access to the ground-state and equilibrium properties of arbitrary lattice models.

Fundamentals of density functional theory $\quad$ A

One of the major breakthroughs in condensed-matter physics and the general quantum many-body problem in general is the development of Hohenberg-Kohn-Sham's density functional theory (DFT), in which the many-particle wave function $|\Psi\rangle$ is replaced by the many-particle density $n(\boldsymbol{r})$ as the central variable [2, 3]. This major simplification opened a completely new perspective to the quantum many-body problem and made it possible to efficiently calculate a large variety of important ground-state properties, such as binding energies of molecules, band structures of solids, or magnetic moments of nanoparticles with high accuracy.

Historically, DFT was not the first attempt to formulate a quantum many-body theory which is solely based on the particle density $n(\boldsymbol{r})$. Already in 1927 Thomas and Fermi (TF) proposed the first, from today's perspective very rudimentary, approach to compute atomic energies on the basis of the electronic density [4, 5]. In the TF theory, the local contribution to the kinetic-energy functional $K[n(\boldsymbol{r})]$ of the interacting many-electron system is approximated by the kinetic energy of *noninteracting* electrons having the homogeneous density $n = n(\boldsymbol{r})$, and the interaction energy $W[n(\boldsymbol{r})]$ is approximated by the classical Hartree-energy $W_{\mathrm{H}}[n(\boldsymbol{r})]$. Shortly after its formulation, it turned out that the TF theory is not able to describe any molecular bonding, which is mainly due to the simple approximation to the kinetic-energy functional, and was therefore rapidly abandoned. After the failure of the TF theory to account for molecular bonding has been discovered, the density functional (DF) approach was not used very intensively, until in 1964 Hohenberg and Kohn (HK) [2] demonstrated that in principle all ground-state observables of a many-particle system can be exactly obtained from the ground-state electron density $n_0(\boldsymbol{r})$ alone. The HK theorem ensures the existence of a universal functional $F_{\mathrm{HK}}[n(\boldsymbol{r})]$, representing the optimal sum of the kinetic and the interaction energy of a many-particle system having the density $n(\boldsymbol{r})$, and the variational principle of the corresponding energy functional gives access to the ground-state density and to all ground-state properties in principle. Just a few month after the formulation of the ground-breaking HK theorem, Mermin [6] extended the HK theorem to finite temperatures by proving that in principle all equilibrium averages of an interacting many-particle system can be obtained from the equilibrium particle density $n_{\mathrm{eq}}(\boldsymbol{r})$.

The actual way to most-current practical applications of DFT was pawed by Kohn and Sham (KS), who showed that the interacting many-particle system can be replaced by an auxiliary system of noninteracting particles [3]. In the same work KS also provided the first local density approximation (LDA) to the nontrivial exchange and correlation (XC) part $E_{xc}[n(r)]$ of the universal functional $F_{HK}[n(r)]$. In the following decades several improvements over the LDA have been developed. Presently, the generalized gradient approximations (GGAs) [8–14] and the so-called hybrid functionals [15–19] are the most widespread approaches for practical applications.

The remainder of this chapter is organized as follows. In Section A.1 a brief overview of the formulation of DFT for the many-particle ground state problem is provided and in Section A.2 the extension of the theory to the equilibrium at finite temperatures is presented.

A.1 Ground-state formalism

In this section we briefly review the formulation of DFT for the ground-state problem of interacting many-particle systems. For simplicity, the focus is on systems having nondegenerate ground states, although the formalism can be easily extended to the degenerate case [132, 133]. Section A.1.1 recalls the HK theorem from which some important conclusions are drawn. The following Section A.1.2 briefly discusses the representability problem for the density functions $n(r)$, some related formal difficulties, and how they can be circumvented by the Levy-Lieb (LL) constrained-search method. The KS method is reviewed in Section A.1.3. Finally, the LDA approximation to the XC energy is presented in Section A.1.4.

A.1.1 The Hohenberg-Kohn theorem

In order to formulate the HK theorem we consider a system of N particles subject to an external potential $v(r)$ (e. g., the lattice potential generated by the ions in a crystal) and to their mutual interaction $w(r, r')$ [e. g., the Coulomb repulsion $w(r, r') = e^2/|r-r'|$]. The corresponding electronic Hamiltonian reads

$$\hat{H} = \hat{K} + \hat{V} + \hat{W}, \tag{A.1}$$

where

$$\hat{K} = -\frac{\hbar^2}{2m} \sum_{\sigma} \int \hat{\psi}_{\sigma}^{\dagger}(r) \, \nabla^2 \, \hat{\psi}_{\sigma}(r) \, dr \tag{A.2}$$

is the kinetic-energy[1] operator,

$$\hat{V} = \sum_\sigma \int \hat{\psi}_\sigma^\dagger(\boldsymbol{r})\, v(\boldsymbol{r})\, \hat{\psi}_\sigma(\boldsymbol{r})\, \mathrm{d}\boldsymbol{r} = \int v(\boldsymbol{r})\, \hat{n}(\boldsymbol{r})\, \mathrm{d}\boldsymbol{r} \tag{A.3}$$

the operator describing the interaction with the external potential, and

$$\hat{W} = \frac{1}{2} \sum_{\sigma\sigma'} \int \hat{\psi}_\sigma^\dagger(\boldsymbol{r})\, \hat{\psi}_{\sigma'}^\dagger(\boldsymbol{r}')\, w(\boldsymbol{r},\boldsymbol{r}')\, \hat{\psi}_{\sigma'}(\boldsymbol{r}')\, \hat{\psi}_\sigma(\boldsymbol{r})\, \mathrm{d}\boldsymbol{r}\, \mathrm{d}\boldsymbol{r}' \tag{A.4}$$

describes the interaction between the particles. In the usual second-quantization notation, $\hat{\psi}_\sigma^\dagger(\boldsymbol{r})$ [$\hat{\psi}_\sigma(\boldsymbol{r})$] stands for the creation [annihilation] operator for an electron with spin polarization σ at the position $\boldsymbol{r}$, and $\hat{n}(\boldsymbol{r}) = \sum_\sigma \hat{\psi}_\sigma^\dagger(\boldsymbol{r})\, \hat{\psi}_\sigma(\boldsymbol{r})$ for the electron-density operator. Notice that the interaction $w(\boldsymbol{r},\boldsymbol{r}')$ is specified by the type of particles under consideration, such that we can consider a system as uniquely characterized by the external potential $v(\boldsymbol{r})$. Before we can formulate the HK theorem we need a small

Lemma A.1. *Two reasonably well-behaved[2] potentials $v(\boldsymbol{r})$ and $v'(\boldsymbol{r})$ lead to the same ground state $|\Psi_0\rangle$ if, and only if, the potentials differ by an additive constant.*

Proof. The fact that two potentials $v(\boldsymbol{r})$ and $v'(\boldsymbol{r})$ which solely differ by an additive constant must lead to the same ground state is obvious. Thus, let us assume that the two potentials differ by more than an additive constant, i. e.,

$$\hat{V} \neq \hat{V}' + c \quad \text{with} \quad c \in \mathbb{R} \tag{A.5}$$

within the given N-particle Hilbert space, but nevertheless lead to the same ground state $|\Psi_0\rangle$, such that

$$\left(\hat{K} + \hat{V} + \hat{W}\right)|\Psi_0\rangle = E_0|\Psi_0\rangle \quad \text{and} \quad \left(\hat{K} + \hat{V}' + \hat{W}\right)|\Psi_0\rangle = E_0'|\Psi_0\rangle. \tag{A.6}$$

Subtracting these two equations leads to

$$(\hat{V} - \hat{V}')|\Psi_0\rangle = \left(E_0 - E_0'\right)|\Psi_0\rangle. \tag{A.7}$$

Thus, since $\hat{V}$ and $\hat{V}'$ are multiplicative operators, we conclude that $\hat{V} - \hat{V}' = E_0 - E_0' \in \mathbb{R}$ if $|\Psi_0\rangle$ does not vanish on a set of positive measure, which is guaranteed by the

[1] Notice that within this Appendix, which provides a formulation of DFT in the continuum, $\hat{K}$ refers to the operator of the *pure* kinetic energy, whereas in the chapters concerning the DFT of lattice models, $\hat{K}$ refers to the *full single-particle part* of the Hamiltonian $\hat{H}$. Nevertheless, as it is common practice, we refer to $\hat{K}$ as "kinetic energy" in these chapters as well.

[2] We call potentials reasonably well-behaved if the unique-continuation theorem applies to them [134, 135]. This excludes, for example, potentials exhibiting infinite barriers.

unique-continuation theorem, which is valid for the reasonably well-behaved potentials under consideration [134, 135]. This, however, contradicts our initial assumption (A.5) which thus must have been wrong. We conclude that there are no reasonably well-behaved potentials which differ by more than a constant but nevertheless lead to the same ground state. □

Theorem A.1 (Hohenberg and Kohn [2]). *The external potential $v(r)$ of a many-particle system is (apart from an irrelevant additive constant) a functional of the electronic ground-state density $n(r)$.*

Proof. Assume that the ground state $|\Psi_0\rangle$ of $\hat{H}$ is non degenerate and that there exists *another* potential $v'(r)$ which differs from $v(r)$ by more than an additive constant but, nevertheless, leads to the *same* ground-state density $n(r)$ as the potential $v(r)$. Then, if $\hat{H}'$ and $|\Psi_0'\rangle$ denote the Hamiltonian and ground state associated with $v'(r)$, the corresponding ground-state energy is given by

$$E_0' = \langle \Psi_0'|\hat{H}'|\Psi_0'\rangle = \int v'(r)\, n(r)\, \mathrm{d}r + \langle \Psi_0'|\hat{K} + \hat{W}|\Psi_0'\rangle\,. \tag{A.8}$$

Since the potentials $v(r)$ and $v'(r)$ differ by more than an additive constant, the corresponding ground states $|\Psi_0\rangle$ and $|\Psi_0'\rangle$ must be different from each other according to Lemma A.1. Therefore, from the minimal principle for the ground-state energy $E_0 = \langle \Psi_0|\hat{H}|\Psi_0\rangle$ of the Hamiltonian $\hat{H}$ it follows that

$$E_0 < \langle \Psi_0'|\hat{H}|\Psi_0'\rangle = \int v(r)\, n(r)\, \mathrm{d}r + \langle \Psi_0'|\hat{K} + \hat{W}|\Psi_0'\rangle =$$
$$= E_0' + \int [v(r) - v'(r)]\, n(r)\, \mathrm{d}r\,. \tag{A.9}$$

Notice that the strict inequality holds, because we assumed that the ground state associated with $v(r)$ is non degenerate. By interchanging primed and unprimed quantities one obtains

$$E_0' \leq \langle \Psi_0|\hat{H}'|\Psi_0\rangle = E_0 + \int [v'(r) - v(r)]\, n(r)\, \mathrm{d}r\,, \tag{A.10}$$

where no strict inequality holds, since the ground state associated with $v'(r)$ could be degenerate. Adding Eqs. (A.9) and (A.10) the contradiction

$$E_0 + E_0' < E_0' + E_0 \tag{A.11}$$

is obtained, which proves that two potentials $v(r)$ and $v'(r)$ differing by more than an additive constant cannot yield the same ground state density $n(r)$. One concludes that $v(r)$ is (apart of a constant) a functional of $n(r)$. □

The HK theorem states that the external potential $v(\boldsymbol{r})$ is a functional of the ground-state density $n(\boldsymbol{r})$. Consequently, as long as the interaction $w(\boldsymbol{r}, \boldsymbol{r}')$ is fixed, the full Hamiltonian $\hat{H}$ and all the physical properties derived from it must be functionals of the ground-state density as well. This applies in particular to the ground state $|\Psi_0\rangle$ but also to all excited states. Notice however, that the one-to-one correspondence between the ground-state density $n(\boldsymbol{r})$ and the external potential $v(\boldsymbol{r})$ established by the HK Theorem A.1 is no longer valid in the presence of ground-state degeneracies. Clearly, if the ground state is degenerate, the ground-state density $n(\boldsymbol{r})$ is no longer unique. Nevertheless, due to the variational principle and the simple fact that all ground states share the same energy, a one-to-one correspondence between the set $\{n(\boldsymbol{r})\}$ formed by the densities of all degenerate ground-states and the external potential $v(\boldsymbol{r})$ can be established [132]. Thus, the density of any one of the degenerate ground-states uniquely determines the external potential $v(\boldsymbol{r})$ and thus defines the Hamiltonian $\hat{H}$ and all its ground-state and excited-state properties. Returning to the case of a nondegenerate ground-state, where the unique ground-state density $n(\boldsymbol{r})$ determines $v(\boldsymbol{r})$ and thus the Hamiltonian $\hat{H}$, we may immediately formulate the important

Corollary A.1. *The ground state $|\Psi_0\rangle$ of a many-particle system is a functional of the ground-state density $n(\boldsymbol{r})$.*

Moreover, the converse statement is also true, i. e., the ground-state density $n(\boldsymbol{r}) = \langle\Psi_0|\hat{n}(\boldsymbol{r})|\Psi_0\rangle$ is a functional of the ground state $|\Psi_0\rangle$. This establishes a bijective map between the set $\boldsymbol{\Psi}_0$ containing all nondegenerate ground states and the corresponding set $\mathcal{N}_v$ of the ground-state densities. Furthermore, from Corollary A.1 we obtain the important

Corollary A.2. *The ground-state expectation value of any observable $\hat{O}$ is a functional of the ground-state density $n(\boldsymbol{r})$.*

Proof. From Corollary A.1 we know, that the ground state $|\Psi_0\rangle = |\Psi_0[n(\boldsymbol{r})]\rangle$ is a functional of the ground-state density $n(\boldsymbol{r})$. Therefore, the ground-state expectation value of any observable $\hat{O}$ can be obtained from the ground-state density as

$$O[n(\boldsymbol{r})] = \langle\Psi_0[n(\boldsymbol{r})]|\hat{O}|\Psi_0[n(\boldsymbol{r})]\rangle \,. \tag{A.12}$$

$\square$

In particular, the kinetic and interaction energies are functionals of $n(\boldsymbol{r})$. One therefore defines the functional

$$F_{\mathrm{HK}}[n(\boldsymbol{r})] = \langle\Psi_0[n(\boldsymbol{r})]|\hat{K} + \hat{W}|\Psi_0[n(\boldsymbol{r})]\rangle \,, \tag{A.13}$$

representing the sum of the kinetic and interaction energies, which is a universal functional of $n(r)$ in the sense that it does not depend on the external potential $v(r)$. Notice that the functional (A.13) is defined for all densities $n(r) = \langle \Psi_0 | \hat{n}(r) | \Psi_0 \rangle$ which can be derived from the N-particle ground state $|\Psi_0\rangle$ associated with *some* external potential $v(r)$. Using Eq. (A.13), the functional corresponding to the ground-state energy is obtained as

$$E[n(r)] = \int v(r)\, n(r)\, \mathrm{d}r + F_{\mathrm{HK}}[n(r)]\,. \tag{A.14}$$

Clearly for the actual ground-state density $n_0(r)$, the energy functional $E[n(r)]$ assumes its minimum and equals the ground-state energy E_0 associated with the given external potential $v(r)$. If the functional $F_{\mathrm{HK}}[n(r)]$ were known, the ground-state energy and density corresponding to arbitrary potentials $v(r)$ could be obtained by minimizing the energy functional $E[n(r)]$. Therefore, the main challenge in practical applications of DFT is to determine the universal functional $F_{\mathrm{HK}}[n(r)]$. In the next section we will see that already the characterization of the domain of definition of $F_{\mathrm{HK}}[n(r)]$ is far from trivial.

A.1.2 The Levy-Lieb constrained-search method

In the previous section we have seen that the ground-state energy and density can be obtained by minimizing the energy functional (A.14) with respect to all functions $n(r)$ that can be derived as the ground-state density of the N-particle problem with interaction $w(r, r')$ and *some* external potential $v(r)$. This class of functions is called *pure-state v-representable*. At first, this does not seem to pose a major restriction on $n(r)$, since all density functions of physical interest for the ground-state many-body problem must be pure-state v-representable. However, any practical implementation of the variational principle for the ground-state energy (A.14) must in principle ensure that the minimization is constrained to the set of pure-state v-representable densities, since otherwise $F_{\mathrm{HK}}[n(r)]$ would be ill-defined and the result of the minimization would be uncontrolled or simply unphysical. This raises the problem of characterizing pure-state v-representable density functions. The early hope that all reasonably well behaved non-negative functions, corresponding to an integer particle-number $N = \int n(r)\, \mathrm{d}r$, are pure-state v-representable has been proven to be wrong. The first kind of non pure-state v-representable density functions has been discovered independently by Levy [136] and Lieb [135]. They considered a system having q degenerate ground states $|\Psi_1\rangle, \ldots, |\Psi_q\rangle$ and constructed the density matrix

$$\hat{\rho} = \sum_{i=1}^{q} p_i\, |\Psi_i\rangle\langle\Psi_i| \quad \text{with} \quad p_i \geq 0 \quad \text{and} \quad \sum_{i=1}^{q} p_i = 1\,. \tag{A.15}$$

The resulting density

$$n(\boldsymbol{r}) = \mathrm{Tr}\{\hat{\rho}\,\hat{n}(\boldsymbol{r})\} = \sum_{i=1}^{q} p_i \langle \Psi_i | \hat{n}(\boldsymbol{r}) | \Psi_i \rangle \qquad (A.16)$$

can be shown to be not pure-state v-representable (except for very special choices of the weights p_i). Density functions $n(\boldsymbol{r})$ of the form (A.16) are called *ensemble v-representable*. One can easily extend the functional (A.14) and the corresponding variational principle to the set of ensemble v-representable densities [137]. However, Englisch and Englisch [137] have shown that even the criterion of ensemble v-representability is not met by all reasonably well-behaved non-negative functions. Therefore, in order to render the variational principle for the ground-state energy useful in practice, the domain of definition of the functional (A.14) must be extended to an even larger set of trial densities.

The first such extension has been proposed by Levy [138] and Lieb [135], who defined the functional

$$F_{\mathrm{LL}}[n(\boldsymbol{r})] = \min_{|\Psi\rangle \to n(\boldsymbol{r})} \langle \Psi | \hat{K} + \hat{W} | \Psi \rangle. \qquad (A.17)$$

The notation $|\Psi\rangle \to n(\boldsymbol{r})$ indicates that the minimization is performed with respect to all normalized N-particle states $|\Psi\rangle$ which yield the given density $n(\boldsymbol{r})$, i. e., which satisfy the condition $\langle \Psi | \hat{n}(\boldsymbol{r}) | \Psi \rangle = n(\boldsymbol{r}) \, \forall \boldsymbol{r}$. The major advantage of the LL functional (A.17), as compared to the HK functional (A.13), is that it is defined for all functions $n(\boldsymbol{r})$ that correspond to the density of *some* normalized N-particle state $|\Psi\rangle$, not necessarily a ground state. These functions $n(\boldsymbol{r})$ are consequently called *pure-state N-representable*, and Gilbert [20], Harriman [139], March [140], Zumbach and Maschke [141] have shown that any non negative function which integrates to the given particle number N is pure-state N-representable.

In order to establish the connection with the many-body problem, and to render the LL functional useful in practice, we have to prove the following statement.

Theorem A.2. *The LL functional* (A.17) *is a reasonable extension of the HK functional* (A.13) *in the sense that*

(a) *it holds*

$$F_{\mathrm{LL}}[n(\boldsymbol{r})] = F_{\mathrm{HK}}[n(\boldsymbol{r})] \qquad (A.18)$$

for any pure-state v-representable density $n(\boldsymbol{r})$, *and*

(b) *the corresponding energy functional*

$$E_{\mathrm{LL}}[n(\boldsymbol{r})] = \int v(\boldsymbol{r})\, n(\boldsymbol{r})\, \mathrm{d}\boldsymbol{r} + F_{\mathrm{LL}}[n(\boldsymbol{r})] \qquad (A.19)$$

assumes its minimum at, and only at, the ground-state density $n_0(\boldsymbol{r})$ which corresponds to the external potential $v(\boldsymbol{r})$, and the minimal value equals the associated ground-state energy E_0.

Proof. According to the Rayleigh-Ritz principle, the ground-state energy E_0 of an interacting N-particle system described by the Hamiltonian (A.1) is given by

$$E_0 = \min_{|\Psi\rangle}\langle\Psi|\hat{H}|\Psi\rangle \,, \tag{A.20}$$

where the minimization is restricted to all normalized N-particle states $|\Psi\rangle$. Denoting by $\mathcal{N}_N$ the set of pure-state N-representable functions, we can perform the minimization in Eq. (A.20) in two consecutive steps:

$$
\begin{aligned}
E_0 &= \min_{n(\boldsymbol{r})\in\mathcal{N}_N} \left\{ \int v(\boldsymbol{r})\,n(\boldsymbol{r})\,\mathrm{d}\boldsymbol{r} + \min_{|\Psi\rangle\to n(\boldsymbol{r})} \langle\Psi|\hat{K}+\hat{W}|\Psi\rangle \right\} = \\
&= \min_{n(\boldsymbol{r})\in\mathcal{N}_N} \left\{ \int v(\boldsymbol{r})\,n(\boldsymbol{r})\,\mathrm{d}\boldsymbol{r} + F_{\mathrm{LL}}[n(\boldsymbol{r})] \right\} = \min_{n(\boldsymbol{r})\in\mathcal{N}_N} E_{\mathrm{LL}}[n(\boldsymbol{r})]\,.
\end{aligned}
\tag{A.21}
$$

This already proves the second part of statement (b), namely that the minimal value of the energy functional (A.19) equals the ground-state energy E_0.

Assuming that the ground state associated with the external potential $v(\boldsymbol{r})$ is nondegenerate, the state $|\Psi_0\rangle$ yielding the minimum in Eq. (A.20) is unique. Consequently, the density yielding the minimum in Eq. (A.21) must be the corresponding unique ground-state density $n_0(\boldsymbol{r})$. More generally, we can state that any N-particle state $|\Psi_0'\rangle$ which minimizes (A.20) for *some* external potential $v'(\boldsymbol{r})$ is a ground state by construction and thus, the corresponding density $n(\boldsymbol{r})$ must be pure-state v-representable. This means, there is no density $n(\boldsymbol{r})$ which does not belong to the set of pure-state v-representable functions but leads to a minimum of $E_{\mathrm{LL}}[n(\boldsymbol{r})]$. Clearly, any pure-state v-representable density $n(\boldsymbol{r})$ that is different from the true ground-state density $n_0(\boldsymbol{r})$ must correspond to a ground state $|\Psi_0'\rangle$ that differs from the true ground state $|\Psi_0\rangle$, and therefore $|\Psi_0'\rangle$ can not yield the minimum in Eq. (A.20) for the given potential $v(\boldsymbol{r})$. Consequently $E_{\mathrm{LL}}[n(\boldsymbol{r})] > E_0$ must hold, which concludes the proof of statement (b).

Let us now assume that $n(\boldsymbol{r})$ is an arbitrary pure-state v-representable function, and let $v(\boldsymbol{r})$ be the external potential associated with it according to the HK Theorem A.1. Then, the state which yields the minimum in Eq. (A.20) for this potential $v(\boldsymbol{r})$ must coincide with the ground state $|\Psi_0[n(\boldsymbol{r})]\rangle$ associated with $n(\boldsymbol{r})$. Therefore, $F_{\mathrm{LL}}[n(\boldsymbol{r})] = \langle\Psi_0[n(\boldsymbol{r})]|\hat{K}+\hat{W}|\Psi_0[n(\boldsymbol{r})]\rangle$ must hold, which coincides with Eq. (A.13). This concludes the proof of statement (a). □

The LL functional (A.17) extends the HK functional (A.13) to the domain of pure-state N-representable densities, i. e., to the set of all non negative functions $n(\boldsymbol{r})$ which

integrate to N. This opens the way to practical implementations of the variational principle (A.19) from which the ground-state energy and density and in principle all ground-state observables can be obtained via Eq. (A.12). The next section addresses the problem of implementing the variational principle for the ground-state energy in practice. It will be shown that the interacting many-particle system can be mapped to a system of N noninteracting particles in an effective potential $v_s([n]; \boldsymbol{r})$, which is a functional of the electronic density $n(\boldsymbol{r})$ itself. In this way, the ground-state problem for N interacting particles can be formally reduced to the selfconsistent solution of single-particle equations.

A.1.3 The Kohn-Sham scheme

In the previous sections we have demonstrated that the ground-state energy and density of a many-particle system can be obtained by from the variational principle of the energy functionals (A.14) and (A.19). In order to formulate a practical implementation of the corresponding minimization procedure, we consider an auxiliary system of noninteracting particles described by the Hamiltonian

$$\hat{H}_s = \hat{K} + \hat{V}_s = \hat{K} + \int v_s(\boldsymbol{r})\,\hat{n}(\boldsymbol{r})\,\mathrm{d}\boldsymbol{r}\,. \tag{A.22}$$

In the following we assume that the electronic ground-state density $n(\boldsymbol{r})$ of a given interacting N-particle system can be obtained from the ground state of N *noninteracting* particles under the action of some external potential $v_s(\boldsymbol{r})$, as described by the Hamiltonian (A.22). Such densities, which can be associated with the ground state of a noninteracting system, are termed *noninteracting pure-state v-representable*. Thus, we assume that all *interacting* pure-state v-representable densities are also *noninteracting* pure-state v-representable. The validity of this hypothesis is discussed, for example, in Ref. [133]. Assuming $v_s(\boldsymbol{r})$ exists, its uniqueness follows from the HK theorem, which, of course, also holds for noninteracting systems.

The ground state of the noninteracting system (A.22) can be obtained from the solution of the corresponding single-particle Schrödinger equation

$$\left[-\frac{\hbar^2}{2m}\nabla^2 + v_s(\boldsymbol{r})\right]\phi_i(\boldsymbol{r}) = \varepsilon_i\,\phi_i(\boldsymbol{r}) \tag{A.23}$$

as the Slater determinant constructed with the single-particle orbitals $\phi_i(\boldsymbol{r})$ having the N lowest single-particle energies ε_i. In the absence of degeneracies, the ground-state density is given by

$$n(\boldsymbol{r}) = \sum_{i=1}^{N} |\phi_i(\boldsymbol{r})|^2\,. \tag{A.24}$$

A Fundamentals of density functional theory

From Corollary A.1 we know that the ground state of a many-particle system is a functional of the ground-state density $n(r)$, and consequently, for a noninteracting system the solutions of Eq. (A.23) must be functionals of $n(r)$, i.e., $\phi_i(r) = \phi_i([n];r)$. Furthermore, for noninteracting particles, the HK functional (A.13) is solely given by the contribution of the kinetic energy. This means that the noninteracting kinetic energy $K_s[n(r)]$ is a universal functional of the electronic density $n(r)$. An explicit expression for $K_s[n(r)]$ is readily obtained in terms of the solutions of Eq. (A.23)

$$K_s[n(r)] = -\frac{\hbar^2}{2m} \sum_{i=1}^{N} \int \phi_i^*([n];r)\,\nabla^2 \phi_i([n];r)\,\mathrm{d}r \,. \tag{A.25}$$

In order to obtain $\phi_i(r)$ and thus $n(r)$, one needs to chose the single-particle potential $v_s(r)$ such that the auxiliary single-particle system (A.22) has the same ground-state density $n(r)$ as the interacting system under consideration. In order to handle this problem, it is useful to write the kinetic- and interaction-energy functional (A.13) or (A.17) in the form

$$F[n(r)] = K_s[n(r)] + \frac{1}{2} \int n(r)\,w(r,r')\,n(r')\,\mathrm{d}r\,\mathrm{d}r' + E_{xc}[n(r)]\,, \tag{A.26}$$

where $K_s[n(r)]$ is the noninteracting kinetic-energy functional (A.25), the second term is the Hartree energy $W_H[n(r)]$, and

$$E_{xc}[n(r)] = F[n(r)] - W_H[n(r)] - K_s[(r)] \tag{A.27}$$

is the *exchange-correlation (XC) energy*. Here and in the following we drop the index to $F[n(r)]$ which distinguishes between the HK and the LL functionals (A.13) and (A.17), since the discussion applies to both. Notice that the XC functional (A.27) includes not only the contribution to $F[n(r)]$ resulting from XC effects on the Coulomb-interaction energy W, but also those caused by XC effects on the kinetic energy K. Just like $F[n(r)]$, the XC energy $E_{xc}[n(r)]$ is a universal functional of the density $n(r)$ in the sense that it does not depend on the external potential $v(r)$, and it applies to arbitrary numbers of particles. For the minimum of the energy-functional (A.14) or (A.19), i.e., for the true ground-state density $n(r)$, the corresponding Euler-Lagrange functional

$$\mathcal{L} = E[n(r)] - \mu \left(\int n(r)\,\mathrm{d}r - N \right) \tag{A.28}$$

must be stationary. Here we have introduced the Lagrange multiplier μ in order to enforce the condition that the density yields the given particle number N. The stationary condition on the Euler-Lagrange functional (A.28) corresponds to the vanishing functional derivative

$$\frac{\delta\mathcal{L}}{\delta n(r)} = \frac{\delta E[n(r)]}{\delta n(r)} - \mu = 0 \,. \tag{A.29}$$

Using Eq. (A.14) or (A.19) together with Eq. (A.26), this condition is equivalent to

$$\frac{\delta K_s[n(\boldsymbol{r})]}{\delta n(\boldsymbol{r})} + v_s([n]; \boldsymbol{r}) - \mu = 0 \tag{A.30}$$

with

$$v_s([n]; \boldsymbol{r}) = v(\boldsymbol{r}) + \int n(\boldsymbol{r}') w(\boldsymbol{r}, \boldsymbol{r}') \, \mathrm{d}\boldsymbol{r}' + v_{\mathrm{xc}}([n]; \boldsymbol{r}), \tag{A.31}$$

where we have introduced the so-called XC potential

$$v_{\mathrm{xc}}([n]; \boldsymbol{r}) = \frac{\delta E_{\mathrm{xc}}[n(\boldsymbol{r})]}{\delta n(\boldsymbol{r})}. \tag{A.32}$$

Equation (A.30) is the same stationary condition that one would obtain for a system of noninteracting particles moving in the external potential $v_s([n]; \boldsymbol{r})$, with the notable difference that the potential $v_s([n]; \boldsymbol{r})$ in Eq. (A.30) depends on $n(\boldsymbol{r})$ in addition to being a function of the electron position $\boldsymbol{r}$. We may identify $v_s([n]; \boldsymbol{r})$ as the unique single-particle potential for which the auxiliary noninteracting system (A.22) yields the same ground-state density $n(\boldsymbol{r})$ as the interacting system with the external potential $v(\boldsymbol{r})$.

Equations (A.23), (A.24), and (A.31) define the KS-scheme. Due to the fact that the effective single-particle potential (A.31) depends on $n(\boldsymbol{r})$, the corresponding problem must be solved in a selfconsistent way: One starts from an assumed $n(\boldsymbol{r})$, constructs $v_s([n]; \boldsymbol{r})$ from Eq. (A.31), and solves Eq. (A.23) from which a new $n(\boldsymbol{r})$ is obtained by means of Eq. (A.24). This procedure is iterated, starting from the new density $n(\boldsymbol{r})$, until the output density obtained from Eq. (A.24) equals the input density that was used to construct the single-particle potential $v_s([n]; \boldsymbol{r})$. After convergence is achieved, the ground-state energy of the interacting system is obtained as

$$E = \sum_{i=1}^{N} \varepsilon_i + E_{\mathrm{xc}}[n(\boldsymbol{r})] - \frac{1}{2} \int n(\boldsymbol{r}) w(\boldsymbol{r}, \boldsymbol{r}') n(\boldsymbol{r}') \, \mathrm{d}\boldsymbol{r} \, \mathrm{d}\boldsymbol{r}' - \int v_{\mathrm{xc}}([n]; \boldsymbol{r}) n(\boldsymbol{r}) \, \mathrm{d}\boldsymbol{r}. \tag{A.33}$$

The question of how the XC energy $E_{\mathrm{xc}}[n(\boldsymbol{r})]$ is obtained, which enters the effective single-particle potential $v_s([n]; \boldsymbol{r})$ through the XC potential (A.32), and which is required in order to compute the ground-state energy (A.33), remains so far open. An explicit expression for $E_{\mathrm{xc}}[n(\boldsymbol{r})]$ is unknown in general, and therefore one has to resort to approximations. In the next section we present the most basic approximation for the XC energy, which is derived from exact results for the homogeneous interacting electron gas.

A.1.4 Local density approximation

The first approximation to the XC energy $E_{\mathrm{xc}}[n(\boldsymbol{r})]$ was introduced by Kohn and Sham [3]. They proposed to approximate the XC energy by

$$E_{\mathrm{xc}}[n(\boldsymbol{r})] = \int \varepsilon_{\mathrm{xc}}(n(\boldsymbol{r})) n(\boldsymbol{r}) \, \mathrm{d}\boldsymbol{r}, \tag{A.34}$$

where $\varepsilon_{\text{xc}}(n)$ is the XC energy per electron of a homogeneous electron gas having the density $n = n(\boldsymbol{r})$. This means, for a given system of interacting electrons, having the density $n(\boldsymbol{r})$, the XC energy per electron at a given point $\boldsymbol{r}$ is approximated by the XC energy of an electron gas having the homogeneous density $n = n(\boldsymbol{r})$. Functionals of this type are called *local*, since they are constructed from a sum of local contributions, i. e., contributions which depend only on the density $n(\boldsymbol{r})$ at the particular point $\boldsymbol{r}$.

The exchange part ε_{x} of the XC energy ε_{xc} can be obtained from the Hartree-Fock (HF) approximation, since exchange effects are treated exactly within the HF method. For the homogeneous electron gas one obtains

$$\varepsilon_{\text{x}} = -\frac{3e^2}{4\pi r_s}\left(\frac{9\pi}{4}\right)^{1/3}, \tag{A.35}$$

where e is the electron charge and r_s the radius of a sphere containing one electron, i. e., $(4\pi/3)\, r_s^3 = n^{-1}$ (see for example Ref. [133]).

The correlation part ε_{c} of the XC energy ε_{xc} is more subtle. Even in the homogeneous case an exact result, which is valid for all values of the electron density n, is unknown at present. Exact results are available for the regimes of high and low densities, as well as parametrizations for intermediate densities. In particular, the two-parameter form suggested by Hedin and Lundqvist [142]

$$\varepsilon_{\text{c}} = -\frac{Ce^2}{a_0}\left\{(1+x^3)\,\log\left(1+\frac{1}{x}\right)+\frac{x}{2}-x^2-\frac{1}{3}\right\} \quad\text{with}\quad x = \frac{r_s}{a_0 A} \tag{A.36}$$

is widely used in practical applications of the LDA. The parameters $C = 0.0225$ and $A = 21$ yield reliable results in the density range characterized by $a_0 \le r_s \le 6a_0$, where a_0 is the Bohr radius.

The LDA (A.34) is by construction exact for the homogeneous electron gas, where the density is uniform. Therefore, one could expect that it would yield accurate results only for systems having slowly varying densities, a condition which is satisfied in some metals but certainly not in atoms and molecules. Nevertheless, it turns out that the LDA gives ionization energies of atoms, dissociation energies of molecules, bond-lengths, and molecular geometries with a satisfying accuracy. The LDA can be easily extended to spin-polarized systems [7]. In addition, noticeable improvements have been proposed [133]. Most notably the GGAs, which take into account the density gradient [8–14], and the hybrid functionals [15–19], which combine the exchange energy computed with the KS orbitals and some appropriate approximation to the XC energy, have been proven to be quite successful.

There are however many situations, where the LDA fails to yield accurate results. One prominent example is the semiconductor band-gap, for example in silicon, which

is largely underestimated by the LDA [33]. Another example are van der Waals inter-actions, which are caused by dynamical density fluctuations, and are therefore beyond the scope of the LDA [34]. Particularly important in the context of the present thesis is the fact that the LDA and its extensions systematically fail to account for the effects caused by strong electronic correlations, such as the physics of spin-fluctuations, the Kondo-screening, heavy-fermion materials [35], high-temperature superconductivity [36, 37], and Mott-insulators [38–40]. It is therefore most desirable to extend the scope of DFT in order to account for systems exhibiting strong electronic correlations. Strongly correlated systems are usually best described in the framework of lattice-model Hamiltonians, which focus on the most relevant many-body dynamics of the valence electrons. Therefore, we present in Chapter 3 a reformulation of DFT which applies to many-body lattice models.

A.2 Extension to finite temperatures

In the previous section we have reviewed the Hohenberg-Kohn-Sham formulation of DFT, which accounts for the ground-state properties of general many-particle systems. There are, however, a myriad of important physical phenomena which can not be described within a ground-state formalism. For example, phase transitions in magnetic or superconducting materials, the Kondo-effect, and metal-insulator transitions are the consequence of specific qualitative features in the many-body spectral density of the electronic system. These effects therefore manifest themselves at specific temperatures, such as the Curie or Néel ordering temperatures in ferromagnets and antiferromagnets or the Kondo temperature for magnetic impurities in metals. Consequently, an extension of the scope of DFT in order to describe the properties of many-particle systems at finite temperatures is indispensable. In fact, shortly after its publication, Mermin [6] demonstrated a finite-temperature version of the fundamental HK theorem, in whose framework it is possible to determine the temperature dependence of the equilibrium properties of a general many-particle system. A finite-temperature formulation of the KS scheme for mixed-states or ensembles had already been provided by Kohn and Sham [3]. Despite some efforts to obtain sound approximations to the functionals involved in Mermin's theory [90, 91], no practical implementation of this method is available so far. However, a number of less rigorous approaches, for example, the functional-integral spin-fluctuation theory [143, 144], or a combination of the LDA and dynamical mean-field theory (DMFT), have been proposed in order to describe remarkable finite-temperature effects such as the magnetism in iron and nickel [145]. In the following we present the foundations of finite-temperature density functional theory (FT-DFT), including the fundamental Mermin theorem in Section A.2.1 and the finite-temperature KS scheme in Section A.2.2.

A.2.1 The Mermin theorem

In contrast to the ground-state formalism of the preceding section, the state of a system at a finite temperature $T > 0$ cannot be described by a pure state but instead by a mixed state. Mixed states are characterized by their density matrix $\hat{\rho}$, which is a hermitian positive semidefinite operator. As such, $\hat{\rho}$ can be expressed in terms of its eigenvalues p_n and orthonormal eigenstates $|\Psi_n\rangle$ in the form

$$\hat{\rho} = \sum_n p_n |\Psi_n\rangle\langle\Psi_n| \quad \text{with} \quad p_n \geq 0 \quad \text{and} \quad \text{Tr}\{\hat{\rho}\} = \sum_n p_n = 1\,, \tag{A.37}$$

where Tr indicates the trace in the corresponding Fock space containing all states with arbitrary particle number. The eigenvalue p_n of the density matrix $\hat{\rho}$ represents the probability of finding the system in the eigenstate $|\Psi_n\rangle$. The sums in Eq. (A.37) go over the complete set of eigenstates, which are not restricted to a fixed particle number. The expectation value of any observable $\hat{O}$ can be expressed in terms of the density matrix $\hat{\rho}$ as

$$O = \text{Tr}\{\hat{\rho}\,\hat{O}\} = \sum_n p_n \langle\Psi_n|\hat{O}|\Psi_n\rangle\,. \tag{A.38}$$

In the following we consider a system which is open with respect to exchange of energy and particles with the environment, where the latter is characterized by a fixed temperature T and chemical potential μ. Before we formulate the Mermin theorem, let us first record Gibbs variational principle for the grand potential, which is the finite-temperature analog of the Rayleigh-Ritz variational principle (A.20) for the ground-state energy. To this aim we consider the functional

$$\Omega[\hat{\rho}] = \text{Tr}\left\{\hat{\rho}\left(\hat{H} + \frac{1}{\beta}\log\hat{\rho} - \mu\hat{N}\right)\right\}, \tag{A.39}$$

where $\hat{H}$ is the Hamiltonian (A.1) of the electronic problem under consideration, which is characterized by the external potential $v(\boldsymbol{r})$. Furthermore, $\beta = (k_{\text{B}}T)^{-1}$ with the Boltzmann constant k_{B}, and

$$\hat{N} = \sum_\sigma \int \hat{\psi}_\sigma^\dagger(\boldsymbol{r})\,\hat{\psi}_\sigma(\boldsymbol{r})\,\text{d}\boldsymbol{r} = \int \hat{n}(\boldsymbol{r})\,\text{d}\boldsymbol{r} \tag{A.40}$$

is the operator counting the number of particles. Gibbs variational principle states that the grand potential is given by

$$\Omega_0 = \min_{\hat{\rho}\in\mathcal{P}} \Omega[\hat{\rho}]\,, \tag{A.41}$$

where the minimization is performed within the set $\mathcal{P}$ of all density matrices of the form (A.37), i.e., within the set of all positive semidefinite density matrices with unit

trace. It is easy to show that the functional (A.39) has a local minimum at the grand-canonical density matrix

$$\hat{\rho}_0 = \frac{e^{-\beta(\hat{H}-\mu\hat{N})}}{\text{Tr}\left\{e^{-\beta(\hat{H}-\mu\hat{N})}\right\}} , \tag{A.42}$$

and Mermin [6] has demonstrated that this minimum is unique and global, i. e., that the strict inequality

$$\Omega[\hat{\rho}] > \Omega[\hat{\rho}_0] = \Omega_0, \quad \hat{\rho} \neq \hat{\rho}_0 \tag{A.43}$$

holds for any density matrix $\hat{\rho} \in \mathcal{P}$ different from $\hat{\rho}_0$. With these preliminaries it is now straight forward to prove the following fundamental statement.

Theorem A.3 (Mermin [6])**.** *For any fixed temperature $T > 0$ and chemical potential μ, the external potential $v(\boldsymbol{r})$ of a many-particle system is a functional of the equilibrium particle density $n(\boldsymbol{r})$.*

Proof. The proof is carried out in close analogy to the one shown for the HK Theorem A.1. Suppose, there would be *another* external potential $v'(\boldsymbol{r})$ different from $v(\boldsymbol{r})$ which, at the given temperature T and chemical potential μ, gives rise to the *same* equilibrium density $n(\boldsymbol{r})$ as $v(\boldsymbol{r})$. If $\hat{H}' = \hat{K} + \hat{V}' + \hat{W}$ and $\hat{\rho}_0'$ denote the Hamiltonian and grand-canonical density matrix of the system with the external potential $v'(\boldsymbol{r})$, the corresponding grand potential is given by

$$\Omega_0' = \int v'(\boldsymbol{r}) \, n(\boldsymbol{r}) \, \mathrm{d}\boldsymbol{r} + \text{Tr}\left\{\hat{\rho}_0'\left(\hat{K} + \hat{W} + \frac{1}{\beta}\log\hat{\rho}_0' - \mu\hat{N}\right)\right\} . \tag{A.44}$$

Here we have used that, by our assumption, the average external-potential energy is given by

$$V' = \text{Tr}\{\hat{\rho}_0' \, \hat{V}'\} = \int v'(\boldsymbol{r}) \, \text{Tr}\{\hat{\rho}_0' \, \hat{n}(\boldsymbol{r})\} \, \mathrm{d}\boldsymbol{r} = \int v'(\boldsymbol{r}) \, n(\boldsymbol{r}) \, \mathrm{d}\boldsymbol{r} . \tag{A.45}$$

Since the potentials $v(\boldsymbol{r})$ and $v'(\boldsymbol{r})$ are by assumption different from each other, the associated grand-canonical density matrices $\hat{\rho}_0$ and $\hat{\rho}_0'$ must differ as well.[3] Thus, from the minimal principle (A.43) it follows that

$$\Omega_0 < \Omega[\hat{\rho}_0'] = \text{Tr}\left\{\hat{\rho}_0'\left(\hat{H} + \frac{1}{\beta}\log\hat{\rho}_0' - \mu\hat{N}\right)\right\} = \Omega_0' + \text{Tr}\{\hat{\rho}_0'\,(\hat{V} - \hat{V}')\} =$$
$$= \Omega_0' + \int \left[v(\boldsymbol{r}) - v'(\boldsymbol{r})\right] n(\boldsymbol{r}) \, \mathrm{d}\boldsymbol{r} . \tag{A.46}$$

---

[3]Notice that the grand-canonical density matrices $\hat{\rho}_0$ and $\hat{\rho}_0'$ are different from each other even in the case where the external potentials $v(\boldsymbol{r})$ and $v'(\boldsymbol{r})$ only differ by a constant energy shift. The grand-canonical density matrix given in Eq. (A.42) depends on $v(\boldsymbol{r}) - \mu$ and therefore, once the chemical potential μ is fixed, there is no ambiguity with respect to a constant energy shift.

By interchanging primed and unprimed quantities one obtains

$$\Omega_0' < \Omega_0 + \int \left[v'(\boldsymbol{r}) - v(\boldsymbol{r})\right] n(\boldsymbol{r}) \, \mathrm{d}\boldsymbol{r} \, . \tag{A.47}$$

Adding Eqs. (A.46) and (A.47) the contradiction

$$\Omega_0 + \Omega_0' < \Omega_0' + \Omega_0 \tag{A.48}$$

is obtained, which proves that two different potentials $v(\boldsymbol{r})$ and $v'(\boldsymbol{r})$ cannot yield the same equilibrium density $n(\boldsymbol{r})$ at a given temperature $T > 0$ and chemical potential μ. Therefore, $v(\boldsymbol{r})$ is a functional of $n(\boldsymbol{r})$. $\qquad\square$

The Mermin theorem states that for a given temperature $T > 0$ and chemical potential μ the external potential $v(\boldsymbol{r})$ is a functional of the equilibrium density $n(\boldsymbol{r})$. Consequently, if the type of interaction defined by $w(\boldsymbol{r}, \boldsymbol{r}')$ is fixed, the full Hamiltonian $\hat{H}$ and all physical properties derived from it must be functionals of the equilibrium density as well. This applies in particular to the grand-canonical density matrix (A.42), which immediately proves the important

Corollary A.3. *For any fixed temperature $T > 0$ and chemical potential μ, the grand-canonical density matrix $\hat{\rho}_0$ is a functional of the equilibrium particle density $n(\boldsymbol{r})$.*

Notice that the converse statement is also true, since the equilibrium density $n(\boldsymbol{r}) = \mathrm{Tr}\{\hat{\rho}_0 \, \hat{n}(\boldsymbol{r})\}$ is a functional of the grand-canonical density matrix $\hat{\rho}_0$. A further important consequence of the Mermin theorem is

Corollary A.4. *For a fixed temperature $T > 0$ and chemical potential μ, the equilibrium average value of any observable $\hat{O}$ is a functional of the equilibrium particle-density $n(\boldsymbol{r})$.*

Proof. From Corollary A.3 we know that for any temperature $T > 0$ and chemical potential μ the grand-canonical density matrix $\hat{\rho}_0 = \hat{\rho}_0[n(\boldsymbol{r})]$ is a functional of the equilibrium particle-density $n(\boldsymbol{r})$. Therefore, the equilibrium average-value of any observable $\hat{O}$ can be obtained from the equilibrium particle-density as

$$O[n(\boldsymbol{r})] = \mathrm{Tr}\{\hat{\rho}_0[n(\boldsymbol{r})] \, \hat{O}\} \, . \tag{A.49}$$

$\qquad\square$

Similar to the ground-state formalism presented in Section A.1, the formulation of FT-DFT requires the construction of a density functional from which the equilibrium density $n(\boldsymbol{r})$ can be obtained by means of a variational principle. We will derive such

a functional by using a constrained search method, which is analogous to the LL formulation of Section A.1.2. This will allow us to bypass all problems related to the representability of equilibrium densities $n(r)$. To this aim we introduce the functional

$$G[n(r)] = \min_{\hat\rho \to n(r)} \mathrm{Tr}\left\{\hat\rho \left(\hat K + \hat W + \frac{1}{\beta} \log \hat\rho\right)\right\},$$
(A.50)

where the notation $\hat\rho \to n(r)$ indicates the minimization with respect to all density matrices $\hat\rho \in \mathcal{P}$ which yield the given density via

$$n(r) = \mathrm{Tr}\{\hat\rho\, \hat n(r)\} = \sum_n p_n \langle \Psi_n | \hat n(r) | \Psi_n \rangle .$$
(A.51)

This means, the functional (A.50) is defined on the set of the density functions $n(r)$, which, via Eq. (A.51), can be associated with *some* density matrix $\hat\rho \in \mathcal{P}$. This type of functions $n(r)$ is called *ensemble representable*, and we denote the set of all ensemble-representable functions by $\mathcal{N}_e$. The question of how ensemble-representable density functions are characterized is easily answered by noting that, according to Eq. (A.51), any $n(r) \in \mathcal{N}_e$ can be expressed as a linear combination of pure-state N-representable density functions $\langle \Psi_n | \hat n(r) | \Psi_n \rangle \in \mathcal{N}_N$ with non-negative coefficients $p_n \geq 0$. Thus, we conclude that $\mathcal{N}_e$ must contain all real valued, non-negative functions, since the sets $\mathcal{N}_N$ with $N \in \mathbb{N}_0$ contain all real valued, non-negative functions that integrate to N, as already discussed in Section A.1.2. The functional (A.50) is valid for arbitrary non-negative particle numbers $N = \int n(r)\,\mathrm{d}r$, and it is universal in the sense that it does not depend on the external potential $v(r)$.

Using the functional $G[n(r)]$, given by Eq. (A.50), we can now define the grand potential density-functional

$$\Omega_v[n(r)] = \int [v(r) - \mu]\, n(r) + G[n(r)] .$$
(A.52)

The minimal value of the functional $\Omega_v[n(r)]$ within the set $\mathcal{N}_e$ of ensemble-representable density functions equals the grand potential Ω_0. This can be most easily seen by performing the minimization in the Gibbs variational principle (A.41) in two consecutive steps:

$$\Omega_0 = \min_{\hat\rho \in \mathcal{P}} \mathrm{Tr}\left\{\hat\rho \left(\hat H + \frac{1}{\beta} \log \hat\rho - \mu \hat N\right)\right\} =$$

$$= \min_{n(r) \in \mathcal{N}_e} \left[\int [v(r) - \mu]\, n(r)\,\mathrm{d}r + \min_{\hat\rho \to n(r)} \mathrm{Tr}\left\{\hat\rho \left(\hat K + \hat W + \frac{1}{\beta} \log \hat\rho\right)\right\}\right] = \quad \text{(A.53)}$$

$$= \min_{n(r) \in \mathcal{N}_e} \left[\int [v(r) - \mu]\, n(r)\,\mathrm{d}r + G[n(r)]\right] = \min_{n(r) \in \mathcal{N}_e} \Omega_v[n(r)] .$$

Furthermore, from Eq. (A.43) it follows that the density matrix $\hat{\rho}$ which yields the minimum in Eq. (A.53) is the grand-canonical density matrix (A.42) associated with the given external potential $v(\boldsymbol{r})$, temperature T and chemical potential μ. Consequently, the minimizing density $n(\boldsymbol{r})$ must be the equilibrium density of the system.

A.2.2 Finite-temperature Kohn-Sham scheme

In order to formulate a finite-temperature extension of the KS scheme, we seek for an auxiliary noninteracting system described by the single-particle Hamiltonian (A.22) with an external potential $v_s(\boldsymbol{r})$, which is chosen such that the corresponding equilibrium density $n(\boldsymbol{r})$ equals the equilibrium density of the interacting system with the external potential $v(\boldsymbol{r})$. Once the existence of $v_s(\boldsymbol{r})$ is granted, its uniqueness follows from the Mermin Theorem A.3.

For a noninteracting system with external potential $v_s(\boldsymbol{r})$, the equilibrium particle density at a given temperature T and chemical potential μ is given by

$$n(\boldsymbol{r}) = \sum_i \frac{|\phi_i(\boldsymbol{r})|^2}{1 + e^{\beta(\varepsilon_i - \mu)}}, \tag{A.54}$$

where $\phi_i(\boldsymbol{r})$ and ε_i are the solutions and corresponding eigenvalues of the single-particle Schrödinger equation

$$\left[-\frac{\hbar^2}{2m} \nabla^2 + v_s(\boldsymbol{r}) \right] \phi_i(\boldsymbol{r}) = \varepsilon_i \, \phi_i(\boldsymbol{r}) . \tag{A.55}$$

From Corollary A.4 we know that the grand-canonical density matrix $\hat{\rho}_s$ of the noninteracting system, and thus the corresponding average values of all physical observables are functionals of the equilibrium density $n(\boldsymbol{r})$. Consequently, the noninteracting kinetic energy

$$K_s[n(\boldsymbol{r})] = \text{Tr}\big\{ \hat{\rho}_s[n(\boldsymbol{r})] \, \hat{K} \big\} \tag{A.56}$$

and the noninteracting entropy

$$S_s[n(\boldsymbol{r})] = -k_\text{B} \text{Tr}\big\{ \hat{\rho}_s[n(\boldsymbol{r})] \, \log \hat{\rho}_s[n(\boldsymbol{r})] \big\} \tag{A.57}$$

are universal functionals of the equilibrium density $n(\boldsymbol{r})$.

In order to find the potential $v_s(\boldsymbol{r})$ which characterizes the noninteracting system whose equilibrium density $n(\boldsymbol{r})$ equals the one of the interacting system under consideration, we write the functional (A.50) in the form

$$G[n(\boldsymbol{r})] = G_s[n(\boldsymbol{r})] + \frac{1}{2} \int n(\boldsymbol{r}) \, w(\boldsymbol{r}, \boldsymbol{r}') \, n(\boldsymbol{r}') \, \mathrm{d}\boldsymbol{r} \, \mathrm{d}\boldsymbol{r}' + G_\text{xc}[n(\boldsymbol{r})] , \tag{A.58}$$

where $G_s[n(r)] = K_s[n(r)] - TS_s[n(r)]$, and $G_{xc}[n(r)]$ is the XC contribution to the free energy of interacting electrons with equilibrium density $n(r)$. Thus, $G_{xc}[n(r)]$ includes the contribution to $G[n(r)]$ resulting from XC effects on the Coulomb-interaction energy W, the kinetic energy K, and the entropy $S = -k_B \text{Tr}\{\hat{\rho} \log \hat{\rho}\}$. The grand potential density-functional $\Omega_v[n(r)]$, defined in Eq. (A.52), assumes its minimal value at the actual equilibrium density, and the corresponding stationary condition reads

$$\frac{\delta\Omega_v[n(r)]}{\delta n(r)} = \frac{\delta G[n(r)]}{\delta n(r)} + v(r) - \mu = 0 \,. \tag{A.59}$$

Writing $G[n(r)]$ in the form (A.58), we obtain

$$\frac{\delta G_s[n(r)]}{\delta n(r)} + v_s([n]; r) - \mu = 0 \tag{A.60}$$

with

$$v_s([n]; r) = v(r) + \int n(r')\, w(r, r')\, dr' + \mu_{xc}([n]; r) \tag{A.61}$$

and

$$\mu_{xc}([n]; r) = \frac{\delta G_{xc}[n(r)]}{\delta n(r)} \,. \tag{A.62}$$

Equation (A.60) is formally the same condition one would obtain for a system of non-interacting particles moving in the effective potential $v_s([n]; r)$. Therefore, we identify $v_s([n]; r)$ as the unique external potential, for which the noninteracting system (A.22) yields the same equilibrium density $n(r)$ as the interacting system in the presence of the external potential $v(r)$. Equations (A.54), (A.55), and (A.61) define the finite temperature KS-scheme. Due to the fact that the effective single-particle potential (A.61) explicitly depends on the density $n(r)$, it must be solved in a selfconsistent way which is analogous to the ground-state procedure described in Section A.1.3.

Hartree-Fock approximation for the interaction-energy functional

<div align="right">

B

</div>

Within the Hartree-Fock method, one assumes that the ground state $|\Psi_0\rangle$ of an interacting many-body system can be approximated by a single Slater determinant. Consequently, one seeks for the Slater determinant

$$|\boldsymbol{n}\rangle = \prod_{\alpha\sigma} \left(\hat{b}_{\alpha\sigma}^\dagger\right)^{n_{\alpha\sigma}} |\text{vac}\rangle \quad \text{with} \quad n_{\alpha\sigma} \in \{0, 1\}, \tag{B.1}$$

which yields the minimal value of the total energy $\langle\hat{H}\rangle = \langle\hat{K}\rangle + \langle\hat{W}\rangle$. Here, the operators $\hat{b}_{\alpha\sigma}^\dagger$ correspond to a complete, yet to be determined, set of single-particle states $\{\varphi_{\alpha\sigma}(\boldsymbol{r})\}$, and $\boldsymbol{n} = \{n_{\alpha\sigma}\}$ represents the corresponding occupation numbers. The minimization procedure in the Hartree-Fock approximation requires one to compute the average value of the two-particle operator

$$\hat{W} = \sum_{\substack{ijkl \\ \sigma\sigma'}} W_{ijkl}^{\sigma\sigma'} \, \hat{c}_{i\sigma}^\dagger \hat{c}_{j\sigma'}^\dagger \hat{c}_{l\sigma'} \hat{c}_{k\sigma}, \tag{B.2}$$

which represents the interaction between the particles. Therefore, we aim to derive an explicit expression for the interaction energy $W = \langle\boldsymbol{n}|\hat{W}|\boldsymbol{n}\rangle$ of a Slater determinant (B.1) in terms of the corresponding single-particle density matrix (SPDM) $\boldsymbol{\gamma}$. Since the operators $\hat{b}_{\alpha\sigma}^\dagger$ in Eq. (B.1) correspond to a complete set of single-particle states, we can expand the operators $\hat{c}_{i\sigma}^\dagger$ which appear in Eq. (B.2) as

$$\hat{c}_{i\sigma}^\dagger = \sum_\alpha u_{i\alpha\sigma} \, \hat{b}_{\alpha\sigma}^\dagger, \tag{B.3}$$

with some coefficients $u_{i\alpha\sigma} \in \mathbb{C}$. Using this relation together with the fact that for a Slater determinant it holds

$$\langle\boldsymbol{n}|\hat{b}_{\alpha\sigma}^\dagger \hat{b}_{\beta\sigma}|\boldsymbol{n}\rangle = \delta_{\alpha\beta} \langle\boldsymbol{n}|\hat{n}_{\alpha\sigma}|\boldsymbol{n}\rangle = \delta_{\alpha\beta} \, n_{\alpha\sigma}, \tag{B.4}$$

one obtains the SPDM of a Slater determinant as

$$\gamma_{ij\sigma} = \langle\boldsymbol{n}|\hat{c}_{i\sigma}^\dagger \hat{c}_{j\sigma}|\boldsymbol{n}\rangle = \sum_{\alpha\beta} u_{i\alpha\sigma} u_{j\beta\sigma}^* \langle\boldsymbol{n}|\hat{b}_{\alpha\sigma}^\dagger \hat{b}_{\beta\sigma}|\boldsymbol{n}\rangle = \sum_\alpha u_{i\alpha\sigma} \, n_{\alpha\sigma} \, u_{j\alpha\sigma}^*. \tag{B.5}$$

Furthermore, using Eq. (B.3) one obtains

$$
\hat{c}^\dagger_{i\sigma} \hat{c}^\dagger_{j\sigma'} \hat{c}_{l\sigma'} \hat{c}_{k\sigma} = \sum_{\alpha\beta\gamma\delta} u_{i\alpha\sigma}\, u_{j\beta\sigma'}\, u^*_{l\delta\sigma'}\, u^*_{k\gamma\sigma}\, \hat{b}^\dagger_{\alpha\sigma} \hat{b}^\dagger_{\beta\sigma'} \hat{b}_{\delta\sigma'} \hat{b}_{\gamma\sigma}\,,
\tag{B.6}
$$

and from the definition (B.1) of a Slater determinant $|\boldsymbol{n}\rangle$ it follows that

$$
\langle \boldsymbol{n}| \hat{n}_{\alpha\sigma} \hat{n}_{\beta\sigma'} |\boldsymbol{n}\rangle = n_{\alpha\sigma} n_{\beta\sigma'}\,.
\tag{B.7}
$$

Thus, it is easy to verify that

$$
\langle \boldsymbol{n}| \hat{b}^\dagger_{\alpha\sigma} \hat{b}^\dagger_{\beta\sigma'} \hat{b}_{\delta\sigma'} \hat{b}_{\gamma\sigma} |\boldsymbol{n}\rangle = n_{\alpha\sigma}\, n_{\beta\sigma'} \left(\delta_{\alpha\gamma}\, \delta_{\beta\delta} - \delta_{\sigma\sigma'}\, \delta_{\alpha\delta}\, \delta_{\beta\gamma} \right).
\tag{B.8}
$$

Combining this relation with Eq. (B.6), one obtains

$$
\langle \boldsymbol{n}| \hat{c}^\dagger_{i\sigma} \hat{c}^\dagger_{j\sigma'} \hat{c}_{l\sigma'} \hat{c}_{k\sigma} |\boldsymbol{n}\rangle = \sum_{\alpha\beta} u_{i\alpha\sigma}\, u_{j\beta\sigma'}\, u^*_{l\beta\sigma'}\, u^*_{k\alpha\sigma}\, n_{\alpha\sigma}\, n_{\beta\sigma'} -
$$

$$
- \delta_{\sigma\sigma'} \sum_{\alpha\beta} u_{i\alpha\sigma}\, u_{j\beta\sigma}\, u^*_{l\alpha\sigma}\, u^*_{k\beta\sigma}\, n_{\alpha\sigma}\, n_{\beta\sigma} \overset{\text{(B.5)}}{=}
\tag{B.9}
$$

$$
= \gamma_{ik\sigma}\, \gamma_{jl\sigma'} - \delta_{\sigma\sigma'}\, \gamma_{il\sigma}\, \gamma_{jk\sigma}\,.
$$

Finally, replacing this result in Eq. (B.2), one obtains the interaction-energy functional in Hartree-Fock approximation as

$$
W_{\mathrm{HF}}[\boldsymbol{\gamma}] = \langle \boldsymbol{n}| \hat{W} |\boldsymbol{n}\rangle = \sum_{\substack{ijkl \\ \sigma\sigma'}} W^{\sigma\sigma'}_{ijkl} \left(\gamma_{ik\sigma}\, \gamma_{jl\sigma'} - \delta_{\sigma\sigma'}\, \gamma_{il\sigma}\, \gamma_{jk\sigma} \right).
\tag{B.10}
$$

In this thesis we refer to Eq. (B.10) as Hartree-Fock approximation for the interaction-energy functional $W[\boldsymbol{\gamma}]$. It is, however, worth noting that this expression is far more general than the usual self-consistent Hartree-Fock (HF) energy, since it corresponds to the exact interaction energy of any Slater determinant yielding the given SPDM $\boldsymbol{\gamma}$.

Uncorrelated mixed-states

In the following we would like to demonstrate that $W_{\mathrm{HF}}[\boldsymbol{\gamma}]$, as given in Eq. (B.10), represents the exact interaction-energy functional not only for pure Slater determinants, but also for an uncorrelated superposition of Slater determinants. By this we mean a special kind of mixed state, which is described by a density matrix of the form

$$
\hat{\rho} = \prod_{\alpha\sigma} p_{\alpha\sigma}(\hat{n}_{\alpha\sigma}) \quad \text{with} \quad p_{\alpha\sigma}(n) = \eta^n_{\alpha\sigma} (1 - \eta_{\alpha\sigma})^{1-n}\,, \quad \eta_{\alpha\sigma} \in [0,1] \quad \forall \alpha\sigma\,.
\tag{B.11}
$$

In Eq. (B.20) below we will demonstrate that the numbers $\eta_{\alpha\sigma}$ represent the average occupation of the orbitals $\varphi_{\alpha\sigma}(\boldsymbol{r})$, i. e., $\eta_{\alpha\sigma}$ is the probability of finding the corresponding orbital occupied in the mixed state described by $\hat{\rho}$. Clearly, the eigenstates of $\hat{\rho}$ are the Slater-determinants $|\boldsymbol{n}\rangle$ defined in Eq. (B.1), and for the corresponding eigenvalues

$$p(\boldsymbol{n}) = \prod_{\alpha\sigma} p_{\alpha\sigma}(n_{\alpha\sigma}) \tag{B.12}$$

it holds $0 \le p(\boldsymbol{n}) \le 1$, which means that $\hat{\rho}$ is positive semidefinite. Furthermore, if we take the Slater determinants (B.1) as basis of the underlying Fock space, it is easy to verify that $\hat{\rho}$ is properly normalized:

$$\mathrm{Tr}\{\hat{\rho}\} = \sum_{n_{1\uparrow}=0}^{1} \sum_{n_{1\downarrow}=0}^{1} \cdots \prod_{\alpha\sigma} p_{\alpha\sigma}(n_{\alpha\sigma}) = \prod_{\alpha\sigma} \sum_{n=0}^{1} p_{\alpha\sigma}(n) = 1 \,. \tag{B.13}$$

Here we have used that $p_{\alpha\sigma}(0) + p_{\alpha\sigma}(1) = 1$ for all $\alpha\sigma$, according to Eq. (B.11). Notice that $\hat{\rho}$ has unit trace in Fock space and not in the N-particle Hilbert space which is relevant in a canonical-ensemble formalism. A density matrix of the form (B.11) would not represent a proper mixed state when working in a canonical ensemble, since its eigenstates do not have a fixed particle number N, and furthermore, since it does not has unit trace in N-particle Hilbert space. We refer to a state described by a density matrix $\hat{\rho}$ of the form (B.11) as *uncorrelated mixed-state*, since its eigenstates are single Slater determinants and the corresponding occupation numbers $n_{\alpha\sigma}$ are uncorrelated due to the product form (B.12) of the eigenvalues $p(\boldsymbol{n})$, which represent the probability for the corresponding occupation-number configuration $\boldsymbol{n} = \{n_{\alpha\sigma}\}$.

One prominent example of an uncorrelated mixed-state is the grand-canonical thermal-equilibrium state of a non-interacting system described by the Hamiltonian

$$\hat{H}_0 = \sum_{\alpha\sigma} \varepsilon_{\alpha\sigma} \, \hat{n}_{\alpha\sigma} \,, \tag{B.14}$$

whose grand-canonical density matrix is given by

$$\hat{\rho}_0 = \frac{\mathrm{e}^{-\beta(\hat{H}_0 - \sum_\sigma \mu_\sigma \hat{N}_\sigma)}}{\mathrm{Tr}\{\mathrm{e}^{-\beta(\hat{H}_0 - \sum_\sigma \mu_\sigma \hat{N}_\sigma)}\}} = \prod_{\alpha\sigma} \frac{\mathrm{e}^{-\beta(\varepsilon_{\alpha\sigma}-\mu_\sigma)\,\hat{n}_{\alpha\sigma}}}{1 + \mathrm{e}^{-\beta(\varepsilon_{\alpha\sigma}-\mu_\sigma)}} = \prod_{\alpha\sigma} p_{\alpha\sigma}(\hat{n}_{\alpha\sigma}) \tag{B.15}$$

with

$$p_{\alpha\sigma}(n) = \eta_{\alpha\sigma}^{n} \, (1 - \eta_{\alpha\sigma})^{1-n} \quad \text{and} \quad \eta_{\alpha\sigma} = \frac{1}{1 + \mathrm{e}^{\beta(\varepsilon_{\alpha\sigma}-\mu_\sigma)}} \,. \tag{B.16}$$

In Eq. (B.15) we have used the well-known grand-canonical partition function of a non-interacting system described the Hamiltonian (B.14)

$$Z = \mathrm{Tr}\{\mathrm{e}^{-\beta(\hat{H}_0 - \sum_\sigma \mu_\sigma \hat{N}_\sigma)}\} = \prod_{\alpha\sigma} \left(1 + \mathrm{e}^{-\beta(\varepsilon_{\alpha\sigma}-\mu_\sigma)}\right) . \tag{B.17}$$

More generally, uncorrelated mixed-states yield the maximal value of the entropy $S = -\text{Tr}\{\hat{\rho} \log \hat{\rho}\}$ for a given distribution of the average occupation numbers $\eta_{\alpha\sigma} = \text{Tr}\{\hat{\rho}\,\hat{n}_{\alpha\sigma}\}$. In order to prove this statement, we seek for the minimum of the Euler-Lagrange functional which corresponds to the negative entropy

$$\mathcal{L}[\hat{\rho}] = \text{Tr}\{\hat{\rho} \log \hat{\rho}\} + \sum_{\alpha\sigma} \varepsilon_{\alpha\sigma} \left(\text{Tr}\{\hat{\rho}\,\hat{n}_{\alpha\sigma}\} - \eta_{\alpha\sigma} \right) =$$

$$= \text{Tr}\left\{ \hat{\rho} \left(\sum_{\alpha\sigma} \varepsilon_{\alpha\sigma}\,\hat{n}_{\alpha\sigma} + \log \hat{\rho} \right) \right\} - \sum_{\alpha\sigma} \varepsilon_{\alpha\sigma}\,\eta_{\alpha\sigma} ,$$

(B.18)

where the Lagrange multipliers $\varepsilon_{\alpha\sigma}$ enforce the condition that the minimizing density matrix $\hat{\rho}$ yields the desired average occupation numbers $\eta_{\alpha\sigma} \in [0, 1]$. Apart from an irrelevant constant, Eq. (B.18) equals the Gibbs functional (3.43) with $\beta = 1$, $\mu_{\sigma} = 0$, and the non-interacting Hamiltonian (B.14). Consequently, the minimum of $\mathcal{L}[\hat{\rho}]$ within the set $\mathcal{P}$ of all positive semidefinite density matrices $\hat{\rho}$ with unit trace is taken for the corresponding grand-canonical density matrix $\hat{\rho}_0 = \text{e}^{-\hat{H}_0}/\text{Tr}\{\text{e}^{-\hat{H}_0}\}$. Thus, $\hat{\rho}_0$ is the mixed state which yields the maximal entropy for the given average occupation numbers $\eta_{\alpha\sigma}$, and in the context of Eq. (B.15) we have already seen that $\hat{\rho}_0$ represents an uncorrelated mixed-state.

In order to show that Eq. (B.10) represents the exact interaction-energy functional for uncorrelated mixed-states, we mainly have to demonstrate that the analog of Eq. (B.7)

$$\text{Tr}\{\hat{\rho}\,\hat{n}_{\alpha\sigma}\hat{n}_{\beta\sigma'}\} = \text{Tr}\{\hat{\rho}\,\hat{n}_{\alpha\sigma}\} \, \text{Tr}\{\hat{\rho}\,\hat{n}_{\beta\sigma'}\}$$

(B.19)

holds for any density matrix $\hat{\rho}$ of the form (B.11). This is most easily seen by taking the Slater determinants (B.1) as basis of the underlying Fock space. In this way one obtains

$$\text{Tr}\{\hat{\rho}\,\hat{n}_{\alpha\sigma}\} = \sum_{n_{1\uparrow}=0}^{1} \sum_{n_{1\downarrow}=0}^{1} \cdots n_{\alpha\sigma} \prod_{\beta\sigma'} p_{\beta\sigma'}(n_{\beta\sigma'}) =$$

$$= p_{\alpha\sigma}(1) \prod_{\beta\sigma'\neq\alpha\sigma} \sum_{n=0}^{1} p_{\beta\sigma'}(n) = p_{\alpha\sigma}(1) = \eta_{\alpha\sigma} ,$$

(B.20)

and similarly

$$\text{Tr}\{\hat{\rho}\,\hat{n}_{\alpha\sigma}\hat{n}_{\beta\sigma'}\} = \sum_{n_{1\uparrow}=0}^{1} \sum_{n_{1\downarrow}=0}^{1} \cdots n_{\alpha\sigma}n_{\beta\sigma'} \prod_{\gamma\sigma''} p_{\gamma\sigma''}(n_{\gamma\sigma''}) =$$

$$= p_{\alpha\sigma}(1)\,p_{\beta\sigma'}(1) \prod_{\gamma\sigma''\neq\alpha\sigma,\beta\sigma'} \sum_{n=0}^{1} p_{\gamma\sigma''}(n) = p_{\alpha\sigma}(1)\,p_{\beta\sigma'}(1) = \eta_{\alpha\sigma}\,\eta_{\beta\sigma'} .$$

(B.21)

Finally, using this relation and the substitutions

$$n_{\alpha\sigma} \to \eta_{\alpha\sigma} \quad \text{and} \quad \langle \boldsymbol{n}|\hat{O}|\boldsymbol{n}\rangle \to \text{Tr}\{\hat{\rho}\,\hat{O}\} \tag{B.22}$$

in Eqs. (B.4) to (B.10), it follows that Eq. (B.10) is the interaction energy functional for uncorrelated mixed-states. In particular, since the grand-canonical density matrix (B.15) of any non-interacting system describes an uncorrelated mixed-state, we conclude that $W_{\text{HF}}[\boldsymbol{\gamma}]$, as given in Eq. (B.10), represents the average interaction energy $W = \text{Tr}\{\hat{\rho}_0\,\hat{W}\}$ in the thermal-equilibrium state $\hat{\rho}_0$ of the unique non-interacting system whose grand-canonical equilibrium single-particle density matrix (eq-SPDM) equals $\boldsymbol{\gamma}$. However, since an uncorrelated mixed-state does not correspond to a fixed particle number, the equivalent statement is not true if one works in a canonical ensemble.

Minimal principle of the Helmholtz functional $F[\hat{\rho}]$

<div align="right">

C
</div>

We wish to demonstrate that the Helmholtz functional

$$F[\hat{\rho}] = \mathrm{Tr}_N\left\{\hat{\rho}\left(\hat{H} + \frac{1}{\beta}\log\hat{\rho}\right)\right\} \tag{C.1}$$

satisfies the strict minimal principle

$$F[\hat{\rho}] > F[\hat{\rho}_N], \quad \hat{\rho} \neq \hat{\rho}_N \tag{C.2}$$

for all positive semidefinite N-particle density matrices with unit trace $\hat{\rho} \in \mathcal{P}_N$, as defined in Eq. (3.17). Here, the canonical density matrix $\hat{\rho}_N$ is given by

$$\hat{\rho}_N = \frac{\mathrm{e}^{-\beta\hat{H}}}{\mathrm{Tr}_N\left\{\mathrm{e}^{-\beta\hat{H}}\right\}} . \tag{C.3}$$

We start by demonstrating that $\hat{\rho}_N$ is in fact a stationary point of the Helmholtz functional $F[\hat{\rho}]$. To this aim we seek for the extremes of the corresponding Euler-Lagrange functional

$$\mathcal{L}[\hat{\rho}] = \mathrm{Tr}_N\left\{\hat{\rho}\left(\hat{H} + \frac{1}{\beta}\log\hat{\rho}\right)\right\} - \varepsilon\left(\mathrm{Tr}_N\{\hat{\rho}\} - 1\right), \tag{C.4}$$

where we have introduced the Lagrange multiplier ε in order to enforce that the minimizing density matrix has unit trace in N-particle Hilbert space. Clearly, if $\hat{\rho}$ is a stationary point of the Euler-Lagrange functional (C.4), its variation

$$\delta\mathcal{L}[\hat{\rho}] = \mathrm{Tr}_N\left\{\delta\hat{\rho}\left(\hat{H} + \frac{1}{\beta}\left(\log\hat{\rho} + 1\right) - \varepsilon\right)\right\} \tag{C.5}$$

must vanish for any infinitesimal $\delta\hat{\rho}$ with $\mathrm{Tr}\{\delta\hat{\rho}\} = 0$. This condition is certainly satisfied if

$$\hat{H} + \frac{1}{\beta}\left(\log\hat{\rho} + 1\right) - \varepsilon = 0 \quad \Rightarrow \quad \hat{\rho} = \frac{\mathrm{e}^{-\beta\hat{H}}}{\mathrm{e}^{1-\beta\varepsilon}} . \tag{C.6}$$

Here, the Lagrange multiplier ε must be chosen such that the condition $\mathrm{Tr}_N\{\hat{\rho}\} = 1$ is satisfied, i.e., we must have $\mathrm{e}^{1-\beta\varepsilon} = \mathrm{Tr}_N\{\mathrm{e}^{-\beta\hat{H}}\}$, which means that $\hat{\rho}_N$, as given in Eq. (C.3), is in fact a stationary point of the Helmholtz functional (C.1) within $\mathcal{P}_N$.

In order to demonstrate that the Helmholtz functional (C.1) is bounded below by $F[\hat{\rho}_N]$, i.e., that Eq. (C.2) holds, we closely follow the proof of Mermin [6] concerning the analog statement for the Gibbs functional $\Omega[\hat{\rho}]$ defined in Eq. (3.43). Let $\hat{\rho} \in \mathcal{P}_N$ be an arbitrary positive semidefinite density matrix with unit trace, and define for $\lambda \in [0, 1]$

$$\hat{\rho}_\lambda = \frac{e^{-\beta\hat{H}_\lambda}}{\text{Tr}_N\{e^{-\beta\hat{H}_\lambda}\}} \quad \text{with} \quad \hat{H}_\lambda = \hat{H} + \lambda\hat{\Delta} \quad \text{and} \quad \hat{\Delta} = -\left(\hat{H} + \frac{1}{\beta}\log\hat{\rho}\right). \tag{C.7}$$

The operator $\hat{H}_\lambda$ is hermitian since $\hat{\rho}$ is positive semidefinite, and consequently we can regard $\hat{\rho}_\lambda \in \mathcal{P}_N$ as the canonical density matrix of a system described by the auxiliary Hamiltonian $\hat{H}_\lambda$. Furthermore, one has $\hat{\rho}_{\lambda=0} = \hat{\rho}_N$ and $\hat{\rho}_{\lambda=1} = \hat{\rho}$, and consequently we can write

$$F[\hat{\rho}] - F[\hat{\rho}_N] = \int_0^1 \frac{\partial}{\partial\lambda} F[\hat{\rho}_\lambda]\, d\lambda. \tag{C.8}$$

In order to evaluate the derivative we write

$$F[\hat{\rho}_\lambda] = \text{Tr}_N\left\{\hat{\rho}_\lambda\left(\hat{H} + \lambda\hat{\Delta} + \frac{1}{\beta}\log\hat{\rho}_\lambda\right)\right\} - \lambda\,\text{Tr}_N\{\hat{\rho}_\lambda\hat{\Delta}\}. \tag{C.9}$$

Here, the first trace is the Helmholtz functional (C.1) for a system described by the Hamiltonian $\hat{H}_\lambda = \hat{H} + \lambda\hat{\Delta}$, and it is therefore stationary with respect to variations of $\hat{\rho}_\lambda$ around the corresponding canonical density matrix (C.7). Consequently, we need to differentiate the first trace in Eq. (C.9) only with respect to the explicit occurrence of λ, which leads to

$$\frac{\partial}{\partial\lambda} F[\hat{\rho}_\lambda] = -\lambda\,\text{Tr}\left\{\frac{\partial\hat{\rho}_\lambda}{\partial\lambda}\hat{\Delta}\right\}. \tag{C.10}$$

In order to compute the derivative $\partial\hat{\rho}_\lambda/\partial\lambda$ we have to take in to account that $\hat{H}$ in general not commutes with $\hat{\rho}$ and consequently also not with $\hat{\Delta}$. In order to handle this difficulty, we will make use of Feynman's ordering technique [146], i.e., we attach an index to each operator, and it is understood that operators act in order of increasing value of their indices. Thus, for two operators $\hat{A}$ and $\hat{B}$ one has $\hat{A}_s\hat{B}_{s'} = \hat{A}\hat{B}$ if $s > s'$ and $\hat{A}_s\hat{B}_{s'} = \hat{B}\hat{A}$ if $s < s'$. In this way we can apply the rules of ordinary commutative calculus to the operators $\hat{A}_s$ and $\hat{B}_{s'}$. However, in a final step we have to disentangle the operators, before we can drop their indices an return to the usual notation. Using

this technique, one can write

$$
\frac{\partial}{\partial \lambda} \mathrm{e}^{-\beta \hat{H}_\lambda} = \frac{\partial}{\partial \lambda} \mathrm{e}^{-\beta \int_0^1 (\hat{H}_{s'} + \lambda \hat{\Delta}_{s'}) \mathrm{d}s'} =
$$

$$
= -\beta \left(\int_0^1 \hat{\Delta}_s \, \mathrm{d}s \right) \mathrm{e}^{-\beta \int_0^1 (\hat{H}_{s'} + \lambda \hat{\Delta}_{s'}) \mathrm{d}s'} =
$$

$$
= -\beta \int_0^1 \mathrm{d}s \, \mathrm{e}^{-\beta \int_0^s (\hat{H}_{s'} + \lambda \hat{\Delta}_{s'}) \mathrm{d}s'} \, \hat{\Delta}_s \, \mathrm{e}^{-\beta \int_s^1 (\hat{H}_{s'} + \lambda \hat{\Delta}_{s'}) \mathrm{d}s'} =
$$

$$
= -\beta \int_0^1 \mathrm{d}s \, \mathrm{e}^{-\beta s \hat{H}_\lambda} \, \hat{\Delta} \, \mathrm{e}^{-\beta(1-s)\hat{H}_\lambda} \; \overset{\beta'=\beta(1-s)}{=}
$$

$$
= -\mathrm{e}^{-\beta \hat{H}_\lambda} \int_0^\beta \mathrm{d}\beta' \, \hat{\Delta}_\lambda(\beta') , \tag{C.11}
$$

where we have introduced $\hat{\Delta}_\lambda(\beta') = \mathrm{e}^{\beta' \hat{H}_\lambda} \hat{\Delta} \, \mathrm{e}^{-\beta' \hat{H}_\lambda}$. Using this result, one obtains

$$
\frac{\partial \hat{\rho}_\lambda}{\partial \lambda} = \frac{\frac{\partial}{\partial \lambda} \mathrm{e}^{-\beta \hat{H}_\lambda}}{\mathrm{Tr}_N \{ \mathrm{e}^{-\beta \hat{H}_\lambda} \}} - \frac{\mathrm{e}^{-\beta \hat{H}_\lambda}}{\left(\mathrm{Tr}_N \{ \mathrm{e}^{-\beta \hat{H}_\lambda} \} \right)^2} \mathrm{Tr}_N \left\{ \frac{\partial}{\partial \lambda} \mathrm{e}^{-\beta \hat{H}_\lambda} \right\} =
$$

$$
= -\hat{\rho}_\lambda \int_0^\beta \mathrm{d}\beta' \, \hat{\Delta}_\lambda(\beta') + \hat{\rho}_\lambda \int_0^\beta \mathrm{d}\beta' \, \mathrm{Tr}_N \{ \hat{\rho}_\lambda \, \hat{\Delta}_\lambda(\beta') \} . \tag{C.12}
$$

Since $\hat{\rho}_\lambda$ commutes with $\hat{H}_\lambda$, we obtain by cyclically permuting operators within the trace

$$
\langle \hat{\Delta}_\lambda(\beta') \rangle_\lambda = \mathrm{Tr}_N \left\{ \hat{\rho}_\lambda \, \mathrm{e}^{\beta' \hat{H}_\lambda} \, \hat{\Delta} \, \mathrm{e}^{-\beta' \hat{H}_\lambda} \right\} = \mathrm{Tr}_N \{ \hat{\rho}_\lambda \, \hat{\Delta} \} = \langle \hat{\Delta} \rangle_\lambda , \tag{C.13}
$$

where we have introduced the shorthand notation $\langle \hat{O} \rangle_\lambda = \mathrm{Tr}_N \{ \hat{\rho}_\lambda \, \hat{O} \}$. Consequently, we can write Eq. (C.12) as

$$
\frac{\partial \hat{\rho}_\lambda}{\partial \lambda} = -\hat{\rho}_\lambda \int_0^\beta \mathrm{d}\beta' \left(\hat{\Delta}_\lambda(\beta') - \langle \hat{\Delta} \rangle_\lambda \right) . \tag{C.14}
$$

Using this result in Eq. (C.10), one obtains

$$
\frac{\partial}{\partial \lambda} F[\hat{\rho}_\lambda] = \lambda \int_0^\beta \mathrm{d}\beta' \, \mathrm{Tr}_N \left\{ \hat{\rho}_\lambda \left(\hat{\Delta}_\lambda(\beta') - \langle \hat{\Delta} \rangle_\lambda \right) \hat{\Delta} \right\} =
$$

$$
= \lambda \int_0^\beta \mathrm{d}\beta' \left(\langle \hat{\Delta}_\lambda(\beta') \, \hat{\Delta} \rangle_\lambda - \langle \hat{\Delta} \rangle_\lambda^2 \right) , \tag{C.15}
$$

and again, by cyclically permuting operators within the trace, similar to Eq. (C.13), it is easy to verify that

$$\langle \hat{\Delta}_\lambda(\beta') \, \hat{\Delta} \rangle_\lambda = \langle \hat{\Delta}_\lambda(\tfrac{1}{2}\beta') \, \hat{\Delta}_\lambda^\dagger(\tfrac{1}{2}\beta') \rangle_\lambda \,. \tag{C.16}$$

By introducing $\hat{\delta}(\beta') = \hat{\Delta}_\lambda(\tfrac{1}{2}\beta') - \langle \hat{\Delta} \rangle_\lambda$, one obtains

$$\langle \hat{\delta}(\beta') \, \hat{\delta}^\dagger(\beta') \rangle_\lambda = \langle \hat{\Delta}_\lambda(\tfrac{1}{2}\beta') \, \hat{\Delta}_\lambda^\dagger(\tfrac{1}{2}\beta') \rangle_\lambda - 2 \underbrace{\langle \hat{\Delta}_\lambda(\tfrac{1}{2}\beta') \rangle_\lambda}_{=\langle \hat{\Delta} \rangle_\lambda} \langle \hat{\Delta} \rangle_\lambda + \langle \hat{\Delta} \rangle_\lambda^2 =$$

$$= \langle \hat{\Delta}_\lambda(\beta') \, \hat{\Delta} \rangle_\lambda - \langle \hat{\Delta} \rangle_\lambda^2 \,, \tag{C.17}$$

and consequently we can write Eq. (C.15) as

$$\frac{\partial}{\partial \lambda} F[\hat{\rho}_\lambda] = \lambda \int_0^\beta \mathrm{d}\beta' \, \langle \hat{\delta}(\beta') \, \hat{\delta}^\dagger(\beta') \rangle_\lambda \,. \tag{C.18}$$

The operator $\hat{\delta}(\beta') \, \hat{\delta}^\dagger(\beta')$ is positive semidefinite, such that the right-hand side of Eq. (C.18) is non-negative and only vanishes if $\hat{\delta}(\beta') = 0$, i. e., if

$$\hat{\Delta}_\lambda(\tfrac{1}{2}\beta') = \mathrm{e}^{\frac{1}{2}\beta'\hat{H}_\lambda} \, \hat{\Delta} \, \mathrm{e}^{-\frac{1}{2}\beta'\hat{H}_\lambda} = \langle \hat{\Delta} \rangle_\lambda \,. \tag{C.19}$$

Since $\langle \hat{\Delta} \rangle_\lambda$ is just a real number, Eq. (C.19) can only be satisfied if $\hat{\Delta}$ is a multiple of the identity operator, which, according to Eq. (C.7), is only the case if $\hat{\rho} = \hat{\rho}_N$. Therefore, Eqs. (C.8) and (C.18) establish the strict inequality (C.2).

Solving Shiba's integral equations

In this Appendix we present a method for solving Shiba's integral equations (2.28) and (2.33), which utilizes the trapezoidal rule in order to approximate the integrals and, in turn, leads to a set of coupled linear algebraic equations. Thus, in order to find a solution $\rho(k)$ of Shiba's integral equation

$$\rho(k) = \frac{1}{2\pi} + \frac{\cos(k)}{u} \int_{-Q}^{Q} R\left(\frac{4\,(\sin k - \sin k')}{u}\right) \rho(k')\,dk'\,, \tag{D.1}$$

we discretize the interval $[-Q, Q]$ into a grid of $M + 1$ equally spaced points $k_m = -Q + m\,\Delta k$, $m = 0, \ldots, M$ with $\Delta k = 2Q/M$, and we approximate the integral on the right-hand side by means of the trapezoidal rule

$$\int_{-Q}^{Q} f(k)\,dk \approx \Delta k \sum_{m=1}^{M} \frac{f(k_{m-1}) + f(k_m)}{2} = \Delta k \left(\sum_{m=1}^{M-1} f(k_m) + \frac{f(k_0) + f(k_M)}{2}\right). \tag{D.2}$$

Here we focus on the trapezoidal rule, since it allows for an easy implementation, however, it is straight forward to generalize the following procedure to higher order quadrature rules. Using the trapezoidal rule (D.2) and $\rho_m = \rho(k_m)$, we can cast Eq. (D.1) into the following set of $M + 1$ coupled linear algebraic equations

$$\rho_n = \frac{1}{2\pi} + \frac{\cos(k_n)}{u} \Delta k \left(\sum_{m=1}^{M-1} R_{nm}\,\rho_m + \frac{R_{n0}\,\rho_0 + R_{nM}\,\rho_M}{2}\right)\,, \tag{D.3}$$

where

$$R_{nm} = R\left(\frac{4\,(\sin k_n - \sin k_m)}{u}\right) \tag{D.4}$$

with $R(x)$ defined in Eq. (2.29). If we introduce

$$A_{nm} = \frac{\Delta k \cos(k_n)}{u}\,R_{nm} \times \begin{cases} 1/2 & \text{if } m \in \{0, M\} \\ 1 & \text{else} \end{cases} \tag{D.5}$$

we can write Eq. (D.3) in the compact form

$$\rho_n - \sum_{m=0}^{M} A_{nm}\,\rho_m = \frac{1}{2\pi} \tag{D.6}$$

or, equivalently,

$$(\mathbb{1} - A)\,\boldsymbol{\rho} = \boldsymbol{v} \quad \text{with} \quad \boldsymbol{v} = \frac{1}{2\pi}(1,\ldots,1)^{\top}. \tag{D.7}$$

Solving this system of linear equations yields a discretized solution $\boldsymbol{\rho}$ for the density function $\rho(k)$, from which the ground-state energy E as well as the electron density $n = N/N_a$ can be obtained by means of

$$-\frac{E}{tN_a} = 2\int_{-Q}^{Q} \rho(k)\,\cos(k)\,\mathrm{d}k \approx \Delta k \sum_{m=1}^{M}\left[\rho_{m-1}\cos(k_{m-1}) + \rho_m\cos(k_m)\right], \tag{D.8}$$

$$n = \int_{-Q}^{Q} \rho(k)\,\mathrm{d}k \approx \Delta k \sum_{m=1}^{M} \frac{\rho_{m-1} + \rho_m}{2}. \tag{D.9}$$

In order to obtain the average number of double occupations

$$D = 2N_a \int_{-Q}^{Q} (\cos Q - \cos k)\,\frac{\partial \rho(k)}{\partial u}\,\mathrm{d}k, \tag{D.10}$$

we need to find $\partial\rho(k)/\partial u$ from the solution of the integral equation

$$\frac{\partial\rho(k)}{\partial u} = \frac{\cos(k)}{u^2} \int_{-Q}^{Q} \Phi\!\left(\frac{4\,(\sin k - \sin k')}{u}\right)\rho(k')\,\mathrm{d}k' + \frac{\cos(k)}{u}\int_{-Q}^{Q}\mathrm{d}k'\,\frac{\partial\rho(k')}{\partial u} \times$$
$$\times \left[R\!\left(\frac{4\,(\sin k - \sin k')}{u}\right) - \frac{1}{2}R\!\left(\frac{4\,(\sin k - \sin Q)}{u}\right) - \frac{1}{2}R\!\left(\frac{4\,(\sin k + \sin Q)}{u}\right)\right] \tag{D.11}$$

with the function $\Phi(x)$ defined in Eq. (2.34). Having the discretized solution $\boldsymbol{\rho}$ for the density function $\rho(k)$, we can approximate the first integral on the right-hand side by means of the trapezoidal rule

$$\frac{\cos(k_n)}{u^2}\int_{-Q}^{Q}\Phi\!\left(\frac{4\,(\sin k_n - \sin k')}{u}\right)\rho(k')\,\mathrm{d}k' \approx$$

$$\approx \frac{\cos(k_n)}{u^2}\,\Delta k\left(\sum_{m=1}^{M-1}\Phi_{nm}\,\rho_m + \frac{\Phi_{n0}\,\rho_0 + \Phi_{nM}\,\rho_M}{2}\right) = \sum_{m=0}^{M} B_{nm}\,\rho_m, \tag{D.12}$$

where we have introduced

$$\Phi_{nm} = \Phi\left(\frac{4\left(\sin k_n - \sin k_m\right)}{u}\right) \tag{D.13}$$

and

$$B_{nm} = \frac{\Delta k \cos(k_n)}{u^2}\, \Phi_{nm} \times \begin{cases} 1/2 & \text{if } m \in \{0, M\} \\ 1 & \text{else.} \end{cases} \tag{D.14}$$

Furthermore, with $\partial \rho_m = \partial \rho(k_m)/\partial u$ and

$$T_{nm} = R\left(\frac{4\left(\sin k_n - \sin k_m\right)}{u}\right) - \frac{1}{2} R\left(\frac{4\left(\sin k_n - \sin Q\right)}{u}\right) - \frac{1}{2} R\left(\frac{4\left(\sin k_n + \sin Q\right)}{u}\right), \tag{D.15}$$

we can approximate the second integral on the right-hand side of Eq. (D.11) by

$$\frac{\cos(k_n)}{u}\, \Delta k \left(\sum_{m=1}^{M-1} T_{nm}\, \partial \rho_m + \frac{T_{n0}\, \partial \rho_0 + T_{nM}\, \partial \rho_M}{2}\right) = \sum_{m=0}^{M} C_{nm}\, \partial \rho_m, \tag{D.16}$$

where, for the sake of simplicity, we have introduced

$$C_{nm} = \frac{\Delta k \cos(k_n)}{u}\, T_{nm} \times \begin{cases} 1/2 & \text{if } m \in \{0, M\} \\ 1 & \text{else.} \end{cases} \tag{D.17}$$

Combining Eqs. (D.12) and (D.16), we can cast Eq. (D.11) into the following set of $M+1$ linear equations

$$(\mathbb{1} - C)\, \partial \boldsymbol{\rho} = \boldsymbol{b} \quad \text{with} \quad \boldsymbol{b} = B\boldsymbol{\rho}\,. \tag{D.18}$$

Finally, having the discretized solution $\partial \boldsymbol{\rho}$ for the function $\partial \rho(k)/\partial u$, we obtain the average number of double occupations D by approximating the integral on the right-hand side of Eq. (D.10) by means of the trapezoidal rule

$$\frac{D}{N_a} \approx \Delta k \sum_{m=1}^{M} \left[\left(\cos Q - \cos k_{m-1}\right) \partial \rho_{m-1} + \left(\cos Q - \cos k_m\right) \partial \rho_m\right]. \tag{D.19}$$

Strongly-interacting limit within the linear IFE-approximation

<div style="text-align: right">**E**</div>

We consider the strongly-interacting limit $U/t \to \infty$ of the half-filled Hubbard model on a hypercubic lattice in d dimensions within the linear independent-Fermion entropy (IFE) approximation (4.17), and derive the corresponding expressions for the ground state total, kinetic, and interaction energy. Our main result is that the ground-state energy obtained in the strongly-correlated limit of the linear IFE-approximation reproduces the expected behaviour $E_0/N_a = -\alpha t^2/U$ of localized Heisenberg spins, where the slope is given by $\alpha = 4d \log(2)$ in the unpolarized case $n_\uparrow = n_\downarrow = 1/2$. Thus, the exact asymptotic behaviour of the ground-state energy is recovered for the one-dimensional Hubbard model ($d = 1$). We also demonstrate that the asymptotic behaviour of the zero-field magnetic susceptibility in the strongly-correlated limit is given by $\chi = UN_a\mu_{\mathrm{B}}^2/(4dt^2)$ within the linear IFE-approximation.

E.1 Ground-state energy and related quantities

We are interested in the ground-state properties of the half-filled Hubbard model on a d-dimensional hypercubic lattice in the thermodynamic limit $N_a \to \infty$ with $n_\sigma = N_\sigma/N_a$ kept fixed for $\sigma = \uparrow,\downarrow$. Therefore, within the linear IFE-approximation (4.17), we consider the energy functional

$$E[\eta] = \frac{N_a}{(2\pi)^d} \sum_\sigma \int_{\mathrm{BZ}} \varepsilon(\boldsymbol{k})\, \eta_\sigma(\boldsymbol{k})\, \mathrm{d}\boldsymbol{k} + W_{\mathrm{HF}} \left(1 - \frac{S[\boldsymbol{\eta}]}{S_\infty}\right). \tag{E.1}$$

Here

$$\varepsilon(\boldsymbol{k}) = -2t \sum_{n=1}^{d} \cos(k_n)\,, \quad k_n \in [-\pi, \pi) \tag{E.2}$$

is the single-particle dispersion relation corresponding to the d-dimensional hypercubic lattice under consideration, $W_{\mathrm{HF}} = UN_a n_\uparrow n_\downarrow$ the Hartree-Fock interaction energy,

$$S[\boldsymbol{\eta}] = -\frac{k_{\mathrm{B}} N_a}{(2\pi)^d} \sum_\sigma \int_{\mathrm{BZ}} \Big[\eta_\sigma(\boldsymbol{k}) \log \eta_\sigma(\boldsymbol{k}) + \big(1 - \eta_\sigma(\boldsymbol{k})\big) \log\big(1 - \eta_\sigma(\boldsymbol{k})\big)\Big]\, \mathrm{d}\boldsymbol{k} \tag{E.3}$$

the IFE, and

$$S_\infty = -2N_a k_B \left(n_\uparrow \log n_\uparrow + n_\downarrow \log n_\downarrow \right) \tag{E.4}$$

its maximal value, which is attained if $\eta_\sigma(\boldsymbol{k}) = n_\sigma$ for all $\boldsymbol{k}$. The integrations in Eqs. (E.1) and (E.3) are taken over the first Brillouin zone (BZ). As discussed in the context of Eq. (4.16), the occupation-number distribution $\eta_\sigma(\boldsymbol{k})$ which minimizes the energy functional (E.1), and thus corresponds to the ground state within the linear IFE-approximation, is given by

$$\eta_\sigma(\boldsymbol{k}) = \frac{1}{z_\sigma e^{\beta\varepsilon(\boldsymbol{k})} + 1} \quad \text{with} \quad z_\sigma = e^{-\beta\mu_\sigma} \quad \text{and} \quad \beta = \frac{1}{k_B T_{\text{eff}}} = \frac{S_\infty}{k_B W_{\text{HF}}}, \tag{E.5}$$

where $T_{\text{eff}} = W_{\text{HF}}/S_\infty \propto U$ is an effective temperature. We conclude that $\beta\varepsilon(\boldsymbol{k}) \propto t/U$, and thus we can expand Eq. (E.5) as

$$\eta_\sigma(\boldsymbol{k}) = \frac{1}{z_\sigma + 1} - \frac{z_\sigma \beta\varepsilon(\boldsymbol{k})}{(z_\sigma + 1)^2} + O\left(\frac{t^2}{U^2}\right). \tag{E.6}$$

We require that the occupation-number distribution $\eta_\sigma(\boldsymbol{k})$ yields the particle density n_σ, and thus we obtain to first order in t/U

$$n_\sigma = \frac{1}{(2\pi)^d} \int_{BZ} \eta_\sigma(\boldsymbol{k}) \, d\boldsymbol{k} = \frac{1}{z_\sigma + 1} \quad \Rightarrow \quad z_\sigma = \frac{1 - n_\sigma}{n_\sigma}, \tag{E.7}$$

where we have used $\int_{BZ} \varepsilon(\boldsymbol{k}) \, d\boldsymbol{k} = 0$, which is obvious from Eq. (E.2). Substituting the result (E.7) back into Eq. (E.6), we obtain to first order in t/U

$$\eta_\sigma(\boldsymbol{k}) = n_\sigma + \delta\eta(\boldsymbol{k}) \quad \text{with} \quad \delta\eta(\boldsymbol{k}) = -n_\uparrow n_\downarrow \beta\varepsilon(\boldsymbol{k}) \propto t/U. \tag{E.8}$$

For the kinetic energy we thus obtain to first order in t/U

$$\frac{K}{N_a} = \frac{1}{(2\pi)^d} \sum_\sigma \int_{BZ} \varepsilon(\boldsymbol{k}) \, \eta_\sigma(\boldsymbol{k}) \, d\boldsymbol{k} = -\frac{2\beta n_\uparrow n_\downarrow}{(2\pi)^d} \int_{BZ} \left[\varepsilon(\boldsymbol{k})\right]^2 d\boldsymbol{k} =$$
$$= -4\beta dt^2 n_\uparrow n_\downarrow = \frac{8dt^2}{U} \left(n_\uparrow \log n_\uparrow + n_\downarrow \log n_\downarrow \right), \tag{E.9}$$

where we have used the well-known result

$$\frac{1}{(2\pi)^d} \int_{BZ} \left[\varepsilon(\boldsymbol{k})\right]^2 d\boldsymbol{k} = 2dt^2, \tag{E.10}$$

which is valid for hypercubic lattices and straight forward to derive from Eq. (E.2). Moving on to the IFE (E.3), we can expand the integrand in powers of $\delta\eta \propto t/U$ using

Eq. (E.8)

$$-\eta_\sigma \log \eta_\sigma - (1 - \eta_\sigma) \log(1 - \eta_\sigma) =$$
$$= -(n_\sigma + \delta\eta) \log(n_\sigma + \delta\eta) - (1 - n_\sigma - \delta\eta) \log(1 - n_\sigma - \delta\eta) =$$
$$= \frac{S_\infty}{2k_B N_a} + \delta\eta \log\left(\frac{1 - n_\sigma}{n_\sigma}\right) - \frac{\delta\eta^2}{2n_\uparrow n_\downarrow} + O(\delta\eta^3) \,. \qquad \text{(E.11)}$$

Thus, we obtain the IFE (E.3) up to second order in t/U as

$$\frac{S - S_\infty}{N_a} = -\frac{k_B}{n_\uparrow n_\downarrow (2\pi)^d} \int_{BZ} \left[\delta\eta(\boldsymbol{k})\right]^2 \mathrm{d}\boldsymbol{k} = -2k_B \beta^2 dt^2 n_\uparrow n_\downarrow \,, \qquad \text{(E.12)}$$

where we have used $\delta\eta(\boldsymbol{k}) = -n_\uparrow n_\downarrow \beta \varepsilon(\boldsymbol{k})$ and Eq. (E.10). With this result we obtain the interaction energy within the linear IFE-approximation as

$$\frac{W}{N_a} = \frac{W_{\mathrm{HF}}}{N_a}\left(1 - \frac{S}{S_\infty}\right) = \frac{1}{k_B \beta}\left(\frac{S_\infty - S}{N_a}\right) = 2\beta dt^2 n_\uparrow n_\downarrow = -\frac{K}{2N_a} \,. \qquad \text{(E.13)}$$

Thus, within the linear IFE-approximation the ground-state energy of the strongly correlated Hubbard model at half band-filling on a d-dimensional hypercubic lattice is, to lowest order in t/U, given by

$$\frac{E_0}{N_a} = \frac{K + W}{N_a} = \frac{K}{2N_a} = \frac{4dt^2}{U}\left(n_\uparrow \log n_\uparrow + n_\downarrow \log n_\downarrow\right) \,. \qquad \text{(E.14)}$$

Therefore, the expected behavior of localized Heisenberg-spins

$$\frac{E_0}{N_a} = -\frac{\alpha t^2}{U} \quad \text{with} \quad \alpha = -4d\left(n_\uparrow \log n_\uparrow + n_\downarrow \log n_\downarrow\right) \qquad \text{(E.15)}$$

is reproduced in the strongly-interacting limit of the linear IFE-approximation. For the case of an unpolarized spin-density ($n_\uparrow = n_\downarrow = 1/2$) the slope of the ground-state energy is given by $\alpha = 4d \log(2)$, such that the exact result $E_0 = -4N_a \log(2)\, t^2/U$ for the strongly-interacting Hubbard chain is recovered, which can be inferred from the exact analytical solution of the one-dimensional Heisenberg model [110].

E.2 Magnetic suseptibility

In order to derive the asymptotic behavior of the zero-field magnetic susceptibility in the strong-coupling limit of the linear IFE-approximation (4.17), let us express the

ground-state energy (E.14) in terms of the spin-polarization $s_z = S_z/N_a = \hbar\,(n_\uparrow - n_\downarrow)/2$

$$
\begin{aligned}
\frac{E_0(s_z)}{N_a} &= \frac{4dt^2}{U}\left[\left(\frac{1}{2}+\frac{s_z}{\hbar}\right)\log\left(\frac{1}{2}+\frac{s_z}{\hbar}\right) + \left(\frac{1}{2}-\frac{s_z}{\hbar}\right)\log\left(\frac{1}{2}-\frac{s_z}{\hbar}\right)\right] = \\
&= \frac{4dt^2}{U}\left(2s_z^2/\hbar^2 - \log 2\right) + O\!\left(s_z^3\right).
\end{aligned}
\tag{E.16}
$$

In the presence of an external magnetic-field $\boldsymbol{B} = B\,\hat{\boldsymbol{e}}_z$ we have to add a Zeeman term to the energy, i. e., $E(s_z) = E_0(s_z) + 2\mu_B B N_a s_z/\hbar$. Thus, leaving terms of the order $O\!\left(s_z^3\right)$ aside, we obtain the magnetization from the necessary condition $\partial E/\partial s_z = 0$ for a local minimum of the energy as

$$
M = -2\mu_B \frac{S_z}{\hbar} = \frac{U N_a \mu_B^2 B}{4dt^2}.
\tag{E.17}
$$

Thus, within the linear IFE-approximation we finally obtain the asymptotic behaviour of the magnetic susceptibility $\chi = \partial M/\partial B$ in the strongly-correlated limit of the half-filled Hubbard model as $\chi = \partial M/\partial B = U N_a \mu_B^2/(4dt^2)$. In the one-dimensional case ($d = 1$) we can compare this result to the exact value $\chi_{1D} = U N_a \mu_B^2/(\pi t)^2$, derived from the Bethe-ansatz solution for the half-filled Hubbard chain [50], which leads to the conclusion that the linear IFE-approximation overestimates the zero-field magnetic susceptibility of the strongly-correlated 1D Hubbard model by a factor $\pi^2/4 \approx 2.47$.

Specific heat of the doublons

<div style="text-align: right">

F

</div>

We are interested in the contribution of the doublons to the specific heat of the half-filled Hubbard model, and thus we would like to investigate the thermal-equilibrium properties of the system described by the Hamiltonian

$$\hat{H} = U \sum_i \hat{n}_{i\uparrow} \hat{n}_{i\downarrow} \,. \tag{F.1}$$

As already discussed in Section 5.2.1, the grand-canonical partition function of the system described by the Hamiltonian (F.1) is given by $Z = Z_1^{N_a}$, where Z_1 is the single-site partition function (5.39), which, in the considered case $\gamma_{11\uparrow} = \gamma_{11\downarrow} = 1/2$, is given by

$$Z_1 = 2 \left(1 + e^{\beta U/2}\right). \tag{F.2}$$

From the corresponding grand-potential $\Omega = -N_a \log(Z_1)/\beta$ we obtain the entropy of the doublons as

$$S = -\frac{\partial \Omega}{\partial T} = N_a k_{\mathrm{B}} \left(\log Z_1 - \frac{\beta U e^{\beta U/2}}{Z_1}\right). \tag{F.3}$$

Finally, the specific heat of the doublons is obtained as

$$C_V = T \frac{\partial S}{\partial T} = \frac{N_a k_{\mathrm{B}} \, x^2}{\cosh^2(x)} \quad \text{with} \quad x = \frac{\beta U}{4} \,. \tag{F.4}$$

In Fig. F.1 the specific heat of the doublons is shown as a function of the ratio $k_{\mathrm{B}}T/U$ between the temperature T and the Coulomb-repulsion strength U. We find a single broad maximum in C_V, which corresponds to the charge excitations across the Hubbard gap, i. e., to the fluctuations in the average number of doublons. In the following we would like to determine the temperature T_C at which the peak in the specific heat occurs. For a local maximum in the specific heat it must hold

$$\frac{\mathrm{d}C_V}{\mathrm{d}x} = \frac{2N_a k_{\mathrm{B}} \, x}{\cosh^2(x)} \left[1 - x \tanh(x)\right] \overset{!}{=} 0 \,. \tag{F.5}$$

This equation has solutions at $x = 0$ and $x \to \infty$, which correspond to the limits $T \to \infty$ and $T = 0$ where the specific heat vanishes. The solution of interest, which
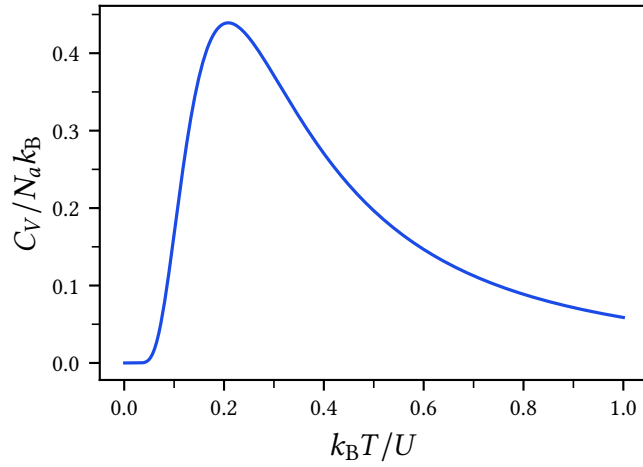
Figure F.1: Specific heat of the doublons as a function of the ratio $k_{\mathrm{B}}T/U$ between the temperature T and the Coulomb-repulsion strength U.

corresponds to a finite non-vanishing temperature, is obtained from $x\tanh(x) = 1$. This equation can be easily solved by numerical methods and one obtains

$$x_C = 1.19968 \quad \Rightarrow \quad k_{\mathrm{B}}T_C \approx 0.21U\,. \tag{F.6}$$

Discontinuities in finite-size domains

G

In this Appendix we briefly discuss the issues arising from a naive generalization of the scaling approximation (5.33) to the regime of spin-polarized electron densities. Within this naive generalization of the scaling idea, one first focuses on a fixed spin polarization $s_z = \hbar(\gamma_{11\uparrow} - \gamma_{11\downarrow})/2$ and one extracts the functional dependence of $G_c[s_z, \gamma_{12}]$ on the degree of nearest neighbor (NN) charge fluctuations γ_{12} from the properly scaled functional of a suitable reference system having the same s_z.

In order to understand the issues arising from this approach, let us notice that the upper bounds γ_{12}^0 and $\gamma_{12}^{\mathrm{rf},0}$ on the degree of NN charge fluctuations, which enter the approximation (5.33) as essential scaling parameters, generally depend on the given spin-polarization s_z. In contrast to the thermodynamic limit $N_a \to \infty$, where $\gamma_{12}^0(s_z)$ is a smooth function of s_z (see Fig. 5.16), one observes that the derivative of $\gamma_{12}^0(s_z)$ exhibits discontinuities at characteristic values of s_z if finite systems are concerned.

This situation is illustrated in Fig. G.1, where the domain of representability is shown for a number of typical reference systems used in the framework of finite-temperature lattice density functional theory (FT-LDFT). We have highlighted the locations where discontinuities in the derivative of $\gamma_{12}^0(s_z)$ occur by red points. These discontinuities are a simple consequence of the fact that the spectrum of the tight-binding Hamiltonian (5.13) is discrete if finite systems are considered. As already discussed in Section 5.1.1, the delocalized limit $\gamma_{12} = \gamma_{12}^0$ is attained when the Bloch states with effective energies (5.10) above the chemical potential μ_σ are fully occupied while Bloch states having $\omega_{\boldsymbol{k}} < \mu_\sigma$ are unoccupied. Thus, as electrons with spin-polarization σ are added to the system the tight-binding energy changes like

$$\frac{\mathrm{d}\langle \hat{H}_{\mathrm{tb}}\rangle}{\mathrm{d}N_\sigma} = zN_a \frac{\mathrm{d}\gamma_{12}^0}{\mathrm{d}N_\sigma} = \mu_\sigma \,, \tag{G.1}$$

where z is the coordination number of the finite cluster under consideration. We conclude that discontinuities in the derivative of γ_{12}^0 occur whenever the Fermi level $\omega_{F\sigma} = \mu_\sigma$ is completely filled and a further increase in the number of spin-σ electrons requires a discontinuous jump of μ_σ. At this point, it is worth mentioning that in the case of finite systems also the correlation contribution $G_c^0(s_z)$ to the free energy in the delocalized limit ($\gamma_{12} = \gamma_{12}^0$), which enters the approximation (5.33) as
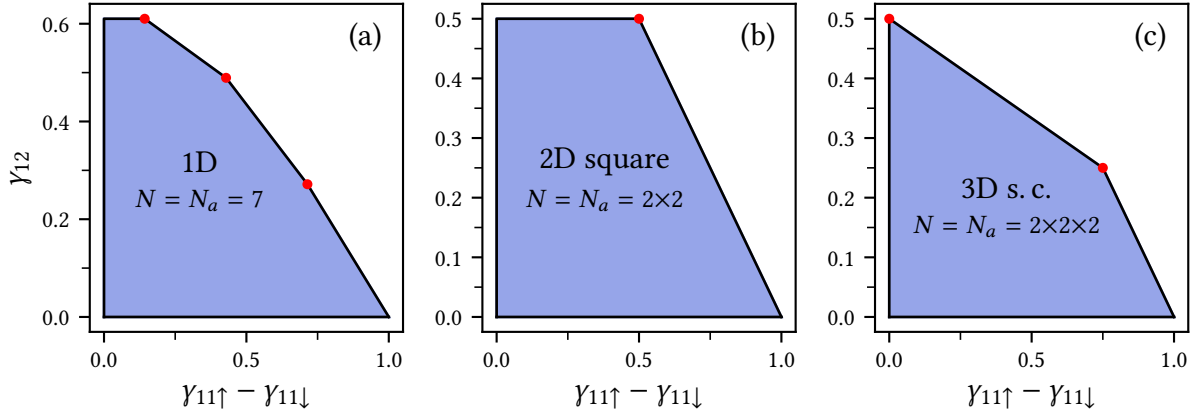
Figure G.1: Representability domains of typical FT-LDFT reference-systems. Results are shown for the half-filled Hubbard model ($n = \gamma_{11\uparrow}+\gamma_{11\downarrow} = 1$) on a (a) 7-site ring, (b) 2×2 square-lattice cluster and (c) 2×2×2 simple-cubic cluster. The spin polarizations $s_z = \hbar\,(\gamma_{11\uparrow}-\gamma_{11\downarrow})/2$ where discontinuities in the derivative of $\gamma_{12}^0(s_z)$ occur are highlighted by red points.

another scaling parameter, displays a discontinuous derivative at the same values of s_z where discontinuities in the derivative of $\gamma_{12}^0(s_z)$ occur. The origin of these discontinuities is, however, more subtle and they usually occur only in the limit $U/k_\mathrm{B}T \to \infty$, i. e., in the case of strong Coulomb repulsions or low temperatures.

Returning to the naive generalization of the scaling idea mentioned above, we must conclude that the discontinuities in the derivative of $\gamma_{12}^{\mathrm{rf},0}(s_z)$, which always occur if a finite reference system is used, would lead to artificial discontinuities in the derivative of the approximate functional $G_c[s_z, \gamma_{12}]$. This ultimately leads to very unphysical discontinuities in the thermal equilibrium averages obtained from the minimization of the corresponding approximations to the free-energy or grand-potential functionals.

Bibliography

[1] T. S. Müller, W. Töws, and G. M. Pastor, "Exploiting the links between ground-state correlations and independent-fermion entropy in the Hubbard model," Phys. Rev. B **98**, 045135 (2018).

[2] P. Hohenberg and W. Kohn, "Inhomogeneous Electron Gas," Phys. Rev. **136**, B864 (1964).

[3] W. Kohn and L. J. Sham, "Self-Consistent Equations Including Exchange and Correlation Effects," Phys. Rev. **140**, A1133 (1965).

[4] L. H. Thomas, "The calculation of atomic fields," Proc. Camb. Phil. Soc. **23**, 542 (1927).

[5] E. Fermi, "Un metodo statistico per la determinazione di alcune priorieta dell'atome," Rend. Accad. Naz. Lincei **6**, 32 (1927).

[6] N. D. Mermin, "Thermal Properties of the Inhomogeneous Electron Gas," Phys. Rev. **137**, A1441 (1965).

[7] U. von Barth and L. Hedin, "A local exchange-correlation potential for the spin polarized case: I," J. Phys. C: Solid State Phys. **5**, 1629 (1972).

[8] H. Stoll, C. M. E. Pavlidou, and H. Preuß, "On the calculation of correlation energies in the spin-density functional formalism," Theor. Chim. Acta **49**, 143 (1978).

[9] H. Stoll, E. Golka, and H. Preuß, "Correlation energies in the spin-density functional formalism," Theor. Chim. Acta **55**, 29 (1980).

[10] A. D. Becke, "Density functional calculations of molecular bond energies," J. Chem. Phys. **84**, 4524 (1986).

[11] J. P. Perdew and W. Yue, "Accurate and simple density functional for the electronic exchange energy: Generalized gradient approximation," Phys. Rev. B **33**, 8800 (1986).

Bibliography

[12] A. D. Becke, "On the large-gradient behavior of the density functional exchange energy," J. Chem. Phys. **85**, 7184 (1986).

[13] A. D. Becke, "Density-functional exchange-energy approximation with correct asymptotic behavior," Phys. Rev. A **38**, 3098 (1988).

[14] J. P. Perdew, K. Burke, and M. Ernzerhof, "Generalized Gradient Approximation Made Simple," Phys. Rev. Lett. **77**, 3865 (1996).

[15] A. D. Becke, "Density-functional thermochemistry. III. The role of exact exchange," J. Chem. Phys. **98**, 5648 (1993).

[16] J. P. Perdew, M. Ernzerhof, and K. Burke, "Rationale for mixing exact exchange with density functional approximations," J. Chem. Phys. **105**, 9982 (1996).

[17] A. D. Becke, "Density-functional thermochemistry. V. Systematic optimization of exchange-correlation functionals," J. Chem. Phys. **107**, 8554 (1997).

[18] H. L. Schmider and A. D. Becke, "Optimized density functionals from the extended G2 test set," J. Chem. Phys. **108**, 9624 (1998).

[19] C. Adamo and V. Barone, "Toward reliable density functional methods without adjustable parameters: The PBE0 model," J. Chem. Phys. **110**, 6158 (1999).

[20] T. L. Gilbert, "Hohenberg-Kohn theorem for nonlocal external potentials," Phys. Rev. B **12**, 2111 (1975).

[21] A. M. K. Müller, "Explicit approximate relation between reduced two- and one-particle density matrices," Phys. Lett. A **105**, 446 (1984).

[22] S. Goedecker and C. J. Umrigar, "Natural Orbital Functional for the Many-Electron Problem," Phys. Rev. Lett. **81**, 866 (1998).

[23] E. J. Baerends, "Exact Exchange-Correlation Treatment of Dissociated H_2 in Density Functional Theory," Phys. Rev. Lett. **87**, 133004 (2001).

[24] M. A. Buijse and E. J. Baerends, "An approximate exchange-correlation hole density as a functional of the natural orbitals," Mol. Phys. **100**, 401 (2002).

[25] O. Gritsenko, K. Pernal, and E. J. Baerends, "An improved density matrix functional by physically motivated repulsive corrections," J. Chem. Phys. **122**, 204102 (2005).

[26] D. R. Rohr, K. Pernal, O. V. Gritsenko, and E. J. Baerends, "A density matrix functional with occupation number driven treatment of dynamical and nondynamical correlation," J. Chem. Phys. **129**, 164105 (2008).

[27] M. Piris, "A new approach for the two-electron cumulant in natural orbital functional theory," Int. J. Quantum Chem. **106**, 1093 (2006).

[28] M. Piris, X. Lopez, F. Ruipérez, J. M. Matxain, and J. M. Ugalde, "A natural orbital functional for multiconfigurational states," J. Chem. Phys. **134**, 164102 (2011).

[29] M. A. L. Marques and N. N. Lathiotakis, "Empirical functionals for reduced-density-matrix-functional theory," Phys. Rev. A **77**, 032509 (2008).

[30] N. N. Lathiotakis and M. A. L. Marques, "Benchmark calculations for reduced density-matrix functional theory," J. Chem. Phys. **128**, 184103 (2008).

[31] N. N. Lathiotakis, S. Sharma, J. K. Dewhurst, F. G. Eich, M. A. L. Marques, and E. K. U. Gross, "Density-matrix-power functional: Performance for finite systems and the homogeneous electron gas," Phys. Rev. A **79**, 040501 (2009).

[32] D. R. Rohr, J. Toulouse, and K. Pernal, "Combining density-functional theory and density-matrix-functional theory," Phys. Rev. A **82**, 052502 (2010).

[33] C. S. Wang and B. M. Klein, "First-principles electronic structure of Si, Ge, GaP, GaAs, ZnS, and ZnSe. I. Self-consistent energy bands, charge densities, and effective masses," Phys. Rev. B **24**, 3393 (1981).

[34] R. O. Jones and O. Gunnarsson, "The density functional formalism, its applications and prospects," Rev. Mod. Phys. **61**, 689 (1989).

[35] A. C. Hewson, *The Kondo Problem to Heavy Fermions* (Cambridge University Press, Cambridge, UK, 1993).

[36] E. Dagotto, "Correlated electrons in high-temperature superconductors," Rev. Mod. Phys. **66**, 763 (1994).

[37] G. D. Mahan, *Many-Particle Physics*, 3rd ed., Physics of solids and liquids (Springer, New York, 2000).

[38] A. Georges and G. Kotliar, "Hubbard model in infinite dimensions," Phys. Rev. B **45**, 6479 (1992).

[39] A. Georges, G. Kotliar, W. Krauth, and M. J. Rozenberg, "Dynamical mean-field theory of strongly correlated fermion systems and the limit of infinite dimensions," Rev. Mod. Phys. **68**, 13 (1996).

[40] M. Imada, A. Fujimori, and Y. Tokura, "Metal-insulator transitions," Rev. Mod. Phys. **70**, 1039 (1998).

[41] R. Pariser and R. G. Parr, "A Semi-Empirical Theory of the Electronic Spectra and Electronic Structure of Complex Unsaturated Molecules. I." J. Chem. Phys. **21**, 466 (1953).

[42] J. A. Pople, "Electron interaction in unsaturated hydrocarbons," Trans. Faraday Soc. **49**, 1375 (1953).

[43] P. W. Anderson, "Localized Magnetic States in Metals," Phys. Rev. **124**, 41 (1961).

[44] J. Hubbard, "Electron Correlations in Narrow Energy Bands," Proc. R. Soc. Lond. A **276**, 238 (1963).

[45] J. Kanamori, "Electron Correlation and Ferromagnetism of Transition Metals," Prog. Theor. Phys. **30**, 275 (1963).

[46] M. C. Gutzwiller, "Effect of Correlation on the Ferromagnetism of Transition Metals," Phys. Rev. Lett. **10**, 159 (1963).

[47] P. Fulde, *Electron Correlations in Molecules and Solids*, 3rd ed., Springer series in solid-state sciences No. 100 (Springer, Berlin, 1995).

[48] N. H. March, *Electron Correlation in Molecules and Condensed Phases* (Springer, New York, 1996).

[49] E. H. Lieb and F. Y. Wu, "Absence of Mott Transition in an Exact Solution of the Short-Range, One-Band Model in One Dimension," Phys. Rev. Lett. **20**, 1445 (1968).

[50] M. Takahashi, "Magnetization Curve for the Half-Filled Hubbard Model," Prog. Theor. Phys. **42**, 1098 (1969); M. Takahashi, "Magnetic Susceptibility for the Half-Filled Hubbard Model," Prog. Theor. Phys. **43**, 1619 (1970).

[51] H. Shiba, "Magnetic Susceptibility at Zero Temperature for the One-Dimensional Hubbard Model," Phys. Rev. B **6**, 930 (1972).

[52] Y. Nagaoka, "Ground state of correlated electrons in a narrow almost half-filled s band," Solid State Commun. **3**, 409 (1965).

[53] H. Tasaki, "Extension of Nagaoka's theorem on the large-U Hubbard model," Phys. Rev. B **40**, 9192 (1989).

[54] E. H. Lieb, "Two Theorems on the Hubbard Model," Phys. Rev. Lett. **62**, 1927 (1989).

[55] H. Tasaki, "The Hubbard model - an introduction and selected rigorous results," J. Phys. Condens. Matter **10**, 4353 (1998).

[56] G. Jüttner, A. Klümper, and J. Suzuki, "The Hubbard chain at finite temperatures: Ab initio calculations of Tomonaga-Luttinger liquid properties," Nucl. Phys. B **522**, 471 (1998).

[57] J. E. Hirsch, "Monte Carlo Study of the Two-Dimensional Hubbard Model," Phys. Rev. Lett. **51**, 1900 (1983).

[58] S. R. White, D. J. Scalapino, R. L. Sugar, E. Y. Loh, J. E. Gubernatis, and R. T. Scalettar, "Numerical study of the two-dimensional Hubbard model," Phys. Rev. B **40**, 506 (1989).

[59] A. Moreo, D. J. Scalapino, R. L. Sugar, S. R. White, and N. E. Bickers, "Numerical Study of the Two-Dimensional Hubbard Model for Various Band Fillings," Phys. Rev. B **41**, 2313 (1990).

[60] N. Furukawa and M. Imada, "Charge Gap, Charge Susceptibility and Spin Correlation in the Hubbard Model on a Square Lattice," J. Phys. Soc. Jpn. **60**, 3604 (1991).

[61] S. R. White, "Density matrix formulation for quantum renormalization groups," Phys. Rev. Lett. **69**, 2863 (1992).

[62] S. R. White, "Density-matrix algorithms for quantum renormalization groups," Phys. Rev. B **48**, 10345 (1993).

[63] D. Duffy and A. Moreo, "Specific heat of the two-dimensional Hubbard model," Phys. Rev. B **55**, 12918 (1997).

[64] C. N. Varney, C.-R. Lee, Z. J. Bai, S. Chiesa, M. Jarrell, and R. T. Scalettar, "Quantum Monte Carlo Study of the Two-Dimensional Fermion Hubbard Model," Phys. Rev. B **80**, 075116 (2009).

[65] T. Paiva, "Fermions in 3D Optical Lattices: Cooling Protocol to Obtain Antiferromagnetism," Phys. Rev. Lett. **107**, 086401 (2011).

[66] E. Khatami and M. Rigol, "Effect of particle statistics in strongly correlated two-dimensional Hubbard models," Phys. Rev. A **86**, 023633 (2012).

[67] E. Kozik, E. Burovski, V. W. Scarola, and M. Troyer, "Néel temperature and thermodynamics of the half-filled three-dimensional Hubbard model by diagrammatic determinant Monte Carlo," Phys. Rev. B **87**, 205102 (2013).

[68] E. Khatami, "Three-dimensional Hubbard model in the thermodynamic limit," Phys. Rev. B **94**, 125114 (2016).

[69] O. Gunnarsson and K. Schönhammer, "Density-Functional Treatment of an Exactly Solvable Semiconductor Model," Phys. Rev. Lett. **56**, 1968 (1986).

[70] A. Svane and O. Gunnarsson, "Localization in the self-interaction-corrected density-functional formalism," Phys. Rev. B **37**, 9919 (1988).

[71] K. Schönhammer, O. Gunnarsson, and R. M. Noack, "Density-functional theory on a lattice: Comparison with exact numerical results for a model with strongly correlated electrons," Phys. Rev. B **52**, 2504 (1995).

[72] A. Schindlmayr and R. W. Godby, "Density-functional theory and the v-representability problem for model strongly correlated electron systems," Phys. Rev. B **51**, 10427 (1995).

[73] A. E. Carlsson, "Exchange-correlation functional based on the density matrix," Phys. Rev. B **56**, 12058 (1997).

[74] R. G. Hennig and A. E. Carlsson, "Density-matrix functional method for electronic properties of impurities," Phys. Rev. B **63**, 115116 (2001).

[75] N. A. Lima, M. F. Silva, L. N. Oliveira, and K. Capelle, "Density Functionals Not Based on the Electron Gas: Local-Density Approximation for a Luttinger Liquid," Phys. Rev. Lett. **90**, 146402 (2003).

[76] C. Verdozzi, "Time-Dependent Density-Functional Theory and Strongly Correlated Systems," Phys. Rev. Lett. **101**, 166401 (2008).

[77] R. López-Sandoval and G. M. Pastor, "Density-matrix functional theory of the Hubbard model: An exact numerical study," Phys. Rev. B **61**, 1764 (2000).

[78] R. López-Sandoval and G. M. Pastor, "Density-matrix functional theory of strongly correlated lattice fermions," Phys. Rev. B **66**, 155118 (2002).

[79] R. López-Sandoval and G. M. Pastor, "Electronic properties of the dimerized one-dimensional Hubbard model using lattice density-functional theory," Phys. Rev. B **67**, 035115 (2003).

[80] R. López-Sandoval and G. M. Pastor, "Interaction-energy functional for lattice density functional theory: Applications to one-, two-, and three-dimensional Hubbard models," Phys. Rev. B **69**, 085101 (2004).

[81] W. Töws and G. M. Pastor, "Lattice density functional theory of the single-impurity Anderson model: Development and applications," Phys. Rev. B **83**, 235101 (2011).

[82] W. Töws and G. M. Pastor, "Spin-polarized density-matrix functional theory of the single-impurity Anderson model," Phys. Rev. B **86**, 245123 (2012).

[83] W. Töws, M. Saubanère, and G. M. Pastor, "Density-matrix functional theory of strongly correlated fermions on lattice models and minimal-basis Hamiltonians," Theor. Chem. Acc. **133**, 1 (2014).

[84] M. Saubanère and G. M. Pastor, "Scaling and transferability of the interaction-energy functional of the inhomogeneous Hubbard model," Phys. Rev. B **79**, 235101 (2009).

[85] M. Saubanère and G. M. Pastor, "Density-matrix functional study of the Hubbard model on one- and two-dimensional bipartite lattices," Phys. Rev. B **84**, 035111 (2011).

[86] M. Saubanère and G. M. Pastor, "Lattice density-functional theory of the attractive Hubbard model," Phys. Rev. B **90**, 125128 (2014).

[87] M. Saubanére, M. B. Lepetit, and G. M. Pastor, "Interaction-energy functional of the Hubbard model: Local formulation and application to low-dimensional lattices," Phys. Rev. B **94**, 045102 (2016).

[88] G. Stefanucci and S. Kurth, "Towards a Description of the Kondo Effect Using Time-Dependent Density-Functional Theory," Phys. Rev. Lett. **107**, 216401 (2011).

[89] J. P. Bergfield, Z.-F. Liu, K. Burke, and C. A. Stafford, "Bethe Ansatz Approach to the Kondo Effect within Density-Functional Theory," Phys. Rev. Lett. **108**, 066801 (2012).

[90] F. Perrot, "Gradient correction to the statistical electronic free energy at nonzero temperatures: Application to equation-of-state calculations," Phys. Rev. A **20**, 586 (1979).

[91] S. Pittalis, C. R. Proetto, A. Floris, A. Sanna, C. Bersier, K. Burke, and E. K. U. Gross, "Exact Conditions in Finite-Temperature Density-Functional Theory," Phys. Rev. Lett. **107**, 163001 (2011).

[92] H. Bethe, "Zur Theorie der Metalle," Z. Physik **71**, 205 (1931).

[93] W. Nolting and W. Borgieł, "Band magnetism in the Hubbard model," Phys. Rev. B **39**, 6962 (1989).

[94] N. Furukawa and M. Imada, "Two-Dimensional Hubbard Model –Metal Insulator Transition Studied by Monte Carlo Calculation–," J. Phys. Soc. Jpn. **61**, 3331 (1992).

[95] P. W. Anderson, "The Resonating Valence Bond State in La_2CuO_4 and Superconductivity," Science **235**, 1196 (1987).

[96] M. Cyrot, "Are high T_c superconductors doped mott insulators?" Solid State Commun. **63**, 1015 (1987).

[97] E. H. Lieb and F. Y. Wu, "The one-dimensional Hubbard model: A reminiscence," Physica A **321**, 1 (2003).

[98] F. H. L. Essler, H. Frahm, F. Göhmann, A. Klümper, and V. E. Korepin, *The One-Dimensional Hubbard Model* (Cambridge University Press, Cambridge, 2005).

[99] J. R. Schrieffer and P. A. Wolff, "Relation between the Anderson and Kondo Hamiltonians," Phys. Rev. **149**, 491 (1966).

[100] P. Fazekas, *Lecture Notes on Electron Correlation and Magnetism*, Series in Modern Condensed Matter Physics, Vol. 5 (World Scientific, Singapore, 1999).

[101] S. M. Valone, "Consequences of extending 1-matrix energy functionals from pure-state representable to all ensemble representable 1 matrices," J. Chem. Phys. **73**, 1344 (1980).

[102] S. M. Valone, "A one-to-one mapping between one-particle densities and some n-particle ensembles," J. Chem. Phys. **73**, 4653 (1980).

[103] R. G. Parr and W. Yang, *Density-Functional Theory of Atoms and Molecules* (Oxford University Press, New York, 1995).

[104] D. Williams, *Weighing the Odds* (Cambridge University Press, New York, 2001).

[105] M. Ogata and H. Shiba, "Bethe-ansatz wave function, momentum distribution, and spin correlation in the one-dimensional strongly correlated Hubbard model," Phys. Rev. B **41**, 2326 (1990).

[106] P. W. Anderson, ""Luttinger-liquid" behavior of the normal metallic state of the 2D Hubbard model," Phys. Rev. Lett. **64**, 1839 (1990).

[107] G. Benfatto, A. Giuliani, and V. Mastropietro, "Fermi Liquid Behavior in the 2D Hubbard Model at Low Temperatures," Ann. Henri Poincaré **7**, 809 (2006).

[108] B. N. Parlett, *The Symmetric Eigenvalue Problem* (SIAM: Philadelphia, PA, USA, 1998).

[109] M. Calandra Buonaura and S. Sorella, "Numerical study of the two-dimensional heisenberg model using a green function monte carlo technique with a fixed number of walkers," Phys. Rev. B **57**, 11446 (1998).

[110] L. Hulthén, "Über das Austauschproblem eines Kristalls," Ark. Mat. Astron. Fys. **26A**, 11 (1938).

[111] D. C. Mattis, *The Theory of Magnetism I: Statics and Dynamics*, Springer Series in Solid-State Sciences (Springer-Verlag, Berlin Heidelberg, 1981).

[112] D. C. Mattis and C. Y. Pan, "Ground-State Energy of Heisenberg Antiferromagnet for Spins $s = \frac{1}{2}$ and $s = 1$ in $d = 1$ and 2 Dimensions," Phys. Rev. Lett. **61**, 463 (1988).

[113] S. Fujiki, "Zero-Temperature Properties of Quantum Spin Models on the Triangular Lattice III: The Heisenberg Antiferromagnet," Can. J. Phys. **65**, 489 (1987).

[114] J. Bardeen, "Theory of Superconductivity," Phys. Rev. **108**, 1175 (1957).

[115] F. D. M. Haldane, "'Luttinger liquid theory' of one-dimensional quantum fluids. I. Properties of the Luttinger model and their extension to the general 1D interacting spinless Fermi gas," J. Phys. C **14**, 2585 (1981).

[116] K. Schönhammer, "Luttinger liquids: the basic concepts," in *Strong interactions in low dimensions*, edited by D. Baeriswyl and L. Degiorgi (Springer Netherlands, Dordrecht, 2004) Chap. 4, pp. 93–136.

[117] H. J. Schulz, "Fermi liquids and non-Fermi liquids," in *Mesoscopic Quantum Physics*, Les Houches, Session LXI, 1994 (Elsevier, Amsterdam, 1995).

Bibliography

[118] E. Koch and S. Goedecker, "Locality properties and Wannier functions for interacting systems," Solid State Commun. **119**, 105 (2001).

[119] J. C. Bonner and M. E. Fisher, "Linear Magnetic Chains with Anisotropic Coupling," Phys. Rev. **135**, A640 (1964).

[120] A. Klümper, "The spin-1/2 Heisenberg chain: Thermodynamics, quantum criticality and spin-Peierls exponents," Eur. Phys. J. B **5**, 677 (1998).

[121] D. Vollhardt, "Characteristic Crossing Points in Specific Heat Curves of Correlated Systems," Phys. Rev. Lett. **78**, 1307 (1997).

[122] N. Chandra, M. Kollar, and D. Vollhardt, "Nearly universal crossing point of the specific heat curves of Hubbard models," Phys. Rev. B **59**, 10541 (1999).

[123] D. F. Brewer, J. G. Daunt, and A. K. Sreedhar, "Low-Temperature Specific Heat of Liquid He^3 near the Saturated Vapor Pressure and at Higher Pressures," Phys. Rev. **115**, 836 (1959).

[124] D. S. Greywall, "Specific heat of normal liquid ^{3}He," Phys. Rev. B **27**, 2747 (1983).

[125] G. E. Brodale, R. A. Fisher, N. E. Phillips, and J. Floquet, "Pressure dependence of the low-temperature specific heat of the heavy-fermion compound CeAl$_3$," Phys. Rev. Lett. **56**, 390 (1986).

[126] N. E. Phillips, R. A. Fisher, J. Flouquet, A. L. Giorgi, J. A. Olsen, and G. R. Stewart, "Pressure Dependences of the Specific Heats of UPt$_3$, UBe$_{13}$ and CeAl$_3$," J. Magn. Magn. Mater. **63-64**, 332 (1987).

[127] J. Jaklič and P. Prelovšek, "Finite-temperature properties of doped antiferromagnets," Adv. Phys. **49**, 1 (2000).

[128] P. Sengupta, A. W. Sandvik, and R. R. P. Singh, "Specific heat of quasi-two-dimensional antiferromagnetic Heisenberg models with varying interplanar couplings," Phys. Rev. B **68**, 094423 (2003).

[129] A. W. Sandvik, "Critical Temperature and the Transition from Quantum to Classical Order Parameter Fluctuations in the Three-Dimensional Heisenberg Antiferromagnet," Phys. Rev. Lett. **80**, 5196 (1998).

[130] E. Khatami and M. Rigol, "Thermodynamics of strongly interacting fermions in two-dimensional optical lattices," Phys. Rev. A **84**, 053611 (2011).

[131] D. W. Hone and P. Pincus, "High-Temperature Properties of the Half-Filled-Band Hubbard Model," Phys. Rev. B **7**, 4889 (1973).

[132] W. Kohn, in *Highlights of condensed-matter theory*, edited by F. Bassani, F. Fumi, and M. P. Tosi (North Holland Physics Publishing, Amsterdam, 1985) p. 1.

[133] R. M. Dreizler and E. K. U. Gross, *Density Functional Theory* (Springer-Verlag, Berlin Heidelberg, 1990).

[134] M. Reed and B. Simon, *Methods of Modern Mathematical Physics*, Vol. 4 (Academic Press, New York, 1978).

[135] E. H. Lieb, "Density Functionals for Coulomb Systems," Int. J. Quant. Chem. **24**, 243 (1983).

[136] M. Levy, "Electron densities in search of Hamiltonians," Phys. Rev. A **26**, 1200 (1982).

[137] H. Englisch and R. Englisch, "Hohenberg-Kohn theorem and non-V-representable densities," Physica A **121**, 253 (1983).

[138] M. Levy, "Universal variational functionals of electron densities, first-order density matrices, and natural spin-orbitals and solution of the v-representability problem," Proc. Natl. Acad. Sci. **76**, 6062 (1979).

[139] J. E. Harriman, "Orthonormal orbitals for the representation of an arbitrary density," Phys. Rev. A **24**, 680 (1981).

[140] N. H. March, "n representability of electron density and first-order density matrix," Phys. Rev. A **26**, 1845 (1982).

[141] G. Zumbach and K. Maschke, "New approach to the calculation of density functionals," Phys. Rev. A **28**, 544 (1983).

[142] L. Hedin and B. I. Lundqvist, "Explicit local exchange-correlation potentials," J. Phys. C: Solid State Phys. **4**, 2064 (1971).

[143] G. M. Pastor and J. Dorantes-Dávila, "Spin-rotational-invariant theory of transition-metal magnetism at finite temperatures: Systematic study of a single-site model," Phys. Rev. B **93**, 214435 (2016).

[144] S. Riemer, J. Dorantes-Dávila, and G. M. Pastor, "Finite temperature magnetic properties of small Fe chains and clusters on Pt(111)," Phys. Rev. B **93**, 134414 (2016).

Bibliography

[145] A. I. Lichtenstein, M. I. Katsnelson, and G. Kotliar, "Finite-Temperature Magnetism of Transition Metals: An ab initio Dynamical Mean-Field Theory," Phys. Rev. Lett. **87**, 067205 (2001).

[146] R. P. Feynman, "An Operator Calculus Having Applications in Quantum Electrodynamics," Phys. Rev. **84**, 108 (1951).